University of Glasgow

Holding the Front Line: Maintaining Barrier Integrity in the Mouth

Krystyna Monika Piela
BDS, BSc (Hons), BSc

Submitted in fulfilment of the requirements
for the Degree of Doctor of Philosophy

School of Medicine, Dentistry and Nursing
College of Medical, Veterinary and Life Sciences

University of Glasgow

October 2025

Abstract

Background

The oral cavity is a unique microenvironment challenged by a wide range of factors including masticatory forces, environmental factors and a diverse oral microbiome. The gingival crevice is lined by non-keratinised sulcular and junctional epithelia; the latter attaches to the tooth surface and is only a few cells thick. It has a uniquely tailored defence system to maintain health, including the presence of distinct subsets of neutrophils displaying characteristic phenotypes following exposure to biofilms. Failure of this barrier homeostasis results in gingival inflammation and – in susceptible patients – in destructive periodontal disease. There is a clinical need for improved preventative and therapeutic options for periodontal disease. There are parallel economic drivers to develop preventative and therapeutic products for the multi-million-pound oral care market. *In vitro* models can offer a reductionist platform for testing novel actives, reducing use of animals and costs of identifying and testing interventions. There has been a recent shift to focus on maintenance of health, rather than aetiopathogenesis of disease. This thesis sought to identify components of the oral mucosal barrier that maintain its integrity with the aim of integrating them into an *in vitro* model that will accurately reflect *in vivo* conditions.

Methods

Literature and data searches were performed, and data were synthesised to identify key components of a healthy oral barrier in three main areas: i) microbiome and microbe-derived soluble mediators; ii) host cells; and iii) host soluble mediators. Cell culture and flow cytometry were used to evaluate potential host cells for use in the model. TR146 epithelial cells and primary human neutrophils were utilised to create a modified chemotaxis assay to mimic the egress of neutrophils at the gingival epithelium upon stimulation with health- and periodontitis-associated biofilms.

Results

The review identified microbial taxa at the phylum, genus and species levels that were associated with periodontal health (Chapter 3). A novel *in vitro* model of multispecies microbial biofilm was developed that emulated certain characteristics of a health-associated subgingival biofilm (Chapter 4). TR146 epithelial cells could be grown on the basolateral side of a porous transwell insert membrane and remain metabolically active. Primary neutrophils were identified as a suitable cell type to model the early immune response *in vitro* (Chapter 5). Multispecies biofilms, TR146 epithelial cells, and primary neutrophils were combined to develop a proof-of-concept *in vitro* model designed to represent the oral barrier at the gingival sulcus (Chapter 6).

Conclusion

The work to date has identified key components of the proposed model system and provided preliminary proof-of-concept evidence that selected components can be combined. Further work is needed to optimise and validate the model across different configurations and challenge conditions, as well as methods for reliable neutrophil tracking and detection of cytokine responses. This work may help to identify potential targetable pathways to maintain oral health.

Table of Contents

List of Tables

List of Figures

Acknowledgement

I would like to extend my sincere gratitude to my thesis supervisors, Professor Shauna Culshaw and Dr Jennifer Malcolm for their invaluable insight and guidance throughout my studies.

As primary supervisor, Professor Culshaw has never wavered in her support and attention for my work and well-being, generously and tirelessly offering help whenever it was needed. She has nurtured my development as a fledgling researcher since 2016 when I came to her lab still as an Erasmus Exchange student. Ever since, she has been an inspiration: an example of a scholar, teacher, clinician and team leader whose footsteps I would love to follow in my own career. The very possibility of this research has been down to her generosity, encouragement and vision. Thank you, Dear Shauna, for this life-changing opportunity – and for all your support throughout the years.

I have known Dr Jennifer Malcolm, my secondary supervisor, since the said Erasmus Exchange, when she was a post-doctoral researcher. Busy with her own work, she spent countless hours of her valuable time to introduce and train the oblivious newcomer that I was, unselfishly sharing her knowledge and skills in ways that eventually formed the foundations of this doctoral research. Later, as my supervisor, she continued to mentor and advise, especially in the difficult lab work where her experience was invaluable. Dear Jennifer – thank you for your openness and guidance.

I would like to express my gratitude to the Biotechnology and Biological Sciences Research Council (BBSRC) for funding this project through Training Grant BB/W510099/1 Industrial CASE CSV.

Many thanks are due to the industry sponsor of the work, Haleon, and specifically to Dr David Bradshaw and Dr Behrad Mahmoodi who provided additional support and opportunity to present my work at the annual Haleon symposia in London.

I would like to thank my friends and peers from the doctoral programme, in particular Suror Shaban, with whom I started my PhD journey, Laurie Rowan,

Lauren Ashcroft and Zainab Bilal. Without your humour and companionship these studies would have been so much more difficult – thank you for being there for me!

I am also grateful to Paddy Watson, Research Assistant in our group, for his tireless help in the early days of this work, and to the Systematic Review Group lead by Professor Magda Feres – participating in her network was instrumental to better planning and contextualisation of my work. Further thanks go to Professor Andrea Sheriff and Dr Tomoko Iwata for their support of the postgraduate student community in our School, as well as to all current and past members of the Oral Sciences group.

Looking back, I wish to extend cordial thanks to Professor Sebastian Kłosek and Dr Anna Dudko of the Medical University of Łódź, for their support and generous help in my application to the PhD programme.

That the past four years have not overwhelmed me – at least not completely – is in no small part to my beloved husband, Piotr Leśniak, whose calm, wisdom, and steadfast support carried me through every challenge. His presence was my greatest source of comfort and strength.

Finally, I would not be who I am without my grandparents, Bronisława and Henryk Kuchta, and my parents Małgorzata and Henryk Piela. I owe much to my grandparents, both dedicated teachers, whose example instilled in me a respect for learning and curiosity about the world. Above all, it was my loving parents' faith in my growth and development, their steadfast backing, comforting words, and countless deeds that made difficult choices easier and allowed me to focus on what truly matters. Mum and Dad – I will always be grateful for everything you have done for me!

I dedicate this work to the memory of my late grandmother, Bronisława Kuchta (1933-2023). Born to a different world and epoch, she kept a sharp mind and a keen eye throughout her long life – always curious of my work, inspiring me to do and be better, to love, look ahead and pursue my dreams.

Dziękuję, Babciu!

Author's Declaration

I certify that the thesis presented here for examination for the degree of PhD of the University of Glasgow is solely my own work other than where I have clearly indicated that it is the work of others (in which case the extent of any work carried out jointly by me and any other person is clearly identified in it) and that the thesis has not been edited by a third party beyond what is permitted by the University's PGR Code of Practice.

Krystyna Monika Piela

October 2025

Abbreviations and definitions

3Rs	Replacement, Reduction and Refinement
AAP	American Academy of Periodontology
ALI	Air-liquid interface
APC	Antigen-presenting cell
aPDT	Antimicrobial photodynamic therapy
APT	Active periodontal therapy
ATRA	All-trans retinoic acid
BHI	Brain heart infusion
BOP	Bleeding on probing
$CaCl_2$	Calcium chloride
CAL	Clinical attachment loss
CBA	Columbia blood agar
CCK-8	Cell Counting Kit-8
CCL	C-C motif chemokine ligand
CD	Cluster of differentiation
CFE	Colony-forming equivalents
CFU	Colony-forming units
Cq	Quantification cycle
CRP	C-reactive protein
CV	Coefficient of variation
CVD	Cardiovascular disease
CXCL	C-X-C motif chemokine ligand
DMARDs	Disease-modifying anti-rheumatic drugs
DMSO	Dimethyl sulfoxide
dPBS(+)	Dulbecco's phosphate-buffered saline with calcium and magnesium
dPBS(−)	Dulbecco's phosphate-buffered saline without calcium and magnesium
ECACC	European Collection of Authenticated Cell Cultures
EDTA	Ethylenediaminetetraacetic acid
EFP	European Federation of Periodontology
ELISA	Enzyme-linked immunosorbent assay
FAA	Fastidious anaerobe agar

FBS	Foetal bovine serum
FCS	Foetal calf serum
FISH	Fluorescence *in situ* hybridisation
fMLF	N-formyl-methionyl-leucyl-phenylalanine
G-CSF	Granulocyte colony-stimulating factor
GCF	Gingival crevicular fluid
GM-CSF	Granulocyte–macrophage colony-stimulating factor
H&E	Haematoxylin and eosin
H_2O_2	Hydrogen peroxide
HaCaT	Immortalised human keratinocyte cell line
HBSS	Hanks' balanced salt solution
HEPES	4-(2-hydroxyethyl)-1-piperazineethanesulfonic acid
HI	Heat-inactivated
HL-60	Human promyelocytic leukaemia cell line
HUVECs	Human umbilical vein endothelial cells
ICAM-1	Intercellular adhesion molecule-1
IFN	Interferon
IHC	Immunohistochemistry
IL	Interleukin
IMPEDE	Inflammation-Mediated Polymicrobial-Emergence and Dysbiotic-Exacerbation model
LOD	Limit of detection
LPS	Lipopolysaccharide
LTB_4	Leukotriene B_4
MCP-1	Monocyte chemoattractant protein-1
MMP	Matrix metalloproteinase
NADPH	Nicotinamide adenine dinucleotide phosphate (reduced form)
NETs	Neutrophil extracellular traps
NF-κB	Nuclear factor-κB
NK cell	Natural killer cell
NSPT	Non-surgical periodontal therapy
NST	Non-surgical therapy
NTC	No-template control
OD	Optical density
OPG	Osteoprotegerin

PBMCs	Peripheral blood mononuclear cells
PBS	Phosphate-buffered saline
PC	Polycarbonate
PD	Probing depth
PDL	Periodontal ligament
PET	Polyethylene terephthalate
PFA	Paraformaldehyde
PGE_2	Prostaglandin E_2
PMA	Phorbol 12-myristate 13-acetate
PMN	Polymorphonuclear neutrophil
PPAR-γ	Peroxisome proliferator-activated receptor-γ
PPD	Probing pocket depth
PRISMA	Preferred Reporting Items for Systematic reviews and Meta-Analyses
PSD	Polymicrobial synergy and dysbiosis
PUFA	Polyunsaturated fatty acid
qPCR	Quantitative polymerase chain reaction
RA	Rheumatoid arthritis
RANK	Receptor activator of nuclear factor-κB
RANKL	Receptor activator of nuclear factor-κB ligand
Rgp	Arginine-specific gingipain
ROS	Reactive oxygen species
RPMI	Roswell Park Memorial Institute medium
SCH	Schaedler anaerobe broth
SD	Standard deviation
SEM	Scanning electron microscopy
SPC	Supportive periodontal care
SPT	Supportive periodontal therapy
STR	Short tandem repeat
TEER	Transepithelial electrical resistance
Th17	T helper 17
THB	Todd-Hewitt broth
TLR	Toll-like receptor
TNF	Tumour necrosis factor
TR146	Human buccal squamous cell carcinoma cell line

TSB	Tryptic soy broth

1 General Introduction

1.1 Oral barrier

1.1.1 Overview of the oral barrier

The oral cavity fulfils several roles important for survival and overall wellbeing of a person. It allows for ingestion and initial digestion of food, mediates taste and general sensory perception, enables speech and resonance and assists in respiration as a secondary airway. These functions require direct contact with external environmental triggers such as food, microbes and airborne antigens and allergens. To protect itself from tissue damage that may arise from these encounters, the oral cavity maintains a mucosal barrier, which consists of epithelium, basement membrane, lamina propria (underlying connective tissue) and, in some areas, submucosa. The oral mucosal barrier displays location-dependent characteristics: areas at risk of mechanical injury (e.g. masticatory or dorsal tongue mucosa) are keratinised, while the floor of the mouth that is not subjected to heavy mechanical stress is not (Moutsopoulos and Konkel, 2018).

Periodontal tissues (periodontium) are structures that surround and support teeth and include cementum, periodontal ligament, alveolar bone and gingiva (see Figure 1.1). Cementum covers and thus protects the root dentin while also acting as an attachment surface for certain periodontal ligament fibers. Periodontal ligament not only anchors the root of the tooth to its socket (alveolus) in the alveolar bone but also distributes and dissipates occlusal forces. It contains mechanoreceptors that provide proprioceptive feedback during mastication and a rich vascular supply that delivers nutrients, and is thought to absorb occlusal forces (Dean, 2017, Matsuo and Takahashi, 2002). The gingiva covers and protects the alveolar processes from mechanical trauma from food and brushing, and forms a protective seal around the teeth to limit penetration by microbes and debris (Schroeder and Listgarten, 1997).

In health, the gingival sulcus is a 0.5 to 3 mm-deep space between the tooth/root surface and the inner aspect of the free (marginal) gingiva. This non-

keratinised epithelium is vulnerable to trauma and microbial invasion. The non-keratinised sulcular epithelium transitions into junctional epithelium that attaches to the tooth surface (Moutsopoulos and Konkel, 2018). Junctional epithelium is highly permeable and allows for a constant outward flow of gingival crevicular fluid (GCF), which is a serum transudate from the (gingival) vascular plexus in the underlying connective tissue (Matsuo and Takahashi, 2002). Within the gingival sulcus reside planktonic bacteria that can adhere to available surfaces and initiate subgingival biofilm formation (Manoil and Belibasakis, 2025). Consequently, this area is subject to a constant surveillance by the immune cells that migrate through the junctional epithelium (Nakamura, 2018), constituting a barrier site.

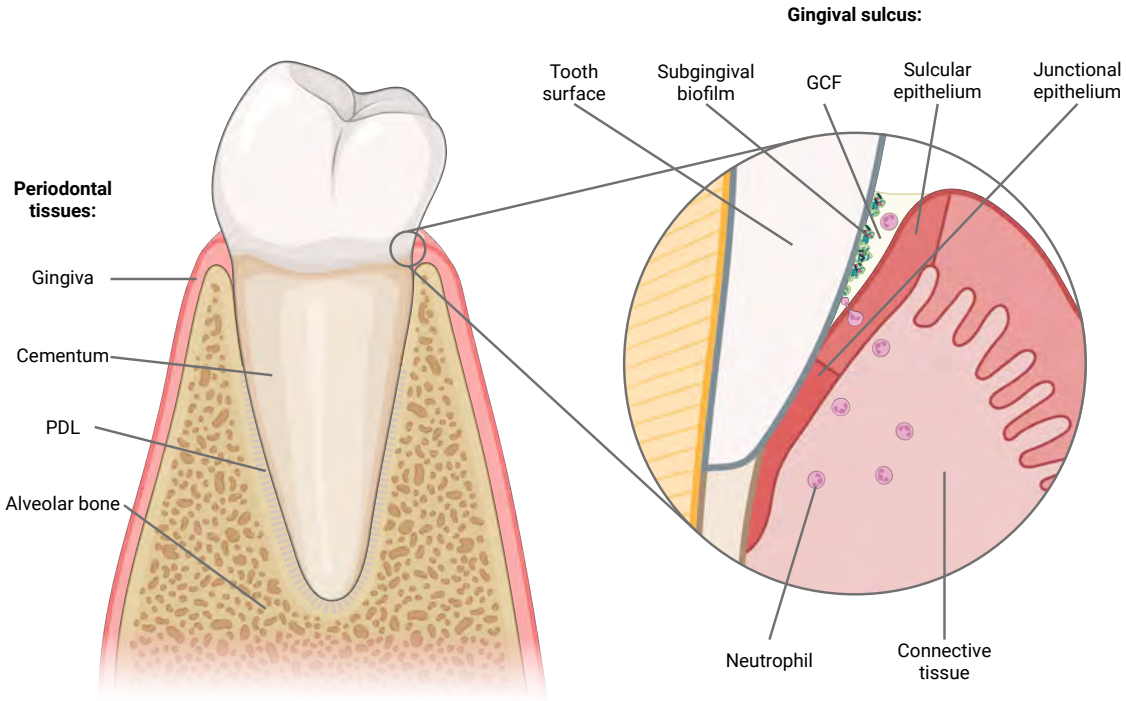

Figure 1.1 Periodontal tissues and oral barrier in the gingival sulcus. (Left) Schematic sectional view of the periodontal tissues surrounding and supporting the tooth. The cementum covering the root surface provides attachment for the periodontal ligament, which anchors the tooth to the alveolar bone. The gingiva overlies the alveolar bone and forms a protective soft tissue seal around the tooth. (Right) Enlarged cross-sectional view of the gingival sulcus indicated on the left panel, showing the key components of the oral barrier at this site. The gingival sulcus is a narrow space below the gumline, bounded by the tooth surface and the sulcular and junctional epithelium. The tooth surface supports subgingival biofilm formation, while the epithelium is associated with gingival crevicular fluid flow and neutrophil migration from the underlying connective tissue into the sulcus. Proportions have been adjusted for clarity and are not representative of actual biological dimensions. GCF, gingival crevicular fluid; PDL, periodontal ligament. Figure created with BioRender.com.

1.1.2 Components of the oral mucosal barrier

The properties of the oral barrier change when affected by disease. Differences between its key components in health versus periodontitis are briefly summarised in Table 1.1.

Table 1.1 Components of the oral mucosal barrier.

	Health	Periodontitis
Neutrophils (Hirschfeld, 2020)	Highly abundant, but efficiently control microbial load and are promptly cleared from the gingival sulcus	Even more abundant, but present hyperactive and hyperreactive phenotype that contributes to non-resolving inflammation and collateral tissue damage
Epithelial cells (Bosshardt and Lang, 2005)	Form a tight seal around the tooth preventing bacterial invasion but allow for GCF flow and controlled passage of immune cells	Become inflamed, destroyed and more permeable to bacteria and their products, contributing to pocket formation
Soluble mediators (Kononen et al., 2019)	Low levels of cytokines (e.g. IL-8) are constitutively expressed to sustain immune surveillance	High levels of pro-inflammatory mediators (e.g. IL-1β, IL-6, IL-8 and TNF-α) and matrix-degrading enzymes are released
Bacteria (Camelo-Castillo et al., 2015)	Facultative anaerobes using carbohydrate metabolism	Obligate anaerobes thriving in peptide-rich, inflammophilic environment

GCF, gingival crevicular fluid; IL, interleukin; TNF-α, tumour necrosis factor-α.

1.1.3 Host responses in the periodontium

The oral mucosal barrier is maintained in a state of dynamic equilibrium between the host immune response and the microbiome. Understanding of the mechanisms that maintain this delicate balance, and of how its disruption may contribute to disease in susceptible individuals, continues to evolve but remains incomplete. The classic model described by Page and Schroeder (1976) provided the original histopathological framework for the transition from periodontal health to disease. This framework has evolved as concepts of polymicrobial dysbiosis, microbial immune subversion and dysregulated host responses emerged (Hajishengallis and Korostoff, 2017). More recently, single-cell and spatial multiomic studies have further refined current understanding of the local organisation of host responses at the gingival barrier by revealing its cellular composition, transcriptional programmes and distinct immune zonation

(Theofilou et al., 2026, Williams et al., 2021). Host response in health, gingivitis and periodontitis is illustrated in Figure 1.2. Gingivitis predicts progression to periodontitis, but progression is not inevitable. For more clinical detail, see Section 1.2.1.

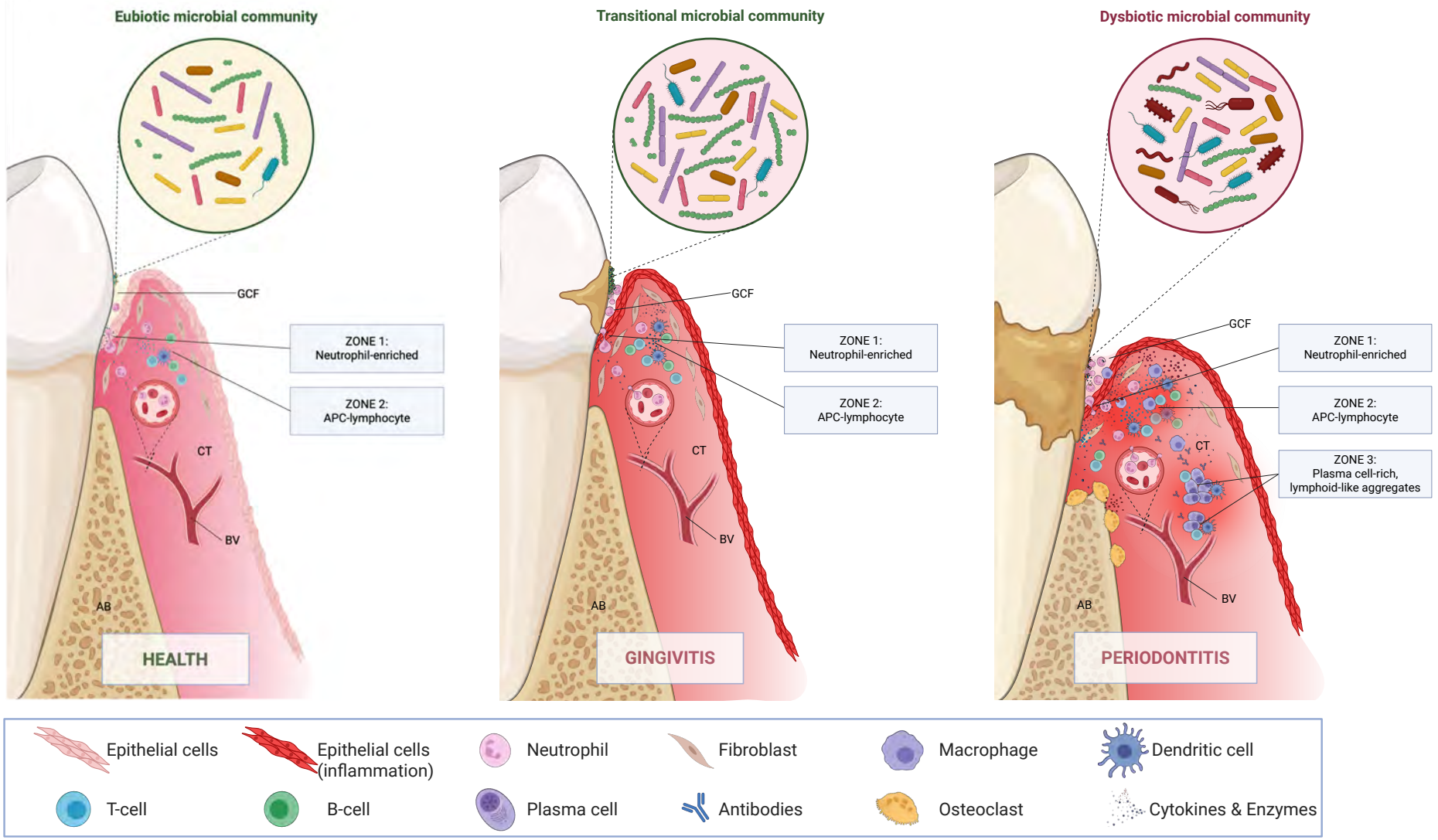
Eubiotic microbial community
GCF
ZONE 1:
Neutrophil-enriched
ZONE 2:
APC-lymphocyte
CT
BV
AB
HEALTH
Transitional microbial community
GCF
ZONE 1:
Neutrophil-enriched
ZONE 2:
APC-lymphocyte
CT
BV
AB
GINGIVITIS
Dysbiotic microbial community
GCF
ZONE 1:
Neutrophil-enriched
ZONE 2:
APC-lymphocyte
ZONE 3:
Plasma cell-rich,
lymphoid-like aggregates
CT
BV
AB
PERIODONTITIS
Epithelial cells
Epithelial cells
(inflammation)
Neutrophil
Fibroblast
Macrophage
Dendritic cell
T-cell
B-cell
Plasma cell
Antibodies
Osteoclast
Cytokines & Enzymes

Figure 1.2 Host response in health, gingivitis and periodontitis. (Left) In health, an eubiotic subgingival biofilm is controlled by homeostatic immunity at the sulcular and junctional epithelium. The local immune response is shown as two spatially organised zones: a neutrophil-enriched zone adjacent to the epithelium (designated as Zone 1) and an underlying APC-lymphocyte zone (designated as Zone 2). (Middle) In gingivitis, increased microbial burden is associated with an expanded but controlled inflammatory response. The same general organisation is shown schematically, with increased immune-cell numbers, while periodontal tissue integrity is preserved. (Right) In periodontitis, a dysbiotic biofilm and persistent inflammation are associated with expansion of the inflammatory infiltrate and altered immune organisation. In addition to the neutrophil-enriched and APC–lymphocyte zones, deeper plasma cell-rich, lymphoid-like aggregates/immature tertiary lymphoid structures are present (designated as Zone 3). Collectively, these changes are associated with irreversible destruction of the periodontal tissues. Based on data from Theofilou et al. (2026) and Williams et al. (2021). Proportions have been adjusted for clarity and are not representative of actual biological dimensions. The visual key identifies the principal cell types represented in the schematic; not all cells are individually annotated. AB, alveolar bone; APC, antigen-presenting cell; BV, blood vessel; CT, connective tissue, GCF, gingival crevicular fluid. Figure created with BioRender.com.

1.1.3.1 Homeostatic inflammation in periodontal health

Within the gingival barrier, particular attention is given to the gingival sulcus and adjacent tissues. This interface is in a state of active homeostatic inflammation rather than immunological silence, such that the local microbiota are generally contained without overt gingival tissue infection. At the transcriptomic level, the sulcular and junctional epithelia, which are directly exposed to the subgingival biofilm, support this homeostatic state through constitutive expression of genes associated with complement and its regulation (*CFH*, *CFHR3*), antimicrobial and anti-inflammatory mediators (*S100A8/S100A9*, *SLPI*) and acute-phase responses (*SAA1*, *SAA2*), alongside genes encoding neutrophil chemoattractants (*CXCL1*, *CXCL2*, *CXCL6*, *CXCL8*) and inflammation regulation (*DNASE1L3*) (Theofilou et al., 2026, Williams et al., 2021). In the superficial epithelial layers, this also includes expression of alarmin-associated cytokine transcripts *IL1A* and *IL36G* (Theofilou et al., 2026). The immune surveillance at this interface is spatially organised; closest to the sulcus lies a neutrophil-rich superficial compartment extending within the sulcular and junctional epithelia and directly beneath them, while a more organised lymphocyte–APC compartment is situated deeper (Theofilou et al., 2026). Among these components, neutrophils appear particularly important to periodontal homeostasis.

1.1.3.1.1 Role of neutrophils in periodontal health

The gingival sulcus is a space constantly flushed by an outward flow of GCF, a transudate originating from the gingival vascular plexus localised underneath the epithelial cell layer. GCF contains transmigrating leukocytes, of which neutrophils, also referred to as polymorphonuclear neutrophils (PMNs), constitute between 70 and 98.6% of all cells (Delima and Van Dyke, 2003). Moreover, a study in rhesus monkeys injected with ^{111}Indium radiolabelled neutrophils revealed that the gingival sulcus is the dominant entry route for neutrophils into the oral cavity and that they can reach it in less than 30 minutes following intravenous injection into the saphenous vein (Scully and Challacombe, 1979). In health, neutrophils actively migrate from blood through gingival connective tissue and junctional epithelium in response to an increasing gradient of IL-8 (interleukin-8; also known as C-X-C motif chemokine ligand 8, CXCL-8),

additionally supported by the intercellular adhesion molecule-1 (ICAM-1) (Tonetti et al., 1998). A recent study in mice suggests that junctional epithelium contains a system of channels that facilitate delivery of neutrophils to the bottom of the gingival sulcus (Oh et al., 2022). After reaching the gingival sulcus, neutrophils engage in immune surveillance activities and exert their effector functions to control commensal bacteria. The three key mechanisms are phagocytosis, degranulation and formation of neutrophil extracellular traps (NETs), as illustrated in Figure 1.3. In phagocytosis, neutrophils use cell-surface receptors (e.g. complement receptors, Fcγ receptors), and pattern recognition receptors such as Toll-like receptors (TLRs) or C-type lectin receptors to engulf bacteria and digest them through the oxidative burst or oxygen independent methods such as releasing antimicrobial peptides and enzymes stored within lysosomal storage granules into phagosomes. This mechanism confines the microbicidal activity within the cell and preserves surrounding tissues from collateral damage (Chapple et al., 2023, Kim and Moutsopoulos, 2024). Neutrophils can also release the granules extracellularly in a highly regulated process called graded exocytosis, where different granule types are released in a threshold-based order. The first released granules are secretory vesicles containing surface receptors whose activation can prime neutrophils. The next set of mobilised granules are the tertiary (gelatinase) granules that contain a more limited set of surface receptors in addition to matrix metalloproteinases, which remodel tissue and can cleave cytokines and chemokines, modifying their biological functions (Catz and McLeish, 2020, Faurschou and Borregaard, 2003, Kim and Moutsopoulos, 2024). As an example, matrix metalloproteinase-9 (MMP-9) is known for amplifying IL-8 chemoattractant potency (Van den Steen et al., 2000). Neutrophil priming is required before exposure to a second stimulus (a ‘two-hit’ model) that will result in the release of the subsequent granule types: secondary (specific) granules containing lactoferrin and nicotinamide adenine dinucleotide phosphate (NADPH) oxidase components and the most toxic, primary (azurophilic) granules with myeloperoxidase, elastase and defensins (Catz and McLeish, 2020, Chapple et al., 2023). Importantly, the two latter types of granules are more likely to be mobilised to phagosomes (Catz and McLeish, 2020), which in combination with graded exocytosis allows for restricting the release of the most harmful enzymes to surrounding tissues. The terms ‘primary granules’, ‘secondary granules’ and ‘tertiary granules’ refer to

the sequence of their formation during granulopoiesis rather than the order of granule mobilisation during activation. The third major mechanism used by neutrophils to kill bacteria is the release of NETs: web-like structures consisting of decondensed chromatin, histones and other proteins which, once again, originate from primary and secondary granules (Delgado-Rizo et al., 2017). Following bacterial killing and clearance, inflammation subsides to enable tissue repair and remodelling. Resolution of inflammation is dependent on efferocytosis, a process of clearance of apoptotic neutrophils by macrophages. This process is mediated by activation of peroxisome proliferator-activated receptor-γ (PPAR-γ) signalling that suppresses nuclear factor-κB (NF-κB), a master regulator of pro-inflammatory gene expression, and results in macrophage reprogramming to a pro-resolving state (Bouchery and Harris, 2019, Cooper et al., 2025).

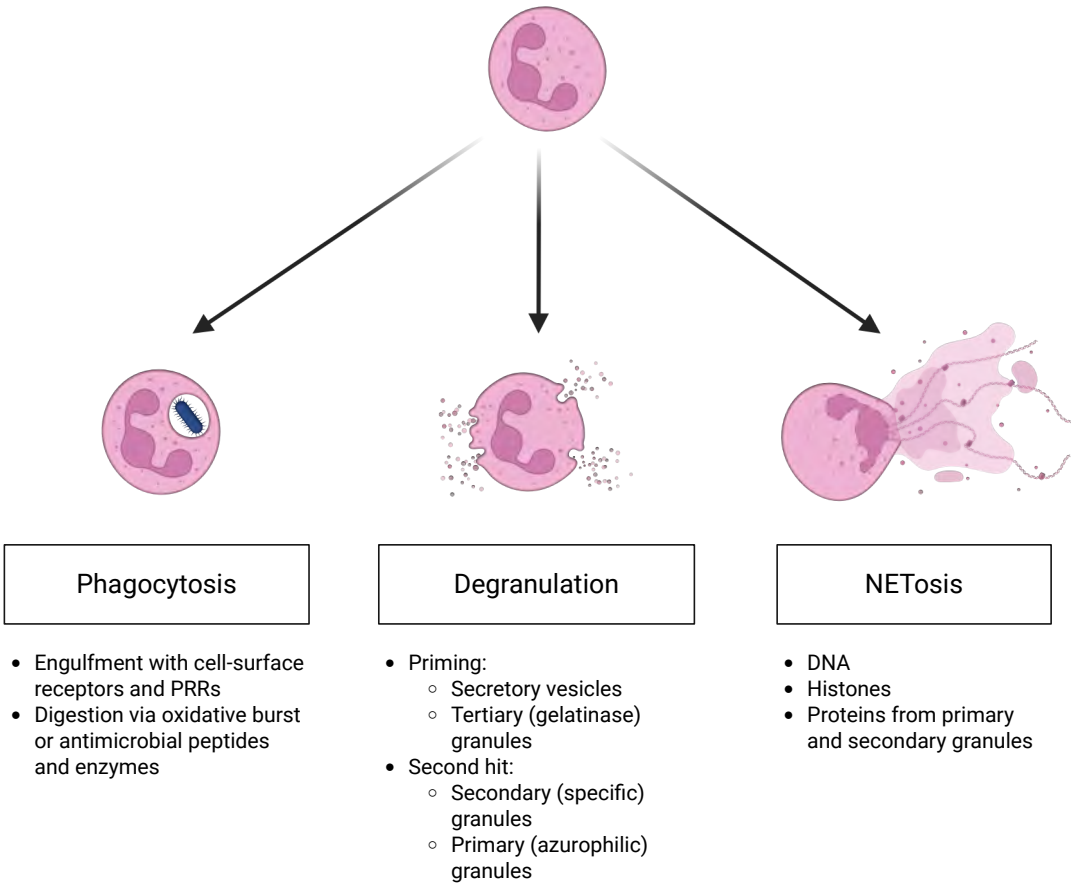

Figure 1.3 Key effector functions of neutrophils. Phagocytosis, degranulation and NETosis represent the three major neutrophil effector mechanisms involved in antimicrobial defence and inflammation. Figure adapted and modified from Kim and Moutsopoulos (2024). Figure created with BioRender.com.

1.1.3.2 Destructive periodontal inflammation

In susceptible individuals, disruption of the homeostatic balance may lead to persistent and dysregulated inflammation. Inflammatory amplification in periodontitis involves coordinated activity across epithelial, stromal and immune compartments, with increased signalling related to adhesion, chemokine activity, antimicrobial responses and cytokine production (Williams et al., 2021). At the transcriptomic level, the pocket-lining epithelium shows increased expression of genes associated with acute-phase responses (*SAA1*, *SAA2*), complement activation (*C3*), neutrophil recruitment (*CXCL1*, *CXCL2*, *CXCL8*) and neutrophil-supporting signalling (*CSF3*) (Theofilou et al., 2026, Williams et al., 2021). Spatially, the neutrophil-rich superficial zone and the deeper lymphocyte–APC zone appear to be largely maintained, although both inflammatory compartments expand. In addition, a deeper plasma cell-rich zone develops, organising into immature tertiary lymphoid structures with potential to support local antibody production (Theofilou et al., 2026). Altogether, this dysregulated inflammatory environment can contribute to connective tissue destruction and alveolar bone resorption (Hajishengallis and Korostoff, 2017).

1.1.3.2.1 Role of neutrophils in periodontitis

Accumulation of bacterial plaque induces an inflammatory response, which manifests as increased vascular permeability, oedema and an increased GCF flow. The upregulation of IL-8 (CXCL8) and other mediators in junctional epithelium, such as CXCL1, CXCL3 and CXCL6, leads to increased neutrophil recruitment into the gingival sulcus (Easter et al., 2024, Tonetti et al., 1994). Upon arrival in the gingival sulcus, already primed neutrophils display a pro-inflammatory and hyper-reactive phenotype by performing their effector functions mentioned above with markedly increased intensity compared to health (Sansores-España et al., 2022). There is also evidence that neutrophils encountering the plaque biofilm attempt to engulf it but inevitably fail and eventually form a ‘leukocyte wall’. Then, in the process known as ‘frustrated phagocytosis’, they release antimicrobial mediators such as reactive oxygen species (ROS) and proteases, causing collateral damage to the surrounding tissues (Ryder, 2010). At the species-specific level, periodontal pathogens have developed various strategies to not only evade neutrophil antimicrobial killing

but also to exploit it to create a nutrient-rich pro-inflammatory environment. For example, *Porphyromonas gingivalis* subverts TLR2–complement crosstalk to inhibit microbicidal mechanisms but not the inflammation itself, creating a favourable environment for other pathogens (Maekawa et al., 2014). *Aggregatibacter actinomycetemcomitans* triggers neutrophil degranulation to obtain epinephrine from azurophilic granules and uses it as a nutrient (Ozuna et al., 2021). *Filifactor alocis* suppresses the respiratory burst and prevents phagosome maturation by impairing recruitment of specific and azurophilic granules (Edmisson et al., 2018). It can also delay neutrophil apoptosis through the TLR2/6 pathway without diminishing their pro-inflammatory effector functions (Miralda et al., 2022). This is noteworthy because efferocytosis of apoptotic neutrophils by macrophages and dendritic cells was shown to reduce granulopoiesis in the bone marrow via suppression of the IL-23–IL-17–granulocyte colony-stimulating factor (G-CSF) axis, also known as 'neutrostat' (Stark et al., 2005). There is evidence that blockade of this axis with Ustekinumab can resolve inflammatory lesions in leukocyte adhesion deficiency type 1-associated severe periodontitis (Moutsopoulos et al., 2017). Interestingly, a recent study has shown that *P. gingivalis* utilises arginine-specific gingipain B (RgpB), a cysteine protease, to modify azurophilic granules which then translocate to the cell surface and act as ligands for $\alpha_M\beta_2$ integrins on macrophages. This allows for 'live entrapment' of neutrophils, which, in contrast to efferocytosis of apoptotic neutrophils, fails to activate the PPAR-γ-dependent pro-resolution pathways, and thus sustains pro-inflammatory milieu (Cooper et al., 2025). Together, bacterial immune evasion and dysregulated host responses lead to a self-perpetuating cycle of chronic inflammation and exacerbating dysbiosis and result in periodontal tissue damage that manifests clinically as deepening pockets and reduced bone levels (Uriarte and Hajishengallis, 2023). What is more, the consequences of this non-resolving inflammation extend far beyond the oral cavity upon reaching the bone marrow. Periodontitis-associated systemic inflammation can cause long term metabolic and epigenetic changes in haematopoietic stem cells, which bias their differentiation, ultimately leading to the production of 'trained' myeloid cell populations of hyperreactive neutrophils and monocytes/macrophages that can in turn be recruited to inflammatory niches within the body (Hajishengallis and Chavakis, 2021).

1.1.3.2.2 Inflammatory amplification, tissue breakdown and bone resorption

Cytokines and chemokines, including C-C motif chemokine ligand 2 (CCL2; also known as monocyte chemoattractant protein-1, MCP-1), interferon-γ (IFN-γ), IL-1β and IL-6 are elevated in GCF in periodontitis (Stadler et al., 2016). Functionally, presence of these mediators indicates that the sulcus is subject to inflammatory cues capable of recruiting and activating inflammatory cells: CCL2 promotes recruitment of monocytes/macrophages and other leukocytes (Hanazawa et al., 1993), while IL-1β and IL-6 amplify inflammatory responses across periodontal tissue cells and immune cells (Pan et al., 2019). However, their detection in GCF should not be interpreted as definitive evidence that they are produced by a distinct cell population within the sulcus itself. In periodontitis, GCF is more accurately described as an inflammatory exudate derived from adjacent periodontal tissues, which bathes the periodontal pocket. Therefore, these mediators most likely reflect contributions from multiple cellular sources, including the sulcular and junctional epithelia, infiltrating neutrophils, stromal cells and immune-cell networks in the underlying gingival connective tissue (Griffiths, 2003). For example, IFN-γ is a cytokine associated with T cells and natural killer (NK) cells, consistent with T cell- and NK cell-associated immune activity rather than production by the sulcular epithelium itself (Schoenborn and Wilson, 2007).

Immune cells other than neutrophils are present in the sulcus-associated region, but they appear to represent a minor component within this compartment. Their more substantial functional contribution is generally in the underlying connective gingival tissues, where adaptive and APC networks sustain and amplify the inflammatory response (Theofilou et al., 2026). APCs, including dendritic cells and macrophages, promote pro-inflammatory T cell responses. In particular, production of IL-1β, IL-6 and IL-23 supports the differentiation and maintenance of T helper 17 (Th17) responses. Th17 cells are a major source of IL-17, a pleiotropic cytokine that acts on epithelial, endothelial, innate immune and stromal cells to amplify antimicrobial and inflammatory responses, which plays both protective and destructive roles in periodontal tissues (Gaffen and Moutsopoulos, 2020). These effects include induction of epithelial antimicrobial mediators; enhancement of neutrophil recruitment through chemokine induction and suppression of developmental endothelial locus-1; and upregulation of

proinflammatory TNF-α, IL-1β, IL-6, and prostaglandin E_2 (PGE_2) by macrophages and other local cellular sources. Together, these processes contribute to tissue destruction, as described further below (Hajishengallis and Korostoff, 2017, Hajishengallis et al., 2020). The broader inflammatory milieu, generated by innate immune, stromal and T cell-derived signals, also supports B cell activation, survival and differentiation into plasma cells, especially through IL-6, IL-21, B cell-activating factor (BAFF; also known as BLyS), and a proliferation-inducing ligand (APRIL) (Abe et al., 2015, Mahanonda et al., 2016).

As this cytokine network develops, recruited leukocytes and activated resident stromal cells increase the local release of host-derived tissue-destructive mediators, including matrix metalloproteinases such as MMP-3, MMP-8, MMP-9, MMP-13, together with neutrophil serine proteases, particularly neutrophil elastase and cathepsin G, and ROS. Collectively, these mediators contribute to degradation of the collagen-rich extracellular matrix and basement-membrane components, promoting connective tissue breakdown in periodontitis (Chapple et al., 2023, Hajishengallis and Korostoff, 2017, Luchian et al., 2022).

Inflammation in periodontitis extends further into deeper periodontal tissues and disrupts physiological bone remodelling. Under normal conditions, bone resorption is coupled to bone formation and regulated by the receptor activator of nuclear factor-κB (RANK)–RANK ligand (RANKL)–osteoprotegerin (OPG) axis. RANKL binds to RANK on osteoclast precursors, promoting osteoclastogenesis, whereas OPG acts as a decoy receptor limiting this process. Inflammatory signalling in periodontitis increases the local RANKL/OPG ratio, thereby promoting osteoclast differentiation and shifting the balance towards net alveolar bone resorption (Hajishengallis and Korostoff, 2017). RANKL is produced by multiple cell populations. In human periodontitis, activated B and T cells are considered major sources (Kawai et al., 2006), while experimental studies also implicate osteoblast-lineage and periodontal ligament cells as important local contributors (Tsukasaki et al., 2018). Th17/IL17 signalling further amplifies periodontal bone loss through RANKL-dependent mechanisms, although the precise cellular pathway remains to be fully elucidated (Tsukasaki et al., 2018).

1.1.4 Dental plaque formation

The oral cavity contains multiple ecological niches that support microbial colonisation. Among these, the tooth and exposed root surfaces are distinctive because, unlike the epithelial surfaces, they are non-shedding. Therefore, these hard tissue surfaces provide a stable substratum for microbial attachment and retention, thereby enabling dental plaque formation (Bertolini et al., 2022, Mark Welch et al., 2019). Dental plaque is a structured polymicrobial biofilm, composed of multiple interacting microbial taxa embedded within an extracellular matrix, rather than a simple bacterial deposit (Costerton et al., 1981, Kolenbrander et al., 2006, Marsh, 2006). Plaque formation occurs through a coordinated, multistep process (Kolenbrander et al., 2002). Within minutes after tooth cleaning, salivary proteins and glycoproteins adsorb onto the enamel surface to form the acquired pellicle, creating binding sites for early bacterial colonisers. These include oral streptococci, such as *Streptococcus gordonii*, *S. mitis*, *S. oralis* and *S. sanguinis*, which attach through adhesins, while other early colonisers such as *Actinomyces* species use surface structures including pili (Bloch et al., 2024, Persson et al., 2012). Following attachment, early colonisers proliferate, form microcolonies and contribute to the developing extracellular matrix. These attached bacteria create new binding surfaces for secondary colonisers and support the later incorporation of late colonisers, including *A. actinomycetemcomitans*, *Prevotella intermedia*, *Treponema denticola*, *P. gingivalis*, *Eubacterium* spp., and *Selenomonas flueggei* (Kolenbrander et al., 2002).

Interbacterial binding is central to multispecies plaque development. This is commonly described as coaggregation when genetically distinct bacteria bind to each other in suspension, whereas co-adhesion refers more specifically to planktonic cells binding to bacteria already attached to a surface. In the oral biofilm literature, however, coaggregation is frequently used more broadly to describe the specific interbacterial interactions that support multispecies plaque development (Kolenbrander et al., 2006, Rickard et al., 2003). In the classical spatiotemporal model of plaque development, *Fusobacterium nucleatum* is particularly important because it can bind both early and late colonisers, allowing it to act as a bridging organism during biofilm maturation (Kolenbrander et al., 2002).

This model was later refined by fluorescence *in situ* hybridisation (FISH)-based analysis of plaque preserved on natural teeth, showing that plaque is both sequentially assembled and spatially organised. In subgingival plaque, a layered biofilm architecture was described, with *Actinomyces* sp. detected in the basal layer and *F. nucleatum* and *Tannerella forsythia* localised in the intermediate layer. The presence of *F. nucleatum* there was consistent with its proposed role in plaque maturation. Presumptive periodontal pathogens, including *P. gingivalis*, *P. intermedia*, *Porphyromonas endodontalis* and *Parvimonas micra*, were mainly observed as microcolonies in the top layer of the organised biofilm, or the fourth, more disorganised outside layer. This outside layer was dominated by *Spirochaetes* and also contained test-tube brush-like structures, with *F. nucleatum* and other filamentous bacteria arranged around central *Lactobacillus* sp. cells. In supragingival plaque, the architecture was more heterogeneous. Two layers were generally observed, with variable basal communities containing *Actinomyces* sp., chains of non-streptococcal cocci, *Streptococcus* sp., yeasts or *Lactobacillus* sp., and an overlying layer containing scattered or surface-associated *Streptococcus* sp. Corncob structures involving *Streptococcus* sp. and *Candida albicans* were also described (Zijnge et al., 2010). A later combinatorial labelling and spectral imaging FISH study of supragingival plaque revealed highly organised 'hedgehog' structures, in which filamentous *Corynebacterium* formed a scaffold-like framework around which eight other taxa were spatially organised: *Streptococcus*, *Porphyromonas, Haemophilus/Aggregatibacter, Neisseriaceae, Fusobacterium*, *Leptotrichia*, *Capnocytophaga*, and *Actinomyces* (Mark Welch et al., 2016).

Collectively, these studies show that dental plaque is not simply a multispecies accumulation, but a spatially organised polymicrobial biofilm. Beyond this structural organisation, plaque microorganisms also interact through metabolic cooperation, including cross-feeding; competition for nutrients and attachment sites; chemical signalling, such as quorum sensing; and modification of local microenvironments. Such interactions can influence nutrient availability, oxygen tension, tolerance of environmental stressors and host–microbe interactions. Therefore, dental plaque should be understood as an integrated microbial community in which structure and function arise from interactions among its

constituent taxa, rather than from properties of individual taxa alone (Hajishengallis et al., 2023, Lamont et al., 2023).

1.2 Periodontitis

Periodontitis is a chronic disease caused by an excessive and unresolving inflammatory response associated with the oral bacterial biofilm, which leads to irreversible destruction of tissues that surround and support teeth, and eventually, tooth loss (Preshaw, 2018).

1.2.1 Clinical features

Clinically, the condition of periodontal tissues can be assessed using a range of signs and measurements that differentiate between health, gingivitis and periodontitis (Figure 1.4). In health, periodontal tissues are intact and show minimal clinical signs of inflammation. Gingivitis is characterised by inflammation limited to the gingiva and is commonly identified clinically by bleeding on probing (BOP). It may also present with visible changes in gingival colour, contour and consistency, such as erythema, swelling, softer and spongy texture and loss of stippling. An important distinction is that these clinical changes remain confined to the gingiva and are reversible, with no destruction of the tooth-supporting structures (Chapple et al., 2018, Trombelli et al., 2018). In some individuals, inflammation may lead to irreversible destruction of the deeper tooth-supporting tissues, including the periodontal ligament, cementum and alveolar bone. Clinically, this is identified as periodontitis and is characterised by clinical attachment loss (CAL) and alveolar bone resorption, often accompanied by increased probing depth (PD; also termed ‘probing pocket depth’ (PPD) when referring specifically to pathological periodontal pockets). In advanced disease, continued loss of tissue support may lead to tooth mobility and ultimately, tooth loss (Papapanou et al., 2018).

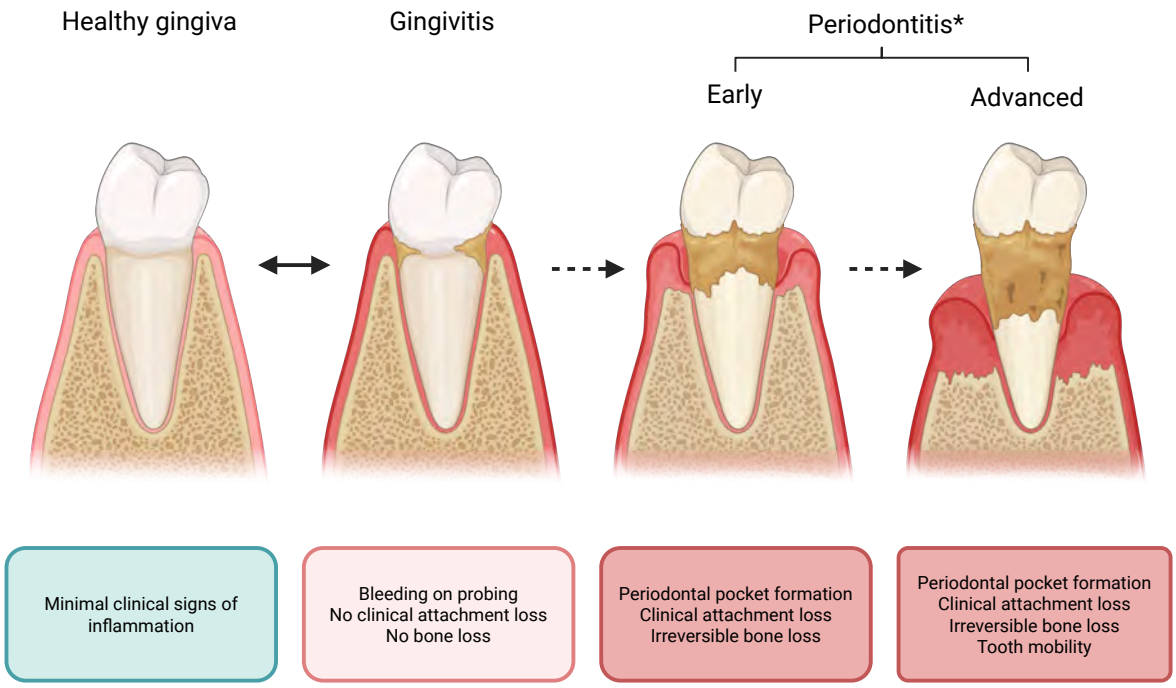

Figure 1.4 Schematic overview of the clinical states of periodontal health, gingivitis, early periodontitis and advanced periodontitis. The transition from periodontal health to gingivitis is reversible, and not all gingivitis lesions progress to periodontitis. Once periodontitis develops, the associated tissue destruction is irreversible. *Early and advanced periodontitis differ in severity and extent of tissue destruction, rather than in the underlying immune mechanisms. Based on data from Chapple et al. (2018) and Papapanou et al. (2018). Figure created with BioRender.com.

1.2.2 Clinical parameters in periodontal assessment

It is currently impossible to identify which gingivitis lesion will progress to periodontitis or how quickly it will happen. It is generally accepted that periodontitis is not a simple infection but dysbiosis that requires a susceptible host. Several risk factors and risk assessment tools have been identified and described (Tonetti et al., 2018). Most of them utilise clinical parameters. In everyday practice, a simplified sextant-based screening system (Basic Periodontal Examination) is used to identify patients requiring further investigations and treatment (Palmer and Floyd, 2023). More detailed clinical parameters include BOP measured around a single tooth or calculated as a percentage of sites with BOP, CAL, PD and number of periodontal pockets with PPD ≥ 5 mm, radiographic horizontal and vertical bone loss, and number of lost teeth (Chapple et al., 2018, Lang and Tonetti, 2003, Papapanou et al., 2018). These clinical measurements can be utilised to quantify inflammatory burden with Periodontal Inflamed Surface Area/Periodontal Epithelial Surface Area

(PISA/PESA) composite indices (Nesse et al., 2008) or to assess periodontal risk (Saleh et al., 2021, Saleh et al., 2022).

1.2.3 Establishment of periodontics and clinical classification systems

The contemporary term 'periodontitis' specifically referring to 'inflammation of the tissues surrounding a tooth' appeared only in the 19th century, with its first known use reported in 1870 (Babcock, 1870, Merriam-Webster, 2025, Waite, 1870). Since then, it started gaining awareness among the general public, as reflected by references in the literature, such as Mark Twain's short story *Happy Memories of the Dental Chair* where he described his own periodontal therapy performed by Dr John Mankey Riggs, often referred to as the 'Father of periodontics' (Maloney, 2010, Twain, 2010). Emergence of periodontology as a distinct dental field was accompanied by the development of various theories and hypotheses on periodontitis aetiology (described in detail in Section 1.2.4) and attempts to characterise and classify periodontal diseases (Armitage, 2002, Highfield, 2009). Currently, only two of them remain in use: the 1999 Classification of Periodontal Diseases and Conditions (established by the American Academy of Periodontology (AAP)) (Armitage, 1999), which is gradually being replaced by its revised version, the 2017 Classification of Periodontal and Peri-Implant Diseases and Conditions (the result of a collaboration between the AAP and the European Federation of Periodontology (EFP)) (Caton et al., 2018).

The 1999 classification introduced the gingival diseases category to distinguish pathologies restricted to gingiva without affecting the underlying tissues (Mariotti, 1999). Periodontitis was grouped into chronic and aggressive forms based on the progression rate, which could be further divided according to the extent of the affected area to localised and generalised (Armitage, 1999).

The 2017 classification distinguished a new periodontal health and gingival health subcategory under the broader periodontal health, gingival diseases and conditions category. The presence of a baseline inflammatory infiltrate and homeostatic host response at a site level was acknowledged, albeit without bleeding on probing, erythema, edema and patient symptoms (Chapple et al.,

2018). The previous chronic and aggressive forms of periodontitis were combined into a single periodontitis category in which a new system of staging (I-IV) and grading (A-C) was introduced (Papapanou et al., 2018, Tonetti et al., 2018). Staging is based on the severity of disease (predominantly periodontal tissue breakdown) and its management complexity (probing depth, bone loss, furcations, tooth mobility, masticatory dysfunction). Furthermore, its extent can be described as localised or generalised. Grading refers to the progression rate based on evidence and anticipated treatment response predicted by risk factor analysis. The new framework also anticipates the future role of biomarkers in individuals that are more susceptible to periodontitis and less responsive to a standard treatment.

Despite initial reluctance of dental professionals due to perceived complexity and time-consuming nature of the system, the 2017 classification is gradually replacing its 1999 predecessor (Jayawardena et al., 2021, Malmqvist et al., 2025, West et al., 2025). It is worth noting the successful attempts to retroactively reclassify patients diagnoses by using available clinical records (Raza et al., 2024, Priyanka et al., 2024, Tokede et al., 2024). Nonetheless, the overlap period in use of both classifications remains relevant in periodontal research as different classifications appear in longitudinal and retrospective studies.

1.2.4 Aetiology

Efforts to explain periodontitis aetiology date back to the late 19th century. Understanding of its causal mechanisms was limited by research tools available at the time. Periodontitis was initially considered to be a disease of bacterial origin driven by increased biofilm biomass (Miller, 1890). Interestingly, this explanation was not universally accepted and there were opinions that emphasised the importance of the ‘lack of resistance’ of the host and claimed that the etiologic factor was of ‘metabolic origin’, assigning bacterial infection a secondary role (Meyer, 1917). This view did not achieve widespread recognition and disappeared from the discourse for several decades.

The 1970s were a transformative period for periodontitis research thanks to the development of technological advancements such as culture-based techniques,

microscopy and the introduction of the anaerobic chamber which enabled isolation and identification of bacterial species implicated in periodontitis, including strict anaerobic ones (Rosier et al., 2014). This led to formulation of the specific plaque hypothesis, which focused on the role of overgrowth of specific pathogenic species (Loesche, 1976). Soon after, interest in the role of the host response slowly began to re-emerge in the form of the updated non-specific plaque hypothesis that recognised the role of both dental plaque (containing different combinations of microorganisms instead of a single species) and the non-specific inflammation it induced that resulted in a change of environment in the gingival crevice (Theilade, 1986). A closely related ecological plaque hypothesis was proposed where the changes in the environment induced selection of bacterial species that led to progressive dysbiosis (Marsh, 1994). Later the hypothesis was revised to underscore the abrupt and substantial character of the disruption in ecology resulting in a large-scale dysbiosis.

The 1990s brough another major shift in technological innovation. Development of targeted high-throughput molecular techniques such as checkerboard DNA-DNA hybridisation allowed for analysis of a much higher volume of plaque samples and quicker identification of microbial species (Feres et al., 2021). This advancement has facilitated identification and definition of Socransky's microbial complexes. In this model of periodontitis aetiology and progression, colour-coded clusters of microbial species colonise the subgingival plaque in a specific order starting with the health associated species (yellow complex) and ending with periodontitis associated species (red complex) (Socransky et al., 1998). The role of the host was again acknowledged in the polymicrobial disruption of host homeostasis hypothesis. It assumed that the host was not just a passive system that acted only in response to microbial triggers but was actively maintaining immune balance. Polymicrobial biofilm disrupted the balance causing periodontal tissue damage (Darveau, 2010). The subsequent keystone pathogen hypothesis bore similarity in that the host actively controlled the biofilm, but the central point was the subversion of the host innate immune response by a low-abundance keystone pathogen. This led to the weakening of the host's ability to clear the pathogens and, as a result, to the development of chronic inflammation and dysbiosis (Hajishengallis et al., 2011). The concept of the keystone pathogen was upheld in the following polymicrobial synergy and

dysbiosis (PSD) model, although it was incorporated into a broader framework of a synergistic microbial community where different species (or even gene combinations) contribute distinct functions in a dysbiotic biofilm. This pathogenic consortium triggers a self-perpetuating inflammatory response in the host (Hajishengallis and Lamont, 2012).

Finally, the most recent hypothesis, the Inflammation-Mediated Polymicrobial-Emergence and Dysbiotic-Exacerbation (IMPEDE) model, was developed to reflect the 2017 Classification of Periodontal and Peri-Implant Diseases and Conditions. It positions the host as a central driver of dysbiosis and subsequent disease process and proposes that resolving inflammation should be the primary objective of therapeutic interventions (Van Dyke et al., 2020).

The most important concepts on periodontitis aetiology are summarised in Table 1.2.

Table 1.2 Conceptual frameworks on periodontitis aetiology.

Reference	Concept	Fundamental principles
(Miller, 1890)	Non-specific plaque hypothesis	Periodontitis is not caused by any specific bacterial species, but collectively by bacteria present in the dental plaque.
(Loesche, 1976)	Specific plaque hypothesis	Most cases of periodontitis are due to the overgrowth of specific pathogenic species.
(Theilade, 1986)	Updated non-specific plaque hypothesis	Non-specific inflammation caused by dental plaque accumulation changes the environment of the gingival crevice and thus composition of the subgingival microflora. Different combinations of microorganisms have a potential to induce destructive periodontitis rather than a single species.
(Marsh, 1994) (Marsh, 2003)	Ecological plaque hypothesis (later ecological catastrophe hypothesis)	Inflammatory response to plaque in gingivitis gradually changes the environment and induces selection of bacterial species contributing to progressive dysbiosis. Later modification highlighted that the changes in ecology are rapid and significant and that this disruption leads to a large-scale dysbiosis.
(Socransky et al., 1998)	Model of microbial complexes in subgingival plaque	Bacteria present in subgingival plaque were grouped into color-coded complexes. Red complex bacteria (*P. gingivalis*, *T. forsythia* and *T. denticola*) were related to clinical parameters associated with periodontitis.
(Darveau, 2010)	Polymicrobial disruption of host homeostasis hypothesis	Several bacterial species are responsible for disruption of mechanisms responsible for host tissue homeostasis, which leads to periodontal tissue damage.
(Hajishengallis et al., 2011)	Keystone pathogen hypothesis	Keystone pathogens play a crucial role by subverting the immune response, disrupting microbial homeostasis and promoting an inflammatory environment
(Hajishengallis and Lamont, 2012)	Polymicrobial synergy and dysbiosis (PSD) model	Broadly-based synergistic and dysbiotic microbiota initiate and exaggerate inflammation. The role of keystone pathogens (e.g. *P. gingivalis*) still recognised, but only as one of the contributing factors.
(Van Dyke et al., 2020)	IMPEDE* model	Complements the 2017 classification of periodontal diseases; inflammation is the primary factor of periodontitis that, if unresolved, changes the subgingival environment leading to dysbiosis and tissue destruction.

*Inflammation-Mediated Polymicrobial-Emergence and Dysbiotic-Exacerbation (IMPEDE)

1.2.5 Risk factors

Dental plaque is required, but insufficient to initiate periodontitis. A landmark study involving Sri Lankan tea plantation workers revealed that they did not follow any conventional oral hygiene routine and all presented with gingival inflammation. Despite having similar plaque indices, only 8% developed rapidly progressing periodontitis, whereas 81% showed signs of moderate progression, and 11% exhibited no signs of worsening of periodontal status (Loe et al., 1986). Progression to periodontitis results from the complex interplay of multiple factors influencing disease pathology and substantial efforts have been made to identify specific risk factors and to create tools that assess individual risk (Chapple et al., 2017, Kornman, 2018). Current evidence identifies genetic predisposition, age, diabetes mellitus and smoking as the major risk factors for periodontitis (Kinane et al., 2017).

1.2.5.1 Genetics

Genetic factors contribute to differences in periodontitis predisposition, its clinical manifestation and progression by affecting pathways regulating host immunity, tissue repair and regeneration. Notably, twin studies attributed 34% of phenotypic variability of periodontitis within the population to genetics (Nibali et al., 2019). Genetic predisposition is particularly important in pre-pubertal and pubertal (early onset) forms of periodontitis, which usually manifest with severe symptoms. Mutations in *CTSC* and *PLG* genes were identified in syndromic presentations of periodontitis. The former leads to uncontrolled inflammation caused by impaired neutrophil function; the latter to inefficient tissue clearance and repair resulting from defective fibrinolysis. Non-synonymous single nucleotide polymorphisms in *SIGLEC5*, *ROBO2*, *ABCA1* and *PF4* genes were implicated by genome-wide association studies as contributing to polygenic risk through altered immune modulation or tissue maintenance mechanisms (Schaefer et al., 2025). Furthermore, candidate gene association studies identified six inflammatory mediator genes whose polymorphisms were linked to significantly elevated periodontitis risk: *IL1A*, *IL1B*, *IL6*, *IL10*, *MMP3* and *MMP9* (da Silva et al., 2017). Interestingly, it has been suggested that genes associated with risky and detrimental health behaviours, including smoking,

could also be involved in periodontitis aetiology (Karlsson Linnér et al., 2019, Schaefer et al., 2025).

1.2.5.2 Age

Advancing age is associated with a higher risk of periodontitis. For a long time, this was attributed to an age-related decline in the capacity of the immune system (immunosenescence) and tissue regeneration and repair, as well as the cumulative effect of exposure to known risk factors such as plaque deposits, smoking or comorbidities (Ebersole et al., 2016, Schaefer et al., 2025). Recently, attention has been drawn to the concept of 'inflammaging' coined in 2000, which describes the presence of low-grade inflammation due to a lifelong exposure to antigenic stimulation, chronic infections, metabolic and environmental stress (Ebersole et al., 2016, Franceschi et al., 2000). This state is characterised by an increase in levels of proinflammatory mediators such as IL-1, IL-6, TNF-α, and C-reactive protein (CRP) in the elderly (Michaud et al., 2013). Furthermore, age-associated acquisition of somatic mutations can also contribute to the risk of developing inflammation-related disorders. It has been reported that mutation of an epigenetic regulator gene *DNMT3A* in hematopoietic stem and progenitor cells in the bone marrow leads to an increased risk of gingival inflammation and periodontitis (Wang et al., 2024).

1.2.5.3 Diabetes mellitus

Diabetes mellitus is the only systemic disease that has been included among the periodontitis grade modifiers of the 2017 classification. Studies report that the risk of developing periodontitis is 2-3 times higher in diabetics than in healthy individuals (Casanova et al., 2014). The rate of progression is influenced by glycaemic status, and glycated haemoglobin (HbA1c) levels are used as grade modifiers in patients with diabetes (Tonetti et al., 2018). Finally, periodontal parameters improve following diabetes control interventions (Ramseier et al., 2020) and therefore are recommended by the EFP (Sanz et al., 2020). It has been proposed that in diabetes mellitus, hyperglycaemia accompanied by adiposity and dyslipidaemia initiate various pathological mechanisms that lead to immune dysfunction, cellular stress and an increase in proinflammatory cytokines such as IL-1, IL-6 and TNF-α. This, together with an ecological shift in

subgingival biofilm, leads to increased destruction of tissue and impairment of the repair processes (Taylor et al., 2013).

1.2.5.4 Smoking

Tobacco smoking is a well-studied risk factor for developing periodontitis; it is estimated that it raises the risk by 85% in active smokers (Leite et al., 2018) and by 28% in passive smokers (Sutton et al., 2017). This has been recognised by the 2017 classification of periodontal diseases where smoking status, defined by the number of cigarettes smoked per day, was recognised as a periodontitis grade modifier (Tonetti et al., 2018). Smoking is thought to exacerbate periodontal disease progression by reducing gingival blood supply (Popescu et al., 2025), accelerating subgingival dysbiosis (Al Kawas et al., 2021, Tamashiro et al., 2023), altering immune response (Bunaes et al., 2017, Popescu et al., 2025), and disrupting gingival connective tissue and bone homeostasis (Popescu et al., 2025). The impact of using electronic cigarettes on periodontal health is not fully understood, but evidence suggests it is also harmful (Tattar et al., 2025). It has been observed that smoking negatively impacts clinical (Kanmaz et al., 2021, Kotsakis et al., 2015) and host responses to periodontal treatment (Hao et al., 2023). Smoking cessation improves clinical parameters in periodontitis patients (Ramseier et al., 2020) and tobacco smoking cessation interventions during periodontitis therapy are recommended by the EFP (Herrera et al., 2022).

1.2.6 Links to systemic health

Periodontitis is associated with multiple chronic systemic conditions including type 2 diabetes mellitus, cardiovascular disease (CVD), rheumatoid arthritis (RA), Alzheimer's disease, non-alcoholic fatty liver disease, inflammatory bowel disease and colorectal cancer (Hajishengallis and Chavakis, 2021).

The associations are hypothesised to be driven by translocation of bacteria and systemic inflammation. Periodontal bacteria have been detected in blood myeloid-derived dendritic cells, atherosclerotic plaque (Carrion et al., 2012), brains of Alzheimer's disease patients (Dominy et al., 2019), the respiratory tract of patients with infectious and non-infectious diseases (Mammen et al.,

2020) and faecal and tumorous samples of colorectal cancer patients (Kerdreux et al., 2023, Lowenmark et al., 2020, Shang and Liu, 2018), suggesting they can spread via haematogenous, oropharyngeal and orodigestive routes. There is evidence that disseminated periopathogens can lead to systemic inflammation, endothelial dysfunction and vascular damage, contribute to increased levels of neurotoxic protein aggregates, cause infections directly or promote growth of cancer cells and their chemotherapy resistance (Hajishengallis and Chavakis, 2021).

Systemic inflammation is observed in patients with periodontitis and is hypothesised to be a direct result of dissemination of proinflammatory mediators from periodontal tissues to the bloodstream. Spillover of IL-1, IL-6 and TNF-α in turn leads to elevated levels of CRP, fibrinogen, and other acute-phase proteins produced by the liver (Genco and Van Dyke, 2010). Increased inflammatory burden possibly leads to deterioration of lipid metabolism that manifests through an increase in serum levels of low-density lipoprotein (LDL) and triglycerides accompanied by a reduction in high-density lipoprotein (HDL), which is a strong risk factor for CVD (Fu et al., 2016, Nepomuceno et al., 2017). Moreover, it has been proposed that an increase in serum inflammatory mediators exacerbates insulin resistance (Gurav, 2012), having negative implications for glycaemic control in diabetes (Casanova et al., 2014).

Additionally, systemic inflammation can prime haematopoietic stem and progenitor cells in the bone marrow towards differentiation into hyperreactive neutrophils and monocytes or macrophages, a process known as trained myelopoiesis. These cells can be trafficked not only to the periodontium but also other sites of the body, contributing to pathologies beyond the initial site, for example CVD or RA. Further highlighting the complexity and bi-directionality of the relationship between periodontitis and systemic health, orally primed cells such as Th17 cells and the mixed phenotype Th17/Th1 cells are believed to exacerbate colitis (Hajishengallis and Chavakis, 2021).

It should be emphasised that the EFP recognises the significance of risk of systemic impact of periodontitis in its 2017 grading system that provisionally stratifies inflammatory burden according to the high sensitivity CRP level, which is used primarily as a prognostic marker of low-grade inflammation in CVD

(Araújo et al., 2009, Mehta et al., 2025, Tonetti et al., 2018). Furthermore, it recommended in collaboration with the European Organisation for Caries Research that medical preventive programmes, especially those targeting diabetes, obesity, metabolic syndrome and CVD, should include an oral health component (Chapple et al., 2017).

In addition to systemic diseases resulting from bacterial dissemination and increased inflammatory burden, periodontitis impacts patients' quality of life. It may affect basic daily activities such as mastication and speech, as well as psychosocial wellbeing due to perceived stigma, impaired aesthetics and oral malodour. Anxiety and fear of losing teeth prematurely are very common among periodontitis patients (Yin et al., 2022)

1.2.7 Treatment

1.2.7.1 Conventional therapy

Removal of plaque deposits has always been central to periodontitis therapy, regardless which hypothesis or classification was favoured at the time (Mills, 1885, Theilade, 1986, American Academy of Periodontology, 2011). Introduction of the 2017 classification was followed by publication of the evidence-based S3 Level Clinical Practice Guideline for a stepwise approach for the treatment of Stage I–III periodontitis by the EFP (summarised in Figure 1.5) (Sanz et al., 2020). It does not cover the treatment of stage IV due to its complexity and multidisciplinary care required (Herrera et al., 2022). The first step of periodontal therapy focuses on a supragingival dental biofilm control through a range of tools, including professional mechanical plaque removal coupled with adjunctive therapies for gingival inflammation, and behavioural change interventions to improve oral hygiene and eliminate or mitigate risk factors such as smoking or diabetes. The second step of treatment is aimed at management of periodontal pockets and teeth with loss of periodontal support through removal of subgingival biofilm and calculus. The two initial steps of the EFP S3-level guideline are collectively referred to using the umbrella term 'non-surgical periodontal therapy' (NSPT), previously described as 'non-surgical therapy' (NST) in earlier publications. This can be accompanied by adjunctive therapies such as physical or chemical agents, local or systemic host-modulating

agents, subgingivally delivered antimicrobials or systemic antimicrobials. However, it is important to acknowledge that some of these therapeutic approaches have limitations; adjunctive antimicrobials and antibiotics pose a risk of driving the development of resistance, while host-modulating therapies are not supported by sufficient clinical evidence. If some of the areas of dentition are not responding to therapy, different surgical interventions may be considered in the third step of therapy to increase access to subgingival areas, regenerate or resect the lesions. The first three steps collectively constitute active periodontal therapy (APT). The fourth and final step includes supportive periodontal care (SPC), also referred to as 'supportive periodontal therapy' (SPT), to monitor and maintain the stability of achieved treatment outcomes (Sanz et al., 2020).

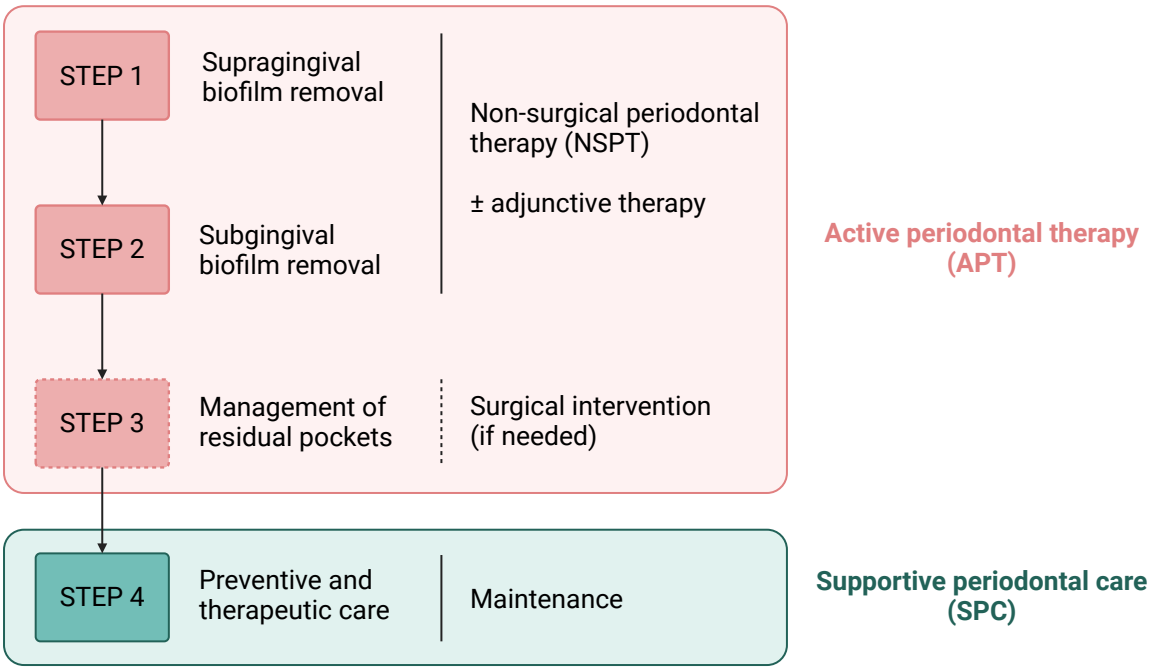

Figure 1.5 Schematic representation of the stepwise approach for the treatment of Stage I–III periodontitis recommended by the EFP. Active periodontal therapy comprises two steps of non-surgical periodontal therapy, which may be accompanied by adjunctive measures, followed, where needed, by surgical intervention for residual pockets. The final step is supportive periodontal care aimed at maintaining periodontal stability. Based on data from Sanz et al. (2020). Figure created with BioRender.com.

1.2.7.2 Emerging therapies

In addition to conventional treatment widely adopted in routine practice and recommended by professional bodies such as the EFP or AAP, several emerging therapies are currently under investigation (Figure 1.6). These novel approaches include host modulation (including the use of pro-resolving mediators, complement inhibitors and probiotics), lasers and antimicrobial photodynamic therapy (aPDT), also known as photoactivated disinfection. There is also growing interest in the use of natural compounds.

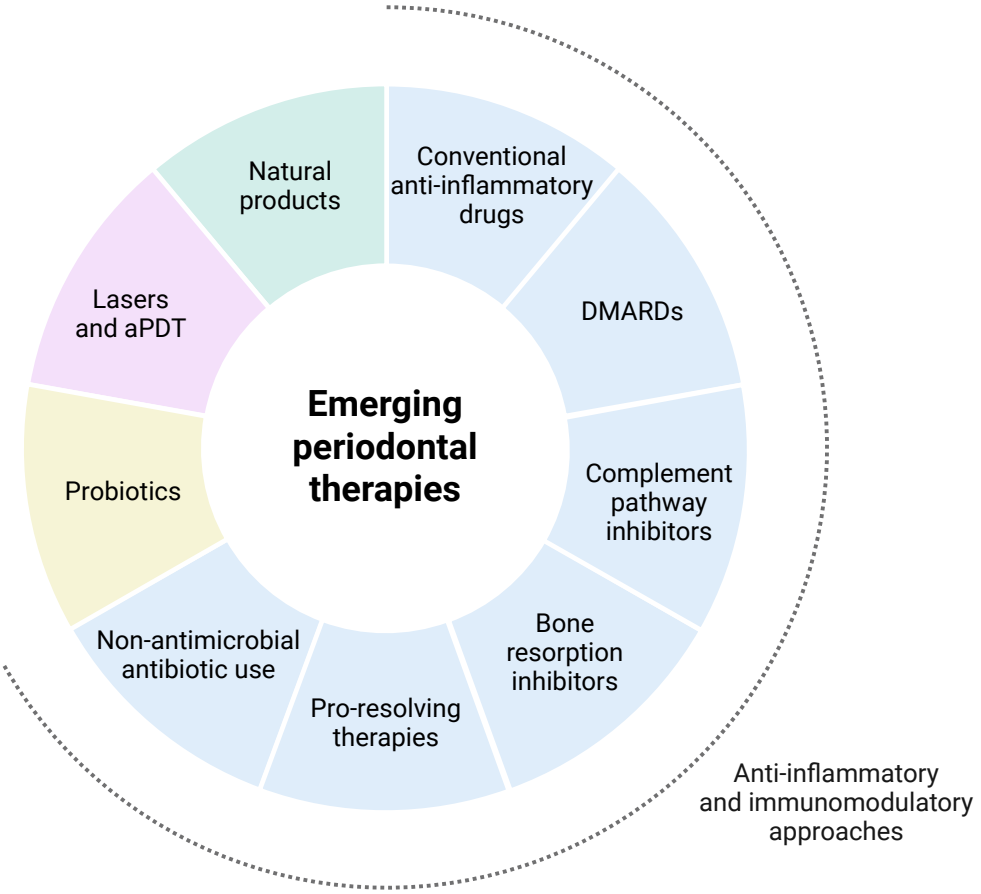

Figure 1.6 Schematic overview of the main categories of emerging periodontal therapies. These include anti-inflammatory and immunomodulatory approaches, such as conventional anti-inflammatory drugs, disease-modifying anti-rheumatic drugs, complement pathway inhibitors, bone resorption inhibitors, pro-resolving therapies, antibiotics used for non-antimicrobial purposes; probiotics; laser therapy and photoactivated disinfection; and natural products. aPDT, antimicrobial photodynamic therapy; DMARDs, disease-modifying anti-rheumatic drugs. Figure created with BioRender.com.

1.2.7.2.1 Anti-inflammatory and immunomodulatory approaches

Recognising periodontitis as a chronic inflammatory disorder rather than a simple infectious disease resulted in a new approach to developing therapeutic strategies. Attention shifted towards investigating various classes of medications with anti-inflammatory or immunomodulatory properties.

Conventional anti-inflammatory drugs such as corticosteroids and non-steroid anti-inflammatory drugs were initially extensively studied, but significant systemic risks associated with their long-term use such as cardiovascular and gastrointestinal events, metabolic dysregulation, immunosuppression and reduced bone density outweighed benefits they offered in periodontitis patients. Disease-modifying anti-rheumatic drugs (DMARDs) were another group of potent systemic anti-inflammatory therapeutics that were considered due to targeting inflammatory pathways shared between RA and periodontitis. While some of the biological DMARDs such as tocilizumab (IL-6 receptor inhibitor) or rituximab (CD20-targeting monoclonal antibody depleting B cells) improved periodontal parameters in RA patients, others such as various TNF-α inhibitors brought inconsistent results across studies. Furthermore, the immunosuppressive nature of these drugs raised concerns about an increased risk of development of malignancies such as lymphoma and reactivation of latent infections such as tuberculosis (Balta et al., 2021, Preshaw, 2018). There is growing interest in targeting C3 and C5a pathways of the complement system; locally delivered C3 inhibitor AMY-101 has been investigated and yielded positive outcomes in patients with gingivitis (Hasturk et al., 2021a).

Another therapeutic direction explored in recent years involved targeting the osteoimmunological mechanisms. One approach was inhibition of osteoclast-mediated bone resorption directly through bisphosphonates or indirectly through targeting their key activator RANKL with denosumab (Preshaw, 2018), while the second approach was stimulation of osteoblast development and activity with metformin or statins, thus supporting bone formation. Systemic use of these drugs was either discouraged due to safety concerns (e.g. risk of osteonecrosis of the jaw elevated by bisphosphonates and denosumab) or did not demonstrate benefits in clinical studies (e.g. bisphosphonates and statins), but local delivery has shown beneficial effects (Balta et al., 2021, Donos et al., 2020).

Statins have been reported to actively resolve inflammation by promoting the biosynthesis of specialised pro-resolving mediators, namely resolvins, protectins and maresins, which are derived from omega-3 polyunsaturated fatty acids (PUFAs), such as eicosapentaenoic acid and docosahexaenoic acid (Preshaw, 2018). Supplementation with omega-3 PUFA brought promising results in a few small periodontitis trials (Balta et al., 2021, Donos et al., 2020). Resolvins demonstrated potential therapeutic value in animal studies (Lee et al., 2016). Moreover, an analogue of another pro-resolving lipid mediator synthesized from omega-6 PUFA, lipoxin, has shown advantageous effects in gingivitis patients (Hasturk et al., 2021b).

Antibiotics are mainly recognised for their ability to eliminate bacteria and are occasionally used in conventional periodontitis therapy. However, recognition of the MMP-inhibitory capacity of tetracyclines, particularly doxycycline, prompted efforts to harness these host-modulatory effects while reducing or removing their antimicrobial properties. This led to the pursuit of two different approaches: optimising doxycycline exposure to maintain serum levels below the threshold required for antibacterial activity, and removing antibiotic activity through modification of its chemical structure (Golub et al., 2016). Currently, only the former, known as subantimicrobial dose doxycycline, has demonstrated a consistent but modest adjunctive benefit in human clinical trials (Donos et al., 2020).

It is important to highlight that the wide range of host modulating agents and considerable heterogeneity of study designs limits clinical recommendations by professional bodies such as the EFP (Sanz et al., 2020). Nonetheless, emergence of more robust evidence in the future may change that.

1.2.7.2.2 Probiotics

Probiotics constitute another novel therapeutic approach. Their proposed mode of action involves direct inhibition of pathogenic species growth through competition for resources and antimicrobial compound production, as well as indirect inhibition by modulating the host response. Unfortunately, despite a considerable number of studies on probiotics as adjuncts in NSPT, only limited studies demonstrate acceptable methodological quality that includes e.g.

adequate reporting of follow-up periods or assessment of long-term outcomes. Additionally, high levels of heterogeneity between different studies poses difficulties for direct comparison (Baddouri and Hannig, 2024, Canut-Delgado et al., 2021). Meta-analysis of 5 studies included in a 2019 systematic review revealed that the use of formulations containing *Lactobacillus rhamnosus* SP1, *L. reuteri*, and a mixture of *Streptococcus oralis* KJ3, *S. uberis* KJ2 and *S. rattus* JH145 yielded a 0.38 mm improvement in PPD, but did not reach statistical significance (Donos et al., 2020) and therefore did not earn an EFP recommendation (Sanz et al., 2020). However, it should be emphasised that two studies that used *L. reuteri* reported above average improvements in PPD (Donos et al., 2020). The first study reported significantly lower BOP as well as higher mean PPD reduction and attachment gain on day 360 following NSPT (Tekce et al., 2015). The second study reported similar improvements in clinical parameters (Ince et al., 2015). Another systematic review that focused exclusively on using *L. reuteri* as an adjunct to NST concluded that most studies supported its use compared to NST alone (Ochôa et al., 2023). These results could be explained by *L. reuteri* antimicrobial and immunomodulatory properties. *L. reuteri* was shown to inhibit periopathogens such as *F. nucleatum*, *P. gingivalis* and *P. intermedia in vitro* through its antimicrobial metabolite reuterin (Jansen et al., 2021) and *P. gingivalis* in subgingival samples *in vivo* (Iniesta et al., 2012). It has been reported to reduce the level of pro-inflammatory cytokines such as TNF-α, IL-1ß and IL-17 in GCF of chronic periodontitis patients following NST (Szkaradkiewicz et al., 2014).

1.2.7.2.3 Lasers

Lasers have been intensively investigated over years as adjuncts to non-surgical mechanical instrumentation to improve debridement of less accessible regions, ablate subgingival calculus, kill bacteria and neutralise their by-products, and improve healing through photobiomodulatory effects (Aoki et al., 2015). aPDT has been introduced as a bactericidal adjunct that utilises a photosensitiser dye with a light source matching its absorption peak to generate ROS to selectively damage bacterial cells (Cieplik et al., 2018). Despite the concepts behind both laser and aPDT appearing promising, clinical trials have not shown measurable improvements on PPD during NST (Salvi et al., 2020) or CAL in supportive therapy (Trombelli et al., 2020).

1.2.7.2.4 Natural products

There is interest in compounds originating from natural products with reported antimicrobial and anti-inflammatory properties. Formulations containing essential oils such as peppermint, chamomile, tea tree, curcumin or vetiver grass used as adjuncts to conventional therapies have been reported to have similar or superior efficacy in improving periodontal parameters when compared to chlorhexidine, which is considered a benchmark treatment (Radu et al., 2024). What is more, mouth rinse formulations containing essential oils are among those recommended by the EFP in supportive treatment of periodontitis patients to control gingival inflammation (Sanz et al., 2020). There is also modest evidence that natural products other than essential oils including, but not limited to, *Camellia sinensis* (green tea) extract, *Aloe vera* gel and propolis extract could be used as adjuncts to scaling and root planing (de Sousa et al., 2021).

1.2.7.3 Response to treatment varies among individuals and sites

It is important to emphasise that response to periodontal therapy varies among patients and depends on the choice of the outcome measures used to assess treatment effects. A systematic review that analysed data from 36 randomized controlled trials established that changes after treatment for CAL and CRP levels displayed higher variability compared to PPD, percentage of sites with BOP and percentage of sites with PD ≤ 3 mm, where responses among study subjects were similar (Raittio et al., 2025). Varied patterns of long-term tooth loss following completion of APT have also been observed among periodontal maintenance patients (Hirschfeld and Wasserman, 1978, Lindhe and Nyman, 1984, McFall, 1982). Moreover, it has been proposed that the changes after treatment can vary even between different sites within the same oral cavity (Byrne et al., 2022).

A longitudinal cohort study investigated differences between microbiome profiles of responsive and non-responsive sites within the same periodontal patients subjected to non-surgical treatment. Subgingival plaque samples displayed low beta diversity at baseline and were dominated by species mostly associated with periodontitis: *P. gingivalis*, *T. denticola*, the *F. nucleatum* group and the *Actinomyces naeslundii* group. After 3 months, responsive sites

displayed a significant reduction in bacterial alpha-diversity and reduction in levels of not only *P. gingivalis*, *T. denticola* and the *F. nucleatum* group, but also *T. forsythia*, *F. alocis*, *Treponema socranskii* and *Fretibacterium* HMT 358/359/361. In contrast, the *A. naeslundii* group, *Streptococcus mitis* group, *Corynebacterium matruchotii*, *Corynebacterium durum*, and *Rothia dentocariosa* increased their relative abundance (Byrne et al., 2022).

1.2.7.4 Factors predicting response to periodontal treatment

There are ongoing efforts to identify factors determining response to periodontal treatment. Variability in response to NST measured as probing depth reduction was attributed to the site (80%), tooth (12%) and patient (8%) level parameters (D'Aiuto et al., 2005). Moreover, machine-learning models have been investigated as methods to predict the outcomes of the first two steps of periodontal therapy using routinely collected clinical data. While the models could predict improving pockets, they were less precise in predicting non-responding sites, implying that other contributing factors including clinician expertise, host genetics and microbiological characteristics should be taken into account (Walter et al., 2025). Indeed, a rare IL-6 (−174) gene polymorphism has been identified as a factor associated with reduced improvement in probing depths following NST (D'Aiuto et al., 2005). Moreover, microbial parameters were identified as potential predictive factors during supportive periodontal therapy. Increased abundance of periodontal pathogens such as *P. intermedia*, *P. micra* or a combination of *P. gingivalis*, *T. denticola* and *T. forsythia* (detected mainly in subgingival biofilm samples) at baseline predicted periodontitis progression (Chew et al., 2023). Significant attention was directed toward Periodontal Risk Assessment (PRA), a composite score used at the end of APT proposed as a tool to predict recurrence of periodontitis during SPT. Multivariate logistic regression analysis showed that a high-risk profile at this time point was associated with recurrence of periodontitis, with smoking being the sole significant variable (Matuliene et al., 2010). Furthermore, the PRA high-risk profile was also shown to be associated with future tooth loss alongside other patient-related factors (IL-1 polymorphism, insufficient plaque management, erratic supportive care, baseline diagnosis, smoking, age and sex) and tooth-related factors (baseline bone loss, furcation involvement and serving

as an abutment tooth) (Eickholz et al., 2008, Perio Tools, 2025, Pretzl et al., 2008).

1.2.8 Epidemiology and socioeconomics of periodontitis

Periodontitis is a widespread disease and a population health challenge. The Global Burden of Disease 2021 Study covering 204 countries reported that more than 1 billion people suffered from severe periodontitis. After accounting for variations in the population age distribution between different countries, the global prevalence reached 12.50% with regional disparities ranging from 9.67% to 17.57%. It is predicted that by 2050 this number will rise to 13.30%, amounting to 1.56 billion people worldwide (Bernabe et al., 2025, Nascimento et al., 2024).

Periodontal disease generates a significant economic burden on healthcare systems and the wider society; it was estimated that in 2018 its direct costs amounted to 3.49 billion US dollars in the USA and 2.52 billion euros in 32 European countries. When indirect costs such as productivity losses, impact on edentulism and root caries were included, the total costs reached 154.06 billion US dollars (0.73% of annual gross domestic product (GDP)) and 158.64 billion euros (0.99% of annual GDP), respectively (Botelho et al., 2022). It must be emphasized, however, that appropriate supportive periodontal care is a cost-efficient alternative to a prosthetic replacement (Pretzl et al., 2009).

Current and projected future burdens highlight the need to improve oral care including both preventive measures and effective treatment strategies. The World Health Organization (WHO) *Global strategy and action plan on oral health 2023–2030* identified severe periodontal disease to be a major public health concern that requires urgent attention of its member states. The strategy has set a target of a 10% relative reduction of the main oral diseases: untreated dental caries of deciduous and permanent teeth, edentulism, severe periodontal disease and other oral disorders (excluding lip and oral cavity cancer and orofacial defects) which, when combined, affect 45% of the world population (World Health Organization, 2024).

1.3 Modelling health and periodontitis

Oral barrier research has made considerable progress over the past decades, however, there are still many gaps in our understanding of both health and periodontitis. This underscores the need for a wide range of models to study those elusive areas. Animal models are invaluable tools to investigate complex mechanisms. The degree of similarity to humans varies depending on the animal model used, and genetic modifications can increase their relevance. Nevertheless, notable differences between humans and animal models exist too. For example, unlike humans, rodents do not produce IL-8 (Matsushima et al., 2022). Another example is that dysbiosis in rodents involves periodontal pathogens distinct from those observed in humans (Van Dyke, 2020). Moreover, the use of larger animal models, such as dogs or non-human primates poses ethical sensitivities and markedly higher costs (National Academies of Sciences Engineering and Medicine, 2020, Padrell et al., 2021). According to the Replacement, Reduction and Refinement (3Rs) principles, efforts should therefore be directed towards the development of alternative methods, such as *in vitro* models (Tannenbaum and Bennett, 2015).

1.3.1 *In vitro* models of gingival sulcus

Several *in vitro* models seeking to recapitulate gingival tissue have been developed (Klausner et al., 2021, Mountcastle et al., 2020). Their key limitation is that while gingiva is an incredibly complex and dynamic environment, studies rarely specify which region is being replicated. These models typically aim to reproduce the ‘full thickness’ of gingiva, which suggests they represent the outer, keratinised gingival tissue rather than the gingival sulcus (Al-Fatlawi et al., 2023). There are models that try to recapitulate junctional epithelium, but usually only in the context of the soft tissue attachment to the tooth or implant abutment surface, not the dynamic interactions e.g. with the immune system or between the host and the microbial biofilms (Gavriiloglou et al., 2024, Gibbs et al., 2019). To date, only a limited number of non-keratinised gingival tissue models incorporating hematopoietic cells have been developed.

In vitro models of non-keratinised gingival tissue can be broadly grouped into three categories, which are summarised in the tables below: co-culture models containing both stromal and hematopoietic cells (Table 1.3), co-culture models containing stromal cells only (Table 1.4), and monoculture models (Table 1.5).

Table 1.3 *In vitro* co-culture models of gingiva containing both stromal and hematopoietic cells.

Composition (Name)	Cell types used	Tests	Reference
Co-culture (3D) ALI Inflammatory human tissue equivalent of gingiva	Primary human gingival fibroblasts (HGF) Immortalised HaCaT human keratinocyte cell line human monocytic leukaemia cell line THP-1 differentiated into macrophage-like cells	H&E staining: morphology IF staining: keratins K8/18, K19; vimentin; TE-7; CD14, CD68 SEM: surface morphology	(Xiao et al., 2018)
Co-culture (3D)	Immortalised HGF-1 human gingival fibroblast cell line U937 monoblastic leukaemia cell line differentiated into macrophage-like cells	MTT assay: viability ELISA: MMP-3, MMP-8, MMP-9	(Morin and Grenier, 2017)
Co-culture (3D)	Primary human gingival fibroblasts (HGF) human $CD4^+$ T cells primed with allogeneic antigen-presenting cells (APCs)	IHC staining: HLA-DR IF staining: HLA-DR, ICAM-1, CD80 RIA: PGE_2 RT-PCR: IFN-γ; GAPDH Southern blotting: IFN-γ	(Shimabukuro et al., 1996)

ALI, air-liquid interface; APC, antigen-presenting cell; CD, cluster of differentiation; ELISA, enzyme-linked immunosorbent assay; GAPDH, glyceraldehyde-3-phosphate dehydrogenase; H&E, haematoxylin and eosin; HGF, human gingival fibroblasts; HLA-DR, human leukocyte antigen-DR; ICAM, intercellular adhesion molecule; IF, immunofluorescence; IHC, immunohistochemistry; IFN-γ, interferon-γ; MMP, matrix metalloproteinase; MTT, 3-(4,5-dimethylthiazol-2-yl)-2,5-diphenyltetrazolium bromide; PGE_2, prostaglandin E_2; RIA, radioimmunoassay; RT-PCR, reverse transcription polymerase chain reaction; SEM, scanning electron microscopy; TE-7, anti-fibroblast antibody clone TE-7. Abbreviations are defined using the relevant protein or protein-family term for clarity.

Table 1.4 *In vitro* co-culture models of gingiva containing stromal cells only.

Composition (Name)	Cell types used	Tests	Reference
Co-culture (3D)	Primary human gingival fibroblasts (HGF) human umbilical vein endothelial cells (HUVECs) Immortalised iHGE (epi 4) human gingival epithelial cell line	H&E staining: morphology IF staining: PECAM-1 IHC staining: *P. gingivalis* qPCR: ZO-1, claudin-1, claudin-4, E-cadherin, collagen IV; mevalonate kinase; *P. gingivalis* 16S rRNA ELISA: IL-6, TNF-α	(Sasaki et al., 2021)
Co-culture (3D) ALI Model of the dentogingival junction (DGJ)	Primary human gingival fibroblasts (HGF) human periodontal ligament fibroblasts (HPDLF) Immortalised H400 oral epithelial cell line	H&E staining: morphology IHC staining: keratins K1, K8, K10, K18, K19; Ki-67	(Lu et al., 2021b)
Co-culture (3D) ALI Gingival tissue equivalent	Immortalised iHGK human gingival keratinocyte cell line iHGF/hTERT human gingival fibroblast cell line	MTT assay: viability ELISA: PGE_2, MMP-1, TIMP-1 Multiplex bead immunoassay: IL-4, IL-6 H&E staining: morphology IHC staining: keratin K17, K19, involucrin, vimentin, Ki-67	(Munar-Bestard et al., 2021) (Ferrà-Cañellas et al., 2021)
Co-culture (3D) ALI Human tissue equivalent of gingiva	Primary Human Gingival Fibroblasts (HGF) Immortalised HaCaT human keratinocyte cell line	H&E staining: morphology SEM: surface morphology IF staining: keratins K8/18, K19, vimentin, TE-7	(Xiao et al., 2018)

Composition (Name)	Cell types used	Tests	Reference
Co-culture (3D) ALI Reconstructed human gingiva (RHG)	Immortalised OKG4/bmi1/TERT gingival keratinocyte cell line iHGF/hTERT human gingival fibroblast cell line	H&E staining: morphology IHC staining: PCNA, Ki-67, elafin, HBD-2 rRNA-FISH: bacterial presence ELISA: IL-6, CXCXL1, CXCL8, CCL20, elafin qPCR: HBD-1, HBD-2, HBD-3, ADM, CAMP; HPRT1 Western blot: TLR1, TLR2, TLR3, TLR4, TLR5, TLR7, TLR8, TLR9 RT² Profiler PCR Array: TLR signalling pathway including transcription factors: *NFKB2, NFKB1, RELA, PPARA, FOS, IRF1, NR2C2, JUN, REL,* receptors: *TLR7, CD14, TNFRSF1A, TLR2, SIGIRR, TLR5, TLR4, MAP2K3, MAP4K4, MAPK8, MAP3K1, MAP2K4;* enzymes: *BTK, IRAK2, PTGS2, IRAK4, EIF2AK2, CASP8, CHUK, IRAK1, TAB1;* cytokines and chemokines: *IL6, CSF3, CXCL8, IL1B, TNF, CSF2, IFNA1, CXCL10, CCL2, IL12A;* activators, inhibitors, & adaptors: *TBK1, NFKBIA, IKBKB, HRAS, PELI1, HSPD1, MYD88, MAPK8IP3, HMGB1, TOLLIP, FADD, HSPA1A, CD86; others: ECSIT, PRKRA; B2M, GAPDH*	(Buskermolen et al., 2016) (Shang et al., 2018) (Shang et al., 2019)
Co-culture (3D)	Immortalised OBA-9 human gingival epithelial cell line HGF-1 human gingival fibroblast cell line	ELISA: IL-6, IL-8 MTT assay: viability multiplex ELISA: EGF, eotaxin-1, FGF-2, Flt3L, fractalkine, G-CSF, GM-CSF, GRO-α, IFN-α2, IFN-γ, IL-1α, IL-1β, IL-2, IL-3, IL-4, IL-5, IL-6, IL-7, IL-8, IL-9, IL-10, IL-12B, IL-12 (p70), IL-13, IL-15, IL-17A, IP-10, MCP-1, MCP-3, MDC, MIP-1α, MIP-1β, PDGF-AA, PDGF-AB/BB, RANTES, sCD40L, TGF-α, TNF-α, TNF-β, VEGF-A; MMP-1, MMP-2, MMP-3, MMP-7, MMP-8, MMP-9, MMP-10, MMP-12, MMP-13; TIMP-1, TIMP-2, TIMP-3, TIMP-4	(Bedran et al., 2014) (Lombardo Bedran et al., 2015)

Composition (Name)	Cell types used	Tests	Reference
Co-culture (3D) ALI Junctional or sulcular epithelium organotypic model	Primary human gingival keratinocytes (HGK) human periodontal ligament fibroblasts (HPLF)	H&E staining: morphology IHC staining: keratins K8, K10, K13, K16, K19, filaggrin, TG, collagen IV, laminin-1, FDC-SP, ODAM, Ki-67	(Dabija-Wolter et al., 2013)
Co-culture (3D) ALI Sulcular or gingival epithelium organotypic model	Primary human gingival keratinocytes (HGK) human gingival fibroblasts (HGF)	H&E staining: morphology IHC staining: keratins K8, K10, K13, K16, K19, filaggrin, TG, collagen IV, laminin-1, FDC-SP, ODAM, Ki-67	(Dabija-Wolter et al., 2013)
Co-culture (3D) ALI Model of human oral mucosa	Primary human oral epithelial cells (HEC) human gingival fibroblasts (HGF)	Protein array: MMP-1, MMP-2, MMP-3, MMP-8, MMP-9, MMP-10, MMP-13; TIMP-1, TIMP-2, TIMP-4	(Johanson et al., 2013)
Co-culture (3D)	Primary human gingival epithelial cells (GEC) human gingival fibroblasts (HGF)	LDH assay: cytotoxicity Sircol Soluble Collagen Assay: residual collagen IHC staining: phospho-VEGFR-1	(Ohshima et al., 2010) (Ohshima et al., 2016)
Co-culture (3D) ALI Organotypic model of the oral mucosa	Immortalised 3T3 mouse embryonic fibroblast cell line OKF6/TERT-2 human oral keratinocyte cell line	H&E staining: morphology IHC staining: E-cadherin, Ki-67 LDH assay: cytotoxicity	(Dongari-Bagtzoglou and Kashleva, 2006)

ADM, adrenomedullin; AL, air-liquid interface; B2M, beta-2-microglubulin; BMI1, B lymphoma Mo-MLV insertion region 1 homolog; BTK, Bruton tyrosine kinase; CAMP, cathelicidin antimicrobial peptide; CASP, caspase; CD, cluster of differentiation; CCL, C-C motif chemokine ligand; CHUK, component of inhibitor of nuclear factor kappa B kinase complex; CSF, colony-stimulating factor; CXCL, C-X-C motif chemokine ligand; DGJ, dentogingival junction; ECSIT, evolutionarily conserved signalling intermediate in Toll pathways; EGF, epidermal growth factor, EIF2AK, eukaryotic translation initiation factor 2 alpha kinase; ELISA, enzyme-linked immunosorbent assay; FADD, Fas-associated via death domain; FDC-SP, follicular dendritic cell-secreted protein; FGF, fibroblast growth factor; FISH, fluorescence *in*

situ hybridisation; Flt3L, Fms-like tyrosine kinase 3 ligand; FOS, Fos proto-oncogene; G-CSF, granulocyte colony-stimulating factor; GM-CSF, granulocyte–macrophage colony-stimulating factor; GAPDH, glyceraldehyde-3-phosphate dehydrogenase; GRO, growth-regulated oncogene; H&E, haematoxylin and eosin; HBD, human beta-defensin; HGF, human gingival fibroblasts; HGK, human gingival keratinocytes; HEC, human oral epithelial cells; HPDLF, human periodontal ligament fibroblasts; HMGB, high mobility group box; HPRT1, hypoxanthine phosphoribosyltransferase 1; HRAS, HRas proto-oncogene; HSPA, heat shock protein family A; HSPD, heat shock protein family D; HUVEC, human umbilical vein endothelial cell; hTERT, human telomerase reverse transcriptase; IF, immunofluorescence; IFN, interferon; IHC, immunohistochemistry; IL, interleukin; IP-10, interferon gamma-induced protein 10; IRAK, interleukin-1 receptor-associated kinase; IRF, interferon regulatory factor; JUN, Jun proto-oncogene; Ki-67, Ki-67 antigen; LDH, lactate dehydrogenase; MAPK, mitogen-activated protein kinase; MAPKIP, mitogen-activated protein kinase interacting protein; MCP, monocyte chemoattractant protein; MDC, macrophage-derived chemokine; MMP, matrix metalloproteinase; MIP, macrophage inflammatory protein; MTT, 3-(4,5-dimethylthiazol-2-yl)-2,5-diphenyltetrazolium bromide; MYD88, myeloid differentiation primary response 88; NFκB, nuclear factor kappa B; NFKBI, nuclear factor kappa B inhibitor; IKBK, inhibitor of nuclear factor kappa B kinase; NR2C2, nuclear receptor subfamily 2 group C member 2; ODAM, odontogenic ameloblast-associated protein; PCNA, proliferating cell nuclear antigen; PDGF, platelet-derived growth factor; PECAM-1, platelet endothelial cell adhesion molecule 1; PELI, pellino E3 ubiquitin protein ligase; PGE_2, prostaglandin E_2; PPAR, peroxisome proliferator-activated receptor; PRKRA, protein kinase, interferon-inducible double stranded RNA dependent activator; PTGS, prostaglandin-endoperoxide synthase; qPCR, quantitative polymerase chain reaction; RANTES, regulated upon activation, normal T cell expressed and secreted; REL, REL proto-oncogene; RHG, reconstructed human gingiva; rRNA, ribosomal RNA; RT² Profiler PCR Array, real-time PCR array for pathway-focused gene expression profiling; sCD40L, soluble CD40 ligand; SEM, scanning electron microscopy; SIGIRR, single immunoglobulin interleukin-1 receptor-related molecule; TAB, TGF-beta activated kinase binding protein; TBK, TANK binding kinase; TE-7, anti-fibroblast antibody clone TE-7; TG transglutaminase; TGF, transforming growth factor; TIMP, tissue inhibitor of metalloproteinases; TLR, Toll-like receptor; TNF, tumour necrosis factor; TNFRSF, tumour necrosis factor receptor superfamily; TOLLIP, toll interacting protein; VEGF, vascular endothelial growth factor, VEGFR, vascular endothelial growth factor receptor; ZO-1, zonula occludens-1. Abbreviations are defined using the relevant protein or protein-family term; where gene symbols are listed, the corresponding protein or protein-family abbreviation is provided for clarity.

Table 1.5 *In vitro* monoculture models of gingiva.

Composition (Name)	Cell types used	Tests	Reference
Monoculture (2D)	Primary human gingival epithelial cells (HGEC)	IHC staining: keratin, involucrin, TLR2, TLR4, CD3 RT-PCR: TLR1, TLR2, TLR3, TLR4, TLR5, TLR6, TLR7, TLR8, TLR9, TLR10 ELISA: IL-8, IL-6, MCP-1	(Kusumoto et al., 2004)
Monoculture (2D)	Immortalised OBA-9 human gingival epithelial cell line	IHC staining: keratin, involucrin, TLR2, TLR4, CD3 RT-PCR: TLR1, TLR2, TLR3, TLR4, TLR5, TLR6, TLR7, TLR8, TLR9, TLR10 ELISA: IL-8, IL-6, MCP-1	(Kusumoto et al., 2004)
Monoculture (2D)	Primary human gingival fibroblasts (HGF)	RT-PCR: TLR1, TLR2, TLR3, TLR4, TLR5, TLR6, TLR7, TLR8, TLR9, TLR10 ELISA: IL-8, IL-6, MCP-1	(Kusumoto et al., 2004)
Monoculture (2D)	Primary human periodontal ligament fibroblasts (HPDLF)	Collagenase assay: collagenase enzymatic activity Western blotting: collagenase proteins	(Ohshima et al., 1994)
Monoculture (2D)	Primary human gingival fibroblasts (HGF)	Collagenase assay: collagenase enzymatic activity Western blotting: collagenase proteins	(Ohshima et al., 1994)
Monoculture (2D)	Primary human gingival fibroblasts (HGF)	LDH assay: cell cytotoxicity Collagen deposition ELISA: PGE_2, MMP-1, TIMP-1	(Ferrà-Cañellas et al., 2021)
Monoculture (2D)	Primary human gingival fibroblasts (HGF)	MTS assay: cell viability LDH assay: cytotoxicity MTT assay: cell viability	(Moghaddam et al., 2016)
Monoculture (2D) Gingival model	Primary human gingival fibroblasts (HGF)	Western blot: collagen I IF staining: collagen fibrils	(Gawron et al., 2014)

Composition (Name)	Cell types used	Tests	Reference
Monoculture (3D)	Primary human gingival fibroblasts (HGF)	H&E staining: morphology alamarBlue assay: cell viability qPCR: EGF, collagen I; ß-actin	(Basso et al., 2016)
Monoculture (3D)	Primary human gingival fibroblasts (HGF)	H&E staining: morphology alamarBlue assay: viability qPCR: collagen I, VEGF ELISA: VEGF, TNF-α, IL-1ß	(Cardoso et al., 2020)
Monoculture (2D)	Primary human gingival fibroblasts (HGF)	Protein array: MMP-1, MMP-2, MMP-3, MMP-8, MMP-9, MMP-10, MMP-13; TIMP-1, TIMP-2, TIMP-4	(Johanson et al., 2013)
Monoculture (3D) Gingival lamina propria model	Primary human gingival fibroblasts (HGF)	Western blotting: S-Gal, MMP-1, MMP-3, TIMP-1, TIMP-2, 4-hydroxyproline RT-PCR: MMP-1, MMP-3, urokinase, TIMP-1, TIMP-2; 18S rRNA	(Cozlin et al., 2006)
Monoculture (2D)	Immortalised iHGF/hTERT human gingival fibroblast cell line	LDH assay: cytotoxicity qPCR: collagen I α1, collagen III α1, decorin, MMP-1, TIMP-1, α-smooth muscle actin, TGF-ß1, endothelin-1; ß-actin, GAPDH, 18S rRNA	(Munar-Bestard et al., 2021)

CD, cluster of differentiation; EGF, epidermal growth factor; ELISA, enzyme-linked immunosorbent assay; GAPDH, glyceraldehyde-3-phosphate dehydrogenase; H&E, haematoxylin and eosin; HGEC, human gingival epithelial cells; HGF, human gingival fibroblasts; HPDLF, human periodontal ligament fibroblasts; IHC, immunohistochemistry; IL, interleukin; LDH, lactate dehydrogenase; MCP-1, monocyte chemoattractant protein 1; MMP, matrix metalloproteinase; MTS, 3-(4,5-dimethylthiazol-2-yl)-5-(3-carboxymethoxyphenyl)-2-(sulfophenyl)-2H-tetrazolium; MTT, 3-(4,5-dimethylthiazol-2-yl)-2,5-diphenyltetrazolium bromide; PGE_2, prostaglandin E_2; qPCR, quantitative polymerase chain reaction; rRNA, ribosomal RNA; RT-PCR, reverse transcription polymerase chain reaction; S-Gal; senescence-associated ß-galactosidase; TGF-ß1, transforming growth factor beta 1; TIMP, tissue inhibitor of metalloproteinases; TNF-α, tumour necrosis factor alpha; VEGF, vascular endothelial growth factor. Abbreviations are defined using the relevant protein or protein-family term for clarity.

1.3.2 Rationale and design requirements for new model development

Although a variety of *in vitro* models of non-keratinised gingival tissue have been developed, none contained all of the relevant components arranged in a spatially representative and appropriately compartmentalised manner that would support physiologically relevant function, including immune cell migration.

Many existing models included an epithelial layer, but its configuration was often not suitable for modelling the gingival sulcus. In some cases, the epithelial layer was established directly on the bottom of the well, rather than on a porous membrane support, thereby precluding transmigration studies. This configuration was also challenging for incorporation of a distinct biofilm compartment: the bottom surface of the well was considered more appropriately reserved for biofilm growth in the sulcus-facing side of the model. In other models, epithelial cells were cultured on the inner surface of a transwell membrane, such that neutrophils introduced into the insert would approach the apical epithelial surface directly. This does not reflect the *in vivo* situation, where neutrophils migrate from the underlying tissue via the basal surface of the epithelial layer, and then into the sulcus. In addition, many models were cultured at an air-liquid interface (ALI), which promotes a keratinised epithelial phenotype and therefore more closely resembles the outer gingiva than the non-keratinised epithelium of the gingival sulcus. Appropriate modelling of the sulcular environment therefore requires correct epithelial polarity and compartmentalisation, with neutrophils approaching from the basal side and migrating towards the apical surface. Such organisation is important because it preserves the correct spatial relationship between host and microbial elements, while governing the directionality of neutrophil movement and the formation of physiologically relevant gradients. Notably, while some models incorporated immune cells, none included neutrophils, despite their key role in immune surveillance in periodontal health (Theofilou et al., 2026, Williams et al., 2021).

Collectively, this provided a clear rationale for development of a new *in vitro* model better suited to investigating immune surveillance and host-microbe interactions at the gingival sulcus, in periodontal health.

Accordingly, several key design requirements were defined for a new model. These included incorporation of the key components of the oral mucosal barrier at the gingival sulcus in a spatially appropriate and compartmentalised arrangement, and preservation of epithelial polarity to support directional processes such as immune cell migration. In addition, the model needed to remain modular and experimentally adaptable, while being reproducible using standard cell culture equipment and widely available materials, without reliance on specialised devices or platforms.

1.4 Thesis Aims

This work sought to identify components of the oral mucosal barrier with the aim of integrating them into an *in vitro* model. Such a model could help explore mechanisms that preserve barrier integrity and, in turn, support oral health. This is important because identifying targetable pathways could provide a platform for screening active compounds with a potential to prevent or treat periodontitis. There is an unmet need for a model that reflects *in vivo* conditions, while still remaining feasible with standard laboratory equipment and versatile enough to be modified to study more focused questions.

The unanswered questions this thesis was to answer were:

- What are the key components of the healthy oral barrier that maintain its integrity?

- Can these components be incorporated into an *in vitro* model that will accurately reflect *in vivo* conditions?

2 Materials and methods

2.1 Bacterial-based methods

2.1.1 Biofilm preparation

2.1.1.1 Growth kinetics of *Neisseria mucosa*

Growth kinetics of *N. mucosa* were determined by inoculating bacterial colonies grown as described in Section 2.1.1.4 into Tryptic Soy Broth (TSB), NutriSelect Basic [Millipore, Merck, Darmstadt, Germany], incubating at 37 °C in 5% CO_2 for 24 h, washing twice in sterile Dulbecco A phosphate-buffered saline (PBS) [Oxoid, Thermo Fisher Scientific, Basingstoke, UK] at 3000 × *g* for 10 minutes, resuspending the pellet in TSB, and adjusting the suspension by dilution to an optical density at 600 nm (OD_{600}) of 0.01. The resulting suspension was added at 100 µL aliquots to 24 wells of a 96-well round-bottom plate [Corning, Corning, NY, USA], placed in a Cerillo Alto Microplate Reader, with 600 nm absorbance operated through the Labrador Software Version 2.3.4 [Cerillo, Charlottesville, VA, USA], and incubated at 37 °C in 5% CO_2. TSB-only wells served as a background control. Absorbance was measured every hour at 600 nm for 24 hours. The experiment was performed on a single occasion.

The growth curve was produced and analysed using GraphPad Prism 10.5.0 (673) software [GraphPad Software, San Diego, CA, USA] and Microsoft Excel (Microsoft 365) [Microsoft, Redmond, WA, USA]. The log phase midpoint was identified by calculating hourly bacterial growth rate and identifying the highest value. The resulting time point was further used to prepare bacterial suspensions for determining absorbance values equivalent to 1×10^7 colony-forming units per mL (CFU/mL).

2.1.1.2 Determining absorbance value of *N. mucosa* suspension

To determine the absorbance value corresponding to 1×10^7 CFU/mL, TSB was inoculated with a loopful of *N. mucosa* colonies grown as described in Section 2.1.1.4 and incubated for 4–5 hours at 37 °C in 5% CO_2. The culture was then

washed twice in sterile PBS at 3000 × *g* for 10 minutes, and the pellet was resuspended in PBS. The suspension was adjusted by dilution to an OD_{600} of 0.05. Next, a two-stage dilution method was used, in which the neat bacterial suspension was initially diluted two-fold, followed by ten-fold dilutions of all suspensions (Table 2.1). Subsequently, the resulting dilutions were used for the Miles and Misra method described in Section 2.1.1.3. Based on preliminary viable count data from a single experiment performed in technical triplicate, the OD_{600} value was adjusted to approximate the target bacterial concentration for subsequent preparation of *N. mucosa* suspensions.

Table 2.1 Dilutions used in the two-stage dilution method.

Primary set of dilutions (↓)	Secondary set of dilutions (→)			
Neat	10^{-6}	10^{-7}	10^{-8}	10^{-9}
1:2	10^{-4}	10^{-5}	10^{-6}	10^{-7}
1:4	10^{-4}	10^{-5}	10^{-6}	10^{-7}
1:8	10^{-2}	10^{-3}	10^{-4}	10^{-5}
1:16	10^{-2}	10^{-3}	10^{-4}	10^{-5}
1:32	10^{-2}	10^{-3}	10^{-4}	10^{-5}
1:64	neat	10^{-1}	10^{-2}	10^{-3}
1:128	neat	10^{-1}	10^{-2}	10^{-3}

The protocol used in this section was based on a method developed by Nasser Binsaif. The experiment was performed by the author.

2.1.1.3 Bacteria quantification and viability assessment: Miles and Misra method

In order to verify the single-species absorbance values equivalent to 1×10^7 (*N. mucosa*) or 1×10^8 CFU/mL (remaining strains), a modified Miles and Misra drop plate method was used (Miles et al., 1938). Single-species suspensions of live bacteria in PBS were standardised to absorbance values mentioned below (see Table 2.2). Following preparation of ten-fold dilutions from neat bacterial suspensions, 10 µL aliquots of the resulting dilutions were dropped in triplicate onto appropriate agar plates: Columbia Blood Agar (CBA), prepared from Columbia agar (NutriSelect Plus) [Millipore, Merck, Darmstadt, Germany], or Fastidious Anaerobe Agar (FAA) [E&O Laboratories, Bonnybridge, UK]. Both media were supplemented with 5% (v/v) defibrinated horse blood [E&O

Laboratories, Bonnybridge, UK]. The inoculated plates were left to dry in a Class II biological safety cabinet before being moved to appropriate culture conditions (see Table 2.2). After completion of the incubation period, the plates were examined for the presence of spots containing between 50 and 200 colonies, and colony counts were recorded primarily from these spots. Where no such spots were present at the dilutions tested – with counts above the preferred range at one dilution and below it at the next consecutive dilution – the counts below 50 were retained for the final estimated viable count calculations. These values were interpreted with caution and indicated on the relevant graph with hash symbols ($^{\#}$). The experiment was performed on a single occasion in technical triplicate. Viable counts were expressed as CFU/mL and calculated using the following formula:

$$\mathrm{CFU/mL} = \frac{\text{Average no. of colonies per spot} \times \text{Dilution factor}}{\text{Volume plated [mL]}}$$

2.1.1.4 Bacterial culture and standardisation

This study utilised a selection of bacterial type strains shown in Table 2.2 alongside their culture conditions and standardisation values. Accession numbers in other collections can be found in Table S1. *N. mucosa* was cultured according to the supplier recommendations [NCTC, Salisbury, UK], while the remaining strains were cultured as described previously (Brown et al., 2023). Following growth on appropriate solid media (either CBA or FAA) and then in liquid media (TSB; Brain Heart Infusion Broth (BHI), NutriSelect Plus [Millipore, Merck, Darmstadt, Germany]; or Schaedler Anaerobe Broth (SCH) [Oxoid, Thermo Fisher Scientific, Basingstoke, UK]), bacterial cultures were washed twice in sterile PBS at 3000 × *g* for 10 minutes. Next, they were standardised to 1×10^8 CFU/mL in PBS, except for *N. mucosa* that was standardised to 1×10^7 CFU/mL. Then they were subsequently diluted to a final working concentration of 1×10^7 CFU/mL in RPMI:THB (1:1) media mixture (described in Section 2.1.1.5), with the exception of *N. mucosa* that was diluted to 1×10^6 CFU/mL.

Table 2.2 Strains, culture conditions, absorbance and OD reference values for species used to grow mono-, 5- and 10-species biofilms.

Microorganism	Strain	Solid medium (plate)*	Time	Liquid medium (broth, 10 mL)	Time	Culture conditions	Absorbance for 1×10^8 CFU/mL (1×10^7 CFU/mL)**	OD
Streptococcus intermedius	DSM 20753	CBA	24 h	TSB	16–18 h	37 °C, 5% CO_2	0.5	550 nm
Streptococcus mitis	NCTC 12261	CBA	24 h	TSB	16–18 h	37 °C, 5% CO_2	0.5	550 nm
Streptococcus oralis	NCTC 11427	CBA	24 h	TSB	16–18 h	37 °C, 5% CO_2	0.5	550 nm
Neisseria mucosa	NCTC 12978	CBA	24 h	TSB	16–18 h	37 °C, 5% CO_2	0.25**	600 nm
Rothia dentocariosa	DSM 43762	CBA	24 h	BHI	16–18 h	37 °C, 5% CO_2	0.5	550 nm
Actinomyces naeslundii	DSM 17233	FAA	48–72 h	BHI	24–48 h	37 °C, AnO_2	0.2	550 nm
Fusobacterium nucleatum subsp. *polymorphum*	ATCC 10953	FAA	48–72 h	SCH	24–48 h	37 °C, AnO_2	0.2	550 nm
Fusobacterium nucleatum subsp. *vincentii*	DSM 19507	FAA	48–72 h	SCH	24–48 h	37 °C, AnO_2	0.2	550 nm
Veillonella dispar	NCTC 11831	FAA	48–72 h	BHI	24–48 h	37 °C, AnO_2	0.5	550 nm
Aggregatibacter actinomycetemcomitans	ATCC 43718	CBA	24–48 h	TSB	16–18 h	37 °C, 5% CO_2	0.2	550 nm
Prevotella intermedia	DSM 20706	FAA	48–72 h	SCH	24–48 h	37 °C, AnO_2	0.2	550 nm
Porphyromonas gingivalis	W83	FAA	48–72 h	SCH	24–48 h	37 °C, AnO_2	0.2	550 nm

*Both solid media were supplemented with 5% (v/v) defibrinated horse blood.
**During biofilm experiments, *N. mucosa* was standardised at 0.025 to establish the 1×10^7 CFU/mL concentration.
AnO_2, anaerobic conditions; BHI, brain heart infusion; CBA, Columbia blood agar; FAA, fastidious anaerobic agar; SCH, Schaedler's broth; TSB, tryptic soy broth.

2.1.1.5 Growth media

All biofilms were cultured in a 1:1 mixture of RPMI 1640 medium (RPMI) [Sigma-Aldrich, Merck, Darmstadt, Germany] and Todd Hewitt broth (THB) NutriSelect Plus [Millipore, Merck, Darmstadt, Germany] supplemented with 0.01 mg/mL hemin [Thermo Scientific Chemicals, Thermo Fisher Scientific, Waltham, MA, USA] and 2 µg/mL menadione [Sigma-Aldrich, Merck, Darmstadt, Germany], as previously described (Brown et al., 2023).

2.1.1.6 Health-associated 5-species biofilm formation

5-species biofilms were designed and optimised to simulate *in vivo* conditions present in a healthy oral barrier of gingival sulcus. Biofilms were generated on a surface of 13 mm Thermanox plastic coverslips [Nunc, Thermo Fisher Scientific, Rochester, New York, USA] in 24-well plates [Corning, Corning, NY, USA]. Assorted combinations of standardised suspensions of 1×10^7 CFU/mL of *Streptococcus* spp. (1:1:1 mixture of *S. intermedius*, *S. mitis*, *S. oralis*) and *R. dentocariosa*, alongside a 1×10^6 CFU/mL suspension of *N. mucosa* were used to seed the coverslips over 2–3 days (see Table 2.3). All 5-species biofilms were incubated under aerobic conditions with 5% CO_2 at 37 °C in a HeraCell 150 incubator [Heraeus Instruments, Hanau, Germany] for 5 days in total. The experiment was performed in triplicate on a single occasion. The final configuration involved adding an equal proportion mixture of *S. intermedius*, *S. mitis*, *S. oralis* suspensions on day 0 followed by an equal proportion mixture of *N. mucosa* and *R. dentocariosa* on day 1 (see Figure 2.1).

Table 2.3 Different combinations of bacterial suspensions used to grow 5-species biofilms.

Combination	Day 0	Day 1	Day 2	Day 3	Day 4	Day 5
SNR	*Streptococcus* spp. *N. mucosa* *R. dentocariosa*	Media change	Media change	Media change	Media change	Move to −80° C storage
NR+S	*N. mucosa* *R. dentocariosa*	*Streptococcus* spp.	Media change			
N+R+S	*N. mucosa*	*R. dentocariosa*	*Streptococcus* spp.			
R+N+S	*R. dentocariosa*	*N. mucosa*	*Streptococcus* spp.			
S+NR	*Streptococcus* spp.	*N. mucosa* *R. dentocariosa*	Media change			
S+N+R	*Streptococcus* spp.	*N. mucosa*	*R. dentocariosa*			
S+R+N	*Streptococcus* spp.	*R. dentocariosa*	*N. mucosa*			

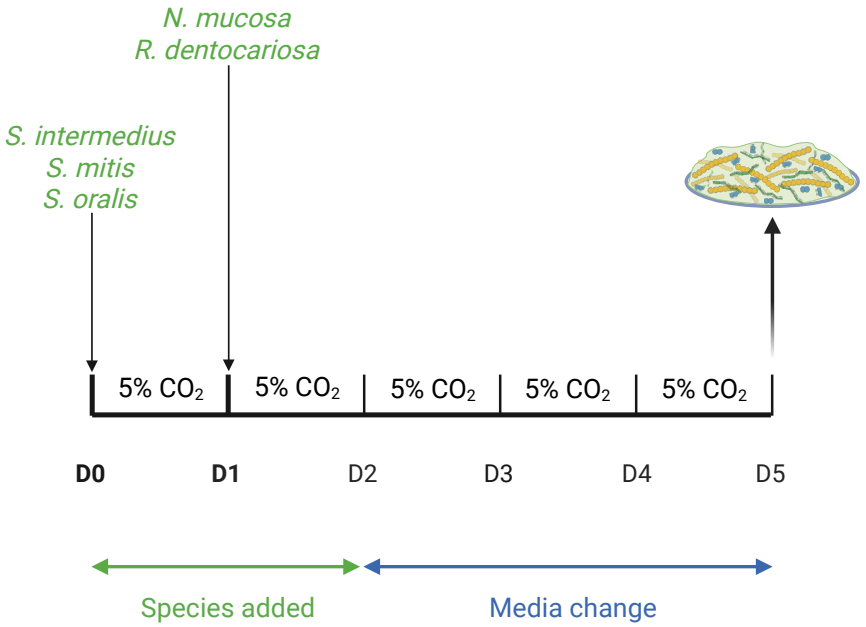

Figure 2.1 Protocol for the final configuration of 5-species biofilm culture. Initially, equal parts of standardised 10^7 CFU/mL suspensions of *S. intermedius*, *S. mitis* and *S. oralis* were added to 13 mm Thermanox coverslips. After 24 hours, a 1:1 mixture of standardised 10^7 CFU/mL suspension of *R. dentocariosa* and 10^6 CFU/mL suspension of *N. mucosa* was added. This was followed by daily media changes. Biofilms were grown in THB:RPMI (1:1) mixture in 5% CO_2 at 37 °C for a total of 5 days. Figure created with BioRender.com.

2.1.1.7 Periodontitis-associated 10-species biofilm formation

10-species biofilms were used to emulate *in vivo* conditions found in the periodontal pocket. They were prepared as previously described (Brown et al., 2023) by sequentially seeding 13 mm Thermanox plastic coverslips placed in 24-well plates with 10 different bacterial species over 3 days (see Table 2.2 and Figure 2.2): *S. intermedius*, *S. mitis* and *S. oralis* on day 0; *A. naeslundii*, *Veillonella dispar*, *F. nucleatum* subsp. p*olymorphum* and *F. nucleatum* subsp. *vincentii* on day 1; and *A. actinomycetemcomitans*, P. gingivalis and *P. intermedia* on day 2.

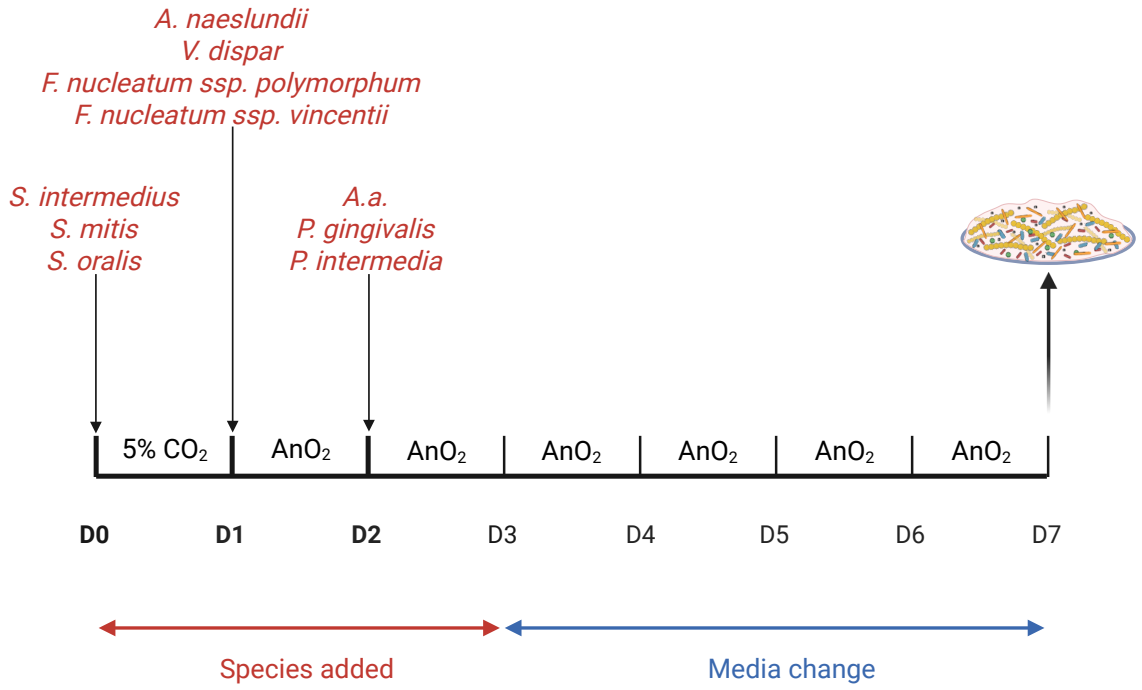

Figure 2.2 Protocol for 10-species biofilm culture. Initially, equal parts of standardised 10^7 CFU/mL suspensions of *S. intermedius, S. mitis* and *S. oralis* were added to 13 mm Thermanox coverslips. After 24 hours, an even mixture of standardised 10^7 CFU/mL suspensions of *A. naeslundii*, *F. nucleatum* subsp. *polymorphum*, *F. nucleatum* subsp. *vincentii* and *V. dispar* was added. Following the next 24 hours, a 1:1:1 mixture of 10^7 CFU/mL suspensions of *A. actinomycetemcomitans*, *P. intermedia* and *P. gingivalis* was added. This was followed by daily media changes. Biofilms were grown in THB:RPMI (1:1) mixture in 5% CO_2 at 37 °C for 1 day and then in an anaerobic chamber at 37 °C for the remaining 6 days. Figure created with BioRender.com.

The first 24 hours of the incubation took place under aerobic conditions with 5% CO_2 at 37 °C, then the coverslips were moved to a Whitley A25 anaerobic workstation [Don Whitley Scientific, Shipley, UK] with 85% N_2, 10% CO_2 and 5% H_2. Biofilms were allowed to mature for a further 6 days.

2.1.1.8 Single species *P. gingivalis* biofilm formation

Single species *P. gingivalis* biofilms were grown on 13 mm Thermanox plastic coverslips placed into 24-well plates as previously described (Connolly et al., 2017) with minor modifications.

500 µL of standardised bacterial suspensions of 1 × 10^7 CFU/mL in RPMI:THB media mix (1:1) were added to the wells and then plates were incubated at 37 °C in an anaerobic chamber with 85% N_2, 10% CO_2 and 5% H_2 for 4 days with daily media changes.

2.1.1.9 Biofilm freezing, long-term storage and revival

Following maturation, biofilms were carefully washed with PBS, then PBS was completely removed from the wells and the plate was placed at −80 °C until further use.

Frozen biofilms were revived by washing them in 500 µL PBS followed by adding 500 µL of THB:RPMI (1:1) media and 24-hour incubation in the appropriate type of cabinet before use.

2.1.2 Biofilm composition quantitative analysis

2.1.2.1 Bacterial DNA extraction

Revived biofilms were sonicated in 1 mL of PBS at 35 kHz in a Fisherbrand FB 11021 ultrasonic bath [Fisher, Loughborough, UK] for 10 minutes. Next, the supernatants were transferred to UV-treated RNase-free 1.5 mL microcentrifuge tubes [Invitrogen, Thermo Fisher Scientific, Paisley, UK] and centrifuged at 10,000 rpm for 5 minutes. When processing planktonic bacterial samples for the standard curves, 1 mL of suspensions were transferred to microcentrifuge tubes directly and centrifuged at 10,000 rpm for 5 minutes.

Following disposal of supernatants, bacterial DNA was extracted using the MasterPure Yeast DNA Purification Kit [LGC Biosearch Technologies, Hoddesdon, UK] as per the manufacturer's instructions. The pellets were resuspended in 300 µL of Yeast Cell Lysis Solution and incubated at 65 °C for 15 minutes. Afterwards, samples were placed on ice for 5 minutes and then 150 µL of MPC Protein Precipitation Reagent was added. Following 10 seconds of vortexing, samples were centrifuged for 10 minutes at 10,000 rpm. Supernatants were then transferred to clean microcentrifuge tubes prior to DNA precipitation. 500 µL of isopropanol (2-propanol) was added and mixed with samples by inversion and centrifuged for 10 minutes at 10,000 rpm. The supernatants were discarded by pipetting and the pellets were washed with 500 µL of 70% ethanol. Ethanol was carefully removed with a pipette and samples were then briefly centrifuged and any remaining ethanol was removed. The pellets containing the DNA were resuspended in 35 µL of TE Buffer and stored at -20 °C until further use.

2.1.2.2 Quantification of bacteria by quantitative polymerase chain reaction

Bacteria in revived biofilms were quantified by quantitative polymerase chain reaction (qPCR). Briefly, a total reaction volume of 20 µL per well was prepared by adding 1 µL of extracted DNA to a master mix containing 10 µL of 2x qPCRBIO Sygreen Mix Hi-ROXSYBR [PCR Biosystems, London, UK], 7.4 µL of UV-treated nuclease-free HyPure Molecular Biology-Grade Water [HyClone, Cytiva, Logan, UT, USA], and 0.8 µL of 10 µM forward/reverse primers for each bacterium (for primer sequences, see Table 2.4) [Life Technologies, Thermo Fisher Scientific, Paisley, UK]. A no-template control (NTC) was prepared by replacing DNA with sterile water. Samples were run in duplicate in MicroAmp Fast 96-Well Reaction Plate (0.1 mL) [Applied Biosystems, Thermo Fisher Scientific, Waltham, MA, USA] with 8-Strip PCR flat and optically clear caps [Starlab International, Hamburg, Germany] using a StepOnePlus Real-Time PCR System with StepOne Software v2.3 [Applied Biosystems, Thermo Fisher Scientific, Waltham, MA, USA]. Fast Cycle protocol was used with the thermal profile presented in Table 2.5. The fluorescence threshold was set at 1.0 ΔRn (baseline-corrected normalised reporter signal), and the baseline was determined automatically. Melting temperature curves were used to assess the purity of the amplification products.

Table 2.4 Primer sequences used for biofilm quantitative analysis.

Target	Forward primer 5'-3'	Reverse primer 3'-5'	Reference
Streptococcus spp. *(S. oralis, S. mitis* and *S. oralis)*	GATACATAGCCGACCTGAG	TCCATTGCCGAAGATTCC	(Sherry et al., 2016)
Neisseria spp. *(N. mucosa)*	CTGGCGCGGTATGGTCGGTT	GCCGACGTTGGAAGTGGTAAAG	(Esposito et al., 2019)
Rothia spp. *(R. dentocariosa)*	GGGTTGTAAACCTCTGTTAGCATC	CGTACCCACTGCAAAACCAG	(Uchibori et al., 2012)
A. naeslundii	GGCTGCGATACCGTGAGG	TCTGCGATTACTAGCGACTCC	(Periasamy et al., 2009)
V. dispar	CCGTGATGGGATGGAAACTGC	CCTTCGCCACTGGTGTTCTTC	(Periasamy and Kolenbrander, 2009)
Fusobacterium spp. *(F. nucleatum* subsp. *polymorphum* and *F. nucleatum* subsp. *vincentii)*	GGATTTATTGGGCGTAAAGC	GGCATTCCTACAAATATCTACGAA	(Sanchez et al., 2014) (Sherry et al., 2016)
A. actinomycetemcomitans	GAACCTTACCTACTCTTGACATCCGAA	TGCAGCACCTGTCTCAAAGC	(van der Reijden et al., 2010) (Loozen et al., 2011)
P. intermedia	CGGTCTGTTAAGCGTGTTGTG	CACCATGAATTCCGCATACG	(Loozen et al., 2011)
P. gingivalis	GCGCTCAACGTTCAGCC	CACGAATTCCGCCTGC	(Park et al., 2011)

Table 2.5 Thermal profile of fast cycle and melt temperature analysis.

Cycle type	No. of cycles	Temperature	Time	Function/role
Initial	1	95 °C	2 minutes	DNA denaturation
Amplification	40	95 °C	3 seconds	DNA denaturation
		55 °C	30 seconds	Primer binding
Melt analysis		55 °C to 95 °C (increments 0.3 °C)		Melting temperature determination

2.1.2.3 Generation of standard curves

The quantity of each bacterial species was determined using standard curves generated from ten-fold serial dilutions of bacterial DNA ranging from 1×10^1 to 1×10^7 CFE/mL (*N. mucosa*) or 1×10^2 to 1×10^8 CFE/mL (remaining strains). To assess DNA extraction efficiency and compare bacterial load with DNA recovery and quantification, an additional standard curve was generated for each bacterial species using DNA extracted from ten-fold serial dilutions of bacterial suspensions prepared within the corresponding CFE/mL ranges. The two dilution series were thereafter referred to as DNA dilution series and bacterial dilution series, respectively. A schematic overview of their preparation is shown in Figure 2.3. Both dilution series were analysed by qPCR to obtain quantification cycle (Cq) values, as described in Section 2.1.2.2. For each species, both the DNA dilution series and the bacterial dilution series were analysed in a single qPCR run on the same plate, under identical conditions and in duplicate, with a shared set of NTCs (4 wells) used for both dilution series.

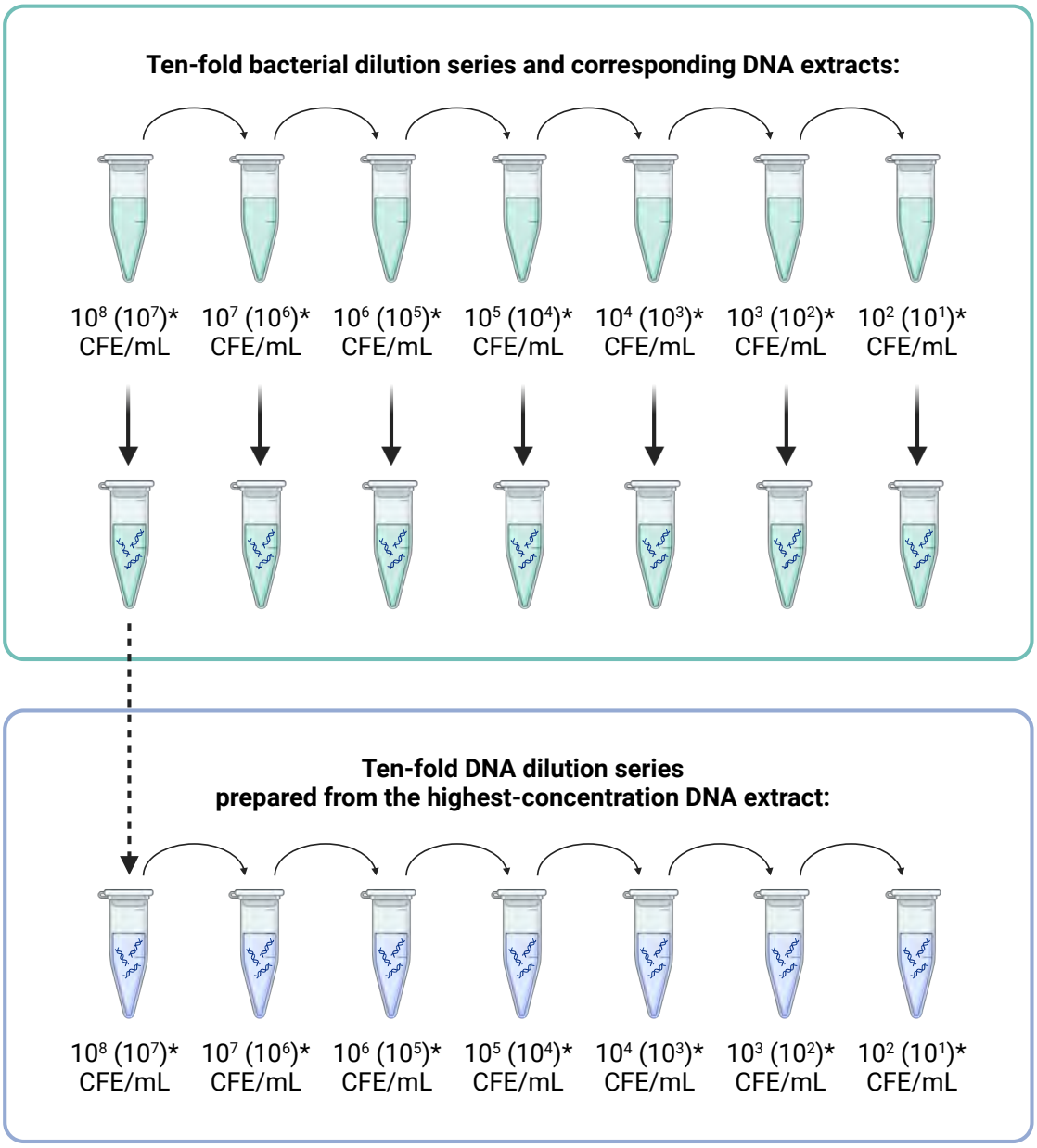

Figure 2.3 A schematic overview of the preparation of bacterial and DNA dilution series. Ten-fold bacterial dilution series were prepared by diluting bacterial suspensions standardised to 1×10^8 CFE/mL, except for *N. mucosa*, which was standardised to 1×10^7 CFE/mL. DNA extracts obtained from the highest-concentration bacterial suspensions were then serially diluted ten-fold to generate the DNA dilution series.
*Values in parentheses indicate the corresponding concentrations used for *N. mucosa*.
CFE/mL, colony-forming equivalents per mL. Figure created with BioRender.com.

Standard curves were generated using GraphPad Prism 10.5.0 (673) software. First, Cq values were plotted against $\log_{10}$-transformed CFE/mL values. Cq values from NTCs and serially diluted DNA samples were used to establish the lower working limit of detection for the assay. Sample dilutions with Cq values equal to or higher than the NTC Cq value were excluded from further analysis. Next, simple regression analysis was performed, and residual plots were analysed to identify residual values deviating by more than ±0.5 Cq. Outliers were then

successively excluded one by one, starting with the largest residual value and running simple regression analysis again until there were no residual values higher than ±0.5 Cq. Assay performance was then assessed using linear dynamic range, correlation coefficient (R^2 value), standard error of estimate ($S_{y.x}$), slope, and amplification efficiency (Bustin et al., 2009, Kralik and Ricchi, 2017), described in more detail in Table 2.6. R^2 values with 0.95–1.0 range satisfied the validation requirements. For *S. intermedius*, *S. mitis* and *S. oralis*, an additional standard curve, named *Streptococcus* spp., was created based on the mean of single-strain Cq values. Similarly, an additional standard curve for *Fusobacterium* spp. was created based on the mean Cq values for *F. nucleatum* subsp. *polymorphum* and *F. nucleatum* subsp. *vincentii*.

Table 2.6 Parameters used for analysis of qPCR standard curve performance.

Value	Description	Determination
Linear dynamic range	Concentration range in which the standard curve shows a linear relationship between Cq values and $\log_{10}$ copy number. Linearity should be demonstrated over a minimum of 3 orders of magnitude and preferably cover 5–6 $\log_{10}$ units.	Established from the range of concentrations meeting predefined residual deviation (±0.5 Cq) range and the goodness of fit (0.9–1.0) following linear regression analysis
Correlation coefficient (R^2)	Evaluates the goodness of fit of the linear regression model to the standard curve data points, with a range 0.95–1.0 indicating a good fit	$R^2 = 1 - \frac{residual\ sum\ of\ squares}{total\ sum\ of\ squares}$
Standard error of estimate ($S_{y.x}$)	Indicates the precision of the standard curve by quantifying the average deviation of observed Cq values around the fitted regression line, with lower values reflecting greater precision	$S_{y.x} = \sqrt{\frac{residual\ sum\ of\ squares}{n-2}}$ where n denotes the number of concentration points included in the regression analysis
Slope (b)	Describes the change in Cq associated with one $\log_{10}$ increase in template concentration, with −3.322 corresponding to E = 100%	Derived from linear regression model: $Cq = a + b \cdot \log_{10}(\text{concentration})$
Amplification efficiency (E)	Reflects the increase in the target amplicon quantity during each qPCR cycle, with 100% representing a doubling	$E = 10^{-1/slope} - 1$

2.1.3 Biofilm visualisation and architecture assessment

2.1.3.1 Evaluation of biofilm structure with scanning electron microscopy

Scanning electron microscopy (SEM) was carried out on mature biofilms stored in −80 °C and revived overnight according to specific required culture conditions (see Section 2.1.1.9).

Following revival, biofilms were carefully washed 3 times with sterile PBS and then fixed overnight at 4 °C with a solution containing 2% glutaraldehyde, 2% paraformaldehyde (PFA), 0.15 M sodium cacodylate, pH 7.4, combined with 0.15% alcian blue as a chemical probe. The fixative was then discarded, and samples were stored in 0.15 M sodium cacodylate buffer at 4 °C until further processing. The fixed biofilms were processed and imaged by Margaret Mullin using SEM at the Electron Microscopy Unit, Cellular Analysis Facility, College Shared Research Facilities, University of Glasgow, whereas regions of interest and magnification settings were selected by the author. Samples were handled as previously described with minor modifications (Erlandsen et al., 2004). Residual fixative was removed by washing samples with 0.15 M sodium cacodylate (1:1) 3 times for 5 minutes. Next, samples were treated with 2% osmium tetroxide in 0.15 M sodium cacodylate buffer for 1 hour in the fume hood. Following this, samples were washed in distilled H_2O three times for 10 minutes and treated with 0.5% uranyl acetate in distilled H_2O for 1 hour in the dark. Next, samples were washed once in distilled H_2O and then they were dehydrated by washes with gradually increasing concentrations of ethanol: single washes in 30, 50, 70 and 90% ethanol for 10 minutes followed by quadruple 5-minute washes in absolute and then dried absolute ethanol. The final drying stage was performed by washing in hexamethyldisilazane 3 times for 10 minutes. Dried samples were mounted onto SEM stubs using double sided carbon tape and silver paint and sputter-coated with approx. 20 nm gold/palladium using a Q150T high-vacuum coating system [Quorum Technologies, Lewes, UK]. The specimens were observed under a JEOL IT 100 SEM [JEOL, Tokyo, Japan] operated at 15 kV. Images were captured using JEOL InTouch Scope software version 1.05 [JEOL, Tokyo, Japan] and saved in TIFF format. This process was performed for one mature biofilm of each type.

2.1.4 Biofilm assays

2.1.4.1 Nitrate reduction assay

All biofilms alongside media-only control coverslips were revived overnight in appropriate conditions as described in Section 2.1.1.9 and carefully washed three times with sterile PBS. Then they were placed in 500 µL of THB:RPMI (1:1) media mix with 100 µM of $NaNO_3$ [Sigma-Aldrich, Merck, Darmstadt, Germany] and incubated for 1 and then 24 hours at 37 °C, 5% CO_2, with sterile PBS triple wash between the incubations. Media mix without $NaNO_3$ served as a background control. Following each incubation, the media were collected into microcentrifuge tubes and centrifuged at 10,000 rpm for 10 minutes. Supernatants were transferred to new microcentrifuge tubes and immediately frozen at −80 °C until required. The experiment was performed in triplicate on a single occasion.

Nitrite (NO_2^-) levels were measured through the Griess diazotisation reaction using Griess Reagent Kit for nitrite quantification [Invitrogen, Thermo Fisher Scientific, Paisley, UK] according to the manufacturer's protocol. In brief, the Griess Reagent was prepared by mixing equal volumes of N-(1-naphthyl)ethylenediamine (Component A) and sulfanilic acid (Component B). Next, 130 µL of deionized water, 20 µL of Griess Reagent and 150 µL of the nitrite-containing supernatant, standard nitrite solution or deionized water (serving as photometric reference sample) were mixed in duplicate wells of a flat bottom 96-well plate. Standards were ranging from 100 to 1 µM of nitrite. Following a 30-minute incubation at room temperature, the plate was read at 548 nm in a FLUOstar Omega Microplate Reader [BMG Labtech, Ortenberg, Germany].

Raw absorbance readings were blank-corrected and averaged for each sample prior to analysis. A standard curve was generated using a sigmoidal four-parameter logistic model with x defined as $\log_{10}$(concentration). Sample values were subsequently interpolated from the fitted standard curve when they fell within the standard range, or extrapolated when they fell outside this range, where possible. Values were then back-transformed using 10^x to obtain nitrite concentrations. Where extrapolated values were present, the lower and/or

upper limits of the standard concentration range were shown as dotted lines on the relevant figures. These extrapolated values were treated as exploratory estimates and interpreted with caution. Values that fell below the extrapolatable range of the fitted standard curve and could not be assigned a concentration were recorded as below the extrapolatable range. A value of 0 was then used for descriptive reporting and calculation of descriptive summary values.

2.1.4.2 Crystal violet biomass assay

All biofilms used in the nitrate reduction assay were re-employed in a subsequent experiment to determine their biomass with a crystal violet assay. Following PBS wash, biofilms were air dried at room temperature for 24 hours. Next, 500 µL of 0.05% w/v crystal violet working solution was added to each biofilm for 30 minutes at room temperature. Solution was then removed from the wells and biofilms were washed 3 times with 1 mL of tap water. At this stage, macroscopic photographs of the plates with coverslips were taken for documentation. Afterwards, 500 µL of absolute ethanol was added to each biofilm for 30 minutes to solubilise the bound dye. 5 × 75 µL aliquots from each well were then transferred to a 96-well flat-bottom microtiter plate. Absorbance was read at 570 nm with a FLUOstar Omega Microplate Reader. The experiment was performed in triplicate on a single occasion.

2.2 Cell-based methods

2.2.1 TR146 cell culture

Human squamous cell carcinoma TR146 cell line obtained from the European Collection of Authenticated Cell Cultures (ECACC) [cat. no. 10032305, ECACC, UK Health Security Agency, Porton Down, Salisbury, UK] was maintained as a monolayer culture in tissue culture flasks and subsequently used to establish epithelial multilayers on transwell insert membranes (see Section 2.2.1.2). A cryovial of frozen TR146 cell stock at a concentration of 1×10^6 cells/mL was rapidly thawed at 37 °C, and the cell suspension was diluted into 9 mL of Ham's F-12 Nutrient Mix modified with L-glutamine and phenol red [Gibco,

Thermo Fisher Scientific, Paisley, UK], supplemented with 20 units/mL of penicillin and 20 µg/mL of streptomycin [Gibco, Thermo Fisher Scientific, Paisley, UK], 10% foetal bovine serum (FBS) [Gibco, Thermo Fisher Scientific, Paisley, UK]. Following centrifugation (1500 rpm for 5 minutes), cells were resuspended in 12 mL of Ham's F-12 medium and seeded into a 75 cm^2 cell culture flask [Corning, Corning, NY, USA]. Cells were grown at 37 °C, 5% CO_2. Culture medium was changed every 2–3 days until confluence reached between 75–90%. Upon reaching confluency, medium was removed and cells were washed twice in calcium- and magnesium-free Dulbecco's phosphate-buffered saline (dPBS(−)) [Gibco, Thermo Fisher Scientific, Paisley, UK]. To detach the cells, 6 mL of 0.05% trypsin-ethylenediaminetetraacetic acid (trypsin-EDTA), with phenol red [Gibco, Thermo Fisher Scientific, Paisley, UK] was used. After incubation at 37 °C in 5% CO_2 for 5–10 minutes, trypsin-EDTA was neutralised with 12 mL of Ham's F-12 medium with 10% FBS. Following centrifugation (1500 rpm for 5 minutes), cells were resuspended in 10 mL dPBS with calcium and magnesium (dPBS(+)) [Sigma-Aldrich, Merck, Darmstadt, Germany] and viable cells were counted using a trypan blue exclusion assay [Sigma-Aldrich, Merck, Darmstadt, Germany] with Neubauer haemocytometer [BRAND, Wertheim, Germany] under a light microscope. Cells were either further passaged at 1–2 × 10^4 cells/cm^2 or cryopreserved for subsequent experiments. For cryopreservation, cells were resuspended at 1 × 10^6 cells/mL in freezing medium consisting of 70% culture medium, 20% FBS and 10% dimethyl sulfoxide (DMSO) [Sigma-Aldrich, Merck, Darmstadt, Germany]. The suspensions were aliquoted into cryovials and placed in a controlled-rate freezing container at −80 °C before being transferred to liquid nitrogen for long-term storage. Cryopreserved stocks were revived as described above. All procedures were carried out using cells between passages 14 and 34. The numbering reported here was based on the ECACC passage designation of +9 (Culture Collections, n.d.-a), and no additional in-house authentication, such as short tandem repeat (STR) profiling, was performed after receipt.

2.2.1.1 Comparison of cell quantification methods for TR146 cells

To compare manual and automated cell quantification methods, serial dilutions of TR146 cells were prepared in dPBS(+) using two-fold dilutions, with the specific dilution range varying depending on the experiment: either 1, 2, 4, and

8×10^5 cells/mL, or 6.25×10^4, 1.25, 2.5 and 5×10^5 cells/mL. Expected cell concentrations were calculated based on the initial haemocytometer count and the dilution scheme. Viable cells in the suspensions were quantified using a trypan blue exclusion assay with a Neubauer haemocytometer under a light microscope, as well as a LUNA-II Automated Cell Counter [Logos Biosystems, Anyang, South Korea] with the manufacturer's exclusion dye: 0.4% trypan blue [Logos Biosystems, Anyang, South Korea]. Each experiment was performed once, with duplicate measurements obtained for each dilution.

The data were analysed using GraphPad Prism 10.5.0 (673). Nonlinear regression with straight line model was performed for the expected as well as manually and automatically obtained results. A global linear fit was performed followed by an extra-sum-of-squares F-test with the null hypothesis that the datasets could be described by a single shared line (i.e., with the same slope and y-intercept).

2.2.1.2 Seeding TR146 cells onto transwell insert membrane

Following passaging, cells were counted and adjusted to varying concentrations depending on the experiment. Fifty microlitres of cell suspension in Ham's F-12 medium was then deposited onto the membrane of each inverted hanging transwell insert (Figure 2.4). Inverted transwell inserts were incubated for 4 hours at 37 °C in 5% CO_2 and then returned to the upright position and carefully transferred to individual wells of a 24-well plate, each containing 600 µL of Ham's F-12 medium. Next, 100 µL of medium was added to the upper chambers to ensure full submersion of the membranes. Transwell inserts were incubated at 37 °C in 5% CO_2 for up to 7 days, with the duration depending on the experiment. Across all brands used in the experiments, transwell inserts were 6.5 mm in diameter and had a 3.0 µm pore size. Other characteristics are summarised in Table 2.7.

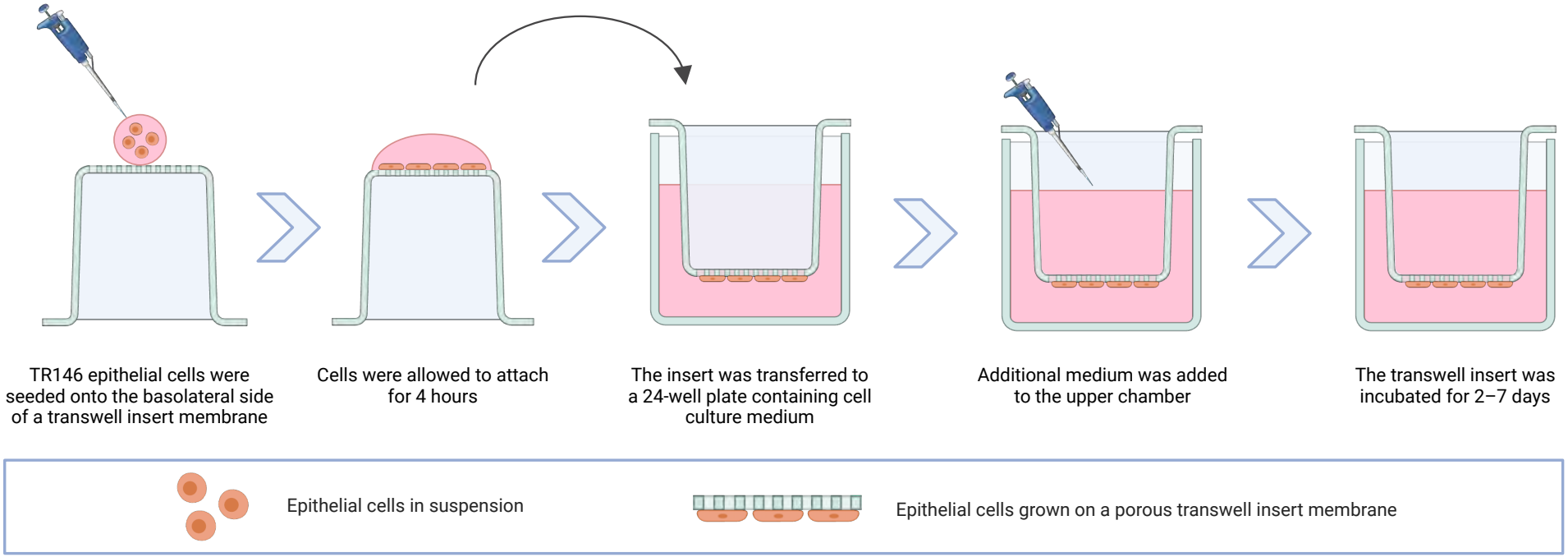

Figure 2.4 Seeding of TR146 cells onto a transwell insert membrane. Fifty microlitres of TR146 cell suspension in Ham's F-12 medium was deposited onto the membrane of an inverted hanging transwell insert. Following incubation for 4 hours at 37 °C in 5% CO_2, the transwell insert was returned to the upright position and carefully transferred to a well of a 24-well plate containing 600 µL of Ham's F-12 medium. Next, 100 µL of medium was added to the upper chamber to ensure full submersion of the membrane. The transwell insert was then incubated at 37 °C in 5% CO_2 for up to 7 days, depending on the experiment. Figure created with BioRender.com.

Table 2.7 Characteristics of transwell inserts used for seeding TR146 cells.

No.	Brand and manufacturer	Membrane	Translucency	Plate
1	Corning Transwell [Corning, Corning, NY, USA]	PC	No	Accompanying plate
2	Corning Transwell [Corning, Corning, NY, USA]	PET	Yes	Accompanying plate
3	Millicell [Millipore, Merck, Darmstadt, Germany]	PET	Yes	Nunc non-treated 24-well plate [Thermo Fisher Scientific, Roskilde, Denmark], except where a cell culture-treated plate is specifically indicated

PC, polycarbonate; PET, polyethylene terephthalate (polyester).

2.2.1.3 Trypsinisation of cells growing on a transwell insert membrane

Following completion of the designated incubation period, transwells were lifted from the wells, and medium was carefully removed from the apical compartments. Transwells were then washed twice in dPBS(−). To detach the cells, transwells were placed in wells filled with 600 µL of trypsin-EDTA and an additional 400 µL of trypsin-EDTA was added to the apical compartments. Transwells were incubated for 30 minutes at 37 °C, 5% CO_2. Next, the contents of the apical compartments were vigorously pipetted to dislodge any remaining adherent cells. The trypsin-EDTA cell suspensions were transferred to 15 mL conical tubes [Corning, Corning, NY, USA] and neutralised with 1 mL of Ham's F-12 medium with 10% FBS. Following centrifugation (1500 rpm for 5 minutes), cells were resuspended in 1 mL of dPBS(+) and viable cells were counted using a trypan blue exclusion assay and a Neubauer haemocytometer under a light microscope.

2.2.1.4 Transwell insert membrane pre-conditioning

For some experiments, transwell insert membranes were pre-conditioned with the following reagents for 30 minutes before seeding with cells:

- filter-sterilised 0.4 mM calcium chloride (CaCl2) [Sigma-Aldrich, Merck, Darmstadt, Germany]
- human collagen type I [Sigma-Aldrich, Merck, Darmstadt, Germany]
- 100% FBS.

2.2.1.5 Lucipher Yellow permeability assay

Permeability of the TR146 cell layer grown on the transwell insert membrane was measured using a Lucifer Yellow assay. Two brands of transwells with PET membranes (see Table 2.7) were seeded with TR146 cells at a total density of 5×10^4 cells/transwell. Unseeded transwells and transwells blocked with nail polish were prepared as positive and negative controls, respectively. For each transwell brand, seeded transwells and both control types were each prepared in four technical replicates. Following a 24-hour incubation, transwells were carefully washed twice in Hanks' balanced salt solution with calcium and magnesium (HBSS(+)) [Gibco, Thermo Fisher Scientific, Paisley, UK]. Next, they were placed in a new 24-well plate with wells filled up with 600 µL HBSS(+). Lucifer Yellow CH dipotassium salt [Sigma-Aldrich, Merck, Darmstadt, Germany] was reconstituted in HyPure Molecular Biology-Grade Water to a 1 mg/mL stock solution and then diluted 1:10 with HBSS(+) to a final concentration of 100 µg/mL. Further Lucifer Yellow dilutions at 50, 25, 12.5 and 6.25 µg/mL were prepared in HBSS(+) and 700 µL of each dilution was added to the wells in duplicate. Then, 100 µL of the 100 µg/mL dilution was added into the upper chambers of the transwell inserts. The plates were incubated for 1 hour at 37 °C, 5% CO_2. Following incubation, inserts were removed from the wells, washed twice in HBSS(+) and placed in a new plate with Ham's F-12 medium and returned to the incubator. Lucifer Yellow assay plates were read in a FLUOstar Omega Microplate Reader using 485 nm wavelength for excitation and 535 nm wavelength for emission. The permeability assay was then performed daily for a further 6 days. The experiment was performed on a single occasion.

Resulting fluorescence values from replicate wells were blank-corrected. A standard curve was generated using a simple linear regression model. Sample concentrations were subsequently interpolated from the fitted standard curve when they fell within the standard range, or extrapolated when they fell outside this range, where possible. Where extrapolated values fell below zero, they were recorded as below the extrapolatable range. A value of 0 was then used for descriptive reporting and calculation of descriptive summary values.

2.2.1.6 Histological processing and analysis

Transwell inserts seeded with TR146 cells were fixed in 10% neutral buffered formalin (4% formaldehyde) [Genta Medical, York, UK] for 3 hours at room temperature or overnight at 4 °C, depending on the experiment and then transferred to dPBS(+). Samples were processed and imaged by the Histology Research Service, School of Veterinary Medicine, University of Glasgow. In short, transwell insert membranes were excised using a scalpel, embedded in paraffin and sectioned. Then they underwent either haematoxylin & eosin (H&E) or immunohistochemical (IHC) staining. Resulting slides were scanned at either 20× or 80× magnification to a .tiff or .svg format. Further analysis was performed by the author using QuPath software version 0.5.1, arm64 build (Bankhead et al., 2017).

2.2.1.7 Cell Counting Kit-8 assay

Transwells seeded at varying cell densities (5×10^4 or 1×10^6 cells/transwell) and incubated for periods required by a specific experiment (2 or 4 days, respectively) were carefully washed twice in dPBS(+) and placed into wells of a new 24-well plate, each filled with 600 µL of Ham's F-12 medium. An additional 100 µL of medium was added into the upper chambers. Next, 70 µL of Cell Counting Kit-8 (CCK-8) [Dojindo Laboratories, Kumamoto, Japan] was added into the wells, and plates were incubated for 1, 2, 3 or 4 hours at 37 °C, 5% CO_2, depending on the experiment. Following incubation, transwells were carefully lifted and medium from the upper chambers was transferred to the corresponding wells. Assay plates were then read in a FLUOstar Omega Microplate Reader using 450 nm wavelength.

Standard curves were prepared separately due to the technical constraints. TR146 cell suspensions in Ham's F-12 medium at 6.125×10^4, 1.25×10^5, 2.5×10^5, 5×10^5 and 1×10^6 cells per 700 µL well were prepared in duplicate and incubated with 70 µL of CCK-8 for 1, 2, 3, and 4 hours in 24-well cell culture-treated plates [Nunc, Thermo Fisher Scientific, Roskilde, Denmark] on 3 different occasions. Obtained OD values were blank-corrected and analysed using GraphPad Prism 10.5.0 (673) software. Nonlinear regression with straight line model was performed separately for each biological repeat. Next, a global

linear fit was performed, followed by an extra-sum-of-squares F-test with the null hypothesis that all three biological repeats could be described by a single shared line (i.e., with the same slope and y-intercept). Top OD values corresponding to 1×10^6 cells/well were excluded due to saturation as indicated by residual analysis, and nonlinear regression was repeated.

2.2.2 HL-60 cell culture and differentiation

Human leukaemia HL-60 cell line obtained from the ECACC [cat. no. 98070106] was used to establish 'neutrophil-like' cells. A cryovial of frozen HL-60 cell stock at a concentration of 1×10^6 cells/mL was rapidly thawed at 37 °C, and the cell suspension was diluted into 9 mL of RPMI 1640 medium modified with L-glutamine and phenol red [Gibco, Thermo Fisher Scientific, Paisley, UK], supplemented with 20 units/mL of penicillin, 20 µg/mL of streptomycin, 20% heat-inactivated (HI) FBS and 25 mM 4-(2-hydroxyethyl)-1-piperazineethanesulfonic acid (HEPES) [Gibco, Thermo Fisher Scientific, Paisley, UK]. Following centrifugation at a low speed (150 × *g* for 5 minutes), cells were resuspended in 12 mL of RPMI 1640 medium and seeded into a 75 cm^2 cell culture flask. The flask was incubated at 37 °C, 5% CO_2 in an upright position. After proliferation was established, the HI FBS concentration was reduced to 10% and the culture was maintained at low density (between 1–9 × 10^5 cells/mL) to avoid spontaneous differentiation. When subculturing was required, cells were removed from the cell culture flask and transferred to a 15 mL conical tube. Following centrifugation at a low speed (150 × *g* for 5 minutes), the cells were resuspended in 10 mL dPBS(−) and viable cells were counted using a trypan blue exclusion assay and Neubauer haemocytometer under a light microscope. Following centrifugation at a low speed (150 × *g* for 5 minutes) and resuspension in a required volume of RPMI 1640 media, cells were either passaged at 3–5 × 10^5 cells/mL or cryopreserved for subsequent experiments. For cryopreservation, cells were resuspended in freezing medium consisting of 90% HI FBS and 10% DMSO, placed in a controlled-rate freezing container at −80 °C and subsequently transferred to liquid nitrogen for long-term storage. Cryopreserved stocks were revived as described above. All procedures were carried out using cells between passages 8 and 10. The numbering reported here was based on the ECACC passage designation of +5 (Culture Collections, n.d.-a),

and no additional in-house authentication, such as STR profiling, was performed after receipt.

2.2.2.1 HL-60 cell differentiation towards neutrophil lineage

To induce the differentiation process of HL-60 cells towards neutrophil lineage, cells were passaged as described above and cultured in their standard growth medium with the addition of 1.25% DMSO or of 1 µmol/L ATRA (all-trans retinoic acid) [Sigma-Aldrich, Merck, Darmstadt, Germany] for 5 days (Manda-Handzlik et al., 2018).

2.2.3 Neutrophil isolation from human blood

Peripheral venous blood was obtained from healthy adult volunteers by venepuncture following informed consent and with approval from the MVLS College Ethics Committee, University of Glasgow (project number 2011002). Neutrophil isolation from human blood followed by erythrocyte depletion was performed with MACSxpress Whole Blood Neutrophil Isolation Kit [Miltenyi Biotec, Bergisch Gladbach, Germany] and MACSxpress Erythrocyte Depletion Kit, human [Miltenyi Biotec, Bergisch Gladbach, Germany], respectively, using manufacturer's protocols.

In short, 8 mL of human blood collected into an EDTA tube was transferred to a 15 mL conical tube. Lyophilised PMN Isolation Cocktail was reconstituted by adding 2 mL of Buffer A. PMN Isolation Mix was prepared in a 15 mL tube by adding 2 mL of reconstituted PMN Isolation Cocktail and then 2 mL of Buffer B. Following gentle mixing, the 4 mL of prepared PMN Isolation Mix was added to 8 mL of blood. After closing the tube tightly and inverting it gently three times, the sample was incubated for 5 minutes at room temperature using the MACSmix Tube Rotator [Miltenyi Biotec, Bergisch Gladbach, Germany] on permanent run at a speed of 12 rpm. Then, the tube was placed in the MACSxpress Separator [Miltenyi Biotec, Bergisch Gladbach, Germany], the cap was opened, and the tube was incubated for 15 minutes. Next, the supernatant was carefully removed and transferred to a new 15 mL tube.

Then, the lyophilised MACSxpress Erythrocyte Depletion Reagent was reconstituted by adding MACSxpress Erythrocyte Depletion Buffer to the vial. A volume of 20 µL of reconstituted MACSxpress Erythrocyte Depletion Reagent was added per 1 mL of cell suspension obtained in the previous step. The tube was closed tightly, inverted gently three times and incubated for 5 minutes at room temperature using the MACSmix Tube Rotator on permanent run speed at 12 rpm. Following incubation, the tube was placed in the MACSxpress Separator, its cap was open and the tube was incubated for 10 minutes. The supernatant was carefully removed and transferred to a new 15 mL tube and centrifuged at low speed (150 × *g* for 5 minutes). After removal of the supernatant, the cell pellet was resuspended in HBSS(+) and the cells were counted using a trypan blue exclusion assay and a Neubauer haemocytometer under a light microscope. Cells were then used in further experiments.

2.2.3.1 Comparison of cell quantification methods for neutrophils

To compare manual and automated cell quantification methods, neutrophil suspensions in HBSS(+) were prepared at defined concentrations: 2, 4, 6, 8 × 10^5 and 1 × 10^6 cells/mL. Expected cell concentrations were calculated based on the initial haemocytometer count and the dilution scheme. Viable cells in the suspensions were quantified using a trypan blue exclusion assay with a Neubauer haemocytometer under a light microscope, as well as a LUNA-II Automated Cell Counter [Logos Biosystems, Anyang, South Korea] with the manufacturer's exclusion dyes: trypan blue (0.4%) and erythrosin B [Logos Biosystems, Anyang, South Korea]. Each experiment was performed once, with duplicate measurements obtained for each dilution.

The data were analysed using GraphPad Prism 10.5.0 (673). Nonlinear regression with straight line model was performed for the expected as well as manually and automatically obtained results. A global linear fit was performed followed by an extra-sum-of-squares F-test with the null hypothesis that the datasets could be described by a single shared line (i.e., with the same slope and y-intercept).

2.2.3.2 Neutrophil quantification using BacLight

Neutrophil suspensions at 0, 2, 4, 6, 8 × 10^5 and 1 × 10^6 cells per mL were prepared in RPMI 1640 medium modified with L-glutamine and phenol red and supplemented with 20 units/mL of penicillin, 20 µg/mL of streptomycin, 10% HI FBS and 25 mM HEPES. The suspensions were then added in duplicate to the wells of 96- and 24-well black clear-bottom plates at volumes of 100 and 600 µL, respectively. Next, either 0.1 µL or 0.6 µL of B-35000 BacLight Green bacterial stain [Invitrogen, Thermo Fisher Scientific, Paisley, UK] was added directly to the wells, and the plates were incubated for 30 minutes at room temperature. Following incubation, fluorescence was measured in a FLUOstar Omega Microplate Reader using 480 nm wavelength for excitation and 516 nm for emission. The experiment was performed on three independent occasions.

Data were blank-corrected and log-transformed [log(x + 1)] prior to analysis to normalise distribution and accommodate zero values. Nonlinear regression with a second-order polynomial (quadratic) model was fitted separately for each biological replicate, with residual plots examined to assess fit quality. Subsequently, a global fit was performed, and an extra-sum-of-squares F-test was applied to test a null hypothesis that all three biological repeats could be described by a single shared curve.

2.2.3.3 Neutrophil quantification using Cell Counting Kit-8 assay

Neutrophil suspensions at 0, 2, 4, 6, 8 × 10^5 and 1 × 10^6 cells per mL were prepared in RPMI 1640 medium modified with L-glutamine and phenol red and supplemented with 20 units/mL of penicillin, 20 µg/mL of streptomycin, 10% HI FBS and 25 mM HEPES. The suspensions were then added in duplicate to the wells of 96- and 24-well plates at volumes of 100 and 600 µL, respectively. Next, either 10 µL or 60 µL of CCK-8 was added directly to the wells, and the plates were incubated for 1, 2, 3 and 4 hours at 37 °C, 5% CO_2. Following incubation, absorbance was measured in a FLUOstar Omega Microplate Reader using 450 nm wavelength. The experiment was performed on three independent occasions.

Data were blank-corrected and log-transformed [log(x + 1)] prior to analysis to normalise distribution and accommodate zero values. Nonlinear regression with

a second-order polynomial (quadratic) model was fitted separately for each biological replicate, with residual plots examined to assess fit quality. Subsequently, a global fit was performed, and an extra-sum-of-squares F-test was applied to test a null hypothesis that all three biological repeats could be described by a single shared curve.

2.2.4 Flow cytometry

Neutrophils, ATRA- and DMSO-differentiated HL-60 cells were washed in PBS at 350 × *g* for 5 minutes and resuspended in cell staining buffer (PBS + 10% HI FBS) to a concentration of 3×10^5 cells/mL. Each cell suspension was aliquoted into round-bottom 5 mL flow cytometry tubes [Falcon, Corning, Corning, NY, USA] at 100 µL per tube.

Cells were incubated on ice and in the dark for 15 minutes with the fluorochrome-conjugated antibodies obtained from BioLegend [BioLegend, San Diego, CA, USA] and summarised in Table 2.8 (5 µL per test added to each tube). Following incubation, cells were washed twice in 200 µL of cell staining buffer at 350 × *g* for 5 minutes. Viability staining was performed using Zombie Violet viability stain (BV421) obtained from BioLegend [BioLegend, San Diego, CA, USA]. Cells in each tube were incubated in a 100 µL volume of the viability stain, diluted 1:1000 in PBS, for 15 minutes at room temperature. Heat-killed cells served as a positive control. Cells were then washed in 200 µL of cell staining buffer at 350 × *g* for 5 minutes and resuspended in 200 µL of cell staining buffer.

Single-stain controls were prepared using the VersaComp Antibody Capture Kit [Beckman Coulter, Brea, CA, USA]. A separate 5 mL tube was prepared for each fluorochrome-conjugated antibody. One drop of each of the positive and negative bead populations was added to each tube, followed by 1 µL of the antibody conjugate. Following a 20-minute incubation in the dark at room temperature, beads were washed in 200 µL of cell staining buffer at 350 × *g* for 5 minutes and resuspended in the same volume of cell staining buffer.

Cells were filtered through 30 µm Nitex mesh [Genesee Scientific, San Diego, CA, USA], and samples were acquired on a FACSCelesta flow cytometer [BD

Biosciences, San Jose, CA, USA]. Data were analysed using FlowJo v10.10.0 [BD Biosciences, San Jose, CA, USA].

Each cell type was stained and acquired once; therefore, data are presented descriptively.

Table 2.8 Fluorochrome-conjugated antibodies used for flow cytometry.

Marker	Fluorophore	Clone	Dilution
CD45	FITC	HI30	1:20
CD11b	PE	ICRF44	1:20
CD14	PerCP/Cyanine 5.5	63D3	1:20
CD15	Brilliant violet 785	W6D3	1:20

2.2.5 Cell stimulation experiments

2.2.5.1 Stimulation of primary neutrophils and ATRA-differentiated HL-60 cells with chemotactic mediators

Suspensions of primary neutrophils or ATRA-differentiated HL-60 cells were prepared at 2×10^5 cells/mL in RPMI 1640 medium modified with L-glutamine and phenol red and supplemented with 20 units/mL of penicillin, 20 µg/mL of streptomycin, 10% HI FBS and 25 mM HEPES. Cell suspensions were added to a 96-well round-bottom plate [Corning, Corning, NY, USA] at 200 µL per well. Cells were stimulated with 40 nM N-formyl-methionyl-leucyl-phenylalanine (fMLF) [Sigma-Aldrich, Merck, Darmstadt, Germany] (Mandeville et al., 1997) or 58.6 µM leukotriene B_4 (LTB_4) [Sigma-Aldrich, Merck, Darmstadt, Germany] (Casale and Abbas, 1990) for 24 hours at 37 °C, 5% CO_2. Supernatants were collected and stored at −80 °C until further use. The experiment was performed in technical triplicate on a single occasion.

2.2.5.2 Stimulation of primary neutrophils with various bacterial, host and synthetic mediators

Suspensions of primary neutrophils were prepared at 2×10^5 cells/mL in RPMI 1640 medium modified with L-glutamine and phenol red and supplemented with 20 units/mL of penicillin, 20 µg/mL of streptomycin, 10% HI FBS and 25 mM HEPES. Cell suspensions were added to 96-well round-bottom plates [Corning, Corning, NY, USA] at 200 µL per well. Cells were stimulated with fMLF, G-CSF

[PeproTech, Gibco, Thermo Fisher Scientific, Paisley, UK], granulocyte–macrophage colony-stimulating factor (GM-CSF) [PeproTech, Gibco, Thermo Fisher Scientific, Paisley, UK], phorbol 12-myristate 13-acetate (PMA) [Sigma-Aldrich, Merck, Darmstadt, Germany], and LPS from *E. coli* O111:B4, using the concentrations summarised in Table 2.9, for 24 or 48 hours at 37 °C, 5% CO_2. The concentrations of stimulants were selected based on previous experiments in the group and on published studies (Castellani et al., 2019, Chen et al., 2012, Jacobsen et al., 2007, Khan et al., 2017, Ledderose et al., 2023, Leoni et al., 2015, Lind et al., 2021, Mahomed and Anderson, 2000, Mandeville et al., 1997, Wen et al., 2021, Wright et al., 1997). Supernatants were collected and stored at −80 °C until further use. The experiment was performed in technical triplicate on a single occasion.

Table 2.9 Concentrations of mediators used to stimulate primary neutrophils.

Mediator	Minimum concentration	Medium concentration	Maximum concentration
fMLF	0.4 nM	40 nM	4 µM
G-CSF	0.1 ng/mL	1 ng/mL	5 ng/mL
GM-CSF	0.1 ng/mL	1 ng/mL	5 ng/mL
PMA	0.042 µM	0.42 µM	4.2 µM
LPS	1 µg/mL	10 µg/mL	50 µg/mL

2.2.6 Transwell migration assays

Due to the iterative approach used in *in vitro* model design, transwell migration assay parameters varied between experiments. This section describes the general workflow. Variable parameters, including transwell insert brand and membrane material, plate brand and surface treatment, assay solution, stimuli, incubation times, experimental outputs and downstream analyses, are specified in the corresponding figure legends. Figure 2.5 shows the workflow for the final protocol, involving TR146-seeded Millicell PET transwell inserts and stimulation with 5- and 10-species biofilms.

2.2.6.1 Well preparation

Wells of 24-well plates were used as the lower chambers for each neutrophil migration assay. Plate manufacturers differed depending on the experiment; details are provided in the relevant figure legends. Plates used with each

transwell insert brand and membrane material are shown in Table 2.7, with one exception indicated in Section 2.2.6.1.1. In all experiments, 600 µL of assay solution was added to each lower chamber. The assay solution consisted of either HBSS(+) or RPMI 1640 medium modified with L-glutamine and phenol red, with the relevant stimuli added according to the experiment, as described below.

2.2.6.1.1 LPS stimulation

In some experiments, LPS from *E. coli* O111:B4 was used as a stimulus. For soluble LPS stimulation, LPS was added directly to the wells to a final concentration of 20 µg/mL. For immobilised LPS stimulation, wells of a 24-well Nunc cell culture-treated plate [Thermo Fisher Scientific, Roskilde, Denmark] were first coated with 500 µL of 1% fibrinogen for 1 hour at room temperature, washed twice with 1 mL of PBS(+), and then coated with 500 µL of 100 ng/mL LPS for 2 hours at room temperature (Nakatomi et al., 1998). Wells were washed twice with 1 mL of PBS(+) before use. Then, 600 µL of RPMI 1640 medium modified with L-glutamine and phenol red was added to each well.

2.2.6.1.2 Multispecies biofilms

Frozen 5- and 10-species biofilms grown on 13 mm Thermanox coverslips were revived as described in Section 2.1.1.9 and washed with 1 mL of PBS(−). They were then placed in wells of a 24-well Nunc non-treated plate [Thermo Fisher Scientific, Roskilde, Denmark]. Next, 600 µL of RPMI 1640 medium modified with L-glutamine and phenol red was added to each well.

2.2.6.1.3 Clean coverslip feasibility platform

Clean coverslips were processed in parallel with each biofilm condition using the same overnight protocol and were used as an exploratory feasibility platform to assess whether neutrophils could be recovered from both transwell compartments.

2.2.6.2 Transwell preparation

In assays without epithelial co-culture, Corning PC or Millicell PET transwell inserts were used. Where TR146-seeded inserts were used, Millicell PET

transwell inserts, prepared as described in Section 2.2.1.2, were carefully washed twice with HBSS(+). For each wash, inserts were placed in wells containing 600 µL HBSS(+), with a further 200 µL HBSS(+) added to the upper chambers. The second wash included a 30–60 min incubation at 37 °C and 5% CO_2 to allow the cells to equilibrate in HBSS(+) as previously described (Kusek et al., 2014). Following incubation and removal of HBSS(+), inserts were transferred to the prepared assay wells.

2.2.6.3 Neutrophil migration

Neutrophil suspensions were prepared at 1×10^7 cells/mL in the appropriate assay solution: HBSS(+) for assays performed without epithelial co-culture, or RPMI 1640 medium modified with L-glutamine and phenol red for co-culture assays. Then, 100 µL of neutrophil suspension, corresponding to 1×10^6 cells, was added to the upper chambers either immediately or following a 1-hour incubation of transwell inserts at 37 °C and 5% CO_2, depending on the experiment. The full setup was then incubated at 37 °C and 5% CO_2 for 1 hour, 2 hours, 24 hours or 48 hours, depending on the experiment. Following incubation, transwell inserts were removed and processed for H&E and IHC staining, while suspensions from both chambers were collected for downstream analysis, including cell quantification using a Neubauer haemocytometer or a CCK-8 assay, and IL-8 quantification by ELISA, depending on the experiment. Additionally, coverslips used in the final migration assay were collected for crystal violet biomass assessment.

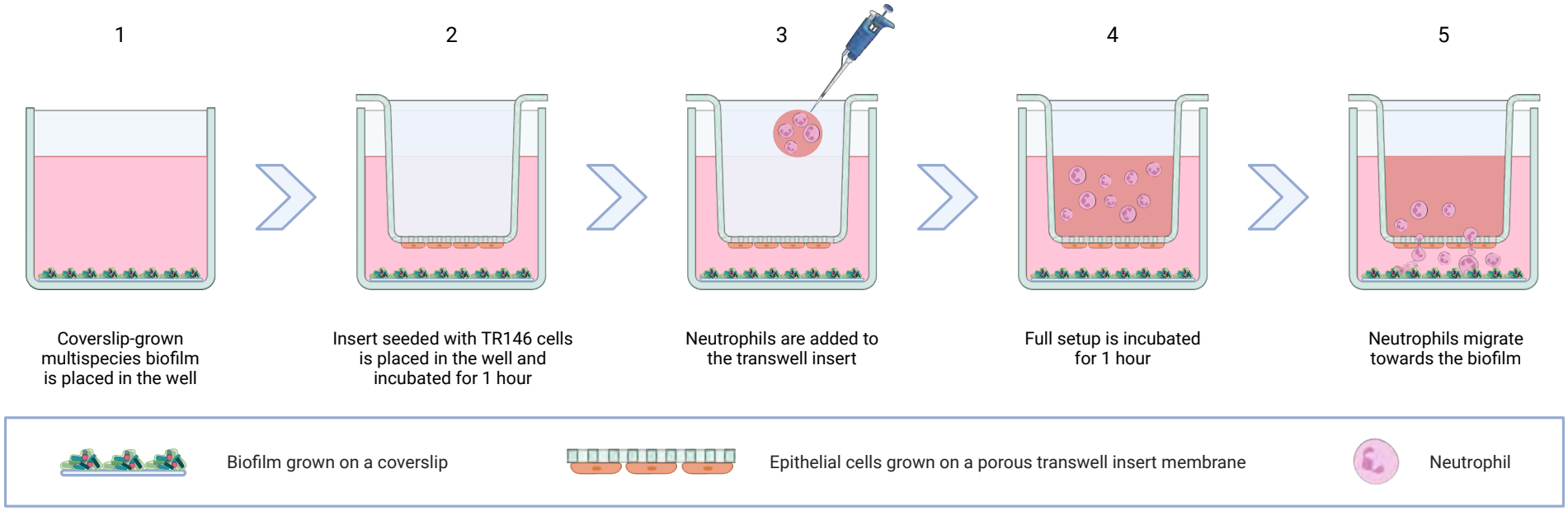

Figure 2.5 Neutrophil transwell migration assay. The assay incorporated coverslip-grown multispecies biofilms as stimuli. (1) Revived 5-species* and 10-species** biofilms grown on 13 mm Thermanox coverslips were placed into wells, followed by addition of 600 µL of RPMI 1640 medium. (2) TR146-seeded Millicell PET transwell inserts were placed into the wells and incubated for 1 hour at 37 °C and 5% CO_2. (3) Then, 100 µL of neutrophil suspension at 1×10^7 cells/mL in RPMI 1640 medium, corresponding to 1×10^6 cells, was added to the upper chambers. (4–5) The full setup was then incubated at 37 °C and 5% CO_2 for 1 hour. Following incubation, transwell inserts, suspensions from both chambers, and coverslips were collected for downstream analysis.
*5-species biofilms included *S. intermedius, S. mitis, S. oralis, N. mucosa* and *R. dentocariosa*.
**10-species biofilms included *S. intermedius, S. mitis, S. oralis, A. naeslundii, F. nucleatum* subsp. *polymorphum, F. nucleatum* subsp. *vincentii, V. dispar, A. actinomycetemcomitans, P. intermedia* and *P. gingivalis*.
PET, polyethylene terephthalate; RPMI 1640 medium, Roswell Park Memorial Institute 1640 medium modified with L-glutamine and phenol red. Figure created with BioRender.com.

2.2.7 ELISA

Concentrations of IL-1ß, IL-6, IL-8 and TNF-α proteins in supernatants were quantified using a range of uncoated ELISA kits from Invitrogen [Invitrogen, Thermo Fisher Scientific, Paisley, UK] according to the manufacturer's instructions (see Table 2.10). For each assay, a Corning Costar 9018 high-binding flat-bottom 96-well plate [Corning, Corning, NY, USA] was coated with 100 µL/well of capture antibody solution at 4 °C overnight. Next, the plate was washed twice with washing buffer and blocked with 200 µL/well of ELISA/ELISPOT Diluent for 1 hour at room temperature. After another wash, standards were prepared as serial two-fold dilutions in ELISA/ELISPOT Diluent and added to the plate alongside samples (100 µL/well each). ELISA/ELISPOT Diluent was also added to the blank wells at 100 µL/well. Following an overnight incubation at 4 °C and a triple wash, 100 µL/well of detection antibody was added for 1 hour at room temperature. The plate was then washed three times before 100 µL/well of the appropriate conjugate/binding system was added for 30 minutes at room temperature. Finally, the plate was washed five times and 100 µL/well of 3,3',5,5'-tetramethylbenzidine (TMB) solution was added for 15 minutes. Once colour developed, the reaction was stopped with 100 µL/well of the Stop Solution and the plate was then read at 450 nm with correction at 570 nm in a FLUOstar Omega Microplate Reader.

Resulting absorbance values from replicate wells were blank-corrected and averaged for each sample prior to analysis. A standard curve was generated using a sigmoidal four-parameter logistic model with x defined as $\log_{10}$(concentration). Sample values were subsequently interpolated from the fitted standard curve when they fell within the standard range, or extrapolated when they fell outside this range, where possible. Values were then back-transformed using 10^x to obtain cytokine concentrations. If remaining sample volume permitted, samples with values above the upper limit of the standard curve were diluted and re-tested; otherwise, extrapolated values were used. Where extrapolated values were present, the lower and/or upper limits of the standard concentration range were shown as dotted lines on the relevant figures. These extrapolated values were treated as exploratory estimates and interpreted with caution. Values that fell below the extrapolatable range of the fitted standard curve and could not be assigned a concentration were recorded

as below the extrapolatable range. A value of 0 was then used for descriptive reporting and calculation of descriptive summary values.

Table 2.10 ELISA kits used for supernatant analysis.

Analyte	Conjugate / Binding system	Lowest standard concentration	Highest standard concentration
IL-1β	Avidin-HRP	2	150
IL-6	Streptavidin-HRP	2	200
IL-8	Streptavidin-HRP	2	250
TNF-α	Avidin-HRP	4	500

HRP, horseradish peroxidase.

2.3 Data analysis and presentation

Illustrations were generated using BioRender [BioRender, Toronto, ON, Canada]. Photographs were taken using a Google Pixel 7 smartphone [Google, Mountain View, CA, USA]. The images' tone was adjusted in Adobe Photoshop CS4 [Adobe Systems, San Jose, CA, USA] using the Levels tool by modifying the white point and midtone (gamma) values to enhance overall brightness and contrast in a linear manner. Outlines and annotations were added for reference. SEM images were annotated using Adobe Photoshop CS4 software.

The number of biological and technical replicates varied across experiments and is specified in the relevant methods, figure legends, and table footnotes. Fits of standard curves were compared using extra-sum-of-squares F-tests to assess whether datasets could be described by a single shared curve. All other results are presented descriptively, and no formal statistical tests were performed. Where appropriate, data are summarised as mean values, with standard deviation (SD) shown where applicable; relative abundance (%); or within-assay variability, expressed as coefficient of variation (CV, %).

Data analysis was performed using Microsoft Excel (Microsoft 365) [Microsoft, Redmond, WA, USA] and GraphPad Prism 10.5.0 (673) [GraphPad Software, San Diego, CA, USA]. Graphs were generated using GraphPad Prism 10.5.0 (673) software.

3 Review based on contribution to systematic review on microbial species associated with periodontal health

3.1 Introduction/Overview

The oral cavity contains more than 700 microbial species (Escapa et al., 2018) that are distributed in varying proportions in different environmental niches such as saliva, soft tissues (tongue, hard palate, buccal mucosa and keratinised gingiva), and tooth surfaces, on which supra- and subgingival plaque develops (Caselli et al., 2020).

A wide range of studies have reported microbial species associated with periodontal health and periodontitis; however, the findings are not entirely consistent. The differences may be attributable to variation in case definition (Costa et al., 2009), sampling technique (Belibasakis et al., 2014, Beyer et al., 2017, Pérez-Chaparro et al., 2015), diagnostic methods used (Caselli et al., 2020, Papapanou et al., 1997) or geographic origin of samples (Arredondo et al., 2025). This highlights the need to identify and synthesise the available data.

There are systematic syntheses of the knowledge of microbial species associated with periodontitis (Antezack et al., 2023, Guerra et al., 2018, Pérez-Chaparro et al., 2014). However, to the author's knowledge, no systematic review focused primarily on microbial species associated with periodontal health.

3.2 Focused question

What is the weight of evidence for the existence of microorganisms associated with periodontal health based on association studies?

3.3 Methods

This chapter is a review based on the author's contribution to a collaborative multi-centre research project led by Professor Magda Feres (currently at Harvard University; at time of initiation of this project from Guarulhos University). The

review was initiated in 2019 and has continued to develop since. The team is continuing to evolve and the members will be named in the final publication.

The methodology of the systematic review was based on previous work of the group (Pérez-Chaparro et al., 2014) and followed the recommendations of the Preferred Reporting Items for Systematic reviews and Meta-Analyses (PRISMA) guidelines 2009 (Moher et al., 2009).

3.3.1 Author's contribution

The author contribution comprised of abstract and full text screening, data extraction and risk of bias assessment. The results in this chapter are from the author's work only, except for the flow chart where both team and author contribution is shown. Full data extraction, risk of bias assessment as well as machine learning-based metanalysis are not reported here. In addition, further publication searches will be undertaken at regular intervals until the final data analysis is completed.

3.3.2 Eligibility

Inclusion criteria:

- Studies of any design that provided a comparison of subgingival microbial data between periodontally healthy and periodontitis patients.
- Studies that were conducted in a systemically healthy population.
- Studies that assessed the presence of at least 1 more organism other than the red complex bacteria or viruses.

Exclusion criteria:

- Studies that were published in languages other than English or Spanish.
- Reviews, case series, case reports, or studies already reported in earlier publications (to avoid duplication of study populations).

- Studies involving participants that were not systemically healthy.

- Lack of baseline data or direct statistical comparison between subgingival plaque samples of periodontally healthy and periodontitis groups.

- Studies that recruited periodontitis patients with localised aggressive periodontitis only.

- Studies that assessed exclusively the presence of red complex bacteria or viruses.

- Studies not reporting results at phylum, genera or species levels, or reporting morphological features only.

3.3.3 Search strategy

3.3.3.1 Title search

Searches were conducted in the MEDLINE (via PubMed), EMBASE and Cochrane Library databases on 18.09.2019 and 27.01.2021 (first search) and 22.11.2023 and 01.05.2024 (second search) using Mesh terms and other key words. This was followed by a manual search of the reference lists of selected publications.

3.3.3.2 Abstract and full text screening

The abstracts and full texts were screened in teams consisting of 2 independent reviewers and discrepancies were resolved through discussion where possible. If consensus could not be reached, a third reviewer was consulted.

Excluded studies were assigned a reason for exclusion in the following order:

- Review

- No human subjects

- No microbial composition data (of oral sample):

    - only *in vitro* data
    - only clinical data
    - only other irrelevant data
- No comparison between periodontal health and periodontitis groups:
    - only periodontitis group
    - only health group
    - only health or periodontitis and other groups
- Subgingival plaque samples not evaluated
- Only known disease-associated species (red complex bacteria) evaluated
- Subjects not systemically healthy
- Samples evaluated for virus presence only
- Case report, case series, or studies already reported in earlier publications

3.3.4 Data extraction

Data were extracted from the full text articles by independent reviewers working in pairs. Disagreements were addressed through discussion if feasible, otherwise an additional reviewer was consulted.

3.3.4.1 Pre-defined Microsoft Excel forms

Extraction was performed using the following pre-defined forms created in Microsoft Excel (Microsoft 365) [Microsoft, Redmond, WA, USA]:

- Form 1: General information (authors, year, country, location (facility type), study design, sample size (volunteers), age, number of males, number of smokers, systemic condition)

- Form 2: Periodontal baseline evaluation in periodontally healthy subjects (sample size, age, number of males, number of smokers, criteria used to define periodontal health, PD, CAL, plaque, bleeding, suppuration)

- Form 3: Periodontal baseline evaluation in periodontally healthy subjects (sample size, age, number of males, number of smokers, criteria used to define periodontitis, PD, CAL, plaque, bleeding, suppuration)

- Form 4: Microbiological baseline outcomes (total number of subgingival samples, number of subgingival samples in periodontally healthy group, number of subgingival samples in periodontitis group, analysis (individual or pooled), diagnostic methods, species assessed, species elevated in periodontal health at phylum, genera and species level, species elevated in periodontitis at phylum, genera and species level)

- Form 5: Other information (source of funding, conflict of interest, other comments)

3.3.4.2 Additional data extraction

In addition to the data extracted as part of the main review, the author extracted data on the subgingival biofilm sampling methods reported in the studies.

3.3.5 Data analysis and presentation

Descriptive analysis was used to summarise characteristics of the included studies (publication year and country), subgingival sample collection methods and microbiological assessment approaches. Country names were matched to alpha-3 ISO 3166-1 codes to generate a choropleth map using Datawrapper [Datawrapper, Berlin, Germany].

Examples of extracted data on microbial species associated with periodontal health and periodontitis are presented in Table S2. Based on all extracted records, the frequency of each taxon in the dataset was calculated using University of Glasgow's Microsoft Copilot AI-powered assistant (based on GPT-5 architecture) [Microsoft, Redmond, WA, USA]. Additionally, this tool was used to detect and remove typographical errors and ensure consistency in taxa nomenclature. Afterwards, the author manually reviewed the output exported to Microsoft Excel (Microsoft 365) files. For the purpose of a more systematic synthesis of the results, inclusion thresholds for the final results tables were applied for taxa at the genera and species levels. The requirement was for genera and species to be reported in at least two and three independent studies, respectively.

Data analysis was performed using Microsoft Excel (Microsoft 365) and GraphPad Prism 10.5.0 (673) [GraphPad Software, San Diego, CA, USA]. Graphs were generated using GraphPad Prism 10.5.0 (673) software. Risk of bias assessment and data analysis using machine learning are not presented in this chapter and will be reported in the main publication.

3.4 Results – Narrative synthesis of data extracted by the author

3.4.1 Characteristics of included studies

During both searches, a total of 4343 titles were identified through database searches and an additional one through manual search. Following abstract screening, 3910 studies were excluded. Then, 350 publications underwent full-text eligibility assessment, after which 197 studies were excluded and 153 studies were included for data extraction and risk of bias assessment. The author contributed to the review by screening 306 abstracts and 88 full texts, and by including 27 papers for the data extraction. Details of both searches are presented in Figure 3.1. Subsequently, the author extracted data from 42 papers and used it to inform the narrative synthesis presented in this chapter.

Manuscripts used for data extraction by the author were published between 2012 and 2021 (see Figure 3.2) and encompassed study populations from 20 countries in total. Most studies originated from Brazil (11), USA (7) and China (5) (see Figure 3.3). Only one study included populations from two different countries – Germany and USA (Hunter et al., 2016).

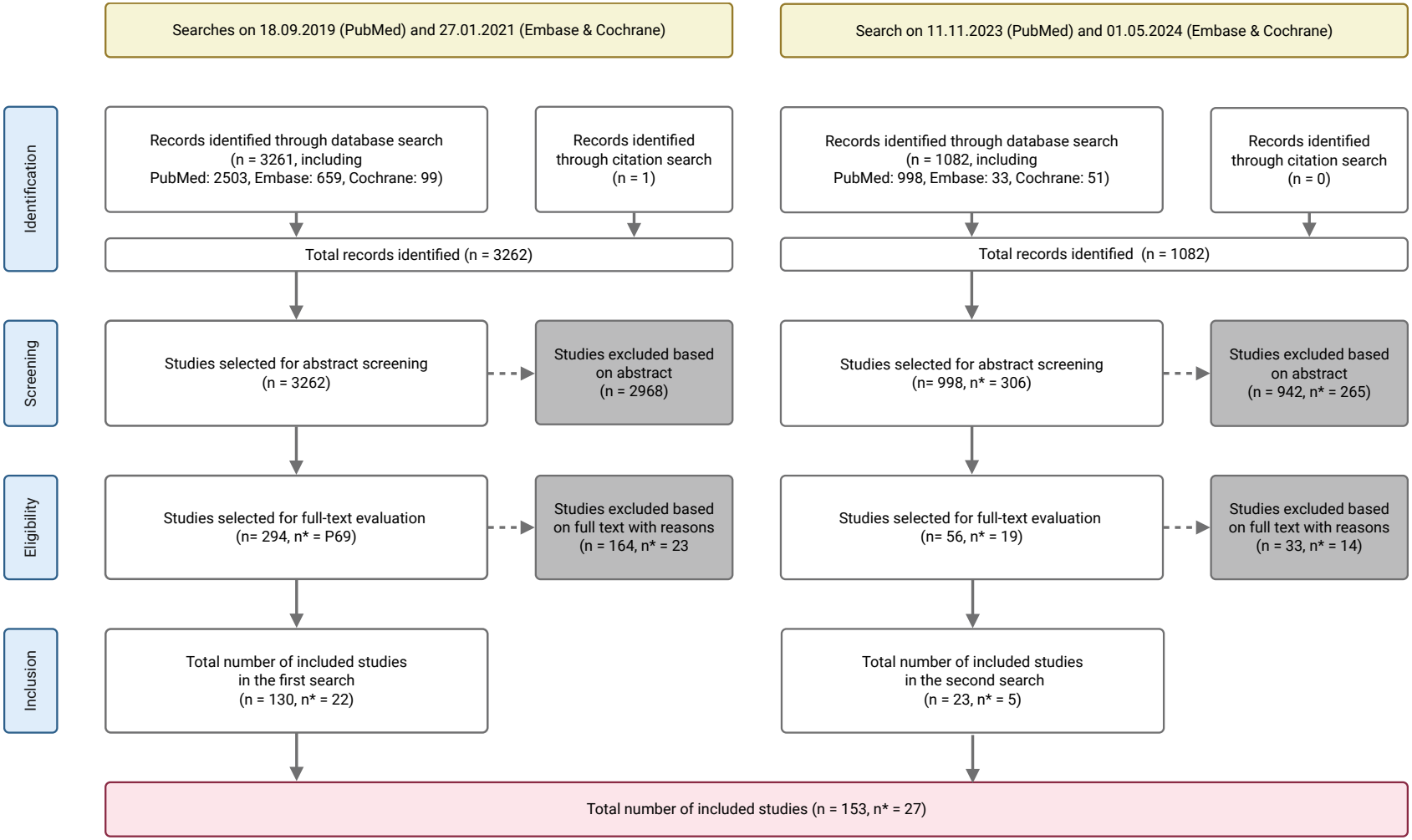

Figure 3.1 Flow chart of the search strategy with results. Values denote the total number of items at each stage (n) and the author's contribution (n*). Figure created with BioRender.com.

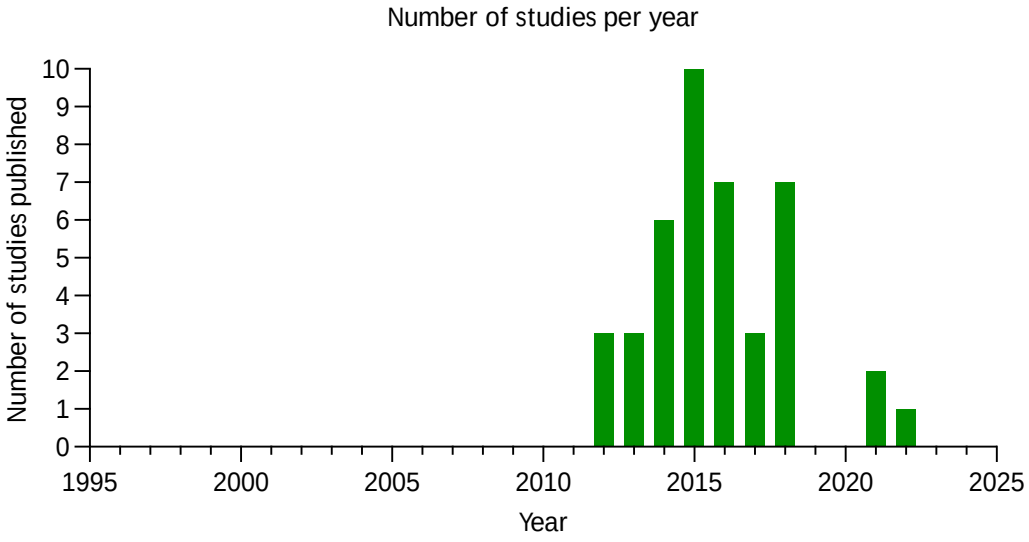

Figure 3.2 Number of studies per year based on studies from which data were extracted by the author. Studies evaluated by other authors are not included.

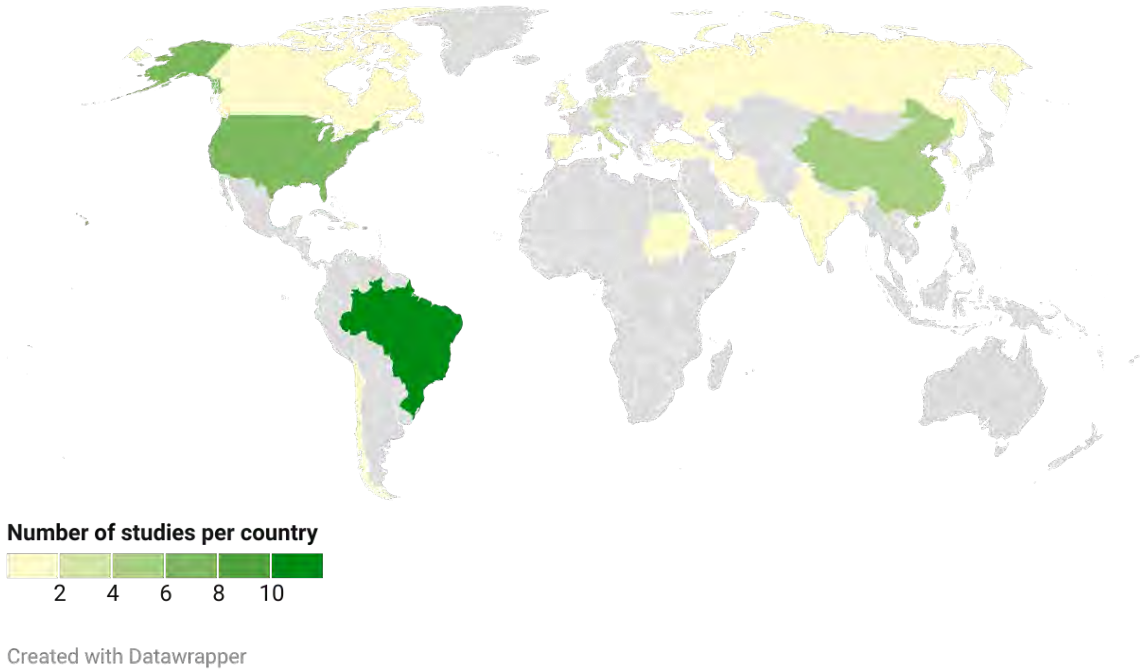

Figure 3.3 Number of studies per country based on studies from which data were extracted by the author. Studies evaluated by other authors are not included. Illustration created with Datawrapper.de.

3.4.1.1 Collection and microbiological assessment of subgingival samples

Methods used for the microbiological assessment varied between the studies. Half of the studies used paper points only to collect subgingival biofilm samples (21, 50.00%) while 19 studies (45.24%) utilised curettes. Only one study used both methods (2.38%). The remaining study (2.38%) did not mention the sample collection method (Figure 3.4A). Most publications analysed pooled samples (24, 57.14% of total), while the remaining ones analysed them individually (17, 40.48% of total) or did not mention analysis strategy at all (1, 2.38% of total) (Figure 3.4B).

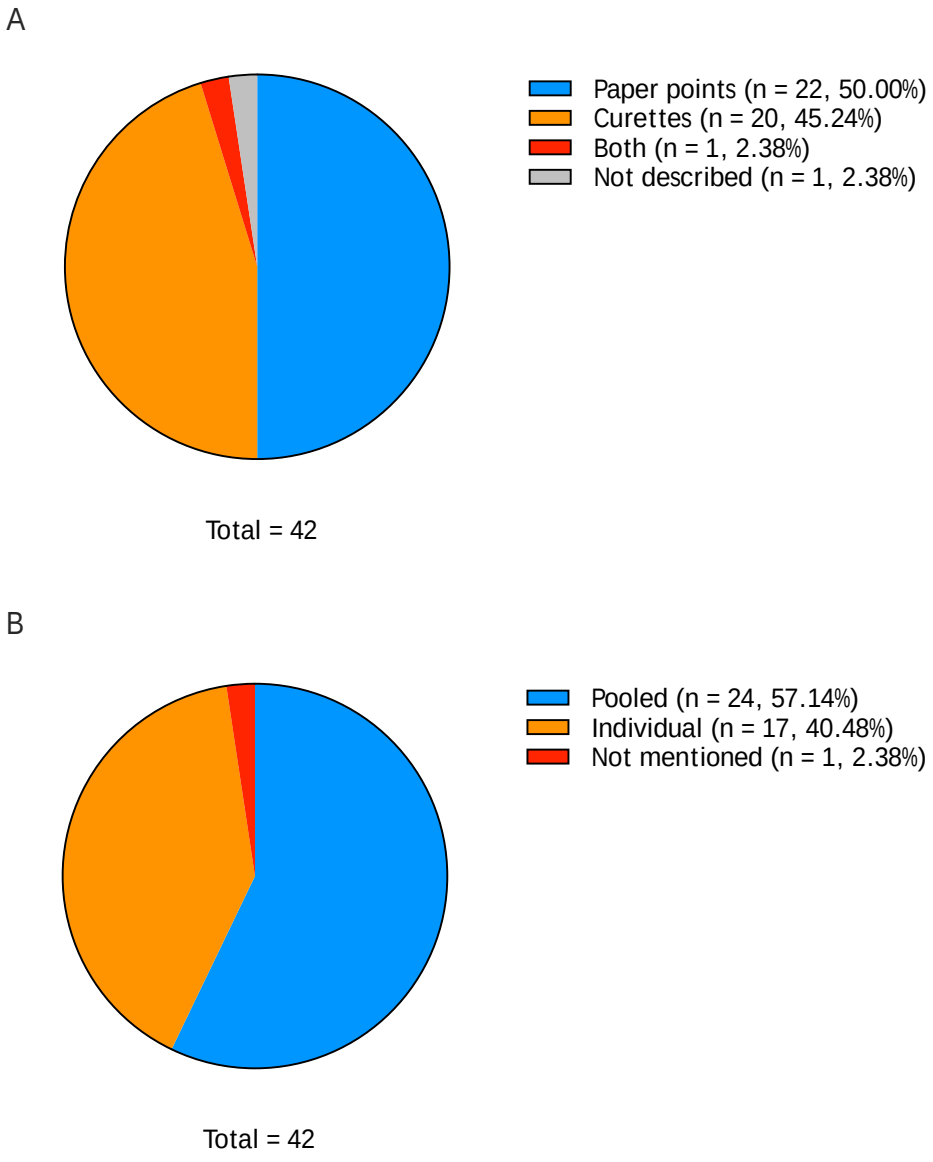

Figure 3.4 Methods used for (A) collection and (B) processing of subgingival biofilm samples.

The majority of studies utilised only one taxa detection method (32, 76.19%), while the others reported using 2 (21.43%) or 3 (2.38%) methods (Figure 3.5A). Sequencing-based approaches, predominantly amplicon sequencing (16S rRNA gene sequencing exclusively) were utilised in 20 studies (38.46%) closely followed by non-sequencing PCR-based methods (conventional, duplex, multiplex, nested and quantitative) that were applied in 17 studies (32.69%). Hybridisation (either checkerboard DNA-DNA hybridisation or microarray) was the third most frequent option used in 10 studies (19.23%) (Figure 3.5B).

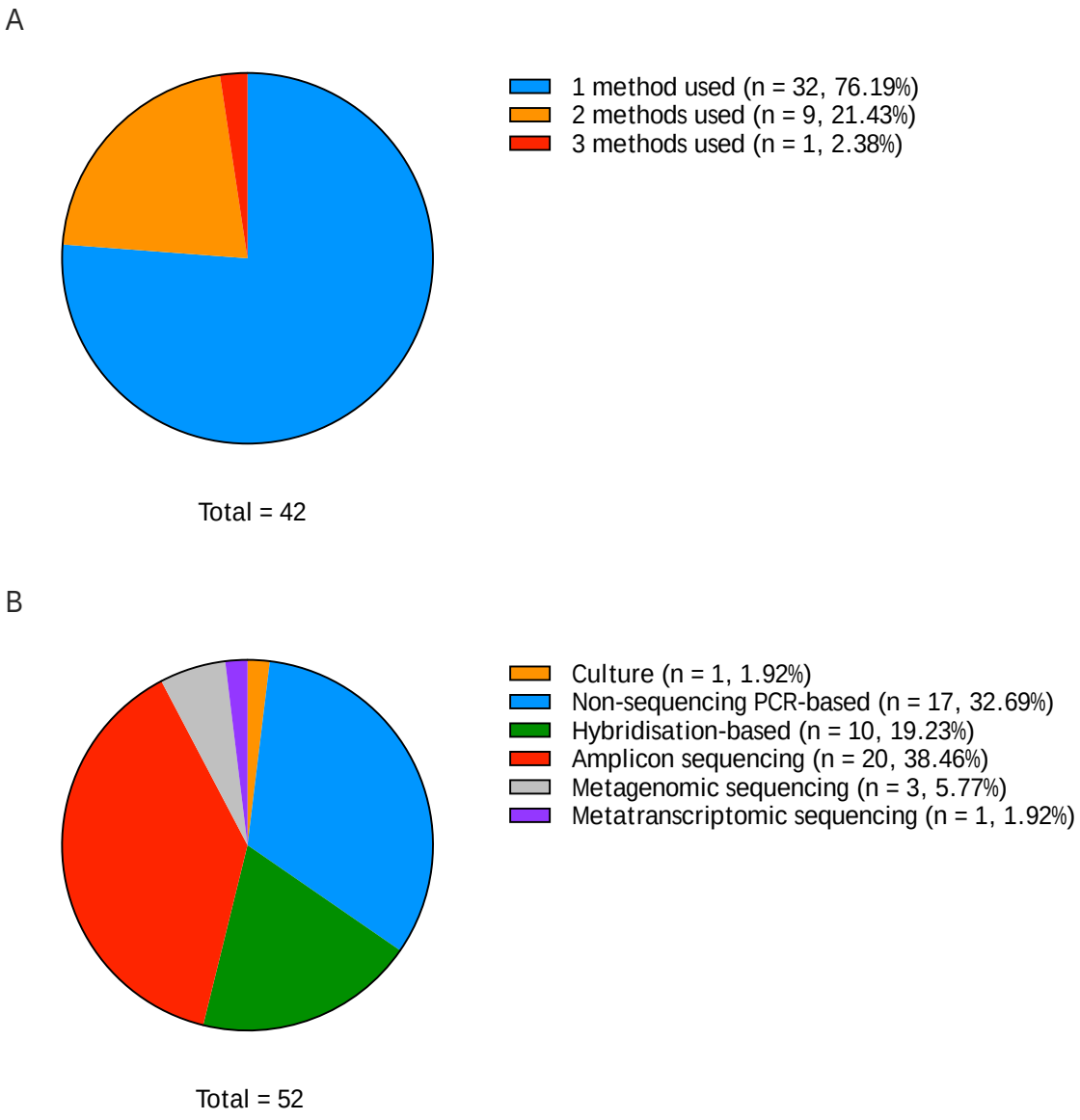

Figure 3.5 (A) Number and (B) types of detection methods used in each study.

3.4.2 Microbial data

There was a variability in taxa associated with periodontal health between the studies.

3.4.2.1 Bacteria associated with health

Most studies (n = 32) did not analyse taxa at the phylum level. Among the few that did, the most frequently reported as more abundant in health were Actinobacteria (3 studies), Proteobacteria (3 studies) and Firmicutes (2 studies) (Table S3). Three studies reported that none of the examined phyla was more abundant in health.

Similarly, the majority of studies (n = 28) did not assess taxa at the genus level. Within the remaining studies, *Corynebacterium* was associated with health in 9 studies, followed by *Actinomyces* (7 studies), *Capnocytophaga* (7 studies) and *Streptococcus* (5 studies) (Table S4). Only a single study suggested that none of the analysed genera were more abundant in health (data not shown).

Interestingly, 20 studies concluded none of the investigated species were associated with health and 7 studies did not evaluate taxa at that level. Species most often associated with health included *Corynebacterium matruchotii* (6 studies*), Cardiobacterium hominis* (5 studies), *Granulicatella adiacens* (5 studies), *Haemophilus parainfluenzae* (5 studies), *Rothia dentocariosa* (5 studies) and *Streptococcus sanguinis* (5 studies) (Table S5).

3.4.2.2 Bacteria associated with periodontitis

Phyla reported to be most abundant in periodontitis included Synergistetes (7 studies), Bacteroidetes (6 studies) and Spirochaetes (5 studies) (Table S6). Of note, all of the studies identified at least one phylum associated with periodontitis.

Filifactor sp. was the most often reported genera (13 studies) next to *Tannerella* sp. (11 studies), *Porphyromonas* (9 studies) and *Treponema* (9 studies)

(Table S7). As with phylum level, all studies reported at least one genus associated with periodontitis (data not shown).

The species most frequently reported to be associated with periodontitis were *Tannerella forsythia* (23 studies), *Porphyromonas gingivalis* (22 studies), *Treponema denticola* (16 studies) and *Filifactor alocis* (15 studies) (Table S8). Three studies reported that none of the species were identified in periodontitis. One study identified that significant differences were lost after adjusting for multiple comparisons (data not shown).

3.5 Discussion

This narrative review aimed to identify taxa present in subgingival plaque that are associated with periodontal health. Such knowledge can establish the reference point for describing the dysbiotic changes that occur during the shift to periodontitis and help to identify commensal communities that support oral homeostasis and potentially prevent dysbiosis.

Most studies provided findings at the species level. The most notable observation was that the most frequently reported periodontitis-associated species, such as the red complex bacteria or *F. alocis,* were indicated roughly 3–4 times more often (Table S8) than the most commonly observed health-associated species (Table S5). The species associated with health identified by both the previous review (Feres et al., 2021) and the current work were: *G. adiacens, S. sanguinis, Rothia aeria, Streptococcus mitis* and *Porphyromonas catoniae.* Species indicated by Feres et al. (2021) as those most associated with health (*Streptococcus* spp., *Capnocytophaga gingivalis* and *Neisseria elongata*) were excluded from the results synthesis as they did not meet the threshold of being reported in at least 3 separate studies. In addition to species identified by Feres et al. (2021), additional species associated with periodontal health were identified. Another review was retrieved, but its search methodology was heavily biased towards already established periopathogens and allowed for inclusion of studies that analysed saliva samples (Antezack et al., 2023). Nevertheless, the results indicated *S. sanguinis*, *S. mitis*, *Corynebacterium matruchotii* and *Peptidiphaga* sp. HMT 183 were associated with health. Among the periodontitis-

associated species, both Feres et al. (2021) and the current work shared 8 out of 25 bacterial species: *Eubacterium brachy, F. alocis, Eubacterium saphenum, Selenomonas sputigena, Dialister pneumosintes, Mogibacterium timidum, Dialister invisus* and *Treponema socranskii*.

A similar pattern regarding the higher frequency and number of reported periodontitis-associated taxa was observed at the genus level (Table S4 and Table S7). Moreover, the most common periodontitis-associated genera identified in this review (*Filifactor*, *Tannerella*, *Porphyromonas* and *Treponema*) were identical to those reported by Feres et al. (2021). Relative prominence of other genera such as *Desulfobulbus*, *Eubacteria*, *Peptostreptococcus*, *Fusobacterium*, *Mycoplasma*, *Prevotella*, *Pseudoramibacter* and *Parvimonas*, that were present in both datasets, differed. Moreover, *Selenomonas* genus was not presented in this chapter's results as it was reported by only one study. The list of health-associated genera listed in this analysis contained more genera, for example *Prevotella*, *Veillonella*, *Granulicatella* and *Lautropia*, but did not contain *Bergeyella* due to being reported by a single study only. Furthermore, *Streptococcus* and *Rothia* reported by Feres et al. (2021) as genera showing the strongest association with periodontal health were less frequently reported by the studies included in this review.

The list of health-associated phyla included more taxa (Table S3), however, in contrast to periodontitis-associated phyla (Table S6), all but one (Firmicutes) were mentioned only by single studies. Of note, Firmicutes were indicated in both groups. When compared to the list of periodontitis-associated phyla in Feres et al. (2021), results of this review include one more phylum – Euryarchaeota.

Taxonomic representation seemed to be imbalanced across studies. Health-associated taxa appeared to be less frequently represented than periodontitis-associated taxa. This imbalance may suggest reporting bias, with disease-associated taxa more frequently reported or emphasised than health-associated taxa. It may also partly reflect methodological detection bias arising from pathogen-focused assay design in targeted non-sequencing approaches, including PCR-based and hybridisation-based methods, where predefined assay targets preferentially included established periopathogens. It could also reflect greater

variability in health-associated subgingival microbiomes, resulting in reduced consistency in taxa identification across studies. The latter interpretation is supported by a study of periodontally healthy individuals, which reported that subgingival microbiome composition varied both between individuals and between sites within the same individual (Tamashiro et al., 2021). Similarly, a study in periodontitis patients found that microbial communities from their clinically healthy sites showed greater diversity and stronger patient-level variation, whereas those from diseased sites appeared more similar across patients (Jorth et al., 2014). In this context, pooling of subgingival plaque samples may also be relevant, as more than half of the included studies combined material from multiple sites rather than analysing each site individually (Figure 3.4B).

In addition to the imbalance in taxonomic representation, differences between taxa indicated by source studies in this review could be attributable to multiple factors related to study design, methods used and geographical variability of the studied populations. Studies adopted multiple definitions of periodontal health and periodontitis that ranged from previously established AAP or Community Periodontal Index of Treatment Needs (CPITN) based criteria to custom, study-specific definitions. Another issue was variability across sampling methods. All studies but one (Zbinden et al., 2014) used either paper points or a curette (Figure 3.4A). One study even used different curettes for healthy and periodontitis subjects (You et al., 2013). Subgingival biofilm samples obtained with a curette contain proportionately more bacterial DNA and less human DNA (Pérez-Chaparro et al., 2015), and display higher microbial diversity (Beyer et al., 2017) compared to samples obtained with a paper point. Furthermore, unused paper points were found to exhibit varying amounts of DNA contamination (Beyer et al., 2017). Curette-collected samples yield higher proportions of *Corynebacterium*, *Prevotella*, *Selenomonas*, *Actinomyces, Treponema* and *Clostridiales* family XIII *incertae sedis*, while paper point-collected samples show elevated proportions of *Streptococcus*, *Gemella*, *Parvimonas*, *Haemophilus* and *Aggregatibacter* (Beyer et al., 2017). Another study demonstrated that although there is no difference in detection levels of red complex species, *Aggregatibacter actinomycetemcomitans* is more reliably detected with paper points (Belibasakis et al., 2014). Another factor, perhaps

the most influential, is that source studies employed a wide range of detection methods that included both targeted and open-ended approaches (Figure 3.5B). While the former are limited by predefined targets, the latter can identify a significantly higher number of taxa, although they are still restricted by the coverage, resolution, curation quality and update frequency of the reference database. An additional consideration is that differences were observed at the population level. Study cohorts differed in their mean ages, and aging has been show to affect the composition of the subgingival microbiome in healthy individuals (Akatsu et al., 2025). Moreover, the geographical origin of the populations also differed (Figure 3.3). A recent study concluded that the country of origin affected beta diversity more than the diagnosis (Arredondo et al., 2025). An interesting example is an observation that all studies suggesting that *Enterococcus faecalis* could be a periodontal pathogen, were conducted on Brazilian populations (Pérez-Chaparro et al., 2014).

The discrepancies between findings in this and review by Feres et al. (2021) may arise due to extracting data from only partially overlapping source publications; the review by Feres et al. (2021) included 20 studies in total, of which 12 studies were used in this review (Table S9). Moreover, all of these 20 studies used next-generation sequencing. This review additionally included studies that utilised targeted non-sequencing approaches such as PCR or hybridisation-based techniques that tend to be biased toward predefined targets and are unable to detect unknown species (Figure 3.5B). Furthermore, the authors of the aforementioned review did not describe their approach to analyse the extracted data, especially the criteria they used to rank the most common taxa.

A clear shortcoming of this review is that it was restricted to studies assigned to the author for data extraction within the systematic review, which was a group project. Nonetheless, it included a substantial number of relatively recent studies across diverse populations. Regions with major research hubs such as Brazil, USA or China were noticeably overrepresented (Figure 3.3). Another limitation is variability in case definitions and detection methods, which makes it difficult to directly compare the studies and to generalise the findings. Application of a cutoff allowed for exclusion of sporadic detections of non-oral bacteria such as *Mycobacterium leprae*, *Mycobacterium tuberculosis* (Dabdoub et al., 2016) or *Yersinia pestis* (Szafrański et al., 2015a), likely attributable to

taxonomic misclassification, reagent or cross-sample contamination. This could, however, lead to the exclusion of some rare taxa.

In addition to taxonomic profiling, a parallel assessment of microbiome functional activity could contribute to a more comprehensive understanding of the role of the subgingival microbiome in maintaining periodontal health. Metatranscriptomic studies suggest that individual species may exhibit context-dependent roles within the microbial community. A study comparing periodontally healthy individuals with periodontitis patients found that disease-associated subgingival communities were characterised by increased expression of genes involved in iron acquisition, LPS synthesis and flagellar synthesis. Interestingly, many upregulated genes encoding putative virulence factors were expressed by taxa not usually regarded as major periodontal pathogens, such as *R. dentocariosa* and *C. matruchotii*, suggesting that disease-associated activity is not restricted to traditionally recognised periodontal taxa (Duran-Pinedo et al., 2014). In a separate study, conserved metabolic differences were reported between microbial communities from clinically healthy sites and diseased pockets within the same periodontitis patients. Diseased communities showed increased expression of pathways related to fermentation and amino-acid catabolism, such as lysine fermentation to butyrate, pyruvate fermentation and histidine catabolism. However, the microbial species contributing to some of these metabolic pathways varied between patients (Jorth et al., 2014). Together, these findings suggest that differences between health and periodontitis may be more consistent at the level of community function than at the level of individual taxa, which could partly explain variability in taxa identified between periodontal health and periodontitis groups in this review.

Within limitations of this study, the findings suggest that the composition of a core periodontal health-associated subgingival microbiome may be not so well defined as that of the periodontitis-associated one. Further studies are needed, preferably using standardised case definitions, sampling methodology and open-ended detection approaches. Such knowledge could guide the design of novel diagnostic and risk assessment tools, as well as the development of preventive and therapeutic strategies focused on restoring ecological balance within the subgingival microbiome.

3.6 Summary and findings

Are there microbial species or taxa associated with periodontal health?

- There are microbial taxa at the phylum, genus and species level that correlate with periodontal health.

These findings corroborate the hypothesis that the subgingival microbiome associated with periodontal health differs when compared to periodontitis.

4 Designing and growing biofilms resembling the human subgingival microbiome associated with health and disease

4.1 Introduction

4.1.1 Role of bacteria in periodontal health

Bacterial colonisation of the oral cavity is essential for maintaining health (Chang et al., 2021). The commensal microbial community within the subgingival plaque occupies the ecological niche constraining available nutrients and limiting binding sites, as well as directly inhibiting the growth of pathogenic species through antimicrobial peptides, thus protecting its host against invading pathogens. There is evidence that subgingival plaque biofilm contributes to immune surveillance and modulates host immune response, supporting healthy oral tissue homeostasis (Chang et al., 2021).

The new 2017 classification scheme for periodontal and peri-implant diseases and conditions acknowledges that that there is a certain 'composition' of subgingival microbiota compatible with gingival health where 'commensal organisms (…) coexist in relative harmony' (Lang and Bartold, 2018). During the shift to periodontitis, this eubiotic microbial community transitions into a dysbiotic one (Lamont et al., 2018, Hajishengallis et al., 2023). Several microbiome studies identified species and genera associated with periodontal health and disease (Abusleme et al., 2013, Feres et al., 2021, Pérez-Chaparro et al., 2014).

4.1.2 *In vitro* modelling of the transition from health to periodontitis through bacterial biofilms

A number of *in vitro* multi-species subgingival biofilm models were developed to explore either a transition from health to periodontitis or to compare characteristics between these two states (see Table 4.1). Janus et al. (2015) modified the Amsterdam Active Attachment model (Exterkate et al., 2010) by

utilising individual and pooled saliva inocula collected from 10 healthy donors. Different buffered semi-defined McBain media compositions – plain or with 10% foetal calf serum (FCS) – were used to differentiate biofilms towards health and periodontitis phenotypes, respectively. Although addition of FCS did not change the biofilm composition, it induced phenotypic differentiation characterised by higher general and specific gingipain protease activities, implying the role of environmental conditions during the shift from health to periodontitis. The 10-species Zurich subgingival biofilm model (Guggenheim et al., 2009) was a modified and expanded version of the earlier 6-species supragingival model (Shapiro et al., 2002). The initial 'supragingival' composition was modified by removing 3 species and adding another 6 species to resemble marginal and subgingival plaque. This model was further developed by evaluating how different culture conditions influenced its composition; biofilms grown in medium containing 50% HI serum resembled more *in vivo* biofilms in periodontitis patients (Ammann et al., 2012). Both models were used not only to study microbial characteristics within biofilms, but also in co-cultures with human epithelial cells to investigate host-microbe interactions (Belibasakis et al., 2013, Belibasakis et al., 2015). Thurnheer et al. (2016) combined both Zurich models into an integrated system to investigate changes in composition and structure occurring during conversion from supragingival to subgingival biofilm (as deep pockets emerge) by means of sequential addition of species accompanied by the gradual change of atmospheric conditions. This approach revealed dynamic structural shifts in characteristics such as specific species counts, biofilm thickness, extracellular polysaccharide presence and biofilm viability. Peyyala et al. (2011b) developed a panel of 3 independent multi-species bacterial biofilms to reflect subgingival biofilm found in 3 distinct environments: healthy sulci, inflamed gingiva and periodontitis. Here, rigid gas-permeable hard contact lenses were used as a support for the biofilms to allow for the equilibration of the gaseous environment at the biofilm-epithelial interface in an ensuing co-culture model (Peyyala et al., 2011a, Peyyala et al., 2012). Finally, Brown et al. (2023) and Millhouse (2015) designed a set of 3 multi-species bacterial biofilms with a shared sequential protocol for 3-, 7- and 10-species biofilms associated with health, gingivitis and periodontitis, respectively. In this case, all biofilm types were cultured in an aerobic environment at first, but introduction of additional species and concurrent

transition from a healthy state to periodontitis required relocating the biofilms to anaerobic conditions.

Table 4.1 Subgingival biofilm model systems including at least two different conditions.

Biofilm model system	Surface	Media	Culture conditions	Health model	Intermediate/gingivitis model	Periodontitis/Disease model
Amsterdam Active Attachment model (Janus et al., 2015)	12 mm glass coverslips	Buffered semi-defined McBain media	Anaerobic (80% N_2, 10% CO_2, and 10% H_2)	Saliva inoculum from 10 healthy donors (individual and pooled) added to plain medium	N/A	Saliva inoculum from 10 healthy donors (individual and pooled) added to medium with 10% FCS
6- & 10-species Zurich model (Ammann et al., 2012, Guggenheim et al., 2009, Shapiro et al., 2002)	10.6 mm HA discs (pellicle-coated)	Initial: 60% saliva, 30% mFUM (0.3% glucose) 10% human serum Modification: 50% human serum, 50% mFUM (4 mM glucose)	Anaerobic (80% N_2, 10% CO_2, and 10% H_2)	6 species to model supragingival biofilm: *S. oralis,* *A. oris/naeslundii,* *V. dispar, F. nucleatum,* *S. mutans, C. albicans* (added later)	N/A	10 species to model subgingival biofilm: *S. oralis, A. oris/naeslundii,* *V. dispar, S. intermedius,* *C. rectus, F. nucleatum* subsp. *vincentii,* *P. intermedia, P. gingivalis,* *T. forsythia, T. denticola*
Modified 12-species Zurich model (Thurnheer et al., 2016)	9 mm HA discs (pellicle-coated)	Phase 1: 70% saliva, 30% mFUM (0.3% glucose) Phase 2&3: 60% saliva, 10% human serum, 30% mFUM (0.3% glucose)	Phase 1: Aerobic Phase 2: Anaerobic (80% N_2, 10% CO_2, and 10% H_2), but manipulations under aerobic Phase 3: Anaerobic (80% N_2, 10% CO_2, and 10% H_2)	Phase 1: 6 species to model supragingival biofilm: *A. oris/naeslundii,* *V. dispar, F. nucleatum,* *S. mutans, S. oralis,* *C. albicans*	Phase 2: Phase 1 + 3 species to model intermediate phase: *C. rectus, P. intermedia,* *S. anginosus*	Phase 3: Phase 2 + 3 species to model subgingival biofilm: *P. gingivalis, T. forsythia,* *T. denticola*

Biofilm model system	Surface	Media	Culture conditions	Health model	Intermediate/gingivitis model	Periodontitis/Disease model
3 × 3-species Kentucky models (Peyyala et al., 2011b)	10.5 mm rigid gas permeable contact lenses (1% FBS in PBS-coated)	Supplemented BHI medium	Anaerobic (85% N_2, 10% H_2, 5% CO_2) at 37 °C	Subgingival biofilm in healthy sulci: *S. gordonii, S. oralis, S. sanguinis*	Subgingival biofilm related to gingivitis *S. gordonii, A. naeslundii, F. nucleatum*	Combination of pioneer, bridging and periopathogenic species: *S. gordonii, F. nucleatum, P. gingivalis*
3-, 7- & 10-species Glasgow models (Brown et al., 2023, Millhouse, 2015)	Thermanox 13 mm coverslips	THB:RPMI (1:1) mix	Health: Aerobic (5% CO_2) Gingivitis & Periodontitis: Anaerobic (85% N_2, 10% CO_2 and 5% H_2)	3-species biofilm associated with health: *S. intermedius, S. oralis, S. mitis*	7-species biofilm associated with gingivitis: Species associated with health and: *A. naeslundii, V. dispar, F. nucleatum* ssp. *polymorphum, F. nucleatum* ssp. *vincentii*	10-species biofilm associated with periodontitis: Species associated with health, gingivitis and: *A. actinomycetemcomitans, P. intermedia, P. gingivalis*

BHI, brain heart infusion; FBS, foetal bovine serum; FCS, foetal calf serum; HA, hydroxyapatite; mFUM, modified fluid universal medium; RPMI, Roslin Park Memorial Institute 1640 medium; THB, Todd–Hewitt broth.

4.1.3 Limitations of currently used *in vitro* biofilm model systems and importance of nitrate-reducing species in periodontal health.

Most biofilm model systems mimic the properties of the periodontitis environment rather than that of periodontal health, with the latter serving merely as a baseline control condition. Recently, nitrate reduction capacity has been suggested to be beneficial for oral homeostasis (Rosier et al., 2022) due to its *in vitro* and *in vivo* dysbiosis-lowering properties (Chen et al., 2022). Moreover, it was reported that periodontitis patients had lower levels of nitrate-reducing bacteria in subgingival plaque compared with healthy controls, and that these increased following treatment and correlated negatively with bacteria associated with periodontitis (Rosier et al., 2024).

Numerous studies and reviews (Feres et al., 2021, Meuric et al., 2017) concluded that *Rothia* and *Neisseria* spp. were associated with health. Many members of their genera are also known nitrate reducers, including *R. dentocariosa* and *N. mucosa* (Barth et al., 2009, Rosier et al., 2020, Rosier et al., 2022). An original study by Abusleme et al. (2013) concluded that the *Rothia* genus was most positively correlated with health, with *R. dentocariosa* numerically dominating the health-associated communities. Results of studies on the effects of experimental gingivitis suggest that the changes in *R. dentocariosa* levels occur in the early stages of periodontal disease. In a study by Kistler et al. (2013), *R. dentocariosa* detected in subgingival plaque was significantly reduced among bacteria species after one and two weeks of experimental gingivitis and was negatively correlated with bleeding on probing (BoP). Another group reported that levels of *R. dentocariosa* consistently decreased over the period of 28 days of experimental gingivitis (Huang et al., 2021a). *N. mucosa* is not as well characterised, but analysis of the oral metagenomes from the Human Microbiome Project revealed that *N. mucosa* populates gingival plaque (Donati et al., 2016). Fukuda et al. (2024) demonstrated that *Neisseria* spp. inhibit *P. gingivalis* invasion into human gingival epithelial Ca9-22 cells *in vitro,* with *N. mucosa* being notably effective. SEM image analysis of a pre-mixed culture system showed interactions between both species, but the specific mechanisms involved remain unknown. There is increasing recognition that defining,

understanding and studying health is as important as studying disease, exemplified by the inclusion of 'periodontal health' for the first time in a classification system in the most recent 2017 classification system.

4.1.4 Designing an *in vitro* model associated with health

In this thesis, a novel 5-species biofilm model was developed to mimic periodontal health *in vitro*. Species present in a previously developed Glasgow 3-species biofilm model (*S. intermedius*, *S. mitis*, and *S. oralis*) (Brown et al., 2023), were retained, given that they are all members of Socransky's yellow complex consisting of early colonisers (Socransky et al., 1998), and that *Streptococcus* is among the genera most commonly associated with periodontal health (Feres et al., 2021). Moreover, two additional health-associated species were incorporated: *N. mucosa* and *R. dentocariosa* due to their associations to periodontal health described recently (see Section 4.1.3). Consistent with this, *S. mitis*, *S. oralis* and *N. mucosa* levels were shown to significantly increase in subgingival plaque of healthy subjects during early microbial succession, with significant increases observed within 7 days without oral hygiene following a full-mouth scaling and root planing (Teles et al., 2012). Taken together, these studies support the role of *S. intermedius*, *S. mitis*, *S. oralis, N. mucosa* and *R. dentocariosa* in the establishment of a health-associated subgingival biofilm and provide a rationale for their inclusion in the *in vitro* biofilm model.

4.1.5 Choosing an *in vitro* model associated with periodontitis

An already established Glasgow 10-species biofilm model (Brown et al., 2023, Millhouse, 2015) was used to emulate the periodontitis-associated microbial biofilm. Earlier studies had demonstrated its ability to induce a pro-inflammatory response in a co-culture with three-dimensional human gingival epithelium model and peripheral blood mononuclear cells or isolated $CD14^+$ monocytes. It was also shown that addition of nitrate during 10-species biofilm growth reduced the numbers of periodontitis-associated bacteria – *F. nucleatum*, *A. actinomycetemcomitans* and *P. gingivalis* (Mazurel et al., 2023).

4.2 Hypothesis and research questions

Hypothesis: There are key differences between health- and periodontitis-associated subgingival biofilms contributing to the integrity of the oral barrier and they can be emulated *in vitro*.

The research questions raised to evaluate this hypothesis included:

1. Can an *in vitro* biofilm reflect some of the key characteristics of a subgingival biofilm associated with a healthy oral barrier such as:

    a. composition?

    b. microarchitecture and structure?

    c. metabolism (nitrate reduction capacity)?

4.3 Results

Preliminary experiments were undertaken to establish a methodology for preparation of the *N. mucosa* suspension for its subsequent incorporation into the 5-species biofilm model associated with periodontal health. This included assessment of *N. mucosa* growth kinetics and viable enumeration to determine the OD_{600} values corresponding to the target bacterial concentration. Viable enumeration of bacteria used for biofilm growth was performed using the Miles and Misra method to confirm the viability of stored bacterial stocks and verify OD-based standardisation. The previously developed 3-species biofilm model associated with health was subsequently expanded by the addition of two more nitrate-reducing species: *N. mucosa* and *R. dentocariosa*. Different 5-species biofilm seeding protocols were evaluated before two variants were selected for further assessment. The Glasgow 10-species biofilm model (Brown et al., 2023, Connolly et al., 2017) was utilised to represent periodontitis conditions *in vitro*. Additionally, a *P. gingivalis* mono-species biofilm was included as a negative control for nitrate reduction in the Griess reaction assay, as *P. gingivalis* is not a known nitrate reducer (Dahlén et al., 2007). In addition to qPCR-based compositional analysis, all biofilms underwent assessment of microarchitecture and structure by SEM, nitrate reduction capacity by the Griess assay, and total biomass by the crystal violet assay.

4.3.1 Optimisation of culture quantification and analytical methods

4.3.1.1 Assessment of *N. mucosa* growth kinetics

The growth kinetics of *N. mucosa* were evaluated by monitoring OD_{600} at hourly intervals over 24 hours to identify the midpoint of the exponential growth phase. Analysis of the growth curve (Figure 4.1) suggested that this occurred during the 5^{th} hour. This time point was then used to prepare a standardised suspension of actively growing *N. mucosa* for the Miles and Misra assay.

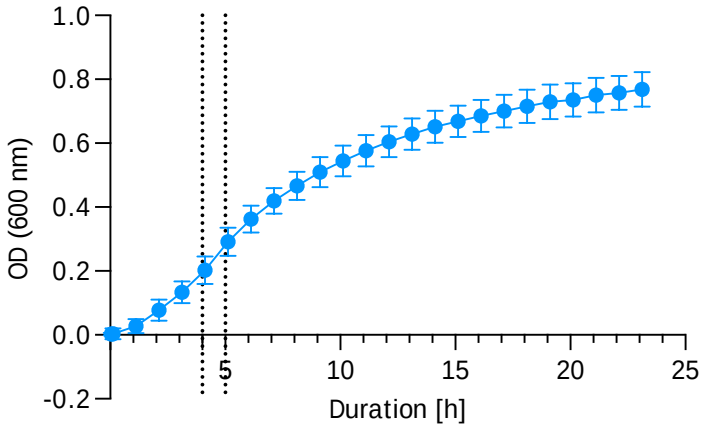

Figure 4.1 Planktonic growth of *N. mucosa* (NCTC 12978) over time. Bacterial planktonic suspension was adjusted to an OD_{600} of 0.01 in TSB and grown for 24 hours at 37 °C in 5% CO_2. The absorbance was measured automatically every hour at 600 nm. Values were corrected for media background. The log phase midpoint (shown between the dotted lines) was identified by calculating hourly bacterial growth rate and identifying the highest value. Data represent mean ± SD of 24 technical replicates from a single experiment (n = 1).

4.3.1.2 Enumeration of *N. mucosa* to determine corresponding OD values

The Miles and Misra method (Miles et al., 1938) was adopted to determine the OD_{600} value corresponding to a *N. mucosa* concentration of 1×10^7 CFU/mL for use in subsequent 5-species biofilm growth experiments. A suspension of actively growing *N. mucosa* was prepared at the midpoint of the log phase between 4 and 5 hours, as identified in the preceding section. The suspension was then adjusted in PBS to an OD_{600} of 0.05 and serially diluted before viable counts were determined using the drop plate method. Only two dilutions produced between 50 and 200 colonies per spot. Total dilution factors of 1600 and 3200 yielded averages of 124.67 ± 3.06 and 71.33 ± 14.47 colonies per spot, respectively. The corresponding numbers of CFU per mL were $1.99 \times 10^7 \pm 5.13 \times 10^5$ and $2.28 \times 10^7 \pm 4.66 \times 10^6$ (Figure 4.2). The results showed that the initial planktonic *N. mucosa* suspension standardised to an OD_{600} of 0.05 in PBS contained $2.14 \times 10^7 \pm 3.36 \times 10^6$ CFU per mL on average; hence, an OD_{600} of 0.025 was further used to obtain 1×10^7 CFU/mL.

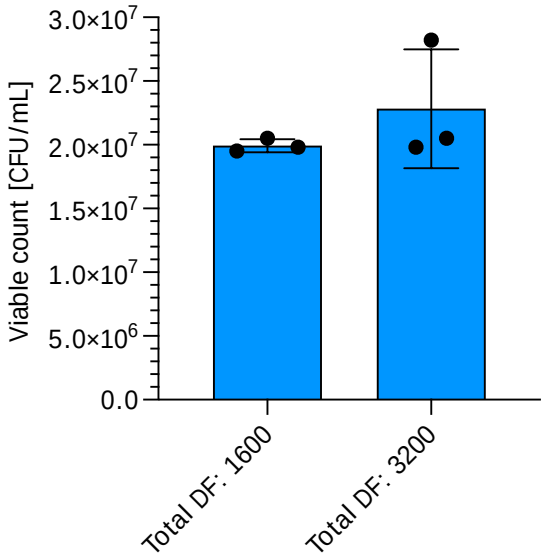

Figure 4.2 Enumeration of standardised *N. mucosa* (NCTC 12978) suspensions. Bacterial planktonic suspension was adjusted to an OD_{600} of 0.05 in PBS followed by a two-stage dilution method. The resulting sets of dilutions were drop-plated and grown for 24 hours at 37 °C in 5% CO_2. The colonies were then counted at each dilution that resulted in growth of between 50 and 200 colonies per spot. The number of CFU per mL was calculated using the following formula: CFU/mL=(No. of colonies)x(DF)/(Volume in mL). Data represent mean ± SD of technical triplicates from a single experiment (n = 1). DF, dilution factor.

4.3.1.3 Enumeration of species used in 5- and 10-species biofilms

The Miles and Misra method (Miles et al., 1938) was also applied to confirm the viability of stored stocks of bacteria used for the preparation of 5- and 10-species biofilms and to verify that OD-based standardisation yielded the expected viable counts. All species except *N. mucosa* were adjusted in PBS to their respective OD_{550} values listed in Table 2.2, corresponding to a target concentration of 1×10^8 CFU/mL. *N. mucosa* was adjusted to the OD_{600} value determined in the preceding section, corresponding to a target concentration of 1×10^7 CFU/mL. The suspensions were then serially diluted and viable counts were determined using the drop plate method. The results (Figure 4.3) show the concentration of viable bacteria, expressed as $\log_{10}$ CFU/mL, present in the suspensions used for biofilm culture.

For *N. mucosa* and *P. gingivalis*, the colony counts fell outside the preferred range of 50–200 colonies per spot at the dilutions tested. Although these values were retained in the final CFU/mL calculations, the resulting viable count estimates should be interpreted with caution. Estimated viable counts were $3.33x10^8 \pm 1.62x10^8$ CFU/mL and $4.43x10^8 \pm 8.5x10^7$ CFU/mL, respectively. No visible colonies were detected for *P. intermedia* under the conditions used for

Miles and Misra plating. In this single experiment, viable counts for the remaining bacterial suspensions ranged from $1.73 \times 10^5 \pm 5.69 \times 10^3$ CFU/mL for *F. nucleatum* subsp. *polymorphum* to $1.88 \times 10^8 \pm 5.86 \times 10^6$ CFU/mL for *S. intermedius*, despite adjustment to the target optical density.

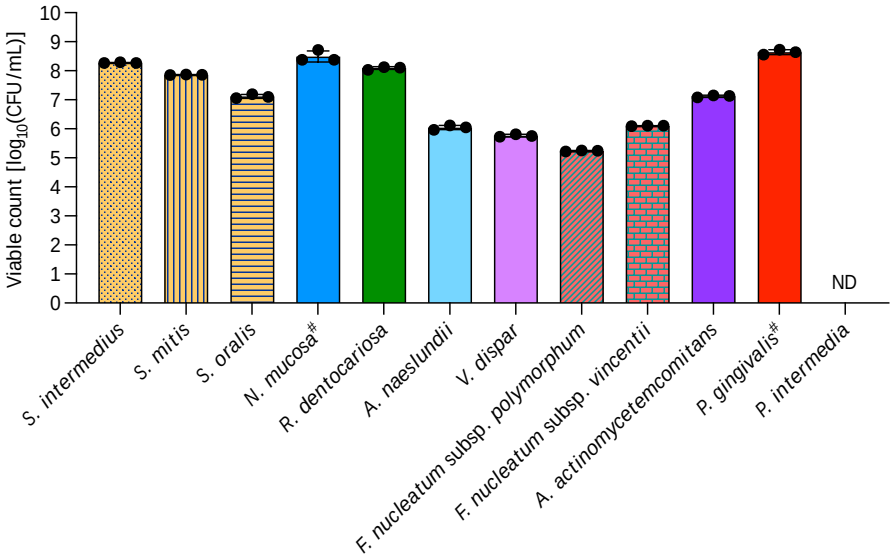

Figure 4.3 Enumeration of standardised bacterial suspensions. Planktonic monocultures of *S. intermedius, S. mitis, S. oralis, N. mucosa, R. dentocariosa, V. dispar, F. nucleatum* subsp. *polymorphum, F. nucleatum* subsp. *vincentii, A. actinomycetemcomitans, P. gingivalis,* and *P. intermedia* were cultured in appropriate broths and adjusted in PBS to target concentrations of 1×10^8 CFU/mL, except for *N. mucosa*, which was adjusted to 1×10^7 CFU/mL. Viable bacteria were quantified using the Miles and Misra drop plate method. Hash symbols (#) indicate species (*N. mucosa and P. gingivalis*) for which colony counts fell below the preferred range of 50–200 colonies per spot at the dilutions tested, but were retained in the final CFU/mL calculations. ND denotes no visible colonies detected for *P. intermedia*. Viable counts were expressed as CFU/mL and calculated using the following formula:
CFU/mL = average no. of colonies per spot × DF / volume plated (mL). Data represent mean ± SD of $\log_{10}$-transformed CFU/mL values from technical triplicates in a single experiment (n = 1), with individual technical replicate values shown as symbols. DF, dilution factor.

4.3.1.4 Optimisation and evaluation of qPCR standard curves

The endpoint composition of all bacterial biofilms following freezing and revival was examined using SYBR-based qPCR. Initially, two standard curves were generated for each species to compare bacterial load with DNA recovery and subsequent quantification. The bacterial standard curve was generated from a ten-fold dilution series of bacterial suspensions, whereas the DNA standard curve was derived from ten-fold dilutions of DNA extracted from the highest-concentration bacterial suspension. Both dilution series were analysed by qPCR to obtain Cq values.

Initial standard curves were generated by plotting Cq values against log_{10}-transformed CFE/mL values and then optimised using iterative residual-based linear regression with sequential removal of outlying data points (Figure S1). In the *A. naeslundii* bacterial dilution series, this process resulted in only two data points remaining; thus, an additional alternative analysis was performed in which data points for 10^2, 10^3 and 10^4 CFE/mL dilutions were removed first due to the flattened shape of the curve. In this single experiment, the first simple linear regression yielded higher R^2 values for dilution series obtained directly from the DNA extracts compared with those generated from DNA extracted from bacterial suspension dilution series. This may reflect a possible reduction in DNA extraction efficiency at lower CFE/mL concentrations and/or reduced amplification efficiency. The performance of both final qPCR standard curves generated by simple linear regression (Figure 4.4) was further evaluated by assessing their linear dynamic range and amplification efficiency (see Table S10 and Table S11). The curves obtained from the dilution series of DNA extracts were then used to determine the composition of all bacterial biofilms.

S. intermedius - final SLR

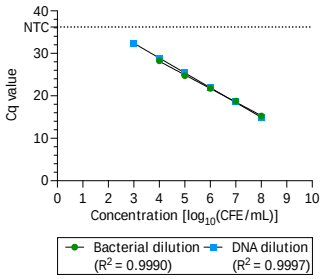

S. mitis - final SLR

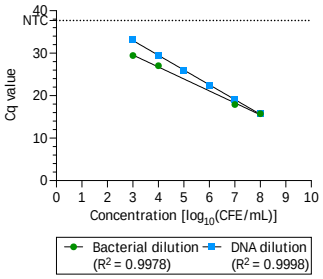

S. oralis - final SLR

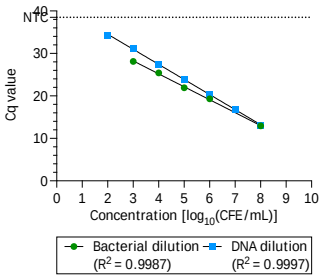

Streptococcus spp. - final SLR

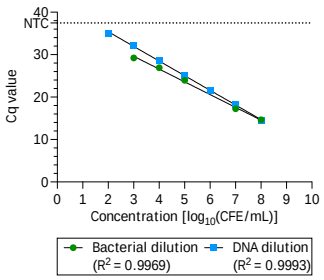

N. mucosa - final SLR

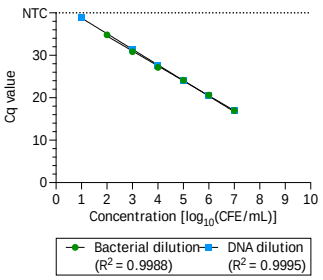

R. dentocariosa - final SLR

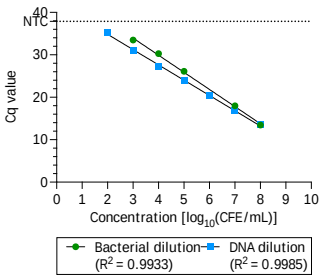

A. naeslundii - final SLR

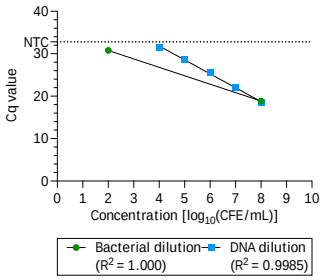

A. naeslundii - final SLR*

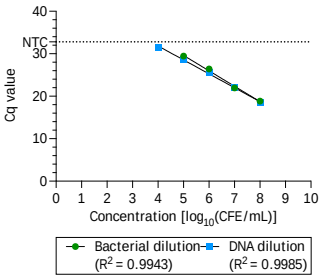

V. dispar - first & final SLR

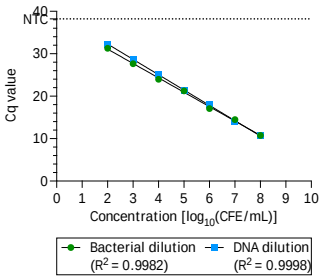

F. nucleatum subsp. *polymorphum* - final SLR

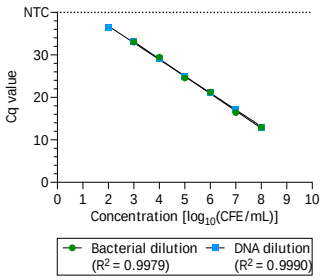

F. nucleatum subsp. *vincentii* - final SLR

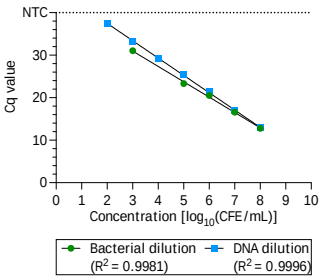

Transform of Fusobacterium spp. - final SLR

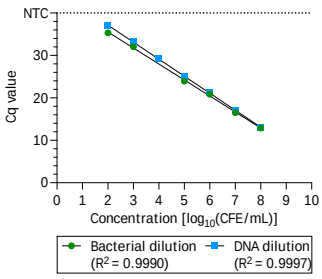

A. actinomycetemcomitans - final SLR

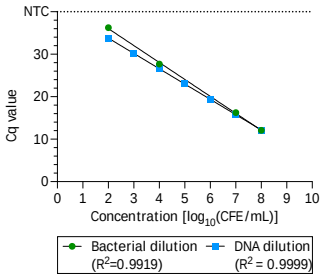

P. gingivalis - final SLR

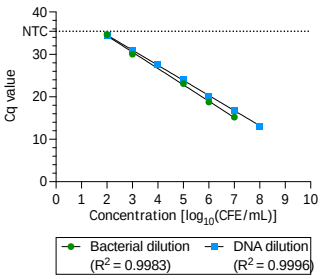

P. intermedia - final SLR

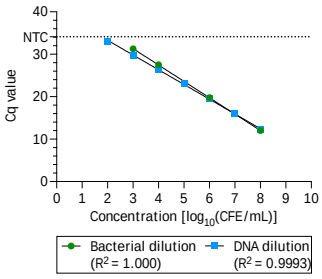

Figure 4.4 Generation of species-specific and genus-level qPCR standard curves. Planktonic monocultures of *S. intermedius, S. mitis, S. oralis, N. mucosa, R. dentocariosa, A. naeslundii, V. dispar, F. nucleatum* subsp. *polymorphum, F. nucleatum* subsp. *vincentii, A. actinomycetemcomitans, P. gingivalis,* and *P. intermedia* were cultured in appropriate broths and adjusted in PBS to target concentrations of 1×10^8 CFE/mL, except for *N. mucosa*, which was adjusted to 1×10^7 CFE/mL. Bacterial suspensions were serially diluted ten-fold before DNA extraction. Additional sets of ten-fold dilutions were prepared from the DNA extracts obtained from the highest-concentration bacterial suspensions. Both dilution series were analysed using qPCR. Standard curves were generated by plotting Cq values against $\log_{10}$-transformed CFE/mL values and fitted using simple linear regression, with iterative residual-based removal of outlying data points. R^2 values indicate the goodness of fit of the final optimised regression models. For *V. dispar*, the first SLR also met the final acceptance criteria and no data points were removed from any dilution series. For *A. naeslundii*, sequential optimisation of the bacterial dilution series yielded only two remaining data points; therefore, an additional alternative analysis, denoted by an asterisk (*), was performed in which the 10^2, 10^3 and 10^4 CFE/mL data points were removed first due to the flattened shape of the curve. For each species, two dilution series were run on a single occasion (n = 1) in duplicate on the same plate under identical conditions, with a single shared set of NTCs (4 wells). Additional genus-level standard curves and corresponding NTC values were generated for *Streptococcus* spp. from the mean Cq values of *S. intermedius, S. mitis*, and *S. oralis*, and for *Fusobacterium* spp. from the mean Cq values of *F. nucleatum* subsp. *polymorphum* and *F. nucleatum* subsp. *vincentii*. A dotted line on each graph denotes the mean Cq value for the NTCs. NTC, no-template control; SLR, simple linear regression.

4.3.2 Developing *in vitro* bacterial biofilm models associated with periodontal health and disease

4.3.2.1 Evaluation of 5-species biofilm seeding protocols

Multiple variants of a 5-species biofilm protocol were evaluated to identify the optimal configuration for generation of a health-associated 5-species biofilm model. Seven different configurations of bacteria seeding timelines were used to produce the initial set of 5-species biofilms. The composition of all configurations was then examined using qPCR (Figure 4.5 and Table 4.2). The biofilms are labelled according to the order in which the bacteria were seeded. For example, S+N+R denotes that *S. intermedius, S. mitis* and *S. oralis* were seeded first, followed by *N. mucosa* 24 hours later, and *R. dentocariosa* a further 24 hours later (see Table 2.3). Across the biofilm variants examined here, *Streptococcus* spp. was the most abundant component, with absolute abundance between $1.54 \times 10^7 \pm 8.66 \times 10^6$ and $3.13 \times 10^8 \pm 8.16 \times 10^7$ CFE/mL and relative abundance between 93.39% and 99.95%. The second most prevalent component was *N. mucosa*, with absolute abundance ranging from $1.99 \times 10^4 \pm 1.74 \times 10^3$ to $4.03 \times 10^6 \pm 7.43 \times 10^5$ CFE/mL and relative abundance from 0.01% to 4.39%. *R. dentocariosa* showed the lowest abundance, with absolute abundance of $3.01 \times 10^4 \pm 3.25 \times 10^4$ to $1.06 \times 10^6 \pm 3.50 \times 10^5$ CFE/mL and relative abundance of 0.04% to 2.22%.

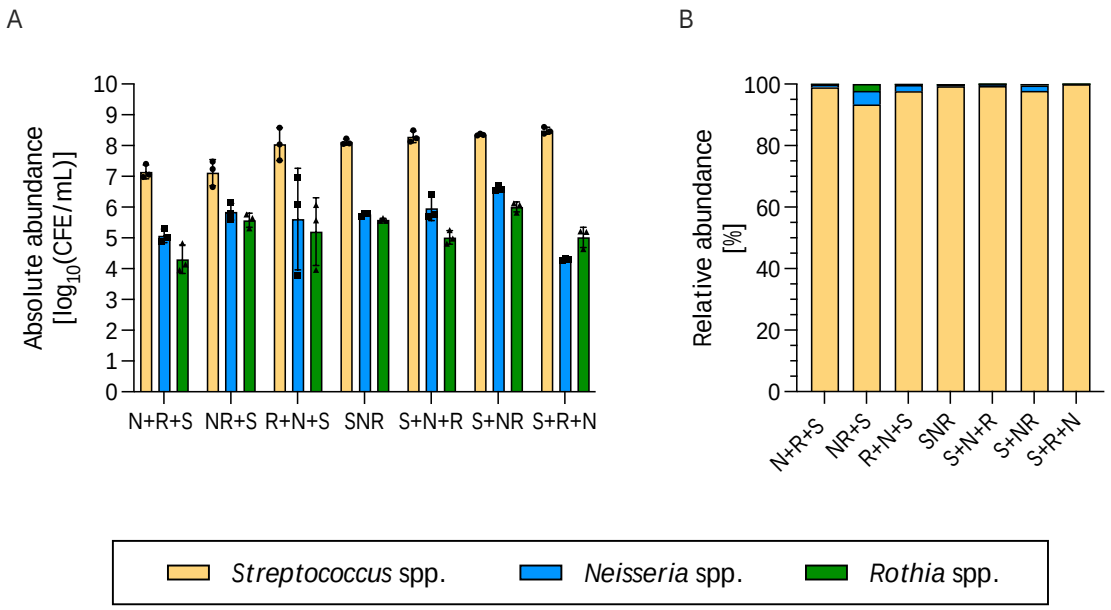

Figure 4.5 Compositional analysis of an initial set of the 5-species biofilms. Panel A shows absolute abundance, expressed as $\log_{10}$(CFE/mL), with data shown as mean ± SD of technical triplicates from a single experiment (n = 1); individual technical replicate values are shown as symbols. Panel B shows relative abundance, expressed as a percentage calculated from the same qPCR-derived values. S, *Streptococcus* spp.; N, *N. mucosa*; R, *R. dentocariosa*.

Table 4.2 Compositional analysis of an initial set of 5-species biofilms using qPCR.

	Absolute [CFE/mL] and relative [%] abundance of each bacterial species or genus in the 5-species biofilms		
Combination	*Streptococcus* spp. (*S. intermedius, S. mitis, S. oralis*)	*N. mucosa*	*R. dentocariosa*
SNR	$1.54 \times 10^7 \pm 8.66 \times 10^6$ (98.99%)	$1.28 \times 10^5 \pm 6.68 \times 10^4$ (0.82%)	$3.01 \times 10^4 \pm 3.25 \times 10^4$ (0.19%)
NR+S	$1.72 \times 10^7 \pm 1.27 \times 10^7$ (93.39%)	$8.08 \times 10^5 \pm 5.17 \times 10^5$ (4.39%)	$4.09 \times 10^5 \pm 1.88 \times 10^5$ (2.22%)
N+R+S	$1.75 \times 10^8 \pm 1.84 \times 10^8$ (97.72%)	$3.55 \times 10^6 \pm 5.12 \times 10^6$ (1.99%)	$5.23 \times 10^5 \pm 6.04 \times 10^5$ (0.29%)
R+N+S	$1.34 \times 10^8 \pm 3.14 \times 10^7$ (99.28%)	$5.85 \times 10^5 \pm 6.86 \times 10^4$ (0.43%)	$3.87 \times 10^5 \pm 5.17 \times 10^4$ (0.29%)
S+NR	$2.06 \times 10^8 \pm 9.26 \times 10^7$ (99.35%)	$1.24 \times 10^6 \pm 1.21 \times 10^6$ (0.60%)	$1.13 \times 10^5 \pm 5.98 \times 10^4$ (0.05%)
S+N+R	$2.27 \times 10^8 \pm 1.71 \times 10^7$ (97.80%)	$4.03 \times 10^6 \pm 7.43 \times 10^5$ (1.74%)	$1.06 \times 10^6 \pm 3.50 \times 10^5$ (0.46%)
S+R+N	$3.13 \times 10^8 \pm 8.16 \times 10^7$ (99.95%)	$1.99 \times 10^4 \pm 1.74 \times 10^3$ (0.01%)	$1.21 \times 10^5 \pm 6.73 \times 10^4$ (0.04%)

Absolute abundance values are shown as mean ± SD of technical triplicates from a single experiment (n = 1), with corresponding relative abundance values shown alongside as percentages (%).

4.3.2.2 Compositional analysis of the 5-species NR+S and S+NR biofilms

Following the preliminary comparison of the different 5-species seeding protocols, two variants, NR+S and S+NR, were chosen for further

characterisation. Their composition was assessed across samples from three independent batches to evaluate the reproducibility of the initial findings. All species added were detected (Figure 4.6), although in the second batch of both variants a strong deviation towards *R. dentocariosa* load in their composition was observed, therefore it was excluded from further analysis. Mean values (Figure 4.7) indicated lower absolute and relative abundances of *Streptococcus* spp. in NR+S biofilms than in S+NR biofilms ($1.12 \times 10^7 \pm 8.49 \times 10^6$ (94.36%) vs. $6.17 \times 10^8 \pm 5.52 \times 10^8$ (99.42%)). Absolute abundances of *N. mucosa* ($4.14 \times 10^5 \pm 5.57 \times 10^5$ vs. $2.48 \times 10^6 \pm 2.19 \times 10^6$) and *R. dentocariosa (*$2.54 \times 10^5 \pm 2.19 \times 10^5$ vs. $1.13 \times 10^6 \pm 1.03 \times 10^5$) were also lower in NR+S biofilms, although their relative abundances were higher (3.49% vs. 0.40% and 2.14% vs. 0.18%, respectively). Data are summarised in Table 4.3 and Table 4.4.

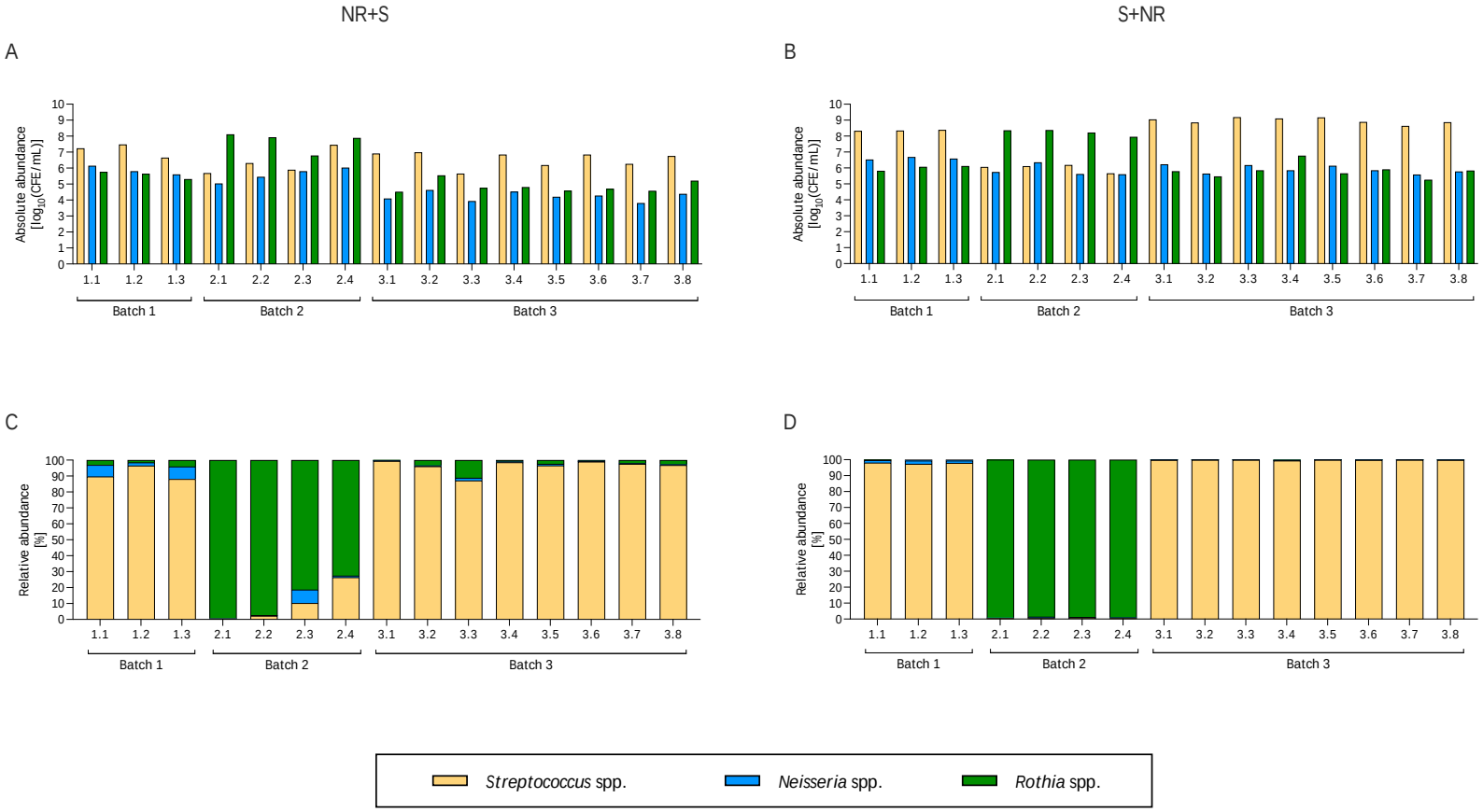

Figure 4.6 Compositional analysis of the 5-species NR+S and S+NR biofilms at the individual coverslip level. Absolute abundance values, determined using qPCR, are shown as $\log_{10}$(CFE/mL) (A, B), with corresponding relative abundance values shown as percentages (%) (C, D). Each x-axis tick label corresponds to an individual biofilm sample grown on a single coverslip.

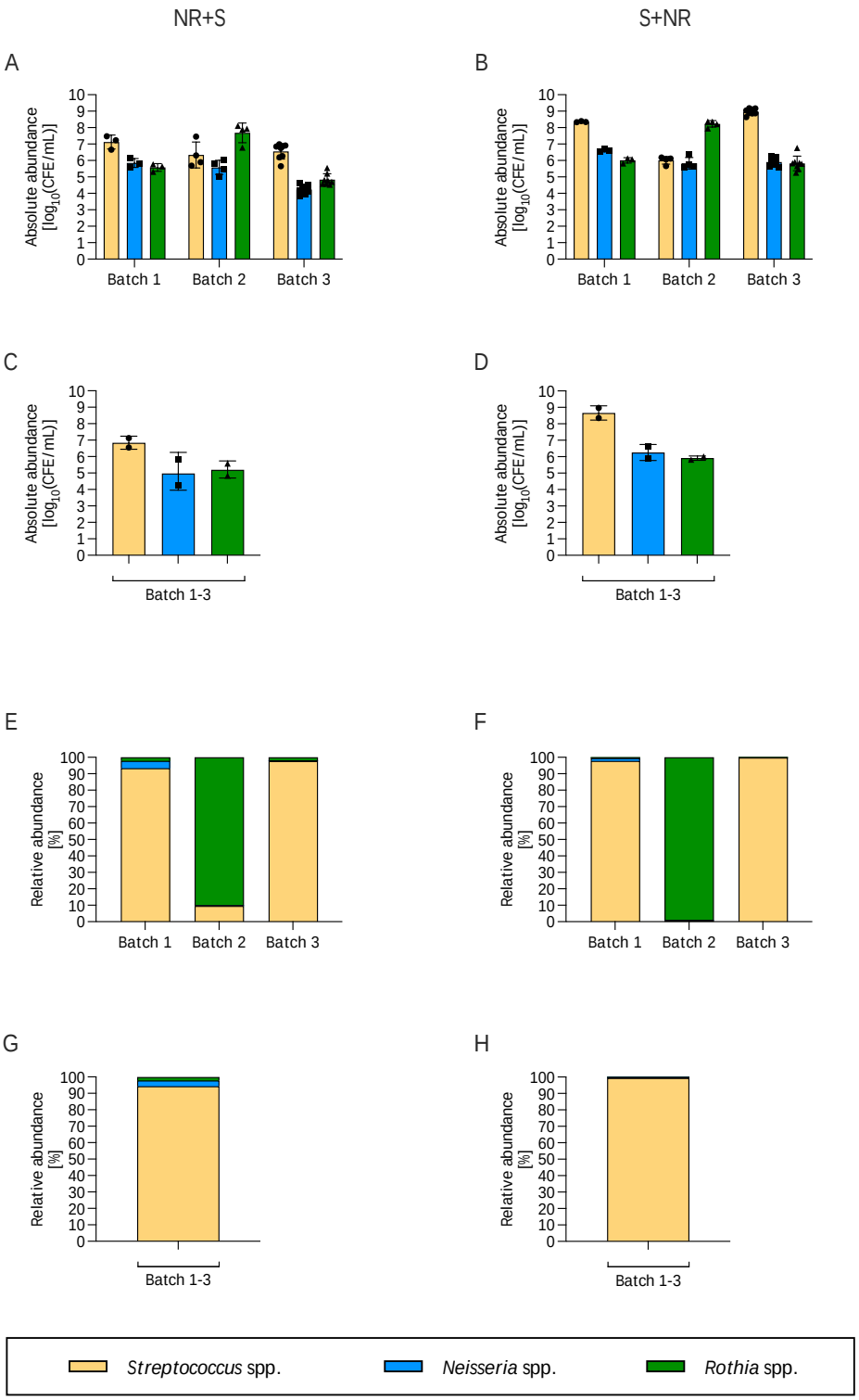

Figure 4.7 Compositional analysis of the 5-species NR+S and S+NR biofilms at the batch and grand mean level. Absolute abundance values, determined using qPCR, are shown as $\log_{10}$(CFE/mL) (A, B, C, D), with corresponding relative abundance values shown as percentages (%) (E, F, G, H). For absolute abundance, values are shown as mean ± SD at the batch level (A, B) and grand mean level (C, D), whereas relative abundance values are shown as mean percentages at the batch level (E, F) and grand mean level (G, H). Batch-level values were calculated from technical replicates within each batch (3, 4 or 8 per batch), with individual technical replicate values indicated by symbols on the batch-level absolute abundance graphs (A, B); grand mean values were calculated from batch means after exclusion of the second batch, with batch means indicated by symbols on the grand mean absolute abundance graphs (C, D).

Table 4.3 Compositional analysis of the 5-species NR+S biofilms.

Bacterial species or genus	Absolute [CFE/mL] and relative [%] abundance of each bacterial species or genus in the 5-species NR+S biofilm			
	Batch 1 (3)	Batch 2 (4)	Batch 3 (8)	Grand mean
Streptococcus spp. (*S. intermedius, S. mitis, S. oralis*)	$1.72 \times 10^7 \pm 1.27 \times 10^7$ (93.39%)	$7.92 \times 10^6 \pm 1.36 \times 10^7$ (9.53%)	$5.18 \times 10^6 \pm 3.44 \times 10^6$ (97.74%)	$1.12 \times 10^7 \pm 8.49 \times 10^6$ (94.36%)
N. mucosa	$8.08 \times 10^5 \pm 5.17 \times 10^5$ (4.39%)	$5.25 \times 10^5 \pm 4.22 \times 10^5$ (0.63%)	$2.05 \times 10^4 \pm 1.27 \times 10^4$ (0.39%)	$4.14 \times 10^5 \pm 5.57 \times 10^5$ (3.49%)
R. dentocariosa	$4.09 \times 10^5 \pm 1.88 \times 10^5$ (2.22%)	$7.46 \times 10^7 \pm 5.09 \times 10^7$ (89.83%)	$9.92 \times 10^4 \pm 1.09 \times 10^5$ (1.87%)	$2.54 \times 10^5 \pm 2.19 \times 10^5$ (2.14%)

Absolute abundance values were determined using qPCR and are expressed as CFE/mL, with corresponding relative abundance values (%) shown in the same cells. For the batch columns, absolute abundance is shown as mean ± SD of technical replicates within each batch (number shown in the column heading), while relative abundance is shown as a mean percentage. Grand mean values were calculated from the corresponding batch-level values after excluding the second batch.

Table 4.4 Compositional analysis of the 5-species S+NR biofilms.

Bacterial species or genus	Absolute [CFE/mL] and relative [%] abundance of each bacterial species or genus in the 5-species S+NR biofilm			
	Batch 1 (3)	Batch 2 (4)	Batch 3 (8)	Grand mean
Streptococcus spp. (*S. intermedius, S. mitis, S. oralis*)	$2.27 \times 10^8 \pm 1.71 \times 10^7$ (97.80%)	$1.11 \times 10^6 \pm 4.60 \times 10^5$ (0.61%)	$1.01 \times 10^9 \pm 4.00 \times 10^8$ (99.79%)	$6.17 \times 10^8 \pm 5.52 \times 10^8$ (99.42%)
N. mucosa	$4.03 \times 10^6 \pm 7.43 \times 10^5$ (1.74%)	$9.05 \times 10^5 \pm 8.97 \times 10^5$ (0.49%)	$9.30 \times 10^5 \pm 5.13 \times 10^5$ (0.09%)	$2.48 \times 10^6 \pm 2.19 \times 10^6$ (0.40%)
R. dentocariosa	$1.06 \times 10^6 \pm 3.50 \times 10^5$ (0.46%)	$1.81 \times 10^8 \pm 6.92 \times 10^7$ (98.90%)	$1.21 \times 10^6 \pm 1.90 \times 10^6$ (0.12%)	$1.13 \times 10^6 \pm 1.03 \times 10^5$ (0.18%)

Absolute abundance values were determined using qPCR and are expressed as CFE/mL, with corresponding relative abundance values (%) shown in the same cells. For the batch columns, absolute abundance is shown as mean ± SD of technical replicates within each batch (number shown in the column heading), while relative abundance is shown as a mean percentage. Grand mean values were calculated from the corresponding batch-level values after excluding the second batch.

4.3.2.3 Compositional analysis of the 10-species biofilms

Prior to its use in subsequent experiments, the 10-species biofilm was assessed to determine whether its composition was consistent with the expected profile (Brown, 2020, Millhouse, 2015). Data were examined on a per-sample basis, at the batch level and as a grand mean. At the sample level (Figure 4.8), all added species and genera were detected. While variability between biofilms within and between batches was observed, the overall composition appeared broadly similar across biofilms, with *A. naeslundii* and *Streptococcus* spp. being the most abundant components. Batch-level variation was most apparent in the abundance values for *V. dispar* and *A. actinomycetemcomitans* (Figure 4.9A and C), with lower values observed in batch 3 ($4.92 \times 10^3 \pm 1.42 \times 10^3$ CFE/mL; 0.0002% and $3.05 \times 10^5 \pm 2.80 \times 10^5$ CFE/mL; 0.02%, respectively) than in batch 1 ($3.56 \times 10^7 \pm 2.50 \times 10^7$ CFE/mL; 3.18% and $6.20 \times 10^6 \pm 7.75 \times 10^6$ CFE/mL; 0.55%, respectively) and batch 2 ($1.75 \times 10^7 \pm 1.72 \times 10^7$ CFE/mL; 1.80% and $3.44 \times 10^6 \pm 5.49 \times 10^6$ CFE/mL; 0.35%, respectively). At the grand mean level (Figure 4.9B and D), the most abundant species was *A. naeslundii* at $9.67 \times 10^8 \pm 4.32 \times 10^8$ CFE/mL (70.98%), followed by *Streptococcus* spp. at $3.45 \times 10^8 \pm 1.34 \times 10^8$ CFE/mL (25.30%). The combined *F. nucleatum* subspecies accounted for $2.85 \times 10^7 \pm 2.15 \times 10^7$ CFE/mL (2.09%), while *V. dispar* was present at $1.77 \times 10^7 \pm 1.78 \times 10^7$ CFE/mL (1.30%). Bacterial species added last comprised the remainder of the biofilm composition: *A. actinomycetemcomitans* ($3.31 \times 10^6 \pm 2.95 \times 10^6$ CFE/mL; 0.24%), *P. gingivalis* ($1.10 \times 10^6 \pm 5.88 \times 10^5$ CFE/mL; 0.08%) and *P. intermedia* ($1.03 \times 10^4 \pm 8.07 \times 10^3$ CFE/mL; 0.0008%). Results at the batch and grand mean levels are summarised in Table 4.5.

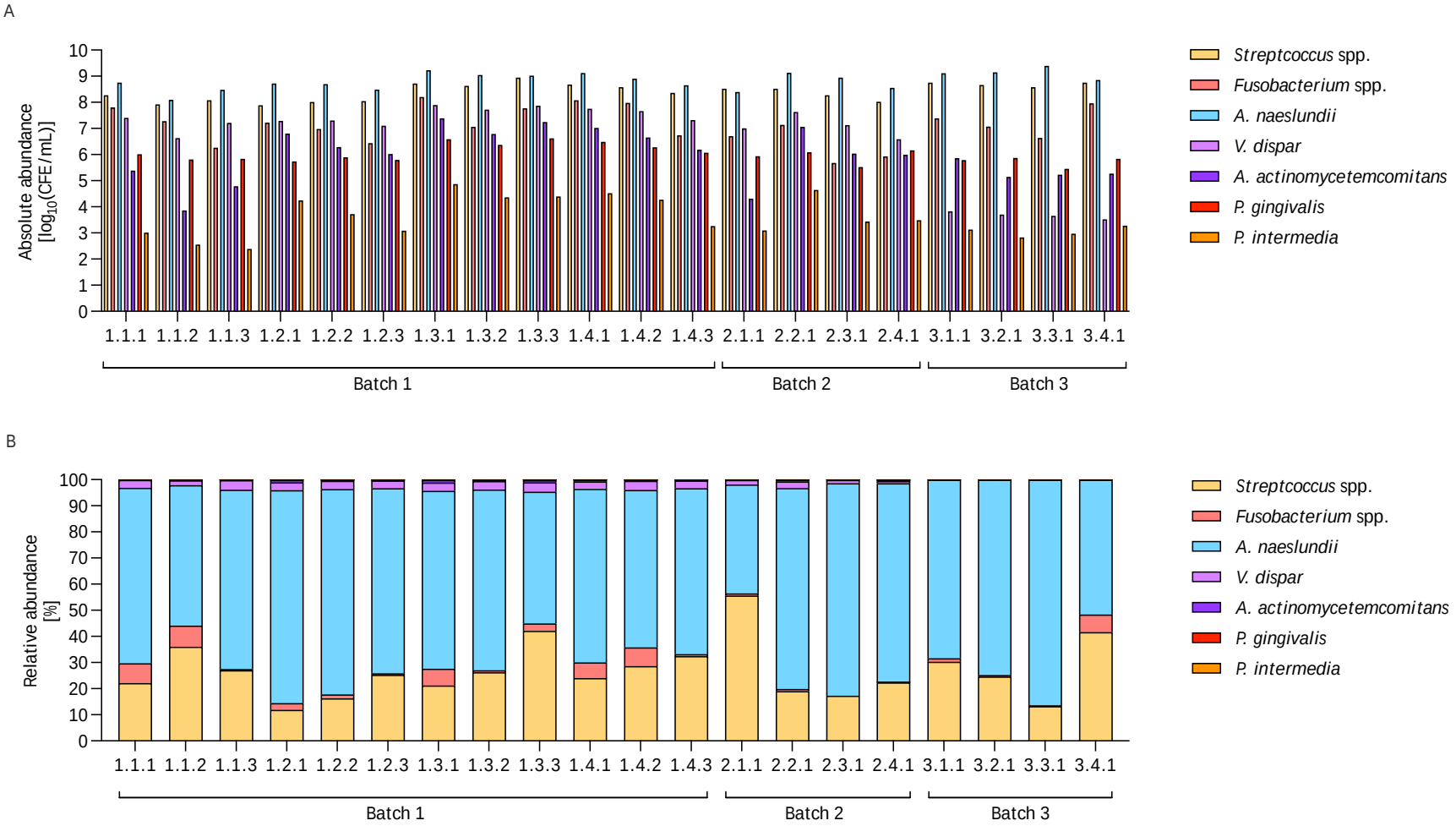

Figure 4.8 Compositional analysis of the 10-species biofilms at the individual coverslip level. Absolute abundance values, determined using qPCR, are shown as $\log_{10}$(CFE/mL) (A), with corresponding relative abundance values shown as percentages (%) (B). Each x-axis tick label corresponds to an individual biofilm sample grown on a single coverslip.

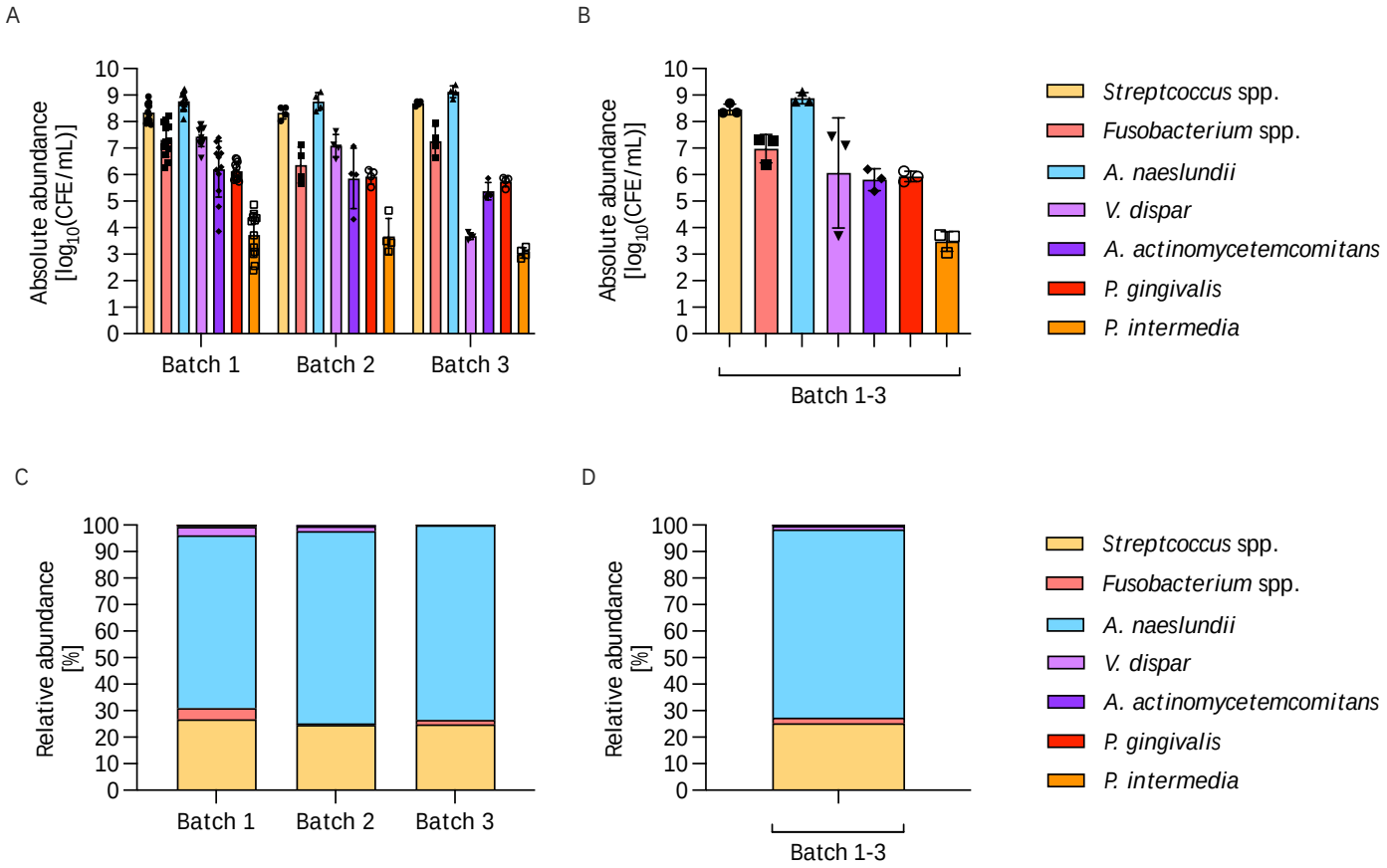

Figure 4.9 Compositional analysis of the 10-species biofilms at the batch and grand mean level. Absolute abundance values, determined using qPCR, are shown as $\log_{10}$(CFE/mL) (A, B), with corresponding relative abundance values shown as percentages (%) (C, D). For absolute abundance, values are shown as mean ± SD at the batch level (A) and grand mean level (B), whereas relative abundance values are shown as mean percentages at the batch level (C) and grand mean level (D). Batch-level values were calculated from technical replicates within each batch (12, 4 or 4 per batch), with individual technical replicate values indicated by symbols on the batch-level absolute abundance graph (A); grand mean values were calculated from batch means, with batch means indicated by symbols on the grand mean absolute abundance graph (B).

Table 4.5 Compositional analysis of the 10-species biofilms.

Bacterial species or genus	Absolute [CFE/mL] and relative [%] abundance of each bacterial species or genus in the 10-species biofilm			
	Batch 1 (12)	Batch 2 (4)	Batch 3 (4)	Grand mean
Streptococcus spp. (*S. intermedius, S. mitis, S. oralis*)	$3.00 \times 10^8 \pm 2.45 \times 10^8$ (26.76%)	$2.39 \times 10^8 \pm 1.12 \times 10^8$ (24.59%)	$4.96 \times 10^8 \pm 9.30 \times 10^7$ (24.83%)	$3.45 \times 10^8 \pm 1.34 \times 10^8$ (25.30%)
F. nucleatum (subsp. *polymorphum* and *vincentii*)	$4.72 \times 10^7 \pm 5.33 \times 10^7$ (4.21%)	$5.01 \times 10^6 \pm 6.13 \times 10^6$ (0.52%)	$3.32 \times 10^7 \pm 4.028 \times 10^7$ (1.66%)	$2.85 \times 10^7 \pm 2.15 \times 10^7$ (2.09%)
A. naeslundii	$7.30 \times 10^8 \pm 4.72 \times 10^8$ (65.14%)	$7.05 \times 10^8 \pm 5.03 \times 10^8$ (72.63%)	$1.47 \times 10^9 \pm 7.35 \times 10^8$ (73.46%)	$9.67 \times 10^8 \pm 4.32 \times 10^8$ (70.98%)
V. dispar	$3.56 \times 10^7 \pm 2.50 \times 10^7$ (3.18%)	$1.75 \times 10^7 \pm 1.72 \times 10^7$ (1.80%)	$4.92 \times 10^3 \pm 1.42 \times 10^3$ (0.0002%)	$1.77 \times 10^7 \pm 1.78 \times 10^7$ (1.30%)
A. actinomycetemcomitans	$6.20 \times 10^6 \pm 7.75 \times 10^6$ (0.55%)	$3.44 \times 10^6 \pm 5.49 \times 10^6$ (0.35%)	$3.05 \times 10^5 \pm 2.80 \times 10^5$ (0.02%)	$3.31 \times 10^6 \pm 2.95 \times 10^6$ (0.24%)
P. gingivalis	$1.74 \times 10^6 \pm 1.32 \times 10^6$ (0.16%)	$9.73 \times 10^5 \pm 4.92 \times 10^5$ (0.10%)	$5.82 \times 10^5 \pm 2.06 \times 10^5$ (0.03%)	$1.10 \times 10^6 \pm 5.88 \times 10^5$ (0.08%)
P. intermedia	$1.67 \times 10^4 \pm 2.13 \times 10^4$ (0.001%)	$1.29 \times 10^4 \pm 2.11 \times 10^4$ (0.001%)	$1.21 \times 10^3 \pm 5.27 \times 10^2$ (0.00006%)	$1.03 \times 10^4 \pm 8.07 \times 10^3$ (0.0008%)

Absolute abundance values were determined using qPCR and are expressed as CFE/mL, with corresponding relative abundance values (%) shown in the same cells. For the batch columns, absolute abundance is shown as mean ± SD of technical replicates within each batch (number shown in the column heading), while relative abundance is shown as a mean percentage. Grand mean values were calculated from the corresponding batch-level values.

4.3.2.4 Quantification of *P. gingivalis* in mono-species biofilms

To provide a negative control for the nitrate reduction Griess assay, a mono-species *P. gingivalis* biofilm was grown, as *P. gingivalis* is not a known nitrate-reducing species (Dahlén et al., 2007). In addition, this model enabled evaluation of *P. gingivalis* characteristics in the absence of other bacterial species from the 10-species biofilm. qPCR analysis (Figure 4.10) showed that, on average, the mono-species biofilms contained $9.58 \times 10^4 \pm 7.66 \times 10^4$ CFE/mL, which was lower than the values observed in the 10-species biofilms.

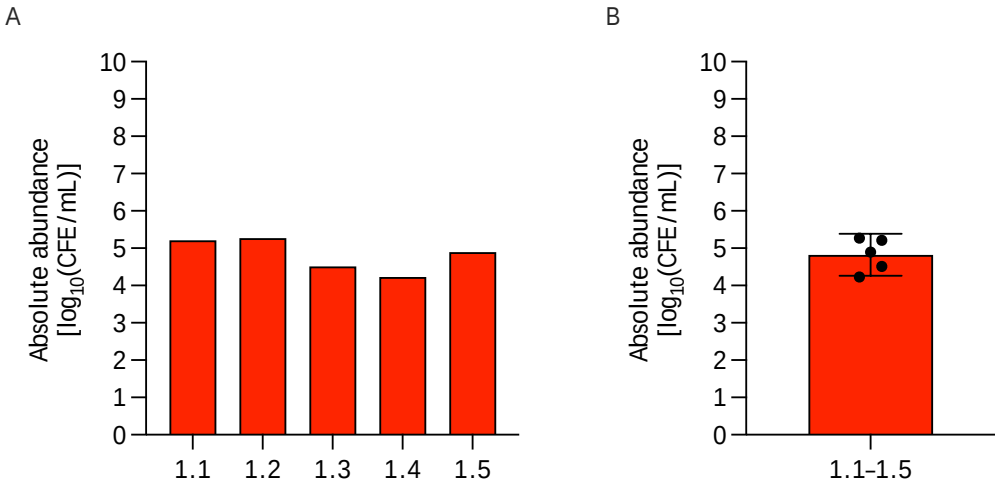

Figure 4.10 Quantification of bacteria in mono-species *P. gingivalis* biofilms. Absolute abundance values were determined using qPCR and are shown as $\log_{10}$(CFE/mL). Individual technical replicates from a single batch are shown separately (A) and summarised as mean ± SD (B), with symbols indicating each replicate value.

4.3.2.5 Assessment of biofilm microarchitecture and structure with scanning electron microscopy

Scanning electron microscopy was used to qualitatively assess biofilm formation and architecture. Following revival, biofilms were processed and imaged by SEM. Images were taken from high-, medium- and low-density areas selected as representative of the observed fields within each coverslip (Figure 4.11). The two types of 5-species biofilms had strikingly different morphologies. The surface of the NR+S biofilm at 18× magnification appeared heterogenous (Figure 4.11A) with modest upward growth and a structure resembling desiccated and fragmented moss at 500× magnification (Figure 4.12). At 5000× magnification, clustered microstructures composed of entangled chains of cocci and diplococci were visible, with distinguishable high-, medium- and low-density regions. The

latter showed the presence of extracellular matrix in central parts of branching bacterial aggregates. The S+NR biofilm was very densely packed and had a homogeneous appearance at 18× magnification (Figure 4.11B). Examination at 500× magnification (Figure 4.13) revealed the presence of a surface with a cracked, desiccated appearance resembling polygonal cracking in dried mud or clay, with three morphologically different areas: one with sparse, wide cracks; one with more numerous, narrower cracks; and one with a dense network of fine cracks. When viewed under 5000× magnification, all areas showed dense aggregation of cocci, with extracellular matrix content difficult to distinguish due to the density of the biofilm. Additionally, sparse elongated bacteria were present. At 18× magnification, the 10-species biofilm showed a distinct, highly heterogeneous surface composed of patches varying in size and distribution; in some regions, the patches formed larger and vertically overlapping structures, while in others they were smaller and dispersed (Figure 4.11C). Under 500× magnification, the aggregates showed a complex fibrous morphology (Figure 4.14). Observation at 5000× magnification revealed a mixture of single and chained cocci, rods and distinctive spindle-shaped bacteria. The abundance of the latter was lower in low-density regions of the biofilm. Biofilm inoculated only with *P. gingivalis* was flattened and showed relatively uniform distribution at 18× and 500× magnifications (Figure 4.11D and Figure 4.15, respectively), although it was still possible to distinguish areas with different growth densities. High-density areas were densely populated by short rods with occasional spaces between them. Pronounced accumulation of thread-like extracellular matrix was observed. In medium-density areas, bacterial cells were uniformly scattered and held together by the extracellular matrix. Low-density areas, on the other hand, displayed a combination of individual bacterial cells and clusters connected by long filaments of the extracellular matrix.

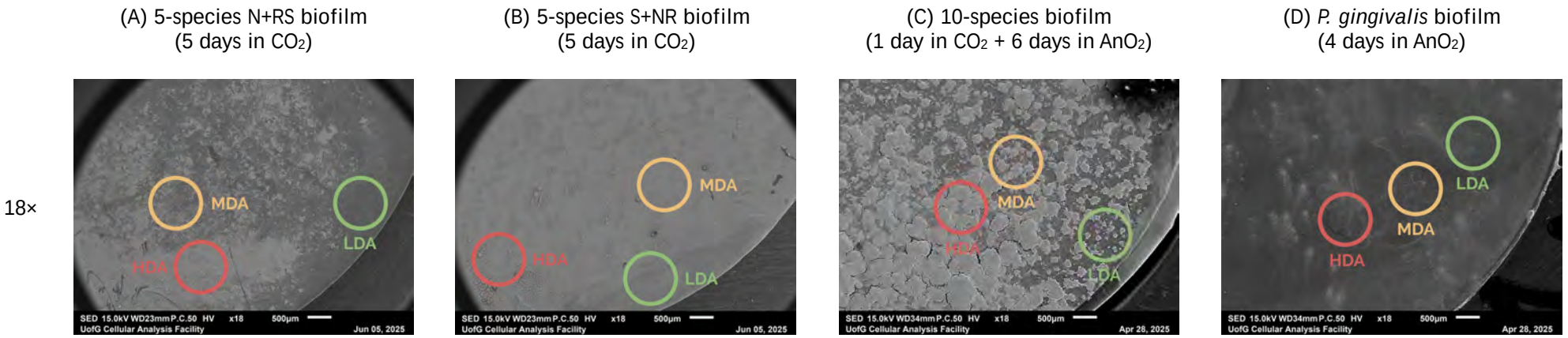

Figure 4.11 Scanning electron microscopy images of 5-species NR+S (A) and S+NR (B), 10-species (C) and mono-species *P. gingivalis* (D) biofilms. Following growth on 13 mm Thermanox coverslips in RPMI:THB (1:1) under conditions shown above each image, biofilms were frozen and revived before being processed for SEM. Specimens were viewed using a JEOL IT100 scanning electron microscope operated at 15.0 kV at 18× magnification. Images were captured using JEOL InTouch Scope software version 1.05. One coverslip containing a mature biofilm of each type was processed. HDA, high-density area; MDA, medium-density area; LDA, low-density area.

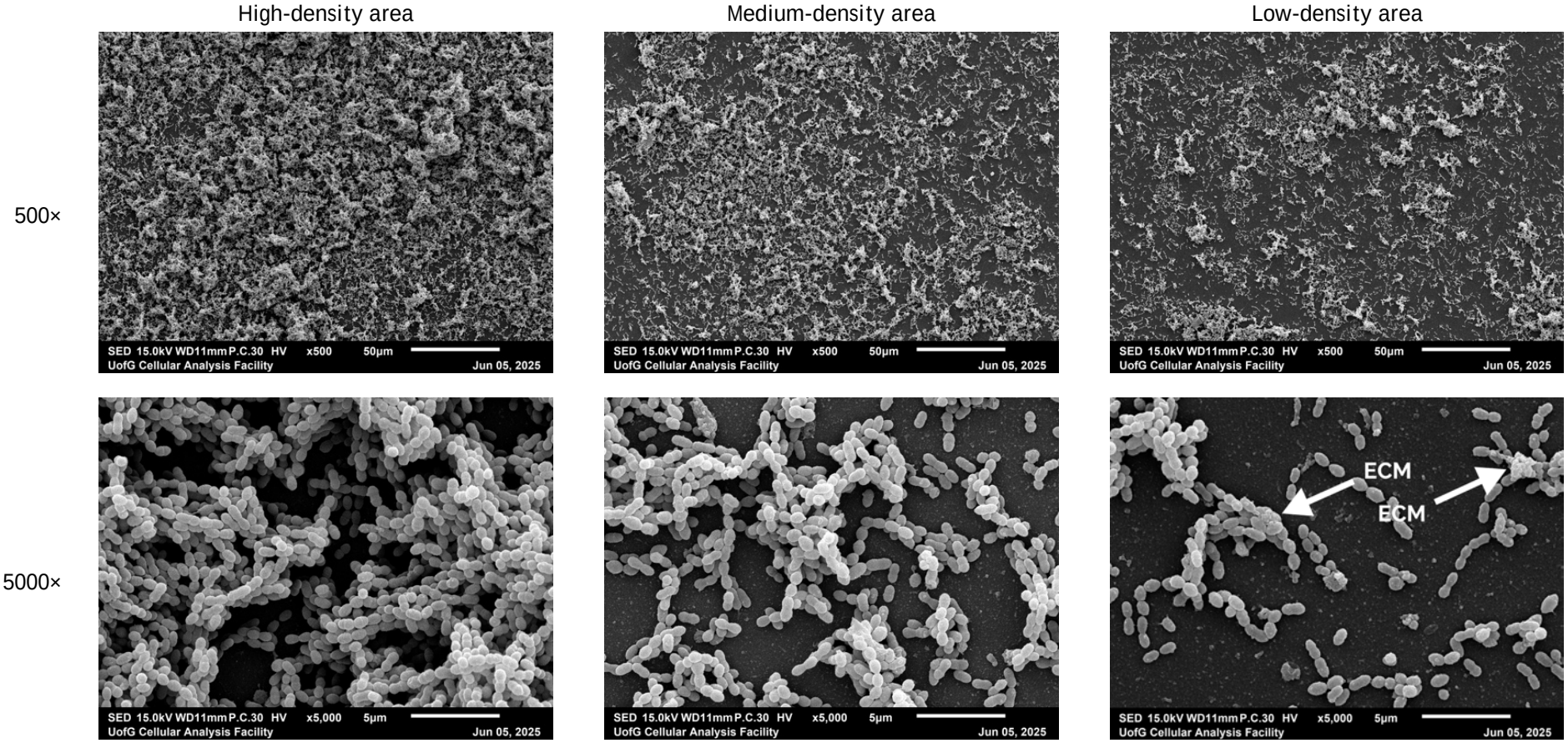

Figure 4.12 Scanning electron microscopy images of a 5-species NR+S biofilm. Following growth on a 13 mm Thermanox coverslip in RPMI:THB (1:1) for 5 days under aerobic (5% CO_2) conditions, the biofilm was frozen and revived before being processed for SEM. The specimen was viewed using a JEOL IT100 scanning electron microscope operated at 15.0 kV at 500× and 5000× magnifications. Images were captured using JEOL InTouch Scope software version 1.05. One coverslip containing a mature biofilm was processed. ECM, extracellular matrix.

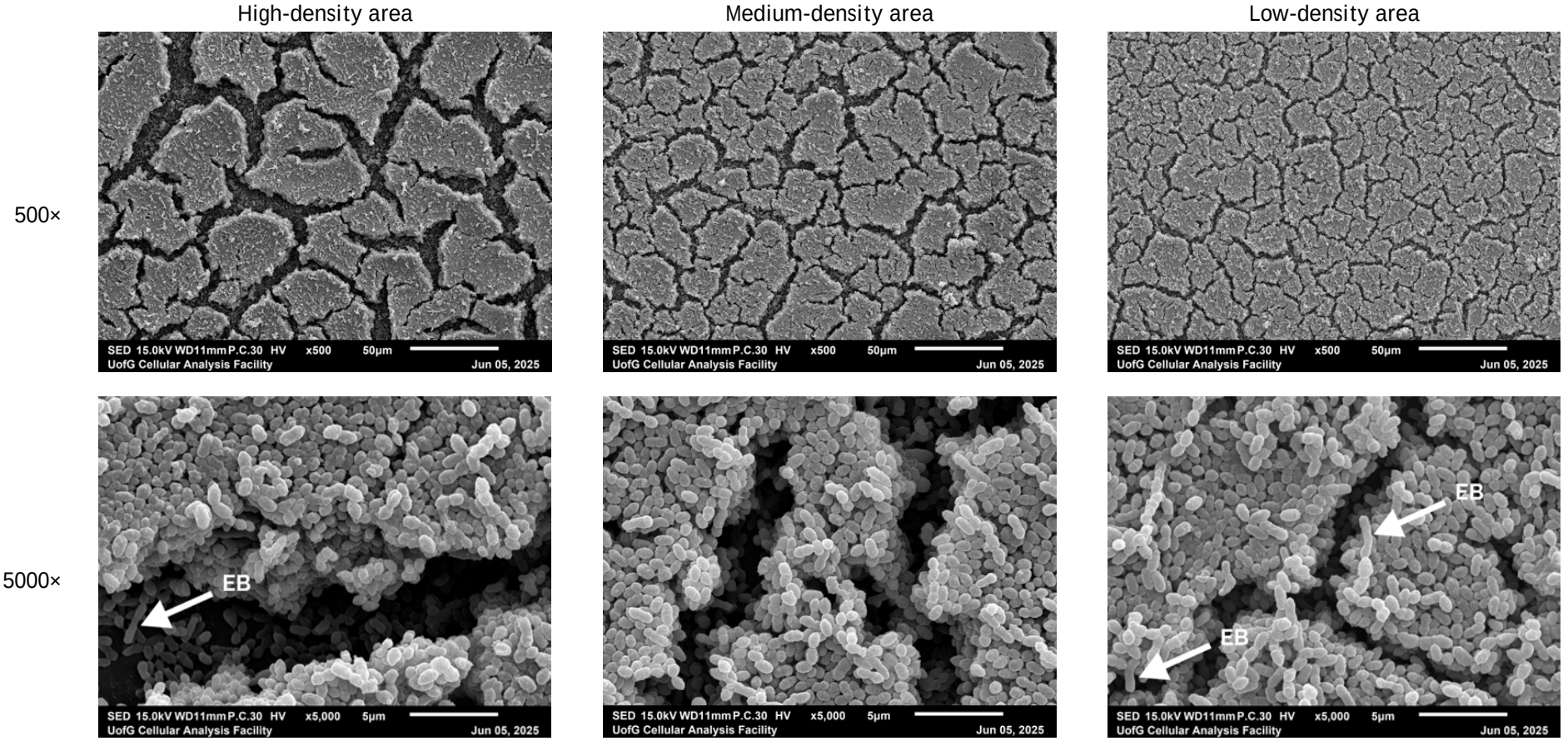

Figure 4.13 Scanning electron microscopy images of a 5-species S+NR biofilm. Following growth on a 13 mm Thermanox coverslip in RPMI:THB (1:1) for 5 days under aerobic (5% CO_2) conditions, the biofilm was frozen and revived before being processed for SEM. The specimen was viewed using a JEOL IT100 scanning electron microscope operated at 15.0 kV at 500× and 5000× magnifications. Images were captured using JEOL InTouch Scope software version 1.05. One coverslip containing a mature biofilm was processed. EB, elongated bacteria.

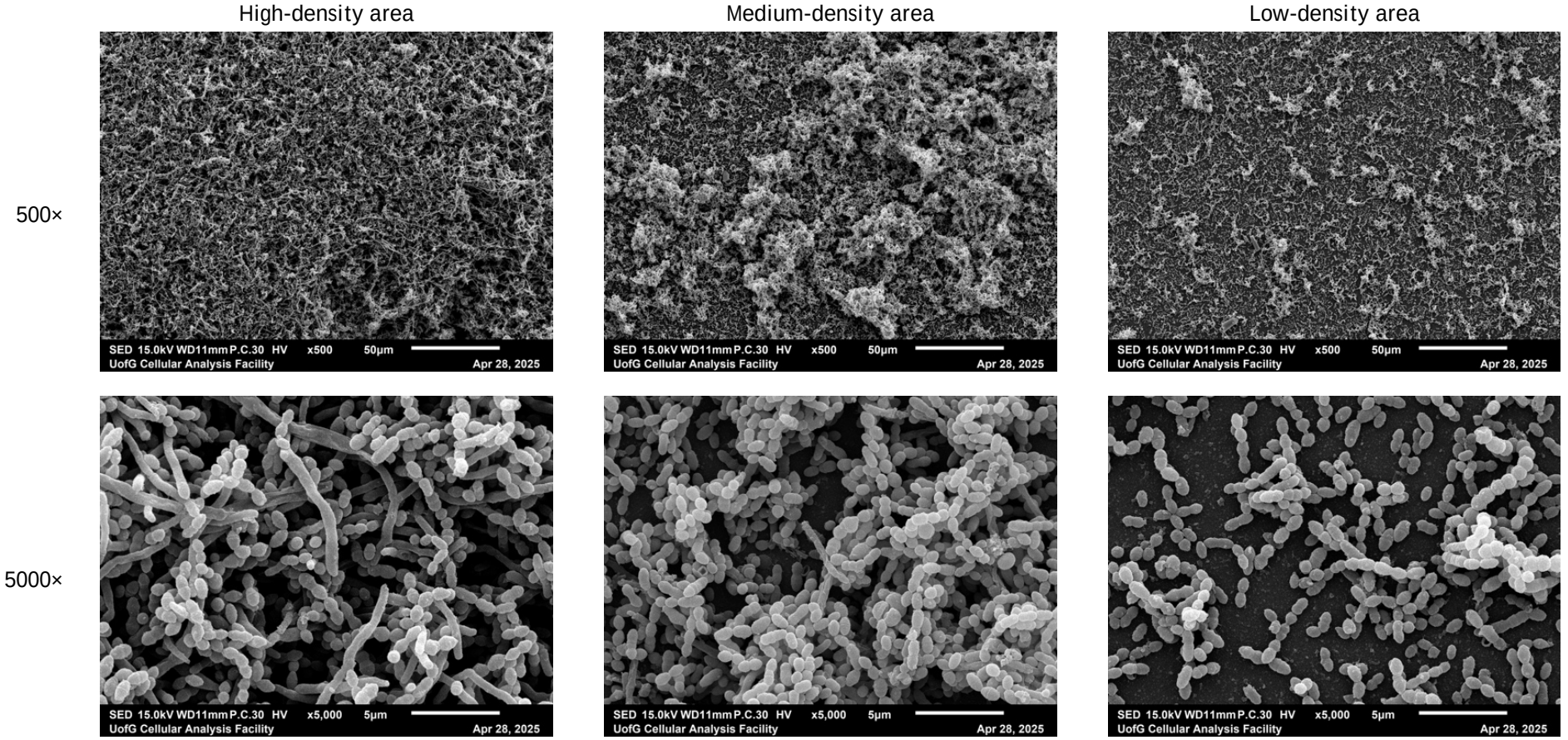

Figure 4.14 Scanning electron microscopy images of a 10-species biofilm. Following growth on a 13 mm Thermanox coverslip in RPMI:THB (1:1) for 1 day under aerobic (5% CO_2) and 6 days under anaerobic conditions (85% N_2, 10% CO_2 and 5% H_2), the biofilm was frozen and revived before being processed for SEM. The specimen was viewed using a JEOL IT100 scanning electron microscope operated at 15.0 kV at 500× and 5000× magnifications. Images were captured using JEOL InTouch Scope software version 1.05. One coverslip containing a mature biofilm was processed.

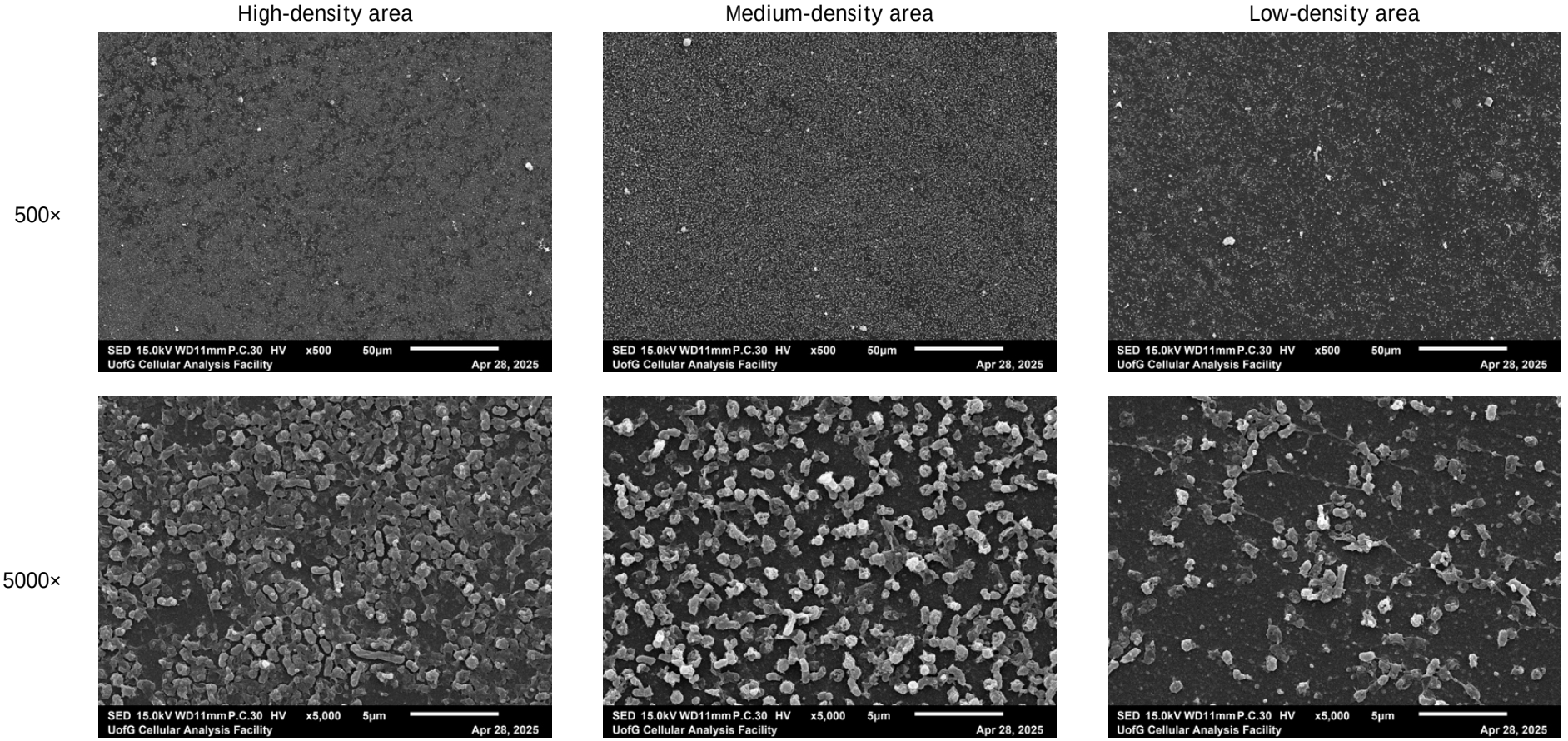

Figure 4.15 Scanning electron microscopy images of a mono-species *P. gingivalis* biofilm. Following growth on a 13 mm Thermanox coverslip in RPMI:THB (1:1) for 4 days under anaerobic conditions (85% N_2, 10% CO_2 and 5% H_2), the biofilm was frozen and revived before being processed for SEM. The specimen was viewed using a JEOL IT100 scanning electron microscope operated at 15.0 kV at 500× and 5000× magnifications. Images were captured using JEOL InTouch Scope software version 1.05. One coverslip containing a mature biofilm was processed.

4.3.2.6 Evaluation of nitrate reduction capacity of biofilms

To evaluate nitrate reduction capacity, mono- and multi-species biofilms were revived under appropriate conditions. Biofilms were incubated with added 100 µM nitrate (treated) or without added nitrate (untreated) for 1 hour at 37 °C, 5% CO_2. The supernatants were then collected and replaced before a further 24-hour incubation under the same conditions. Supernatant nitrite (NO_2^-) levels were measured using the Griess diazotisation reaction (Figure 4.16).

Overall, nitrite levels in supernatants collected from the S+NR and NR+S biofilms and media-only control coverslips revived under the same conditions appeared broadly comparable between the nitrate-treated and untreated control groups. At 1 hour, nitrite levels in S+NR biofilm supernatants from both groups were below the lower limit of detection (LOD) of the assay (1.0 µM). In the NR+S untreated group, the mean nitrite level was also below the assay LOD, although not all readings were below this limit. Measurable nitrite concentrations were observed in NR+S biofilm supernatants from the treated group (1.31 ± 0.23 µM) and in control coverslip supernatants from both treated and untreated groups (1.33 ± 0.19 µM and 1.29 ± 0.06 µM, respectively). After 24 hours, nitrite concentrations in supernatants were 8.11 ± 3.58 µM and 6.35 ± 1.52 µM in S+NR, 3.23 ± 0.15 µM and 4.98 ± 0.84 µM in NR+S, and 1.67 ± 0.39 µM and 1.64 ± 0.17 µM in control coverslips, respectively, for the treated and untreated groups.

Supernatants collected from the 10-species and mono-species biofilms and media-only control coverslips revived under the same conditions showed different nitrite accumulation patterns. Some values exceeded the upper LOD of the assay (100 µM) and are therefore reported as extrapolated estimates and interpreted cautiously. At 1 hour, 10-species biofilm supernatants had a higher estimated nitrite concentration in the treated group (306.47 ± 40.54 µM) compared to the untreated group (227.45 ± 136.96 µM). These concentrations decreased after 24 hours to an estimated 151.10 ± 4.53 µM (treated group) and 99.65 ± 37.58 µM (control). In contrast, supernatants collected at 1 hour from the *P. gingivalis* mono-species biofilms contained 3.21 ± 0.28 µM nitrite in the treated group and 3.18 ± 1.18 µM in the untreated group. These values increased after 24 hours to estimated concentrations of 334.83 ± 12.29 µM and 311.53

± 14.99 µM, respectively. Supernatants from the media-only control coverslips in this group showed slightly higher nitrite concentrations than their counterparts revived in 5% CO_2. At 1 hour, nitrite levels were 2.15 ± 0.67 µM and 2.62 ± 0.96 µM, increasing at 24 hours to 3.44 ± 0.22 µM and 3.78 ± 2.36 µM in the treated and untreated groups, respectively.

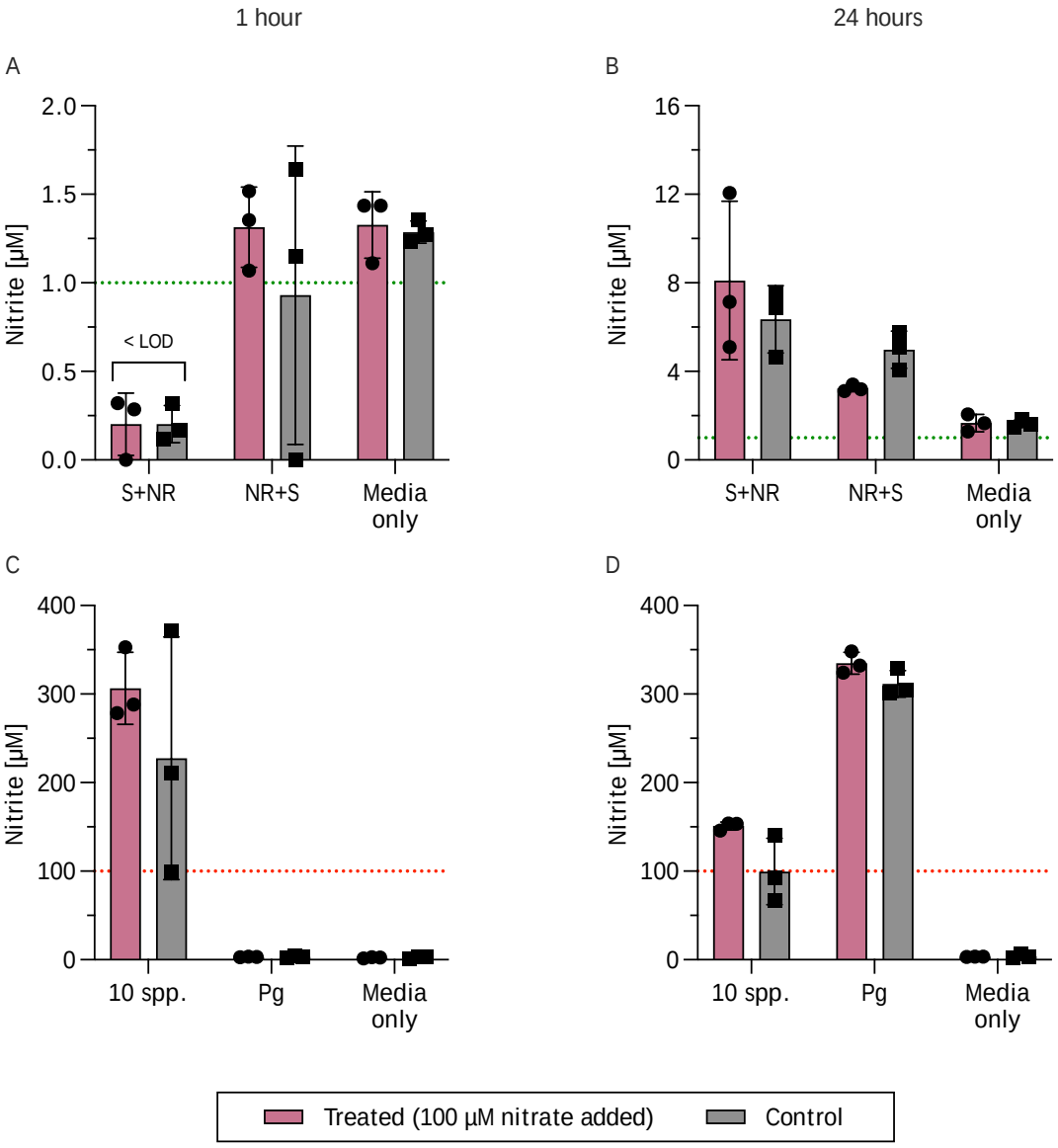

Figure 4.16 Nitrite accumulation in biofilm supernatants evaluated through the Griess diazotisation reaction. Biofilms were incubated in RPMI:THB (1:1) with added 100 µM nitrate (Treated) or without added nitrate (Control) for 1 hour and then for a further 24 hours at 37 °C, 5% CO_2. Data are shown as mean ± SD from one experiment (n = 1) with three technical replicates. Individual technical replicate values are shown as symbols. The green and red dotted lines denote the lower and upper limits of the standard curve, respectively. Samples outside the limits of the standard curve were extrapolated where possible; values below the lower limit that could not be extrapolated were assigned a value of 0 before calculation of the mean.
< LOD, below the lower limit of detection; S+NR, 5-species biofilm initiated with *Streptococcus* spp.; NR+S, 5-species biofilm initiated with *N. mucosa* and *R. dentocariosa*; 10 spp., 10-species biofilm; Pg, mono-species *P. gingivalis* biofilm; Media only, control coverslip.

4.3.2.7 Assessment of biofilms biomass

Following assessment of the nitrate reduction capacity, the remaining biofilms were reused in a crystal violet assay to assess their biomass. At the macroscopic level, there were no visible differences between biofilms treated with nitrate and untreated controls. 5-species S+NR and 10-species biofilms showed strong dye retention, however, notable variations were observed in the uptake pattern (Figure 4.17A). S+NR biofilms appeared to be more uniformly stained, which contrasted with 10-species biofilms that had a heterogeneous morphology with confluent patches caused by colony coalescence. 5-species NR+S biofilms exhibited moderate dye retention with the presence of patches that were heterogeneous in size and shape. In *P. gingivalis* mono-species biofilms, on the other hand, only faint staining was observed, although this was still distinguishable from the control coverslips. Colorimetric analysis of the released crystal violet dye showed that both nitrate-treated and untreated control biofilms had similar biomass within the same biofilm types (Figure 4.17B). The highest OD values were observed among 10-species biofilms, with values of 2.48 ± 0.22 and 2.44 ± 0.38 for treated and control groups, respectively. This was followed by S+NR biofilms, with OD_{570} values of 1.98 ± 0.41 (treated) and 1.82 ± 0.41 (control) and NR+S biofilms with 1.40 ± 0.33 (treated) and 1.17 ± 0.28 (control). The lowest biomass was observed in *P. gingivalis* mono-species biofilms, with values of 0.45 ± 0.02 and 0.45 ± 0.07 (treated and control, respectively).

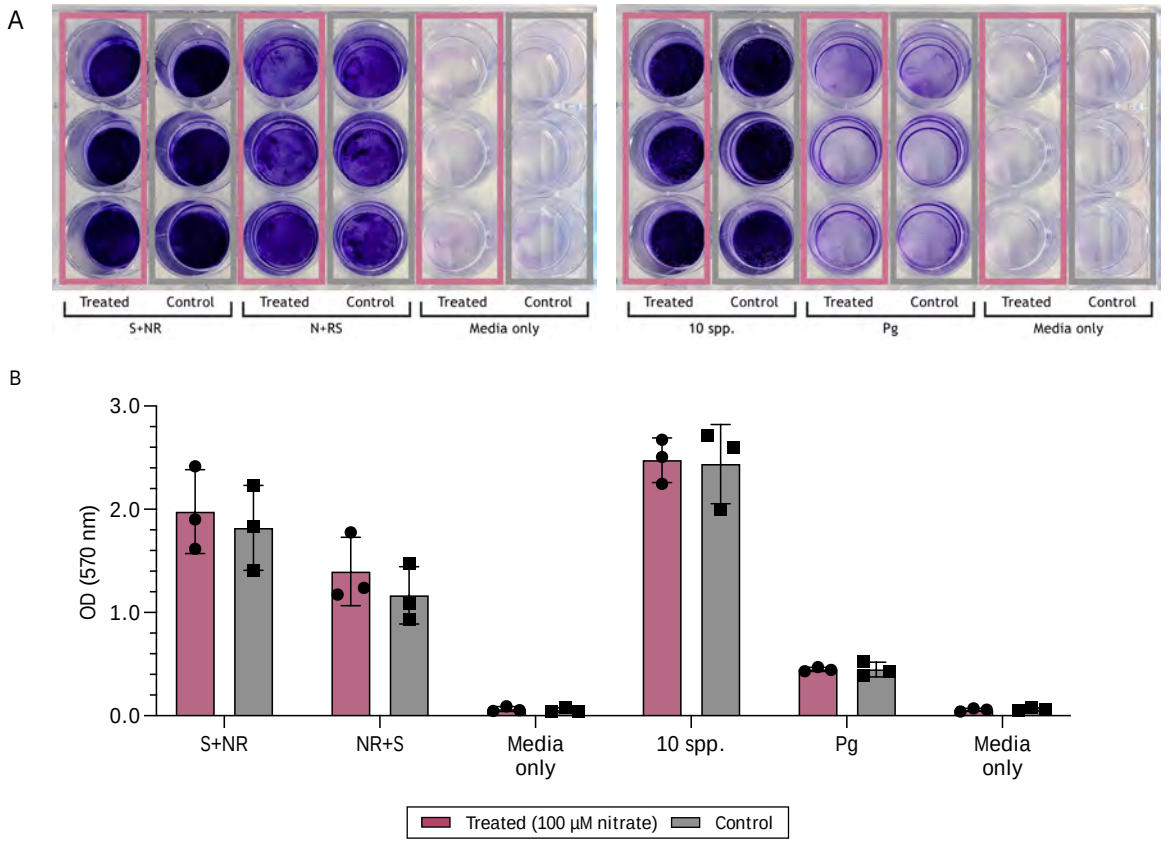

Figure 4.17 Crystal violet biomass assessment of biofilms following the Griess diazotisation reaction. (A) Biofilms stained with crystal violet; (B) crystal violet biomass assessment. Images and data are from a single experiment (n = 1) performed in technical triplicate. Data represent mean ± SD, with individual technical replicate values shown as symbols. S+NR, 5-species biofilm initiated with *Streptococcus* spp.; NR+S, 5-species biofilm initiated with *N. mucosa* and *R. dentocariosa*; 10 spp., 10-species biofilm; Pg, mono-species *P. gingivalis* biofilm; Media only, control coverslip.

4.4 Discussion

This chapter presents the process of development and validation of the first multispecies *in vitro* biofilm model associated with periodontal health that goes beyond mimicking a supragingival plaque or being a baseline for the growth of a periodontitis model. While the biofilm was built on a previously developed 3-species Glasgow model containing *S. intermedius*, *S. mitis* and *S. oralis*, it additionally incorporated two health-associated species – *N. mucosa* and *R. dentocariosa*. Using a 10-species periodontitis model for comparative evaluation suggested differences between 5- and 10- species biofilm models.

4.4.1 Optimisation of culture quantification and analytical methods

Preliminary characterisation of *N. mucosa* growth kinetics (Figure 4.1) was performed solely to identify the optimal culture incubation time point for Miles and Misra plating (Figure 4.2), and to correlate OD with viable CFU counts. These experiments therefore represented a methodological optimisation step rather than a biological endpoint.

In the subsequent experiment, viable counts appeared to differ from the expected values for species used in biofilm seeding (Figure 4.3), despite adjustment of each bacterial suspension to its predefined target OD. This observation should be interpreted in light of the limitations of both OD-based standardisation and CFU/mL-based viable count estimation. Single-point OD measurements provide an indirect estimate of bacterial suspension density based on light scattering, but do not distinguish between single cells and aggregates, viable and non-viable cells, or cells in different physiological states. Therefore, OD adjustment alone may not reliably predict the viable bacterial load expressed as CFU/mL (Mira et al., 2022). CFU/mL measurements also have limitations as an estimate of viable bacterial numbers in the initial suspension. Colony counts assume that each visible colony arises from one colony-forming unit, which may not correspond to a single bacterial cell, and that colonies are sufficiently separated to be distinguished accurately (Sutton, 2012). These measurements may also be affected by the physiological state of cells and differences in the ability to initiate colony growth after plating (Davey, 2011).

In line with this, viable count estimates for *N. mucosa* and *P. gingivalis* appeared higher than the intended seeding targets, particularly for *N. mucosa*. However, as these estimates were derived from colony counts outside the preferred range of 50–200 colonies per spot, the exact CFU/mL values should be interpreted cautiously. These findings suggest that, in this experiment, adjustment to predefined OD values may not have produced the intended viable bacterial loads. The lack of visible colonies for *P. intermedia* may in part reflect failure to recover culturable cells under the conditions used, potentially due to oxygen exposure during droplet drying. Despite the observed variability, the Miles and Misra assay was useful in confirming the presence of viable culturable bacteria in

the stored stocks, although recovery was not observed for all species. Furthermore, it provided an approximate indication of the extent to which OD-based standardisation corresponded to viable CFU counts across species. As this optimisation experiment was conducted on a single occasion (n = 1), these findings should be interpreted with caution and regarded as preliminary observations rather than definitive quantitative comparisons between species.

In addition to culture-based quantification, qPCR standard curve optimisation (Figure S1) was performed to support downstream assessment of biofilm composition. Small differences were observed between the two versions of the qPCR standard curves generated for each species or genus (Figure 4.4), which may be consistent with the presence of qPCR inhibitors. Such inhibitors may arise from residual media components, bacterial cell material, or extracellular polymeric substances within the biofilm matrix (Schrader et al., 2012). This introduces a possibility of reduced DNA extraction efficiency or co-purification of inhibitory substances with the DNA samples, thereby potentially altering the Cq values obtained from the assigned CFE/mL standards. Further investigation would be required to determine the exact nature of the inhibition mechanism, as amplification may improve when inhibitory effects are reduced by dilution or worsen if inhibitory substances are co-purified and concentrated within the sample (Huggett et al., 2008). This could be assessed by adding a known quantity of external DNA to a biofilm sample before DNA extraction (also known as a 'spike-in') to assess the entire workflow, or employing an internal amplification control (IAC) to detect inhibition in already extracted biofilm DNA samples. Nolan et al. (2006) developed a quantitative TaqMan-based version of IAC called a 'SPUD' assay that uses a synthetic DNA template derived from the *phyB* gene region of the potato species *Solanum tuberosum*. Similarly, Kavlick (2018) described a TaqMan-based method in which a fully synthetic universal exogenous internal positive control could be customised. These techniques would require validation with SYBR Green-based qPCR. Once the underlying mechanism of amplification inhibition has been identified, an appropriate method for PCR inhibitor removal should be selected (Schrader et al., 2012). The better performance of the DNA-derived standard curves is likely attributable to the fact that serial dilutions were prepared directly from a single extracted DNA stock in ultrapure water, thereby minimising variability associated with repeated

extraction steps and dilution of potential inhibitory substances. While this method provided a consistent basis for qPCR quantification, it cannot fully account for variability introduced during DNA extraction from low biomass samples. Consequently, quantification of biofilm samples may still be influenced by extraction-related variability not captured by these standard curves. It is important to note, however, that each standard curve was based on a single serial dilution series assessed in technical duplicate. Therefore, the results demonstrate consistency within the assay but do not capture variability between independently prepared standard curves, and the reported curve performance should be interpreted as assay-specific. Despite these limitations, the selected qPCR standard curves remained appropriate for comparative assessment of bacterial abundance across all biofilm samples.

4.4.2 Development and compositional characterisation of health-associated biofilms

The next part of the chapter was to determine the order of introduction of species during the seeding phase of biofilm growth. All tested modifications of the seeding protocol resulted in the added species being detected, with notable dominance of *Streptococcus* spp. (that included *S. intermedius*, *S. mitis* and *S. oralis*) observed across all conditions (Figure 4.5), which may be consistent with antagonistic interactions with the remaining species. Based on these findings, the NR+S and S+NR, were selected for further characterisation and assessment of reproducibility across three independent batches.

Compositional analysis showed similar patterns in batches 1 and 3 for both biofilm combinations, with *Streptococcus* spp. being the most abundant component. This contrasted with the marked predominance of *R. dentocariosa* in batch 2 at both the individual coverslip level (Figure 4.6) and batch level (Figure 4.7). Although the cause remains unclear, one unplanned variation in the protocol was noted. During the preparation phase, Thermanox coverslips were placed in the plate; however, seeding with bacterial suspensions was delayed by 4 days for logistical reasons. Thermanox coverslips are made of a proprietary polyester film with a surface treatment that confers hydrophilicity and thereby promotes cell adherence. Evidence from studies on plasma-treated PET, a type

of polyester, suggests that exposure to air may result in partial hydrophobic recovery, particularly within the first few days (Vesel et al., 2020). Altered surface properties may therefore have promoted differential attachment of bacterial cells from the seeding suspensions. *R. dentocariosa* has been reported to show greater affinity for a hydrophobic silicone rubber surface than the other bacterial strains included, although the comparison set was limited (Rodrigues et al., 2007). This raised the possibility that the observed dominance of *R. dentocariosa* was influenced by unintended changes in surface properties, and the batch was therefore excluded from further analysis. This highlights the importance of strict adherence to the protocol and of validating the composition of each batch before use in downstream assays.

4.4.2.1 Comparison of *in vitro* biofilm composition with *ex vivo* biofilms

Although the human oral microbiome encompasses over 700 species and around 150 genera (Escapa et al., 2018), it appears that the majority of both supra- and subgingival plaque in periodontally healthy volunteers is composed of a relatively small number of genera. For example, in one study, around 80–85% of the sequences identified in *ex vivo* plaque from healthy volunteers were accounted for by around 13 genera, including *Streptococcus*, *Rothia* and *Neisseria* (Mark Welch et al., 2016). The composition of a health-associated subgingival microbiome is less well defined than that associated with periodontitis. As discussed in Chapter 3, findings are highly variable between studies, and no single health-associated profile can be defined. Nevertheless, a review of 20 next-generation sequencing association studies identified *Streptococcus* and *Rothia* as the genera most strongly associated with periodontal health (Feres et al., 2021). A reanalysis of publicly available datasets from 10 studies likewise identified *Streptococcus* and *Rothia* taxa among the dominant members of health-associated communities (Abusleme et al., 2021). The taxon with the highest mean relative abundance in health was the aggregated *Streptococcus* HMT 423 mitis/pneumoniae group, although this classification could not distinguish *S. mitis*, *Streptococcus pneumoniae* and *Streptococcus* sp. HMT 423. *R. dentocariosa* was also among the most abundant taxa in health. Nonetheless, compared with the 5-species *in vitro* biofilms generated in the present study (Figure 4.7), the most abundant taxa reported in health-associated *in vivo* communities comprised a broader range, including

additional *Streptococcus* (*S. sanguinis* and *Streptococcus* sp. HMT 064), *Rothia* (*R. aeria*) and *Neisseria* (*Neisseria flava*) taxa, as well as *Corynebacterium, Lautropia, Actinomyces*, *Fusobacterium, Veillonella*, *Capnocytophaga* and *Haemophilus*. Notably, the mean relative abundance of individual taxa did not exceed 20%. The current work provides a foundation for future studies to incorporate a broader range of species.

4.4.2.2 Role of included species in initial colonisation and early biofilm development

The final selected 5-species biofilm variant (S+NR) was initiated with *Streptococcus* spp., an approach commonly used in previous Glasgow 3-, 7- and 10-species biofilm models (Brown et al., 2023, Millhouse, 2015). This was consistent with the fact that *Streptococcus* spp. are the most abundant colonisers of virtually all sites of the oral cavity and possess a variety of mechanisms ensuring successful adhesion to different surfaces. These include adhesins, matrix-interacting proteins and pili (Bloch et al., 2024, Nobbs et al., 2015). *S. mitis* and *S. oralis* are among pioneer colonisers that adhere directly to the surface providing a foundation for attachment and growth of early colonisers such as *S. intermedius* through cell-to-cell interactions. This sequence is essential for subsequent colonisation by bridging species and the late colonisers such as members of the red complex (Kolenbrander et al., 2010, Rosan and Lamont, 2000). The role of early colonisers in biofilm structure and composition *in vitro* was demonstrated through delayed addition or complete removal of *S. oralis, S. anginosus,* and *A. oris* from the Zurich subgingival 10-species biofilm model (Ammann et al., 2013). While there were no significant differences in total bacterial counts, species-specific shifts were observed accompanied by looser biofilm structure and more homogenous bacterial distribution. Furthermore, a study on *in vivo* biofilm development on enamel chips in 3 healthy human subjects provided evidence that streptococci comprised from 66 to 80% of genera present in newly formed biofilm samples (Diaz et al., 2006). At the species level, a group consisting of *S. oralis* and *S. mitis* was dominant at 4- and 8-hour time points. A similar study utilising hydroxyapatite discs in 10 healthy volunteers also indicated *Streptococcus* as the most abundant genus, reaching ≥ 20%, but only up to the 16-hour time point (Wake et al., 2016). Its numbers started declining at 24 hours and constituted less than 5% after

96 hours. These somewhat contradicting results could be explained by different methods employed in both studies: 16S rRNA gene cloning and Sanger sequencing accompanied by FISH (Diaz et al., 2006) vs. Ion Torrent PGM sequencing of the V5–V6 region of the 16S rRNA gene (Wake et al., 2016). The latter is a modern next-generation sequencing method that can better detect rare and low-abundance taxa. Further studies of the *in vitro* biofilms described in this chapter could employ such more sophisticated methods of *Streptococcus* spp. discrimination. However, for the current work the benefits of these approaches were not deemed.

Although *Rothia* spp. are less dominant in subgingival plaque than *Streptococcus* spp., *R. dentocariosa* was found to be the most abundant species in health-associated subgingival plaque (Abusleme et al., 2013). Studies on *in vivo*-formed biofilms collected at a 6-hour time point, either using polyvinylidene difluoride membrane swabs in 11 healthy subjects (Heller et al., 2016) or from hydroxyapatite discs placed in the mouth in 74 healthy subjects (Ihara et al., 2019), indicated that *R. dentocariosa* is involved in early plaque formation. Its potential role was indicated in a study that mapped specific interbacterial adhesion networks in early (4- and 8-hour) *in vivo* biofilms grown on human enamel chips through FISH combined with confocal microscopy. *Rothia* spp. (which included *R. dentocariosa* and *R. mucilaginosa*) formed distinct islands within the biofilm, indicating a potential role as a nucleation point for bacterial interactions. Of note, *R. dentocariosa* isolates coaggregated mainly with streptococci (Palmer et al., 2017). In another study, *R. dentocariosa* isolated from dental plaque was identified as a coadhesion partner of *S. oralis* strain 34 (Ruhl et al., 2014). Interestingly, 2-day old *R. dentocariosa* monospecies biofilms were shown to form only moderate biofilms with OD_{590} values ranging between 0.2 and 0.3 (Alshatti et al., 2023).

Neisseria spp. are abundant in health-associated subgingival plaque (Feres et al., 2021, Meuric et al., 2017). Analysis of the oral metagenomes obtained from the Human Microbiome Project dataset revealed that the gingival plaque was populated mainly by *N. sicca*, *N. mucosa* and *N. elongata* (Donati et al., 2016). *Neisseria* spp. were indicated as early colonisers; in the aforementioned study by Wake et al. (2016) they comprised more than 20% of the biofilm population from 4 hours until the final study endpoint at 96 hours. It has also been described that

Neisseria spp. form islands within the biofilm similarly to *Rothia* spp. (Palmer et al., 2017).

4.4.2.3 Possible mechanisms underlying antagonistic interactions within health-associated biofilms

The predominance of *Streptococcus* spp. in the 5-species health-associated biofilms may partly reflect antagonistic interactions with other community members. In addition to directly competing for binding sites and nutrients in the medium, oral streptococci can also modify the surrounding environment and inhibit growth of other bacteria through production of antimicrobial compounds, e.g. organic acids lowering pH (Assinder, 1995, Mashimo et al., 1985) and hydrogen peroxide introducing oxidative stress (Herrero et al., 2016, Okahashi et al., 2014, Redanz et al., 2018).

4.4.2.3.1 pH

Streptococci isolated from different tooth surfaces are capable of lowering pH in broth to as low as 4.2 (van Houte et al., 1996). Furthermore, of the three *Streptococcus* species used in the health-associated biofilm, *S. oralis* is known for its remarkably high acid tolerance even at pH as low as 3.5 (Boisen et al., 2021). There is no specific data available on pH range tolerated by *R. dentocariosa* and *N. mucosa*, however, both species have been reported to be isolated from initial carious lesions alongside other cariogenic bacteria, suggesting they can survive low pH environments (Bizhang et al., 2011).

4.4.2.3.2 Hydrogen peroxide

Hydrogen peroxide (H_2O_2) is produced by nearly all oral *Streptococcus* species. It serves a variety of roles in the microbial community and thus provides competitive advantage for their producers during the early stages of biofilm development. H_2O_2 is generated from superoxide anions inside the bacterial cells and diffuses into the external environment, where it is quickly reduced to highly reactive hydroxyl radicals that induce DNA damage (Redanz et al., 2018). Several oral commensals can prevent this H_2O_2-induced cytotoxicity through production of catalase that neutralises H_2O_2 to H_2O and O_2, and this comprises most *Neisseria* spp. (including *N. mucosa*) (Tønjum and van Putten, 2017), some

Rothia spp. (with most *R. dentocariosa* strains (Ergin et al., 2002)), and some *A. naeslundii* strains (Ellen, 1976, Jakubovics et al., 2008). Interestingly, streptococci do not express catalase, indicating that effects of H_2O_2 might provide them with a better competitive advantage (Redanz et al., 2018). Indeed, H_2O_2 was reported to cause extracellular release of streptococcal DNA, thus promoting genetic transformation (Itzek et al., 2011). Furthermore, based on studies on other species, it has been suggested that extracellular DNA may enhance aggregation and initial adhesion in oral commensal streptococci (Zhu and Kreth, 2012). Activity of the main pathway responsible for H_2O_2 production in oral streptococci, pyruvate oxidase SpxB, yields yet additional benefits for its host by producing adenosine triphosphate (ATP) in addition to other metabolites from the oxidative decarboxylation of pyruvate (Redanz et al., 2018). At later stages of biofilm development, when biofilm biomass increases and oxygen becomes less available, H_2O_2 production decreases, allowing for growth of H_2O_2-sensitive periopathogens such as *A. actinomycetemcomitans*, *P. intermedia* and *P. gingivalis* (Herrero et al., 2016). If subsequent experiments confirm that a high initial H_2O_2 concentration in 5-species biofilms is detrimental to *N. mucosa* and *R. dentocariosa*, this could potentially be mitigated by introducing more catalase-positive species that are still associated with periodontal health, either to counteract oxidative stress or to provide a physical or diffusion barrier.

4.4.2.3.3 Polysaccharide foraging

Palmer et al. (2017) suggested the presence of a potentially interesting interaction between oral streptococci and *R. dentocariosa*. The latter expresses polysaccharide in its cell wall that consists of fructose (contributing to the majority of its dry weight), glucose, galactose and ribose (Hammond, 1970). Some streptococci are either predicted to have fructosidases on their cell surface, e.g. *S. gordonii* and *S. sanguinis* (Lombard et al., 2014), or to express soluble fructan-hydrolising enzymes and utilise fructan as an energy source, e.g. *S. salivarius* (Takahashi et al., 1983, Takamori et al., 1985). Early colonisers of dental plaque, *A. viscosus* and *S. gordonii*, were found to use fructans in adhesion *in vitro* (Rozen et al., 2001). It was therefore hypothesised that streptococci can use *R. dentocariosa* as a carbon source at the expense of their contribution to the biofilm biomass (Palmer et al., 2017).

4.4.3 Compositional characterisation of previously established periodontitis-associated and mono-species biofilm models

Both 10-species and mono-species *P. gingivalis* biofilms were grown as described previously, providing reference models for comparison with the 5-species biofilms. The qPCR assay suggested minor differences in the composition of the 10-species biofilms (Figure 4.9) and in the abundance of *P. gingivalis* in mono-species biofilms (Figure 4.10) compared to the previously reported data (Brown, 2020, Millhouse, 2015). This could, at least in part, be explained by the use of different culture media, with THB:RPMI (1:1) used here and artificial saliva used previously.

The 10-species biofilm model was reproduced from an established protocol (Brown et al., 2023) rather than developed *de novo* in the present study. Its composition can be considered in the context of naturally occurring dysbiotic subgingival biofilms. The model includes species indicated as strongly associated with periodontitis – *P. gingivalis* and *P. intermedia* (Feres et al., 2021). Similarly, *F. nucleatum* subsp. *vincentii* and *F. nucleatum* subsp. *polymorphum* are reported to have high relative abundance in periodontitis (Abusleme et al., 2021) and are also included in the model. Nevertheless, the model lacks several taxa frequently associated with periodontitis, including *T. forsythia*, *T. denticola* and *F. alocis*. Notably, *T. forsythia* and *T. denticola* have been incorporated into the Zurich 10-species biofilm model, indicating that their absence from the Glasgow 10-species consortium reflects simplification of community composition rather than an absolute technical barrier. In addition, the Glasgow 10-species biofilm contains high proportions of *Streptococcus* spp. and *A. naeslundii*, taxa more typically associated with health or gingivitis than with periodontitis in clinical microbiome studies (Abusleme et al., 2021).

Taken together, this model biofilm is better viewed as a simplified, disease-associated model with periodontitis-related features rather than a full representation of dysbiotic periodontal plaque. This level of simplification was appropriate for the present study, in which the established 10-species biofilm (Brown et al., 2023) was used primarily as a comparator against the newly developed 5-species health-associated biofilm.

4.4.4 Limitations of biofilm compositional analysis

4.4.4.1 qPCR-related limitations

The first challenge relates to recovery of bacterial DNA from biofilm samples, which are more structurally and chemically complex than bacterial suspensions (Jakubovics et al., 2021). Although sonication of the biofilm-coated coverslips prior to extraction improves dispersion of the biofilm biomass and partially mitigates this issue, extracellular matrix components would still have been present during DNA extraction and may have contributed to variability in DNA recovery. In addition, the complexity of biofilm-derived samples may have increased the likelihood of carryover of substances capable of inhibiting qPCR, which could have further contributed to underestimation of CFE/mL values. Methods for detection and removal of qPCR inhibitors have already been discussed in detail in Section 4.4.1. A further limitation of using qPCR is that these assays amplify target sequences regardless of bacterial viability and therefore cannot determine which species were alive at the endpoint of biofilm maturation. This limitation could be addressed by utilising a live/dead qPCR assay, where samples are pre-treated with propidium monoazide to prevent amplification of DNA in dead cells (Nocker et al., 2006). This method has been successfully utilised to assess viability of bacterial species in oral biofilms (Alvarez et al., 2013, Loozen et al., 2011). Finally, while specific abundance values were presented for each biofilm model, these should be interpreted as qPCR-derived quantitative estimates rather than exact absolute counts, given the methodological limitations discussed in Section 4.4.1.

4.4.4.2 Potential effects of freezing and revival on biofilm composition

Freezing and subsequent revival were used pragmatically to facilitate preparation of the biofilm models in larger batches and to ensure sample availability for downstream analyses. However, the effect of this approach on biofilm composition and post-thaw metabolic recovery was not assessed in the present study. Freezing may cause structural injury to bacterial cells and reduce viability, with the extent of damage varying between species (Guo et al., 2020, Ray and Speck, 1973). In cells that survive, freezing may also result in metabolic injury and impaired recovery, although such damage can be at least partly

reversible under appropriate post-thaw conditions (Postgate and Hunter, 1963, Ray and Speck, 1972). In multispecies biofilms, these effects may differ from those observed in planktonic cultures, as the biofilm matrix and community context could influence both freezing injury and subsequent recovery. Previous work has shown that the composition of the Glasgow 3-, 7- and 10-species biofilm models was not significantly affected by freezing and revival, as measured by qPCR (Brown et al., 2019). Similarly, in the 10-species Zurich model, only minor differences in culture-based species enumeration were observed following freezing, thawing and revival (Guggenheim et al., 2009). Together, these findings support the use of this approach. Nevertheless, a potential impact of freezing and revival on the relative abundance of individual species within the health-associated biofilm was not directly assessed in this study and therefore cannot be fully excluded. However, because all comparable biofilm samples were subjected to the same freezing, revival, and compositional analysis workflow, any bias introduced by this step would be expected to affect those samples consistently.

Cryoprotective additives, or cryoprotectants, such as glycerol and DMSO, have long been used for the storage of individual bacterial isolates (Hubálek, 2003). In addition, 20% glycerol has been used for the storage of plaque-derived oral microbiome microcosms prior to re-propagation (Zhou et al., 2022). To the author's knowledge, the use of cryoprotectants has not been reported for intact model oral biofilms. Their application during biofilm freezing may therefore be explored as a potential means of improving the preservation of viability and species composition. However, this would require validation, as the effects of different cryoprotectants may vary across bacterial species and formulations (Alessandri et al., 2024), with potential consequences for post-thaw recovery and downstream analyses, particularly in co-culture with mammalian cells.

4.4.5 Structural characterisation of biofilm models by SEM

In vitro biofilm models cannot fully replicate the structural complexity of biofilms occupying gingival sulci and periodontal pockets. Nevertheless, some morphological features of the 10-species *in vitro* biofilms (Figure 4.14) appeared to be broadly consistent with those reported for *ex vivo* subgingival biofilms imaged on extracted teeth from periodontitis patients (Friedman et al., 1992,

Holliday et al., 2015). These included the presence of mixed bacterial morphologies and evidence of matrix formation. However, spirochaete-like forms reported in *ex vivo* periodontitis-associated biofilms were not observed in the present *in vitro* model, as no spirochaete species were included in its composition. The bacterial morphology observed in the health-associated NR+S (Figure 4.12) and S+NR (Figure 4.13) biofilms was much more homogeneous than that reported in healthy *ex vivo* specimens. However, both *in vitro* and *ex vivo* health-associated biofilms shared a predominance of cocci.

While SEM provides high-resolution morphological data, it cannot assess viability or metabolic activity. Furthermore, the desiccated appearance of the NR+S biofilm (Figure 4.12) suggests it underwent structural changes during processing, such as loss of the extracellular matrix, despite the use of alcian blue in the fixative (Erlandsen et al., 2004). Alternative imaging modalities could be explored, such as fluorescence confocal microscopy, with all bacteria labelled with the same fluorophore or different labels used for each species. Previous experience in the group suggests that autofluorescence of the biofilms can be extremely challenging to manage.

4.4.6 Nitrate reduction assay

Detected nitrite levels were comparable between the nitrate-treated and untreated groups (Figure 4.16). This may indicate that the addition of nitrate to the culture media did not produce a measurable effect on net nitrite accumulation under the conditions tested. In the 5-species biofilms, low nitrite accumulation was detected throughout the experiment. This may reflect the low abundance of the nitrate-reducing species *N. mucosa* and *R. dentocariosa*. In addition, aerobic conditions may have been less favourable for nitrate-reducing activity, as nitrate reduction in oral bacteria and *Neisseria* has been described or assessed under anaerobic conditions (Barth et al., 2009, Doel et al., 2005). Extensive optimisation of the culture conditions would be required to assess the effect of exogenous nitrate addition more fully.

Commercially available nitrate reduction assays are a widely used method in nitrite level determination in biological samples; however, this technique has several limitations. It assesses only the total amount of nitrite present at a

chosen endpoint, without the ability to account for further reduction to NO or re-oxidation to nitrate, which may occur in a biological setting. Moreover, false-positive and false-negative results may arise for several reasons. Nitrate may not be able to penetrate deeper layers of biofilm or it could be sequestered or retained within the biofilm environment. Conversely, the RPMI:THB media mix used in the experiment contains components that might have interfered with the assay reagents. Similarly, oxidative stress markers released from anaerobic bacteria that were moved to an aerobic atmosphere also could have interfered with nitrite measurement. Furthermore, appropriate sample processing and storage are critical, and the requirement to handle samples quickly and at low temperatures was technically demanding. These limitations could have been explored further by testing bacterial suspensions alongside intact biofilms. In addition, performing the assay on freshly prepared biofilms without a freezing and revival step may have helped determine whether sample preservation influenced nitrate-reducing activity or assay performance. A potential approach to detect and mitigate problems related to the inability to directly detect nitrate and the presence of compounds interfering with the Griess reaction could be the use of a complementary nitrite/nitrate detection method such as high-performance liquid chromatography or ion chromatography, which allows separation of the components of the sample and measures the concentration of analytes of interest (Bryan and Grisham, 2007).

4.4.7 Crystal violet biomass assessment

Biofilms used for the 1-hour and 24-hour nitrate reduction capacity assays were subsequently repurposed for the crystal violet biomass assay. Although staining revealed variations in macroscopic structure (Figure 4.17A), no notable differences were observed between the multi-species biofilms in the assay (Figure 4.17B). The crystal violet biomass assay is widely used in biofilm characterisation, despite several potential sources of bias and error. Crystal violet has limited sensitivity to detect small differences between samples, is prone to experimental handling variations and may underestimate biomass in biofilms that are prone to detachment (Kragh et al., 2019). While experimental handling variation was reduced by processing all samples simultaneously, it was noted that the 5-species biofilms, especially the NR+S variant, were more prone

to detachment in patches a few millimetres in size during washing, introducing the risk of biomass loss before staining and measurement.

4.5 Summary and findings

1. Can we design and develop an *in vitro* biofilm that reflects the key characteristics of a subgingival biofilm associated with a healthy oral barrier such as:

    a. composition?

    - There are bacterial genera and species more abundant in a healthy subgingival biofilm, and they were successfully incorporated into an *in vitro* model.

    b. microarchitecture and structure?

    - Similar to *in vivo* conditions, health-associated *in vitro* biofilm models had a more homogenous surface, less complex structure and exhibited lower biomass than a periodontitis-associated biofilm model. This may reflect the smaller number of species in the health-associated biofilm. Nonetheless, this could be considered to reflect the reduced microbiome diversity observed in healthy gingival sites compared with periodontitis sites.

    c. metabolism (nitrate reduction capacity)?

    - More studies are needed to determine the conditions where nitrate reduction capacity contributes to the maintenance of the healthy oral barrier.

These findings supported the hypothesis that there are key differences between health- and periodontitis-associated subgingival biofilms. Further studies are needed to evaluate how these different biofilms influence oral barrier integrity in an *in vitro* model.

4.6 Publications

Work from this chapter has been presented at the following conferences/symposia:

- Haleon Symposium, January 2025, Weybridge
- University of Glasgow School of Medicine, Dentistry and Nursing IEE Day Away, April 2025, Glasgow
- Oral Microbiology and Immunology Group ECR Meeting, May 2025, Glasgow.

5 Investigating host cell lines for use in an *in vitro* model of neutrophil migration into the gingival sulcus

5.1 Introduction

5.1.1 Available models of neutrophil transepithelial migration *in vitro*

Previous studies report attempts at reconstructing junctional epithelium *in vitro* using a combination of different epithelial and fibroblast cell types (Gavriiloglou et al., 2024). However, to date, only one study has described development of an *in vitro* model of neutrophil transepithelial migration into the gingival sulcus. The authors developed a system consisting of the 'oral' epithelial KB cells seeded onto the basolateral side of the transwell insert membrane and ^{51}Cr-labelled primary neutrophils. Neutrophil transepithelial migration was assessed in the context of a prior infection of the epithelial layer with *P. gingivalis* (Madianos et al., 1997). The KB cell line employed in this study was initially misidentified as oral epidermoid carcinoma, but it was later attributed as HeLa or cervical adenocarcinoma (Vaughan et al., 2017). Comparable *in vitro* setups employing apical-to-basolateral migration have been utilised to model bacterial infection-induced neutrophil transepithelial migration in other organs such as intestines (Chu et al., 2017), lungs (Kusek et al., 2014) and brain (Wewer et al., 2011).

5.1.2 Choosing components of an *in vitro* model of neutrophil migration through the junctional epithelium

In this thesis, a novel 3D *in vitro* model was developed to mimic neutrophil migration through the junctional epithelium. The components intended to constitute the host part of the model, together with their spatial arrangement, are shown in Figure 5.1. The inverted transwell setup, with the epithelial cells seeded on the basolateral side, was retained because of its physiological

relevance. *In vivo*, neutrophils first cross the basement membrane and then traverse the epithelial cell layer. A pore size of 3 µm was chosen to allow for active migration of neutrophils that have a diameter of 8.3 µm, while preventing their passive passage (Downey et al., 1990).

Primary junctional epithelial cells are challenging to isolate and culture, and have a limited proliferative capacity (Matsuyama et al., 1997). Thus, employing an established immortalised cell line was deemed the most suitable approach. The candidate epithelial cell line for the *in vitro* model was the TR146 cell line, a buccal mucosa squamous cell carcinoma cell line isolated from a metastatic lesion in a cervical lymph node of a 67-year-old female (Rupniak et al., 1985). It has been extensively used in oral barrier property studies (Bierbaumer et al., 2018) and is known to form permeable multilayers (Jacobsen et al., 1995, Jacobsen et al., 1999). It constitutively expresses IL-8 (CXCL-8) (Molero-Abraham et al., 2019) and has been shown to increase *IL8* gene expression in response to stimulation with multi-species bacterial suspensions (Brown et al., 2019).

Primary human neutrophils are used extensively in *in vitro* studies. However, they are short lived (hours to days) and as terminally differentiated cells, they do not divide (Rosales, 2018). It is recommended that they are used for functional assays within 24 hours following isolation. Their long-term storage in liquid nitrogen is not advised as it significantly compromises their chemotactic and polarisation responses (Avci et al., 2019). There are several established alternatives to the use of primary neutrophils in *in vitro* models. The most widely used are immortalised myeloid cell lines of leukaemic origin, such as HL-60, PLB-985, NB4 and, less often, Kasumi-1 (Blanter et al., 2021). All of them, with the exception of the last one, are comparable to the promyelocyte stage of neutrophil development in the bone marrow (see Figure 5.2). Kasumi-1 is more closely associated with the myeloblast stage of myeloid differentiation. The most commonly used is the HL-60 cell line that was originally isolated from a 36-year-old Caucasian female with acute promyelocytic leukaemia (Collins et al., 1977, Gallagher et al., 1979). It can be differentiated into neutrophil-like cells using a wide range of treatments including DMSO and ATRA, among others (Blanter et al., 2021, Manda-Handzlik et al., 2018). These two treatments allow for differentiation into neutrophil-like cells that are more responsive to IL-8 (CXCL-8)-induced chemotaxis than the untreated HL-60 cells (Sham et al., 1995).

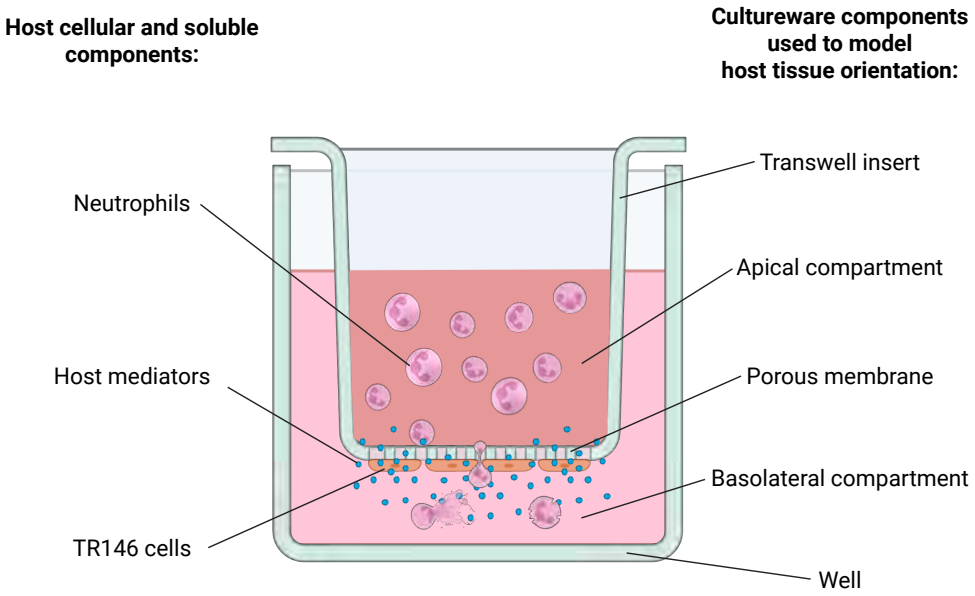

Figure 5.1 Intended spatial orientation of host components in an *in vitro* model of neutrophil migration through the junctional epithelium. TR146 epithelial cells are seeded on the basolateral side of a porous transwell insert membrane to mimic the *in vivo* orientation of the junctional epithelium, where the basement membrane is adjacent to the connective tissue and the outermost epithelial layers face the sulcus. In this configuration, neutrophils migrate from the apical transwell compartment, representing the connective tissue side, towards the basolateral compartment, representing the gingival sulcus, in response to a chemokine gradient. They first cross the porous membrane, representing the basement membrane underlying the junctional epithelium, and then move through the epithelial layers towards the sulcular-facing surface. Figure created with BioRender.com.

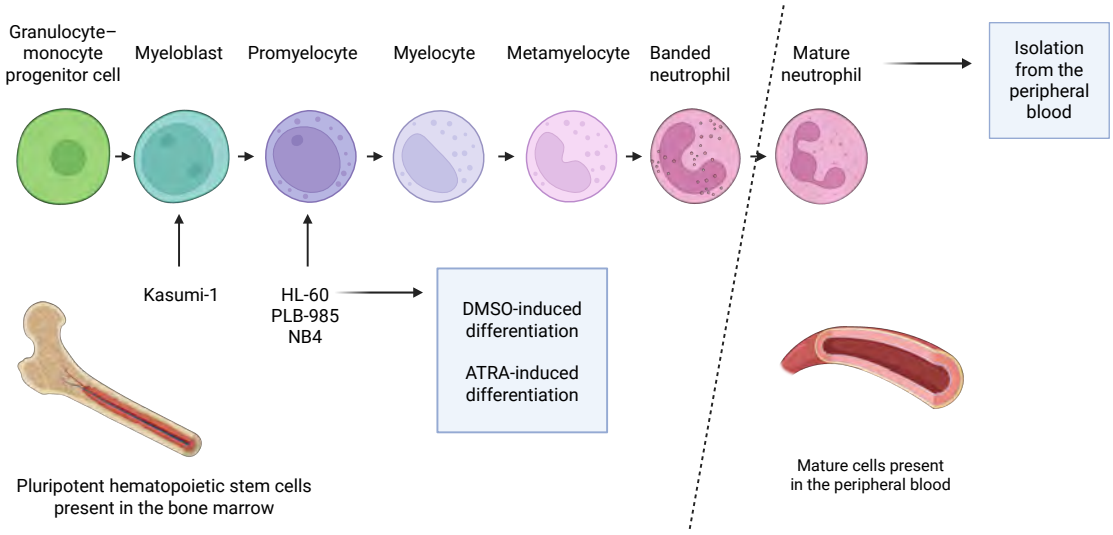

Figure 5.2 Granulopoiesis. Neutrophils develop in the bone marrow from granulocyte–monocyte progenitor cells originating from haematopoietic stem cells. Neutrophil precursors progress through different stages of development with distinct phenotypes. The promyelocyte stage is marked by the development of primary (azurophilic) granules and the ability to divide, which is lost by the metamyelocyte stage. Other types of granules appear during later stages of

granulopoiesis. Once a neutrophil matures, it is released into the blood. The HL-60, PLB-985 and NB4 cell lines are comparable to the promyelocyte stage of development, while the Kasumi-1 cell line is analogous to the myeloblast stage. Figure adapted and modified from Blanter et al. (2021). ATRA, all-trans retinoic acid; DMSO, dimethyl sulfoxide. Figure created with BioRender.com.

5.1.2.1 Cell line identity and provenance considerations

Careful identification and assessment of incorporated components and methods involved in developing any *in vitro* model is crucial to maintain credibility, reproducibility of the work and its relevance to *in vivo* systems.

A 2017 study using the International Cell Line Authentication Committee database identified 32,755 articles based on misidentified cell lines (Horbach and Halffman, 2017). Version 13 of the register lists 593 cell lines from various species that were either misidentified or cross-contaminated (International Cell Line Authentication Committee, 2024). The HeLa cell line, reported as the contaminant in 145 other cell lines, is the most notable example. Among the known HeLa cross-contaminants is the KB subline initially thought to be an oral epidermoid carcinoma (Masters, 2002, Vaughan et al., 2017). Interestingly, this KB cell line was used in the only other known attempt to model neutrophil transepithelial migration into the gingival sulcus *in vitro* (Madianos et al., 1997), described in more detail in Section 5.1.1. The candidate cell lines investigated in this chapter, TR146 and HL-60, were not listed in the database and were obtained from the ECACC, a cell culture collection that routinely authenticates the identity of human cell lines using STR profiling (Culture Collections, n.d.-b).

5.2 Hypothesis and research questions

Hypothesis: Certain cell types and lines can be used as components of an *in vitro* model of neutrophil migration at the junctional epithelium.

The following research questions were posed to test the hypothesis:

1. Can TR146 epithelial cells be grown on the basolateral side of a porous transwell insert membrane?

2. What are the differences between primary peripheral blood neutrophils and HL-60 cells differentiated into neutrophil-like cells with respect to:

    a. expression of surface receptors?

    b. responsiveness to relevant stimulants?

Question 2 sought to validate the suitability of differentiated HL-60 cells for use in the proposed model system.

5.3 Results

Preliminary experiments were undertaken to determine whether TR146 epithelial cells could be grown on the basolateral side of porous transwell insert membranes, with the aim of establishing an *in vitro* epithelial layer suitable for modelling neutrophil migration through the junctional epithelium. The experiments first assessed methods for quantifying cell number, comparing manual haemocytometer counts and automated cell counter measurements against expected values calculated from serial dilutions. Subsequent experiments evaluated TR146 cell attachment, metabolic activity and layer formation on different transwell insert membranes using the CCK-8 assay and H&E histology. The effect of membrane pre-coating with $CaCl_2$, FBS or type I collagen was also explored. Lucifer yellow permeability assays were then used to assess whether epithelial layer formation altered membrane permeability over time. Based on the initial findings, further optimisation was performed using a higher seeding density and selected membrane conditions.

The second part of this chapter aimed to characterise primary neutrophils and HL-60 cells differentiated with either DMSO or ATRA towards a neutrophil-like phenotype, and to optimise readouts relevant to the planned neutrophil transepithelial migration model. Surface expression of CD45, CD11b, CD14 and CD15 was first compared between primary neutrophils and DMSO- or ATRA-differentiated HL-60 cells by flow cytometry to assess whether either treatment generated cells with a neutrophil-like phenotype, as previously reported. The functional responsiveness of primary neutrophils and ATRA-differentiated HL-60 cells was then explored by measuring IL-8 release following stimulation with fMLF and LTB_4, two rapid neutrophil-activating mediators. Primary neutrophil responses were further assessed following stimulation with fMLF, G-CSF, GM-CSF or PMA across selected concentration ranges and incubation periods, with IL-1ß, IL-6, IL-8 and TNF-α measured by ELISA. Finally, several methods for quantifying neutrophil number as a migration-related readout were evaluated, including manual and automated cell counting using trypan blue and erythrosin B dyes, as well as standard curves generated using the CCK-8 and BacLight assays for indirect cell quantification.

5.3.1 Epithelial cell layer grown on transwell insert membrane

5.3.1.1 Assessment of quantification methods for TR146 cells

To determine if TR146 epithelial cells could be grown on the basolateral side of a porous transwell insert membrane, methods were sought to quantify the cells forming the epithelial layer. There are various methods of cell counting, including use of a manual haemocytometer and an automated cell counter. In order to compare these two methods, freshly passaged TR146 cells were used to prepare serial dilutions of cell suspensions at 1, 2, 4, and 8 × 10^5 cells/mL. Cells were then quantified with a trypan blue exclusion assay using a Neubauer haemocytometer and a Luna II Automated Cell Counter. Obtained data (two technical replicates per method obtained from a single biological sample) were used to generate standard curves (Figure 5.3). Following nonlinear regression (straight line), extra-sum-of-squares F-tests revealed that both methods yielded curves comparable in shape ($F(2,12) = 0.5329$, $p = 0.6002$) but positioned below the expected curve. Furthermore, the dataset obtained with the Luna II Automated Cell Counter suggested higher variability and lower R^2 values (0.6581) compared to manually counted cells ($R^2 = 0.9810$).

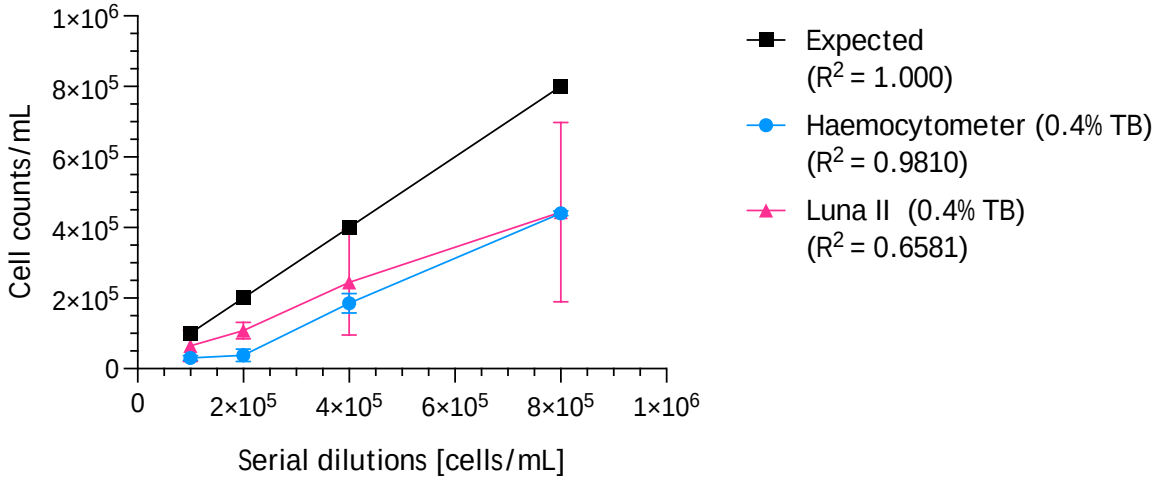

Figure 5.3 Cell counts of TR146 cells using a haemocytometer and an automated cell counter. Cell counts were performed on a set of dilutions (1, 2, 4, 8 × 10^5 cells/mL) using a Neubauer haemocytometer or a Luna II automated cell counter. Cells were stained with 0.4% trypan blue. Expected cell counts were calculated using the initial haemocytometer count and serial dilution factors. Data are presented as mean ± SD from technical duplicate measurements obtained in one experiment (n = 1). TB, trypan blue.

In the subsequent cell counting experiment, a different set of dilutions (6.25×10^4, 1.25, 2.5 and 5×10^5 cells/mL) was prepared to target lower concentrations. Trypan blue was used either at its original stock concentration of 0.4% or as a 1:10 dilution (0.04%) to reduce background staining. Among the standard curves generated (Figure 5.4), only the one representing manually counted cells stained with stock trypan blue shared its parameters with the expected standard curve ($F(2,8) = 1.140$, $p = 0.3668$), although it had the lowest R^2 value (0.8114), indicating a poorer fit of the data. This was considered a valid compromise. Therefore, the manual cell counting method using stock 0.4% trypan blue was selected as the method of choice for quantifying TR146 cells in suspension, to ensure an accurate estimate of the number of cells seeded onto membranes in each experiment.

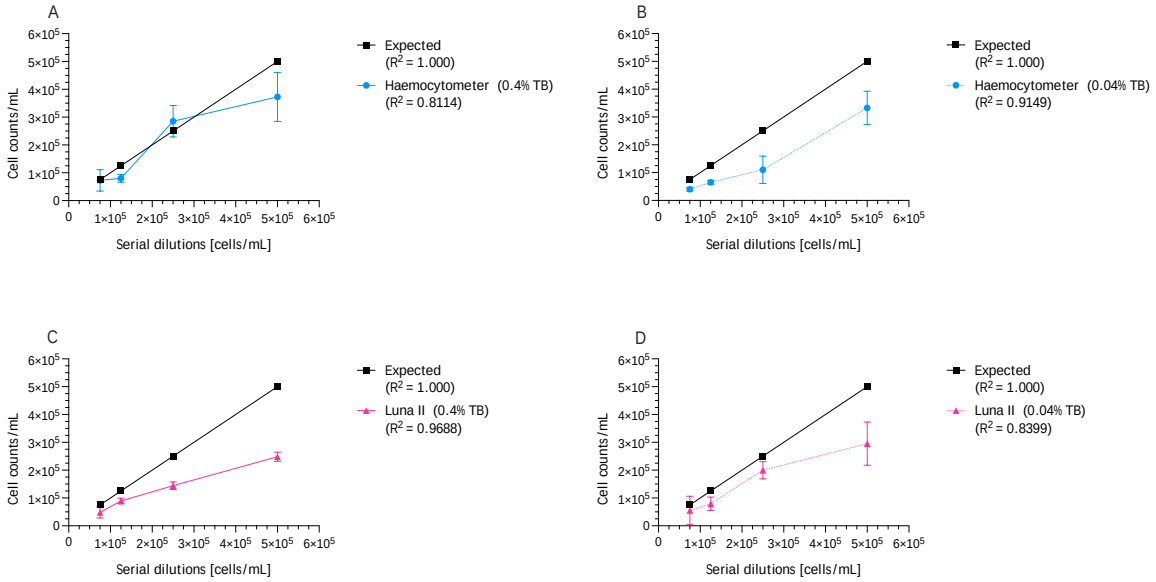

Figure 5.4 Cell counts of TR146 cells using a haemocytometer and an automated cell counter. Cell counts were performed on a set of dilutions (6.25×10^4 and 1.25, 2.5, 5×10^5 cells/mL) using a Neubauer haemocytometer (A, B) or a Luna II automated cell counter (C, D). Cells were stained with 0.4% trypan blue (A, C) or 0.04% trypan blue (B, D). Expected cell counts were calculated using the initial haemocytometer count and serial dilution factors. Data are presented as mean ± SD from technical duplicate measurements obtained in one experiment (n = 1). TB, trypan blue.

The next step involved an attempt to quantify TR146 cells cultured on a transwell insert membrane. However, even prolonged trypsinisation for 30 minutes (compared with 5–10 minutes used in routine culture), combined with vigorous pipetting, was insufficient to detach the cells from the membrane. Therefore, other methods were sought to quantify the cells attached to the membrane.

The CCK-8 assay measures the metabolic activity of cells, which is assumed to be proportional to cell number. It is non-toxic and does not require cell detachment, potentially preserving the epithelial layer structure and permitting the use of the same transwells in subsequent assays. To evaluate the capacity of the CCK-8 assay to enumerate TR146 cells, freshly passaged TR146 cells were used to prepare serial dilutions (ranging from 6.125×10^4 to 1×10^6 cells per 700 µL well) in a 24-well plate. Plates were read in a FLUOstar Omega Microplate Reader at 450 nm wavelength following incubation with CCK-8 for 1, 2, 3 and 4 hours. Initial visual inspection (Figure 5.5) and nonlinear analysis (Figure S2) indicated saturation of the top OD values corresponding to 1×10^6 cells/well, which were excluded from further analysis. Subsequent nonlinear regression and comparison of fits using the extra-sum-of-squares F-test revealed that the curves within each time point ($F(4,23–24) = 14.6\text{-}45.0$, $p < 0.005$) differed significantly, indicating that the 3 repeats could not be described by one shared line. Therefore, the standard curves could not be used to interpolate values obtained during the following CCK-8 assays performed with transwell inserts seeded with TR146 cells. Instead, blank-corrected OD values were reported in subsequent experiments, which are referred to as metabolic activity assays.

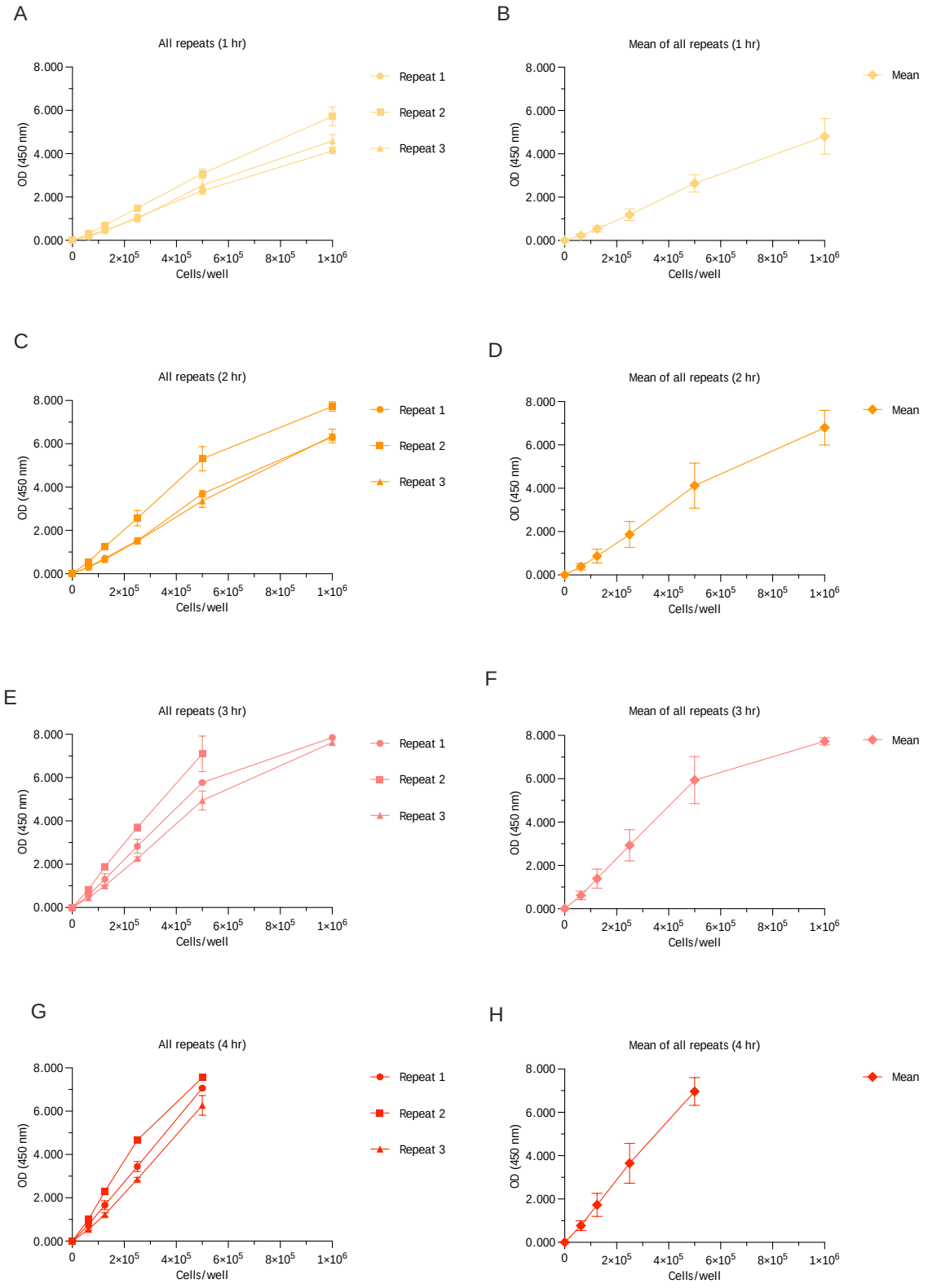

Figure 5.5 CCK-8 assay of serial dilutions of TR146 cell suspensions. Serial dilutions of TR146 cell suspensions were incubated with CCK-8 for 1 hour (A, B), 2 hours (C, D), 3 hours (E, F) and 4 hours (G, H). Data are presented as mean ± SD of blank-corrected OD values from each of three independent experiments (n = 3) performed in technical duplicate (A, C, E, G) and as mean ± SD from all experiments (B, D, F, H) for each time point. For the 4-hour time point, the OD values for the top concentration exceeded the plate reader's measurable range and were unavailable for analysis.

5.3.1.2 Assessment of metabolic activity of TR146 cells forming the epithelial cell layer

To explore if TR146 cells could attach to the basolateral side of the transwell insert membrane and remain metabolically active, Corning and Millicell PET transwells were seeded with 5×10^4 cells per transwell and incubated at 37 °C, 5% CO_2 for 4 days. Additionally, three membrane pre-coating conditions were included (0.24 M $CaCl_2$, FBS or type I collagen) to explore if these could improve TR146 cell adhesion and layer formation. CCK-8 assay results (Figure 5.6) suggested that cells grown on Millicell PET inserts achieved higher OD values after 1-hour incubation, although there was considerable variability between the technical replicates. After the 3-hour incubation, all Corning PET transwells (except for those with untreated membranes) appeared to achieve higher average OD values, but this was attributable to one technical replicate giving higher readings. These pilot observations were exploratory and not designed to support statistical inference. These data suggested that additional pre-coating did not provide a measurable improvement in cell metabolic activity, as measured by the CCK-8 assay.

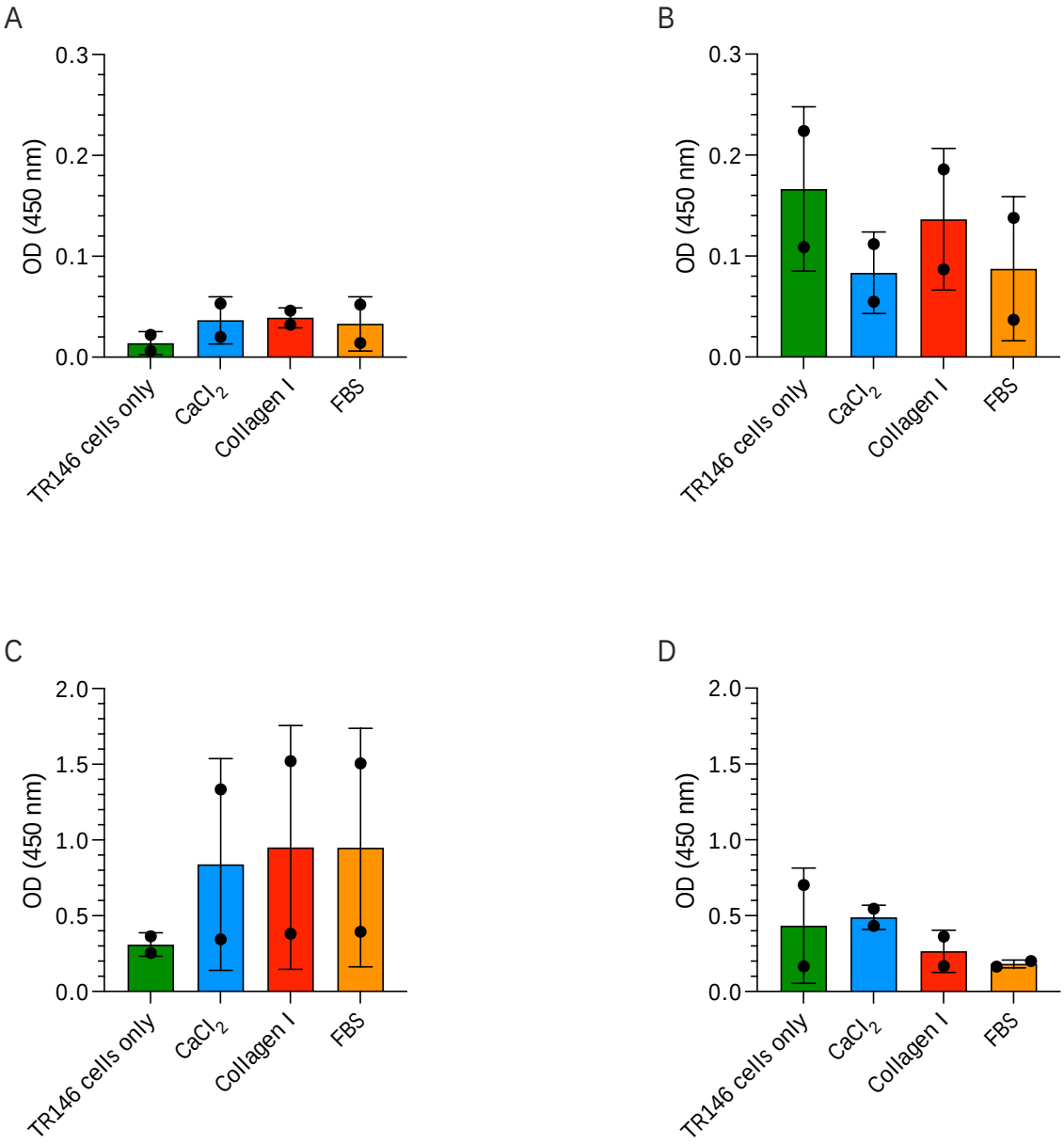

Figure 5.6 CCK-8 assay of TR146 cells seeded onto transwell insert PET membranes with or without pre-coating with $CaCl_2$, type I collagen or FBS. Corning (A, C) and Millicell (B, D) transwell inserts with PET membranes of 6.5 mm diameter and 3 µm pores were seeded with 5×10^4 cells per transwell and incubated for 4 days at 37 °C, 5% CO_2. Following incubation, the metabolic activity of the TR146 epithelial cell layer on each transwell was evaluated with the CCK-8 assay. Data are presented as mean ± SD of blank-corrected OD values obtained after either 1 hour (A, B) or 3 hours (C, D) of incubation with CCK-8 at 37 °C in 5% CO_2. Each condition was tested in a single experiment (n = 1) with two technical replicates represented as dots. $CaCl_2$, calcium chloride; FBS, foetal bovine serum; PET, polyethylene terephthalate.

5.3.1.3 Architecture of TR146 epithelial cell layers grown on transwell insert membranes

The presence and morphology of the epithelial cell layers formed on transwell insert membranes were assessed by histological examination of H&E-stained sections. Membranes from the previous experiment were fixed in 10% neutral buffered formalin (4% formaldehyde) overnight at 4 °C and then transferred to PBS. Next, they were carefully excised, embedded in paraffin blocks, sectioned and stained with H&E. The staining revealed heterogeneous cell distribution both between and within membranes (Figure 5.7, Figure 5.8 and Figure S3). None of the tested transwell insert brands or conditions produced a consistently uniform epithelial coverage of the membranes.

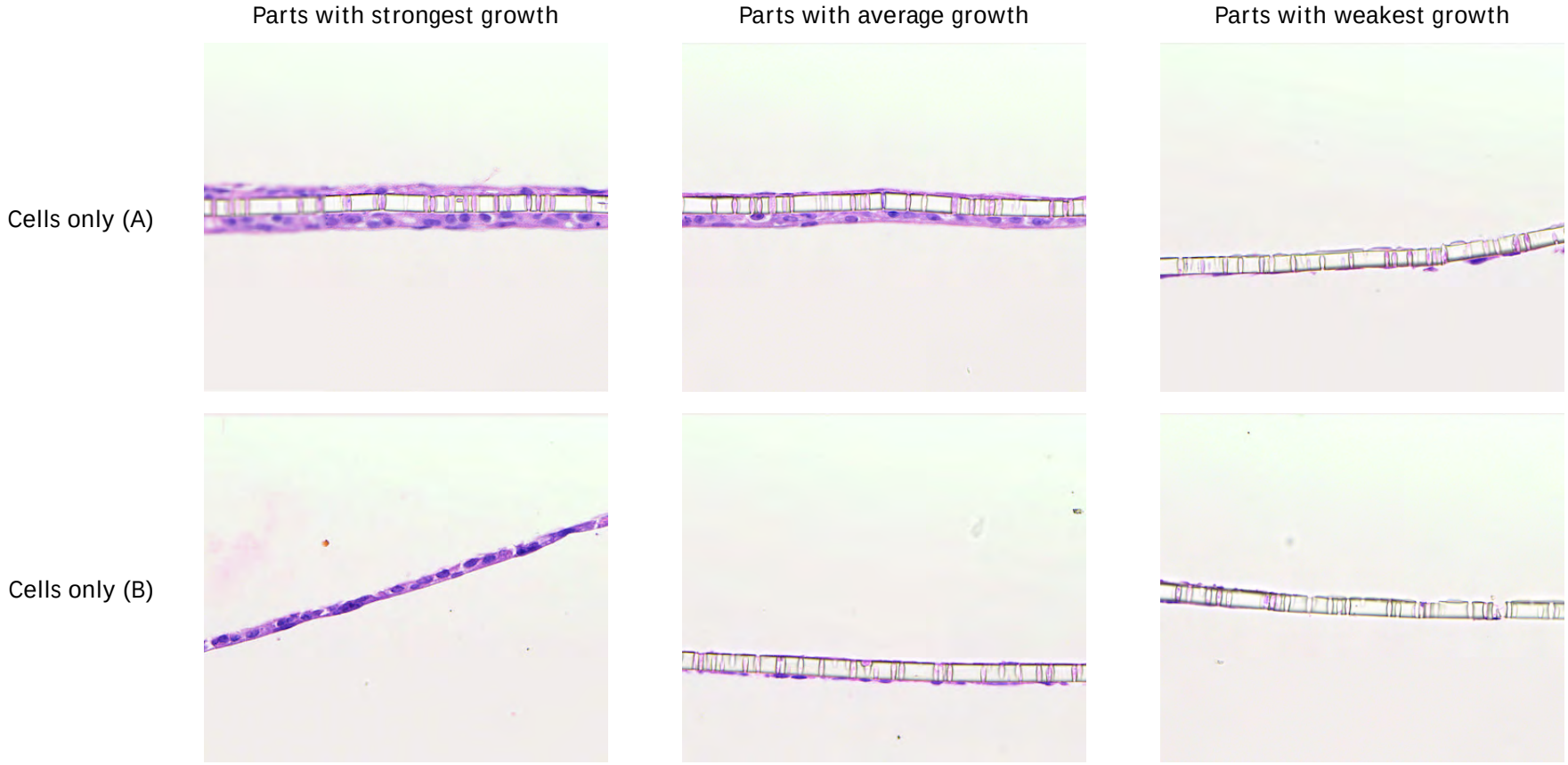

Figure 5.7 Histology of TR146 epithelial cell layers grown on Corning PET transwell insert membranes. Panels A and B show duplicate membranes, each seeded with 5×10^4 cells without any pre-coating and incubated for 4 days at 37 °C, 5% CO_2. Subsequently, they were fixed, excised, embedded in paraffin blocks, sectioned and stained with H&E. Slides were scanned at 80× magnification. Each image is representative of a part of a single membrane showing the strongest, average or weakest cell growth. Membrane thickness is 10 µm. PET, polyethylene terephthalate.

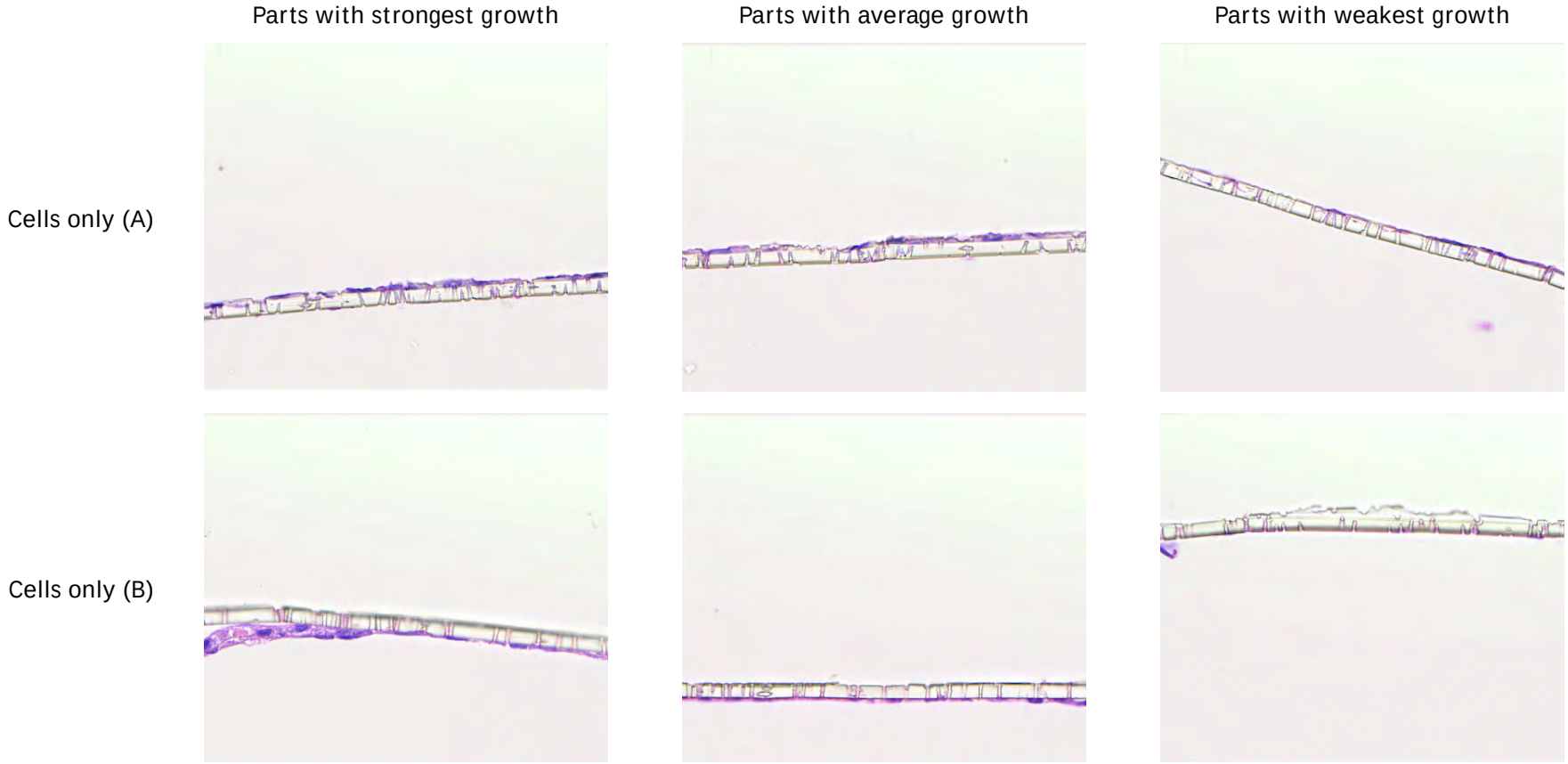

Figure 5.8 Histology of TR146 epithelial cell layers grown on Millicell PET transwell insert membranes. Panels A and B show duplicate membranes, each seeded with 5×10^4 cells without any pre-coating and incubated for 4 days at 37 °C, 5% CO_2. Subsequently, they were fixed, excised, embedded in paraffin blocks, sectioned and stained with H&E. Slides were scanned at 80× magnification. Each image is representative of a part of a single membrane showing the strongest, average or weakest cell growth. Membrane thickness is 9–16 µm. PET, polyethylene terephthalate.

5.3.1.4 Permeability of the epithelial barrier

Permeability of the TR146 epithelial cell layer was assessed over the course of 7 days using Corning and Millicell transwell inserts with PET membrane. A 100 µL solution of 100 µg/mL Lucifer Yellow was added into the apical chamber of the transwell inserts and the full setup was incubated for 1 hour in 37 °C, 5% CO_2. Lucifer Yellow is a synthetic fluorescent dye with a low molecular weight that has a capacity to diffuse through gaps in the cell layer and is commonly used to assess paracellular permeability (Bierbaumer et al., 2018). Following incubation, the fluorescence intensity was measured as its relative indicator. The results of this single experiment (Figure 5.9) suggested that the permeability of the TR146 epithelial cell layer appeared similar to the unseeded membrane of the same brand throughout the experiment, although unseeded Millicell membranes displayed higher variability compared to Corning membranes. Seeded Corning PET transwells maintained relatively stable levels of permeability over the period of 7 days except for day 2 when it slightly decreased. Permeability of seeded Millicell transwells showed a subtle reduction towards day 4, but then it approached the initial levels by day 7. Blocked inserts, in which the porous membrane was sealed with nail polish, produced positive raw fluorescence values, but blank-correction and extrapolation below the lower end of the standard curve resulted in calculated negative concentrations. These values were recorded as below the extrapolatable range. A value of 0 was then used for descriptive reporting and calculation of descriptive summary values.

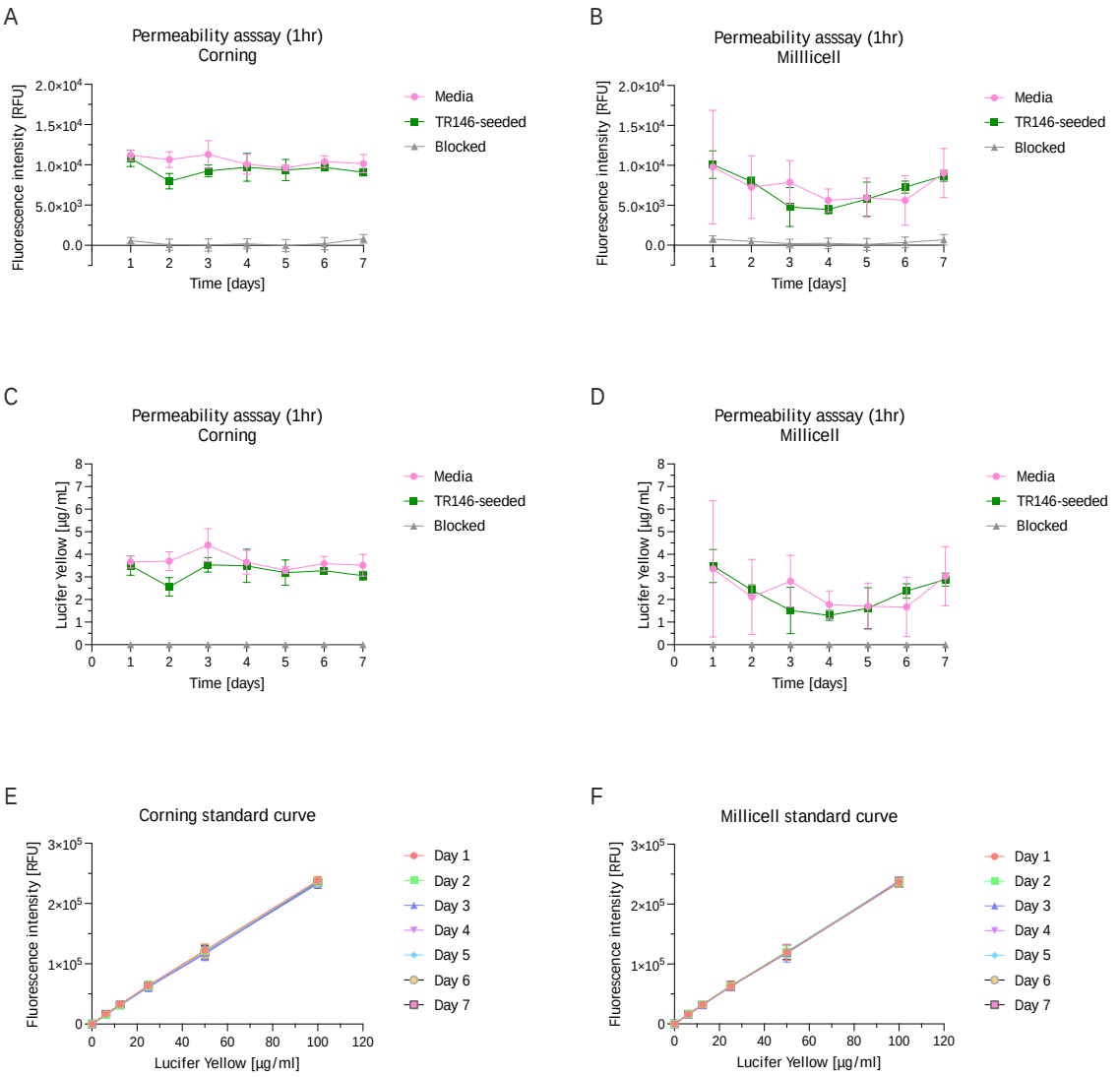

Figure 5.9 Lucifer Yellow permeability assay of TR146 cells seeded onto transwell insert membranes. TR146 cells were seeded onto Corning or Millicell PET transwell insert membranes at 5 × 10^4 cells per transwell and cultured for 1 day at 37 °C, 5% CO_2. Unseeded transwells and transwells blocked with nail polish were prepared as positive and negative controls, respectively. Lucifer Yellow was added to the apical compartment of the transwell inserts, which were incubated for 1 hour at 37 °C, 5% CO_2. Following incubation, the inserts were removed and the fluorescence signal in the wells was measured using a plate reader. The permeability assay was then performed daily for a further 6 days. Data are presented as mean ± SD from a single experiment (n = 1), with 4 technical replicates for blank-corrected values (A, B) and calculated concentrations (C, D). Standards used to generate the standard curves for concentration calculation (E, F) were run in duplicate and are also presented as mean ± SD. Samples outside the limits of the standard curve were extrapolated where possible. Values extrapolated below zero were recorded as below the extrapolatable range and assigned a value of 0 before calculation of descriptive summary values. PET, polyethylene terephthalate; RFU, relative fluorescence units.

5.3.1.5 Assessment of metabolic activity of TR146 cells seeded at a higher density

Initial experiments conducted at 5 × 10^4 cells per transwell did not show a clear advantage of any brand or pre-treatment in the context of cell attachment and

metabolic activity. Therefore, an expanded set of transwell insert types (including previously tested Corning and Millicell PET transwells and an additional Corning PC transwell type; for further details see Table 2.7) was tested using a substantially higher seeding density (1×10^6 cells per transwell), under the assumption that this might enhance cell attachment and metabolic activity. The incubation time was shortened to 2 days to prevent nutrient depletion and waste build-up.

The following CCK-8 assay (Figure 5.10) suggested that cells growing on both Corning transwell types generally showed a consistently low OD signal (0.250 ± 0.032 and 0.139 ± 0.061 for PC and PET membranes, respectively). By contrast, cells growing on Millicell PET membranes appeared to produce higher OD values, which varied more between transwells (0.725 ± 0.281). Nevertheless, all technical replicates of Millicell PET transwells showed a tendency to exceed the maximum OD reached by the other transwells. Histological assessment of 3 out of 4 transwells representing each tested brand and membrane type was attempted. However, no epithelial layers were observed in the sections, which contained occasional sparse individual cells or cell-free membranes (data not shown).

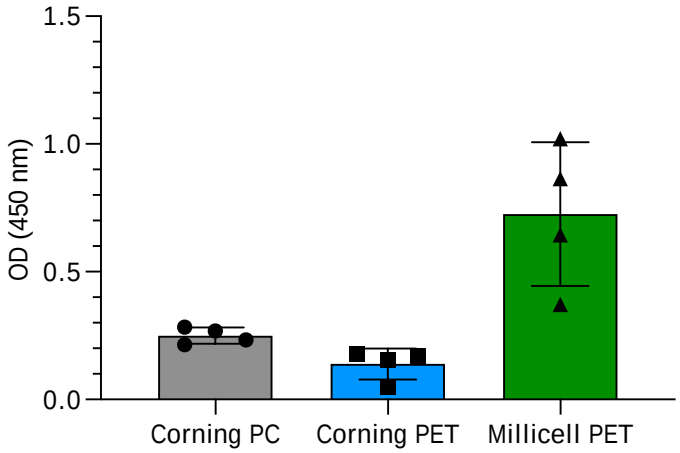

Figure 5.10 CCK-8 assay of TR146 cells seeded onto three different transwell insert types. Corning PC and PET membranes alongside Millicell PET membranes were seeded with 1×10^6 cells per transwell and incubated for 2 days at 37 °C, 5% CO_2. Following incubation, the metabolic activity of the TR146 epithelial cell layer on each transwell was evaluated with the CCK-8 assay. Data are presented as mean ± SD of blank-corrected OD values obtained after a 2-hour incubation with CCK-8 at 37 °C, 5% CO_2. Data are from a single experiment (n = 1) with 4 technical replicates represented as symbols. PC, polycarbonate; PET, polyethylene terephthalate.

5.3.1.6 Assessment of metabolic activity of TR146 cells seeded onto Millicell PET transwell insert membranes

The Millicell PET transwell insert membranes were considered the most promising due to their tendency to yield higher OD values in the CCK-8 assay and were prioritised for further evaluation. Metabolic activity of TR146 cells grown on Millicell membranes was assessed in three independent experiments at 4 different time points (Figure 5.11). The first and second experiments produced comparable and relatively consistent OD values at each time point. Compared to initial measurements obtained after the first hour, the signal seemed to decrease at 2 hours, but then showed an increase towards the 4-hour time point. By contrast, the third experiment appeared to produce higher OD values, while variability between technical replicates remained relatively low.

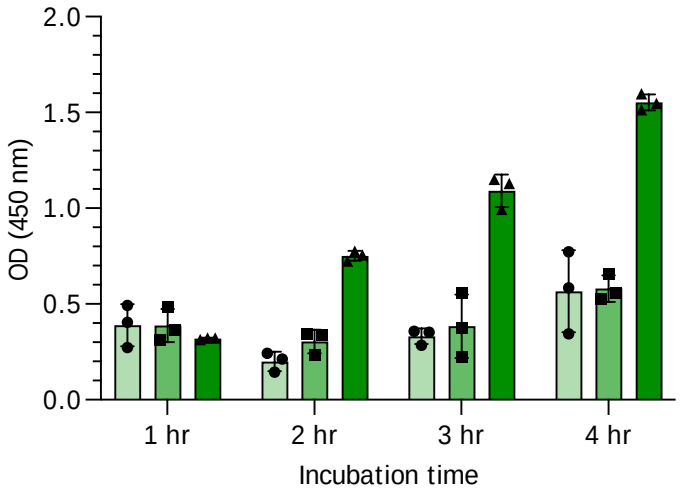

Figure 5.11 CCK-8 assay of TR146 cells seeded onto Millicell PET transwell inserts. Membranes were seeded with 1×10^6 cells per transwell and incubated for 2 days at 37 °C, 5% CO_2. Following incubation, the metabolic activity of the TR146 epithelial cell layer on each transwell was evaluated with the CCK-8 assay. Data are presented as mean ± SD of blank-corrected OD values obtained after 1, 2, 3 and 4 hours of incubation with CCK-8 at 37 °C in 5% CO_2, using separate sets of transwells for each time point. The experiment was performed on 3 independent occasions (n = 3; shown as different bar colours) with 3 technical replicates represented as symbols. PET, polyethylene terephthalate.

5.3.1.7 Architecture of TR146 epithelial cell layers grown on Millicell PET transwell insert membranes

During the preparation of transwells for the final repeat of the previous experiment, additional transwell inserts were seeded with TR146 cells for the

purpose of histological analysis. H&E staining of the membranes revealed the presence of a uniform multilayer of epithelial cells across all examined specimens (Figure 5.12).

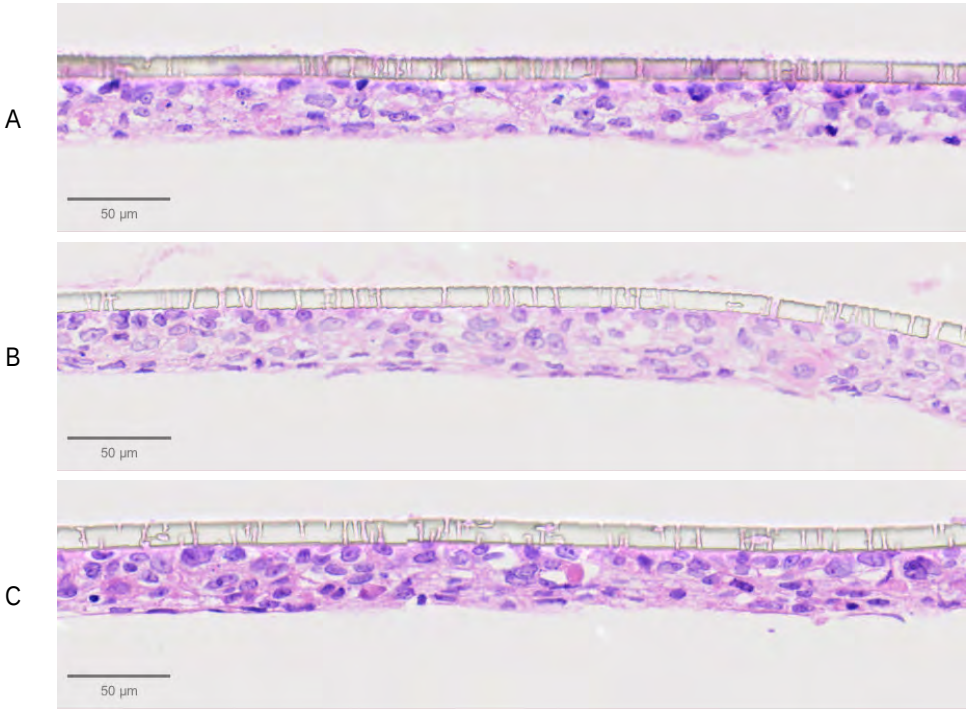

Figure 5.12 Histology of TR146 epithelial cell layers grown on Millicell PET transwell insert membranes. Membranes were seeded with 1 × 10^6 cells per transwell and incubated for 2 days at 37 °C, 5% CO_2. Subsequently, they were fixed, excised, embedded in paraffin blocks, sectioned and stained with H&E. Slides were scanned at 80× magnification. Each image is representative of one of three seeded transwells from a single experiment (n = 1).
PET, polyethylene terephthalate.

5.3.2 Selection of an immune cell type

5.3.2.1 Expression of cell surface receptors

As a preliminary validation step, the suitability of differentiated HL-60 cells for use in the proposed model system was assessed by comparing their cell surface receptor expression with that of primary neutrophils (Blanter et al., 2021, Manda-Handzlik et al., 2018). Primary neutrophils, undifferentiated HL-60 cells and ATRA- and DMSO-differentiated HL-60 cells were stained with fluorochrome-conjugated antibodies against CD45, CD11b, CD14 and CD15, together with a viability dye, and analysed by flow cytometry. The gating strategy involved gating all events based on forward scatter area (FSC-A) and side scatter area (SSC-A) to identify cells (Figure 5.13A), which was followed by exclusion of

doublets using forward scatter area (FSC-A) and forward scatter height (FSC-H). Next, singlets were gated on CD45 and CD11b expression, indicative of leukocytes and myeloid cells, respectively. Then, $CD14^+$ monocytic-like events were excluded. The final gated population was displayed on a CD11b/CD15 dot plot (Figure 5.13B). DMSO-differentiated cells were $CD45^+$, $CD11b^+$, $CD14^-$ and $CD15^-$, while both primary neutrophils and ATRA-differentiated HL-60 cells showed a phenotype consistent with the expected $CD45^+$, $CD11b^+$, $CD14^-$ and $CD15^+$ profile and were therefore used in the subsequent experiments.

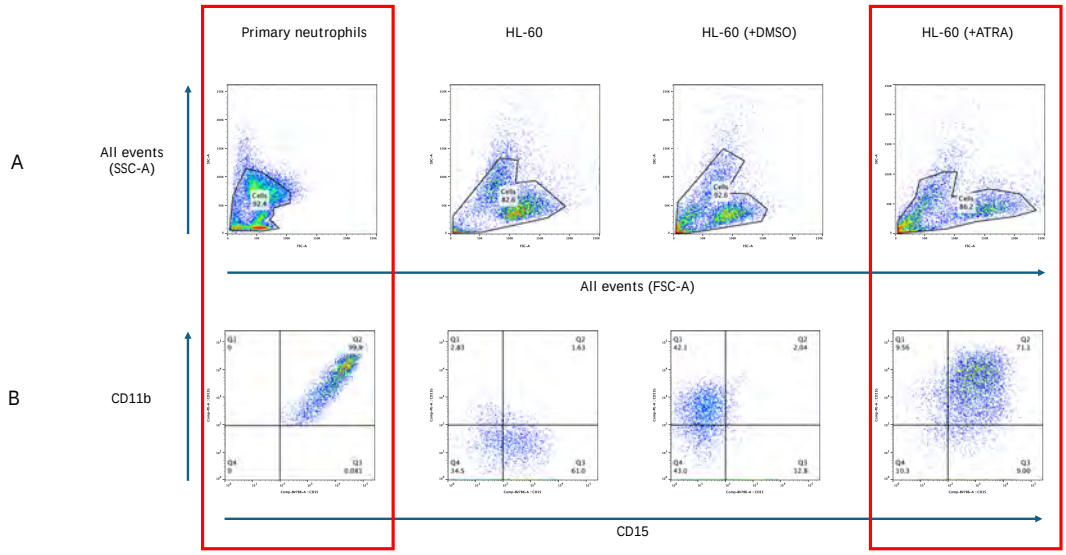

Figure 5.13 Comparison of primary neutrophils, undifferentiated HL-60 cells and DMSO- and ATRA-differentiated HL-60 cells by flow cytometry. The cell types investigated are shown in the column headings. Row A shows SSC-A/FSC-A profiles of all acquired events, with the cell gates indicated. Row B shows CD11b/CD15 profiles of the final gated populations, with CD11b-positive events in the upper quadrants and CD15-positive events in the right quadrants. Each cell type was stained and acquired once; therefore, data are presented descriptively. Values shown on the plots indicate the percentage of events within the corresponding gate or quadrant. ATRA, all-trans retinoic acid; CD, cluster of differentiation; DMSO, dimethyl sulfoxide; FSC-A, forward scatter area; SSC-A, side scatter area.

5.3.2.2 Pro-inflammatory cytokine production following neutrophil and neutrophil-like cell stimulation

Release of pro-inflammatory mediators such as IL-8 is one of the effector functions of neutrophils following activation by bacterial components such as

fMLF or host mediators such as LTB_4. Both fMLF and LTB_4 are rapid G protein-coupled receptor agonists and key molecules in neutrophil signalling (Metzemaekers et al., 2020) and therefore were used to stimulate both neutrophils and neutrophil-like cells to investigate if they produced comparable levels of IL-8. After 24 hours, supernatants were collected and assessed for IL-8 concentration using an ELISA (Figure 5.14). It was observed that fMLF and LTB_4 were associated with increased IL-8 release in primary neutrophils, with concentrations of 73.174 ± 23.496 and 50.113 ± 15.051 pg/mL, respectively. By contrast, fMLF- and LTB_4-stimulated ATRA-differentiated HL-60 cells produced on average 3.694 ± 1.761 and 3.405 ± 2.537 pg/mL of IL-8, which was below the levels detected in the media-only control (17.681 ± 2.884 pg/mL). This suggested that ATRA-differentiated HL-60 cells did not appear to show increased IL-8 release in response to well-characterised neutrophil agonists, and thus only primary neutrophils were used in further experiments.

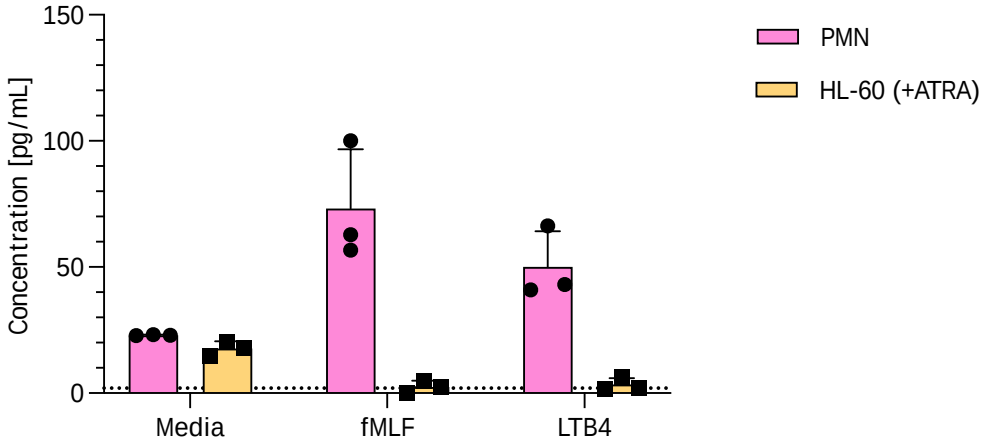

Figure 5.14 IL-8 protein release from primary neutrophils and ATRA-differentiated HL-60 cells. Primary neutrophils and ATRA-differentiated HL-60 cells were stimulated for 24 hours with fMLF or LTB_4 at 37 °C, 5% CO_2. IL-8 concentrations were measured by ELISA and are shown as mean + SD from a single experiment (n = 1) with three technical replicates. The dotted line denotes the lower limit of the standard curve. Samples outside the limits of the standard curve were extrapolated where possible; one value below the extrapolatable range was assigned a value of 0 before calculation of descriptive summary values. PMN, primary neutrophils; HL-60 (+ATRA), ATRA-differentiated HL-60 cells; fMLF, N-formyl-methionyl-leucyl-phenylalanine; IL-8, interleukin-8; LTB_4, leukotriene B_4.

The aim of the next experiment was to investigate neutrophil responsiveness to mediators and cytokines that could be utilised in the neutrophil transepithelial migration model. Neutrophils were stimulated with a range of bacterial (fMLF and LPS), host (G-CSF and GM-CSF) or synthetic (PMA) mediators at three

different concentrations designated as minimum, medium and maximum based on published literature (see Table 2.9), for 24 and 48 hours. Following incubation, cell-containing supernatants were assessed for the concentrations of IL-1β, IL-6, IL-8 and TNF-α by ELISA (Figure 5.15). All cytokines except for IL-8 were detected at generally higher levels at the 24-hour time point compared to 48 hours. Across the mediators, LPS was associated with the highest release of cytokines from neutrophils and was therefore used as the mediator of choice in further experiments.

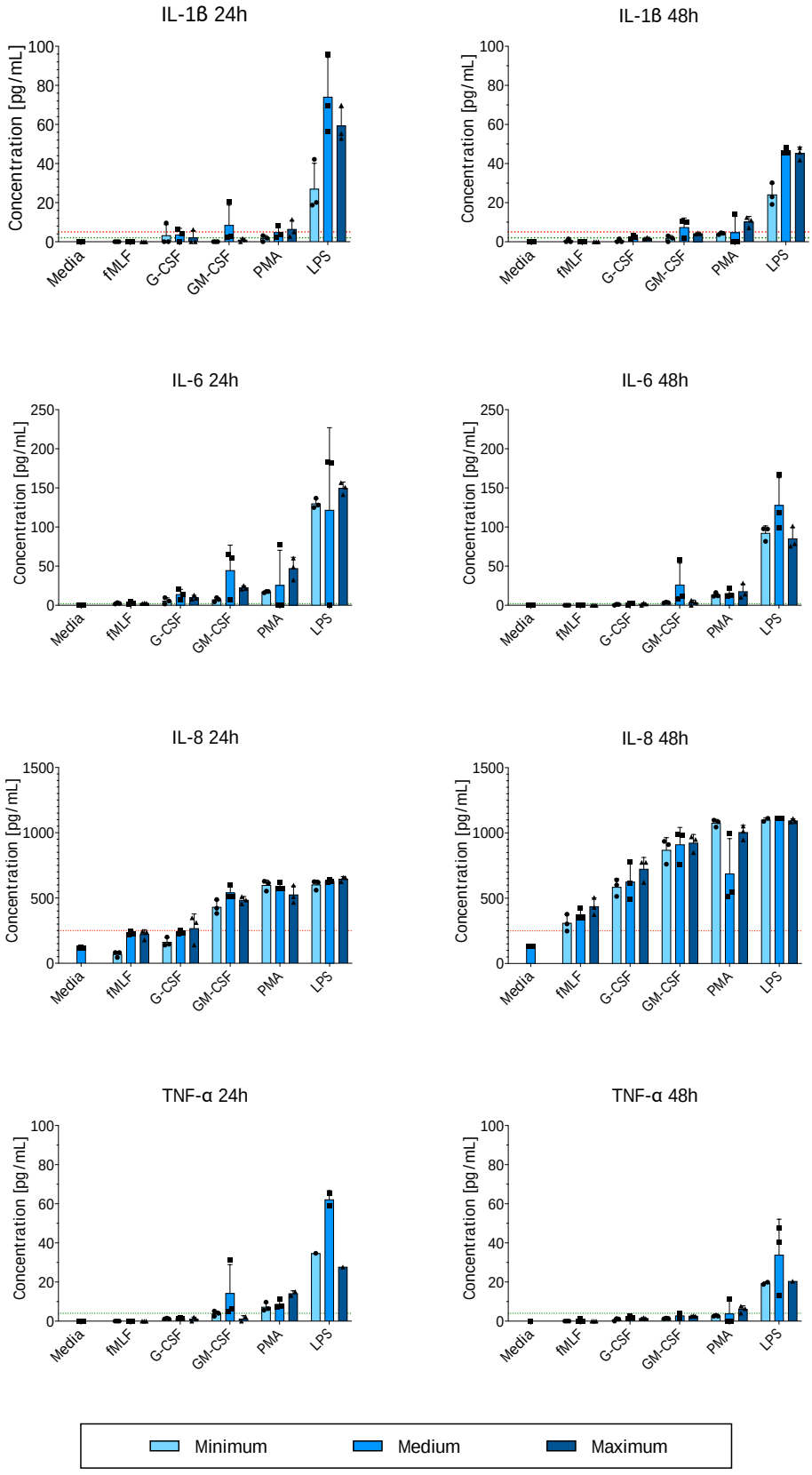

Figure 5.15 IL-1**β**, IL-6, IL-8 and TNF-**α** protein release from primary neutrophils. Primary neutrophils were stimulated for 24 and 48 hours at 37 °C in 5% CO_2 with a range of bacterial, host and synthetic mediators at three different concentrations designated as minimum, medium and maximum. The minimum, medium and maximum concentrations were 0.4, 4 and 40 nM for fMLF; 0.1, 1 and 5 ng/mL for G-CSF; 0.1, 1 and 5 ng/mL for GM-CSF; 0.042, 0.42 and 4.2 µM for PMA; and 1, 10 and 50 µg/mL for LPS. Cytokine concentrations were measured by ELISA and are shown as mean + SD from one experiment (n = 1) with three technical replicates. Individual

technical replicate values are shown as symbols. Samples with insufficient volume were excluded from analysis. The green and red dotted lines denote the lower and upper limits of the standard curve, respectively. Samples outside the limits of the standard curve were extrapolated where possible; values below the lower limit that could not be extrapolated were assigned a value of 0 before calculation of descriptive summary values. fMLF, N-formyl-methionyl-leucyl-phenylalanine; G-CSF, granulocyte colony-stimulating factor; GM-CSF, granulocyte-macrophage colony-stimulating factor; IL, interleukin; LPS, lipopolysaccharide; PMA, phorbol 12-myristate 13-acetate; TNF-α, tumour necrosis factor-α.

5.3.2.3 Neutrophil quantification

Migration efficiency is one of the primary measures of the cell transmigration assay. It can be measured directly by counting the cells that migrated through the porous membrane into the well, or those that remained within the transwell insert apical compartment. For that purpose, manual and automated methods of neutrophil quantification were assessed. A set of neutrophil suspensions at 0, 2, 4, 6, 8 × 10^5 and 1 × 10^6 cells per mL were prepared and quantified using trypan blue viability dye and either an improved Neubauer haemocytometer or a Luna II automated cell counter. Additionally, 0.4% trypan blue and erythrosin B were used at two different dilutions (neat and 1:10) in the latter method. The resulting curves were compared to a hypothetical reference curve. Following nonlinear regression (straight line), extra sum-of-squares F-tests revealed that none of the datasets (Figure 5.16) could be described by a single common curve (all p-values < 0.0001). Nevertheless, the lowest F value of the dataset generated using a manual haemocytometer ($F(2, 20) = 18.92$) suggested that it was the closest match, although this was not accompanied by the best curve fit (R^2 value = 0.9150 compared to the highest R^2 = 0.9467) achieved with Luna II and neat trypan blue.

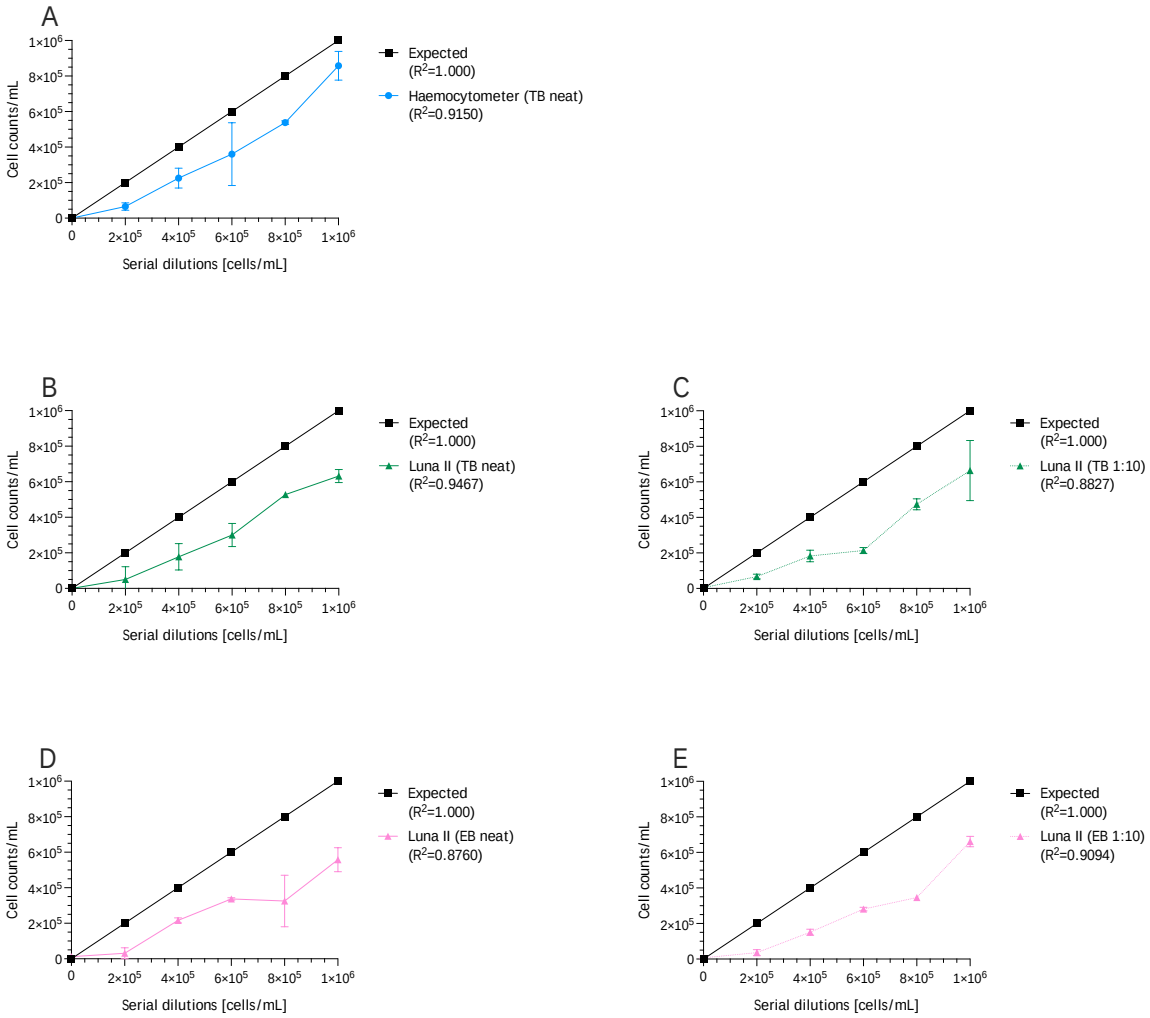

Figure 5.16 Cell counts of neutrophils using a haemocytometer and an automated cell counter. Cell counts were performed on a set of dilutions (0, 2, 4, 6, 8 × 10^5 and 1 × 10^6 cells/mL) using a Neubauer haemocytometer (A) and a Luna II automated cell counter (B, C, D, E). Cells were stained with neat trypan blue (0.4%; A, B), trypan blue diluted 1:10 (0.04%; C), neat erythrosin B (D) or erythrosin B diluted 1:10 (E). Expected values were calculated from the initial haemocytometer count and serial dilutions. Data are presented as mean ± SD from two technical replicates obtained in one experiment (n = 1). TB, trypan blue; EB, erythrosin B.

Next, the same set of dilutions was used to evaluate if the CCK-8 assay could generate a reliable standard curve after 1, 2, 3 or 4 hours in both 24- and 96-well plates. Furthermore, a 30-minute membrane integrity-based BacLight fluorescent assay was performed in parallel.

Results from the 96-well plate format (Figure 5.17) indicated that BacLight standard curves displayed greater variability between technical replicates within each biological repeat compared to CCK-8 standard curves, with mean intra-assay CVs ranging from 25.13% to 47.96% compared with 2.94% to 5.44%, respectively. Each dataset was then analysed by applying a second-order polynomial nonlinear regression in log-space (Figure S4). Extra sum-of-squares

F-tests showed that, within each assay and time point, biological repeats could not be described by a single curve (p-value < 0.0001).

A

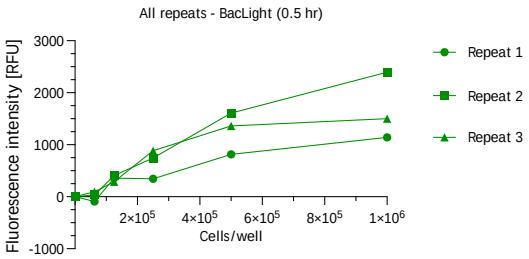
All repeats - BacLight (0.5 hr)
Fluorescence intensity [RFU]
3000
2000
1000
0
-1000
2×10^5
4×10^5
6×10^5
8×10^5
1×10^6
Cells/well
Repeat 1
Repeat 2
Repeat 3

B

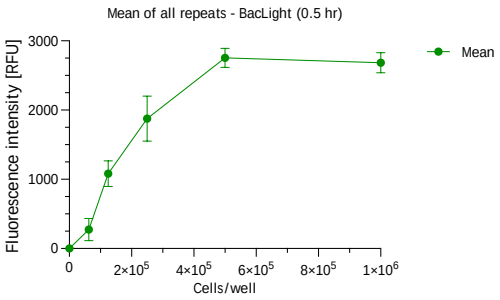
Mean of all repeats - BacLight (0.5 hr)
Fluorescence intensity [RFU]
3000
2000
1000
0
2×10^5
4×10^5
6×10^5
8×10^5
1×10^6
Cells/well
Mean

C

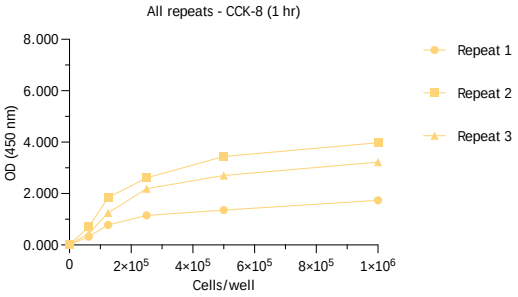
All repeats - CCK-8 (1 hr)
OD (450 nm)
8.000
6.000
4.000
2.000
0.000
0
2×10^5
4×10^5
6×10^5
8×10^5
1×10^6
Cells/well
Repeat 1
Repeat 2
Repeat 3

D

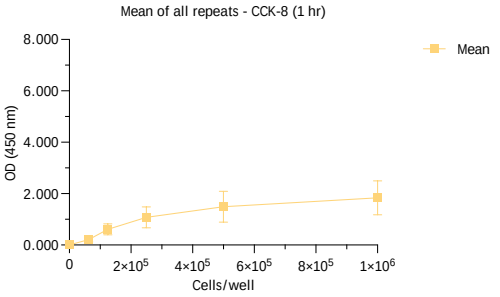
Mean of all repeats - CCK-8 (1 hr)
OD (450 nm)
8.000
6.000
4.000
2.000
0.000
0
2×10^5
4×10^5
6×10^5
8×10^5
1×10^6
Cells/well
Mean

E

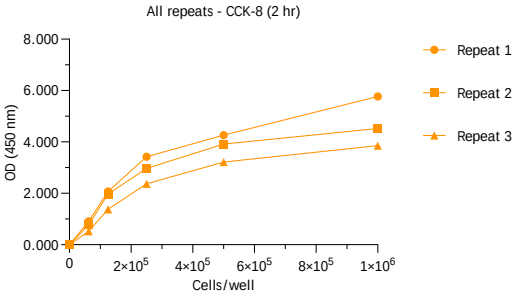
All repeats - CCK-8 (2 hr)
OD (450 nm)
8.000
6.000
4.000
2.000
0.000
0
2×10^5
4×10^5
6×10^5
8×10^5
1×10^6
Cells/well
Repeat 1
Repeat 2
Repeat 3

F

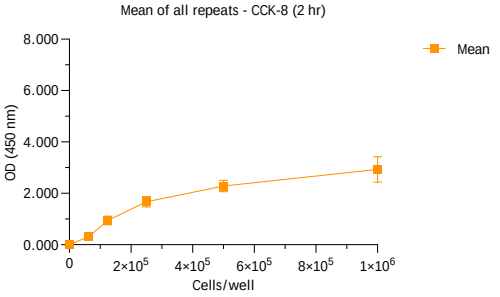
Mean of all repeats - CCK-8 (2 hr)
OD (450 nm)
8.000
6.000
4.000
2.000
0.000
0
2×10^5
4×10^5
6×10^5
8×10^5
1×10^6
Cells/well
Mean

G

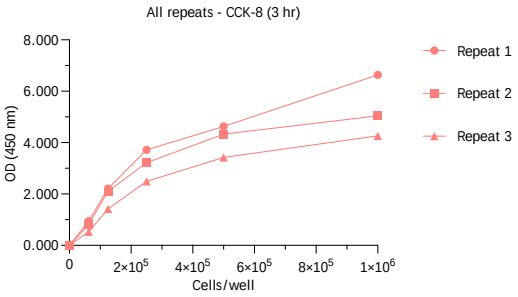
All repeats - CCK-8 (3 hr)
OD (450 nm)
8.000
6.000
4.000
2.000
0.000
0
2×10^5
4×10^5
6×10^5
8×10^5
1×10^6
Cells/well
Repeat 1
Repeat 2
Repeat 3

H

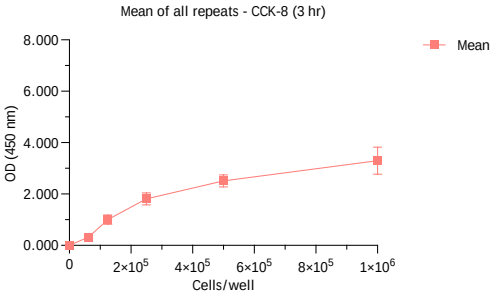
Mean of all repeats - CCK-8 (3 hr)
OD (450 nm)
8.000
6.000
4.000
2.000
0.000
0
2×10^5
4×10^5
6×10^5
8×10^5
1×10^6
Cells/well
Mean

I

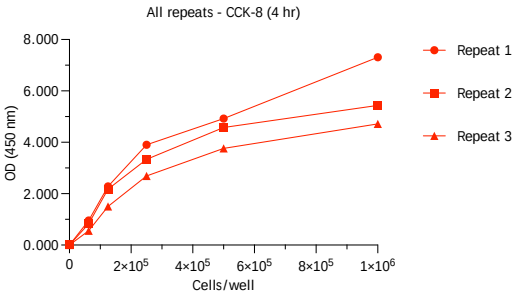
All repeats - CCK-8 (4 hr)
OD (450 nm)
8.000
6.000
4.000
2.000
0.000
0
2×10^5
4×10^5
6×10^5
8×10^5
1×10^6
Cells/well
Repeat 1
Repeat 2
Repeat 3

J

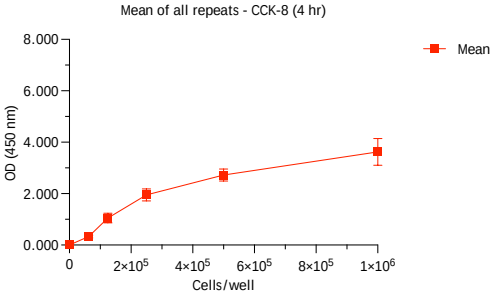
Mean of all repeats - CCK-8 (4 hr)
OD (450 nm)
8.000
6.000
4.000
2.000
0.000
0
2×10^5
4×10^5
6×10^5
8×10^5
1×10^6
Cells/well
Mean

Figure 5.17 BacLight and CCK-8 assays of serial dilutions of neutrophil suspensions in 96-well plates. Serial dilutions of neutrophil suspensions were incubated in 96-well plates with BacLight for 0.5 hours (A, B) or with CCK-8 for 1 hour (C, D), 2 hours (E, F), 3 hours (G, H) and 4 hours (I, J) at 37 °C, 5% CO_2. Data are presented as mean ± SD of blank-corrected fluorescence values for the BacLight assay and blank-corrected OD values for the CCK-8 assay from each of 3 independent experiments (n = 3) performed in technical duplicate (A, C, E, G, I), and as mean ± SD from all experiments (B, D, F, H, J) for each time point. RFU, relative fluorescence units.

In a 24-well plate format (Figure 5.18), BacLight standard curves showed slightly lower variability (CVs ranged from 9.36% to 20.71%) than in 96-well plates, while the CCK-8 CVs increased, ranging from 1.46% to 14.10%. A second-order polynomial nonlinear regression in log-space was applied to each dataset (Figure S5). The extra sum-of-squares F-test results showed that, for each assay and time point, biological repeats required separate curve fits (p-values ranging from < 0.0001 to 0.0074).

A

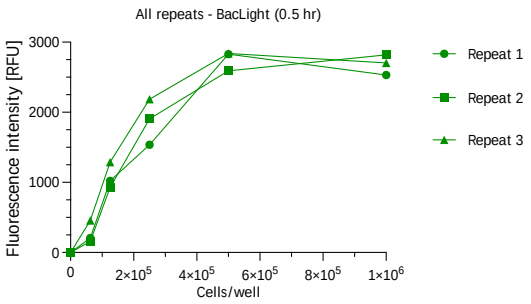
All repeats - BacLight (0.5 hr)
Fluorescence intensity [RFU]
3000
2000
1000
0
0
2×10^5
4×10^5
6×10^5
8×10^5
1×10^6
Cells/well
Repeat 1
Repeat 2
Repeat 3

B

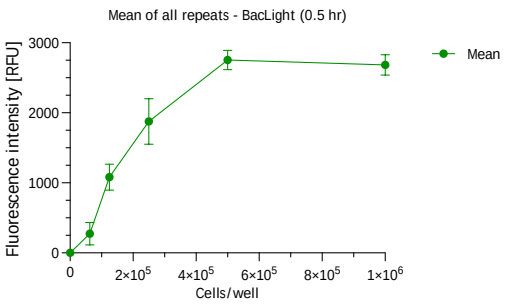
Mean of all repeats - BacLight (0.5 hr)
Fluorescence intensity [RFU]
3000
2000
1000
0
0
2×10^5
4×10^5
6×10^5
8×10^5
1×10^6
Cells/well
Mean

C

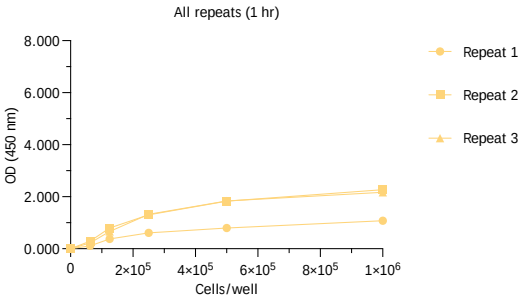
All repeats (1 hr)
OD (450 nm)
8.000
6.000
4.000
2.000
0.000
0
2×10^5
4×10^5
6×10^5
8×10^5
1×10^6
Cells/well
Repeat 1
Repeat 2
Repeat 3

D

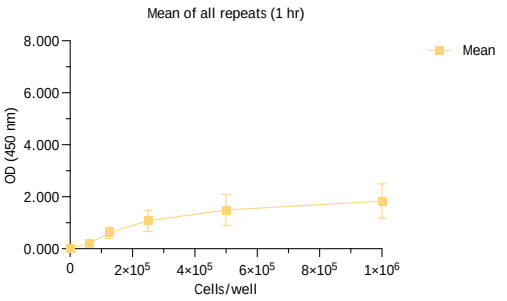
Mean of all repeats (1 hr)
OD (450 nm)
8.000
6.000
4.000
2.000
0.000
0
2×10^5
4×10^5
6×10^5
8×10^5
1×10^6
Cells/well
Mean

E

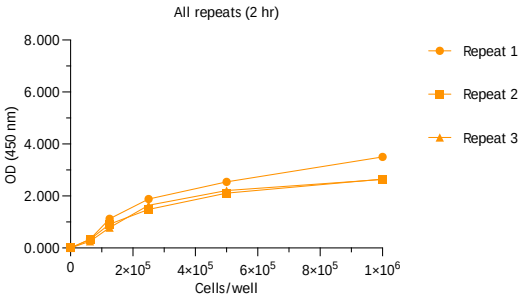
All repeats (2 hr)
OD (450 nm)
8.000
6.000
4.000
2.000
0.000
0
2×10^5
4×10^5
6×10^5
8×10^5
1×10^6
Cells/well
Repeat 1
Repeat 2
Repeat 3

F

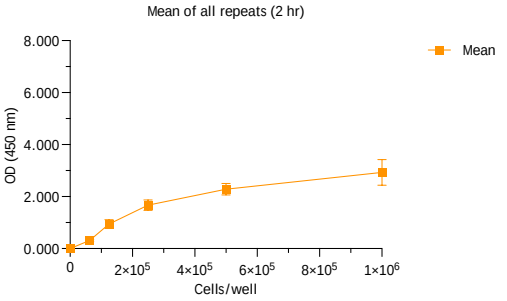
Mean of all repeats (2 hr)
OD (450 nm)
8.000
6.000
4.000
2.000
0.000
0
2×10^5
4×10^5
6×10^5
8×10^5
1×10^6
Cells/well
Mean

G

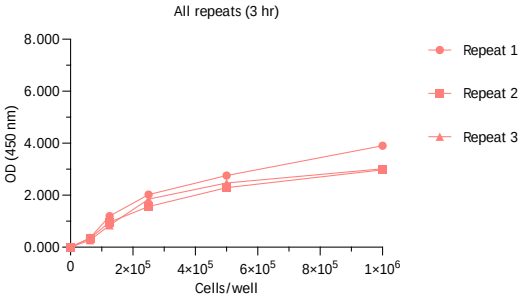
All repeats (3 hr)
OD (450 nm)
8.000
6.000
4.000
2.000
0.000
0
2×10^5
4×10^5
6×10^5
8×10^5
1×10^6
Cells/well
Repeat 1
Repeat 2
Repeat 3

H

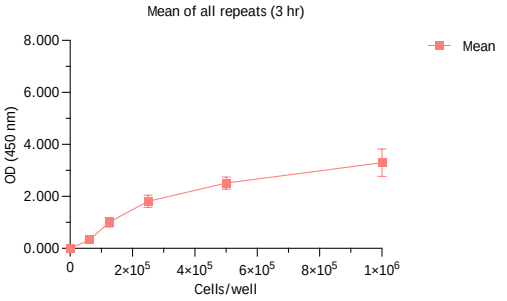
Mean of all repeats (3 hr)
OD (450 nm)
8.000
6.000
4.000
2.000
0.000
0
2×10^5
4×10^5
6×10^5
8×10^5
1×10^6
Cells/well
Mean

I

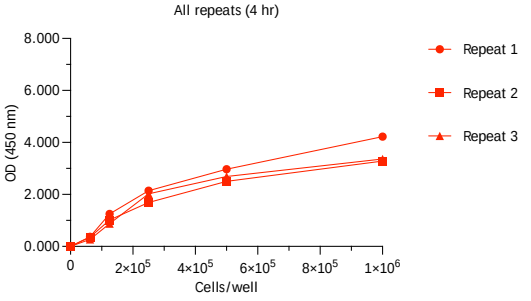
All repeats (4 hr)
OD (450 nm)
8.000
6.000
4.000
2.000
0.000
0
2×10^5
4×10^5
6×10^5
8×10^5
1×10^6
Cells/well
Repeat 1
Repeat 2
Repeat 3

J

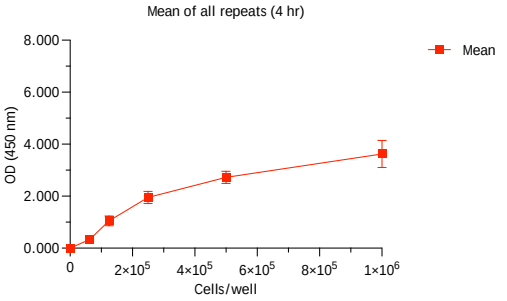
Mean of all repeats (4 hr)
OD (450 nm)
8.000
6.000
4.000
2.000
0.000
0
2×10^5
4×10^5
6×10^5
8×10^5
1×10^6
Cells/well
Mean

Figure 5.18 BacLight and CCK-8 assays of serial dilutions of neutrophil suspensions in 24-well plates. Serial dilutions of neutrophil suspensions were incubated in 24-well plates with BacLight for 0.5 hours (A, B) or with CCK-8 for 1 hour (C, D), 2 hours (E, F), 3 hours (G, H) and 4 hours (I, J) at 37 °C, 5% CO_2. Data are presented as mean ± SD of blank-corrected fluorescence values for the BacLight assay and blank-corrected OD values for the CCK-8 assay from each of 3 independent experiments (n = 3) performed in technical duplicate (A, C, E, G, I), and as mean ± SD from all experiments (B, D, F, H, J) for each time point. RFU, relative fluorescence units.

5.4 Discussion

5.4.1 Assessment of methods used to quantify TR146 cells growing on a transwell insert membrane

Haemocytometers are widely used for manual cell counting due to the ease of use, versatility and affordability. However, this method may be time-consuming for large sample sets and is susceptible to user-to-user variability. Automated cell counters are claimed to offer a convenient alternative to manual cell counting, providing higher reproducibility, as well as reduced analysis time and operator bias. The disadvantages are inaccuracies at very low or very high cell densities, presence of cell clumping or debris (Camacho-Fernandez et al., 2018, Sarkar et al., 2017) and cell line-specific performance (Huang et al., 2010). Results obtained in this chapter (Figure 5.3 and Figure 5.4) suggested that using an improved Neubauer haemocytometer and 0.4% trypan blue may provide better apparent accuracy, as measured values were closer to the expected cell counts, but lower apparent precision, as variability between replicate measurements was higher (Menditto et al., 2007). Reliability of results could be improved by increasing the number of replicates. A pragmatic decision was taken to use the method which appeared most reliable, rather than continuing to pursue this line of enquiry. In addition, using serial dilution rather than preparing each dilution independently may have propagated pipetting errors, and the stability of the target cell sample was not assessed (Huang et al., 2021b).

In the trypsinisation experiments TR146 cells did not fully detach from the transwell insert membrane even after prolonged periods of trypsinisation and vigorous pipetting. Therefore, other methods were sought to quantify the cells attached to the membrane. The CCK-8 assay, which is based on the reduction of

water-soluble tetrazolium salt-8 by metabolically active cells, has previously been used to assess the viability of TR146 cells (Guo et al., 2022, Shin et al., 2025). It is often preferred over other methods due to its non-toxicity. However, it has been reported that it can interfere with the metabolic activity of the cells and caution is advised when performing additional testing immediately after CCK-8 assay (Fan et al., 2024). In this chapter, TR146 serial dilutions were incubated with CCK-8 in 3 independent experiments, and OD values at 450 nm were used to generate standard curves (Figure 5.5). Each standard curve was fitted using nonlinear regression (straight line), and fits were compared using extra-sum-of-squares F-tests. This was followed by exclusion of the outliers caused by saturation, after which the analysis was repeated. Comparison of fits revealed that the independently obtained standard curves should not be averaged to generate a global fit used to interpolate results from unknown samples. The differences between the curves' parameters could have been caused by variation in experimental conditions such as different passage number or metabolic activity of the cells. To the author's knowledge, no study has reported generating standard curves using TR146 cell suspensions treated with CCK-8 or other compounds such as XTT or MTT. One study reported using standard curves to quantify the immortal human keratinocytes HaCaT growing in wells, but authors did not include details of the standard curve validation (Baik et al., 2014). Furthermore, freshly passaged TR146 cells seeded into wells may have different metabolic activity compared to established TR146 layers growing on a PET membrane.

5.4.2 TR146 epithelial layer grown on different transwell insert membranes

The preliminary seeding experiments investigated whether TR146 cells could attach to the basolateral side of porous transwell insert membranes. Basolateral seeding is not a common approach for establishing an epithelial layer mimicking the oral barrier. However, this orientation more closely mimics the *in vivo* orientation of the junctional epithelium, where the basement membrane faces the connective tissue and the outermost epithelial layers face the sulcus. In contrast, most studies utilise the apical compartment of a transwell insert in order to grow cells at the ALI upon reaching confluency. TR146 cells are typically

cultured for 3–4 weeks to form stratified, multilayered epithelium with stable transepithelial electrical resistance (TEER) and permeability parameters (Bierbaumer et al., 2018, Keum et al., 2022, Lin et al., 2020, Shin et al., 2025). In the standard apical seeding approach, cells settle onto the membrane under the influence of gravity. Basolateral seeding, however, requires temporary inversion of the transwell so that gravity can similarly promote cell attachment to the membrane (Kusek et al., 2014, Madianos et al., 1997).

Pre-coating of membranes with $CaCl_2$, type I collagen and FBS to increase TR146 cell adhesion was explored. Addition of $CaCl_2$ to the cell culture medium was reported during TR146 cell seeding onto transwell insert membranes (Lin et al., 2020). Optimising calcium supplementation has been shown to improve TEER values in human colonoid-derived epithelial cells (McClintock et al., 2020) and Madin-Darby canine kidney (MDCK) epithelial cells (Gonzalez-Mariscal et al., 1990) by improving desmosome formation or expression of tight junction proteins, respectively. Type I collagen is used in scaffolds employed in various *in vitro* oral mucosa models (Moharamzadeh et al., 2007) and to coat transwell membranes, e.g. in primary airway epithelial cells (Ashraf and Bruce, 2025, Bluhmki et al., 2020). Improved adhesion and spreading of epithelial cells on type I collagen-coated surfaces is mediated through $\alpha_2\beta_1$ integrins (Leitinger, 2011). FBS contains various adhesion proteins such as fibronectin or vitronectin and is widely used in *in vitro* cell cultures as a medium supplement to improve integrin-mediated cell attachment to culture surfaces (Piazza et al., 2024, Wilson et al., 2005). In the pilot transwell experiment, TR146 cells were seeded onto Corning and Millicell PET transwell membranes and then their metabolic activity was assessed by a CCK-8 assay (Figure 5.6). The obtained results did not suggest that the use of either brand or pre-coating protocol promoted metabolic activity. This may have been due to the small number of transwells tested in each group, which could have limited the ability to detect differences. Likewise, histological assessment with H&E staining (Figure 5.7 and Figure 5.8) also did not reveal any detectable differences.

Consistent with these findings, permeability testing using Lucifer Yellow fluorescent dye (Figure 5.9) did not indicate a clear difference between TR146 cell-seeded and unseeded transwell membranes from either manufacturer. To

the author's knowledge, no study has reported the use of a Lucifer Yellow permeability assay in this cell line. TEER assessment was attempted, but the results were inconsistent and inconclusive (data not shown). Findings from other tracer flux assays and TEER studies showed that the TR146 *in vitro* barrier is more permeable than healthy epithelium (Mazzinelli et al., 2023) and much less restrictive than Caco-2 and MDCK strain I *in vitro* barriers that are known to form tight junctions (Bashyal et al., 2018). The TR146 cell line has been reported to lack tight junctions (Jacobsen et al., 1995) and to show poor expression of zonula occludens (Teubl et al., 2013). Taken together, these reports suggest that TR146 cells may not be expected to form a highly restrictive barrier in transwell culture. Therefore, the lack of a clear difference between seeded and unseeded membranes in this experiment may be consistent with the relatively permeable phenotype of this cell line.

Increased TR146 cell seeding concentration and decreased incubation time (Figure 5.10 and Figure 5.11) appeared to reduce transwell-to-transwell variability in metabolic activity as measured by a CCK-8 assay. Successful histological processing of epithelial multilayers into H&E-stained sections (Figure 5.12) coincided with reducing the PFA fixation time from overnight to 3 hours. Earlier failed attempts could have been caused or exacerbated not by prolonged PFA exposure per se, but by the relative thinness of the epithelial multilayer compared to typical specimens usually fixed overnight, which may have made it more susceptible to fixation-induced shrinkage (Kiser et al., 2018). An alternative explanation could be that in previous experiments, TR146 cells directly attaching to the membrane were less adherent, which led to their detachment during membrane processing. Furthermore, a study on epithelial monolayers has shown that they maintained intrinsic tension via the acto-myosin cytoskeleton, which was balanced by the substrate, but once this tension was no longer opposed, the monolayer curled (Fouchard et al., 2020). Similar curling could potentially happen during the excision of the membrane from the transwell.

5.4.3 Comparison of neutrophils and 'neutrophil-like' cells

Several different protocols have been published for HL-60 differentiation, and these are reported to generate cells with varying neutrophil-like features. The extent of this methodological heterogeneity was highlighted in a recent systematic review, which identified 71 studies published between 2020 and 2025 that used 41 distinct protocols for HL-60 neutrophil-like differentiation (Cázares-Preciado et al., 2025). Nonetheless, the potential benefits of using a cell line in the model, compared with using primary cells, meant that the use of HL-60 cells was deemed worth exploration. In the flow cytometry validation experiment (Figure 5.13), only ATRA-differentiated HL-60 cells appeared to be predominantly CD15-positive, suggesting they may have acquired a neutrophil-like phenotype, while DMSO-differentiated HL-60 cells remained CD15-negative. This is in contrast to the results reported in the literature, in which both treatment groups showed CD15 expression (Cázares-Preciado et al., 2024, Manda-Handzlik et al., 2018, Trayner et al., 1998).

A possible explanation is that the DMSO-differentiated cells may have reached their maximum maturity stage earlier than anticipated by the protocol, and initiated apoptosis-driven reorganisation of the cell surface, similar to one seen in primary neutrophils cultured *in vitro*, marked by a 78% reduction in CD15 expression (Hart et al., 2000).

Nevertheless, there is a consensus that HL-60 differentiation with ATRA, compared to DMSO, leads to a more mature phenotype reflected by higher NADPH oxidase activity, higher phagocytic efficacy, and a more frequent later-stage nuclear morphology, including banded or segmented forms (Manda-Handzlik et al., 2018, Martin et al., 1990). This could be due to the different mechanisms of action of the two differentiation agents. ATRA binds to retinoic acid receptor-α, a nuclear receptor, and activates the mitogen-activated protein kinase (MAPK) and phosphoinositide 3-kinase/Akt pathways that lead to growth arrest and cytoskeletal reorganisation, which are essential for differentiation. Additionally, it suppresses c-Myc transcription through a receptor-independent mechanism (Blanter et al., 2021). Interestingly, ATRA is used successfully in treatment regimens for acute promyelocytic leukaemia, a subtype of acute

myeloid leukaemia (Johnson and Redner, 2015, Nguyen et al., 2020). By contrast, DMSO induces HL-60 differentiation via multiple indirect routes. It arrests transcriptional elongation of the c-Myc gene, inhibits its splicing and eliminates its amplicons. DMSO also upregulates Ras and protein kinase C (PKC), initiating the MAPK pathway (Blanter et al., 2021). Of note, it was recently reported that the combination of ATRA and DMSO produces a synergistic effect on HL-60 differentiation (Hornstein and Unfried, 2025).

ATRA-differentiated HL-60 cells were chosen for further experiments to compare their responsiveness to bacterial and host mediator stimulation with that of primary neutrophils. Results from the fMLF- and LTB_4-stimulation assay (Figure 5.14) suggested that only primary neutrophils released IL-8 in response to stimulation. The observed results in primary neutrophils were in line with the literature (Hidalgo et al., 2015, McCain et al., 1994). It has been reported that compared to primary neutrophils, ATRA-differentiated HL-60 cells exhibited poor migration towards fMLF, LTB_4 and IL-8. The same study confirmed the expression of LTB_4 receptors and secretion of LTB_4 (Babatunde et al., 2021). Another study found that retinoic acid differentiation impaired fMLF but not LTB_4 signalling in HL-60 cells (Erbeck et al., 1993). Nevertheless, both cell types can secrete IL-8 in response to TLR2 stimulation (Wen et al., 2021). There was no obvious explanation for the lack of response in ATRA-differentiated HL-60 cells, nor for the observation that IL-8 levels in the stimulated conditions were below those in the media-only condition. However, IL-8 release was low across all three conditions. As these cells did not seem to function as required or expected, and the primary neutrophils appeared to behave as predicted in this experiment, a decision was made to progress with the model using primary cells to minimise further loss of time and resources.

Responsiveness of primary neutrophils to bacterial, host and synthetic mediators was evaluated further (Figure 5.15). These cells produced detectable levels of IL-1β, IL-6, IL-8 and TNF-α, which was in line with the literature (Tecchio et al., 2014). IL-8 appeared to show a differential release pattern with higher levels detected after 48 hours, whereas the remaining cytokines were detected at increased concentrations at the 24-hour time point. This may reflect differences in cytokine release kinetics, with early pro-inflammatory mediators such as IL-1β

and TNF-α potentially contributing to later IL-8 production as part of a sustained chemokine response following stimulation (DeForge et al., 1992, Strieter et al., 1992). However, this was not directly tested in this experiment. Alternatively, the lower detected concentrations of some cytokines at 48 hours may reflect differences in cytokine stability, cellular uptake, receptor binding or adsorption to the well surface. LPS was associated with the release of the highest levels of all cytokines at both time points and was therefore used in further experiments as the main stimulus for primary neutrophils.

5.4.4 Neutrophil quantification

Results obtained in this chapter suggested that using the improved Neubauer haemocytometer and 0.4% trypan blue provided better accuracy than the Luna II automated cell counter (Figure 5.16). In contrast to TR146 quantification experiments, each neutrophil dilution was prepared independently, thus preventing the propagation of pipetting errors. Similar to the TR146 findings, a decision was taken to use the method which appeared most reliable. Because the stability of the target cell sample was not assessed, potential effects of cell settling, aggregation or time-dependent changes in viability on the measured counts cannot be excluded (Huang et al., 2021b).

Two indirect methods of neutrophil quantification were evaluated: BacLight staining, measured using SYTO 9-associated fluorescence, and the CCK-8 colorimetric assay, which is based on cellular metabolic activity and therefore generates a readout that correlates with the number of viable cells. BacLight-based standard curves displayed higher technical variability than CCK-8 curves prepared in 96-well plates (Figure 5.17) but were comparable in 24-well plates (Figure 5.18). Furthermore, neither method yielded a dataset in which all biological repeats could be represented by one global curve fit, highlighting the need to prepare individual curves for each assay. This did not pose a technical limitation, as neutrophils are non-adherent cells and curves can be established simultaneously with the assay.

Overall, this chapter highlights the technical difficulties of reproducibly and reliably working with small cell numbers within individual wells or transwell inserts used in *in vitro* model systems. It also emphasises the need to consider

the sensitivity and limitations of different cell counting methods to achieve reasonable reliability in these model systems. Nonetheless, the methods devised showed that primary human neutrophils and the TR146 epithelial cell line could be combined into a model system.

5.5 Summary and findings

1. Can TR146 epithelial cells be grown on the basolateral side of a porous transwell insert membrane?

- TR146 epithelial cells could be grown on the basolateral side of a porous transwell insert membrane and remain metabolically active.

2. Can HL-60 cells be differentiated into neutrophil-like cells that display a phenotype consistent with primary neutrophils including:

    a. expression of surface receptors?

    b. responsiveness to stimulants?

- HL-60 cells could be differentiated with ATRA into neutrophil-like cells that expressed surface markers characteristic of primary neutrophils, as previously reported, but these cells did not mimic primary neutrophil responsiveness to stimuli, contrary to the results of earlier studies.

These findings supported the hypothesis that certain cell types and lines can be used as potential components of an *in vitro* model of neutrophil migration at the junctional epithelium.

6 Development of an *in vitro* 3D co-culture model of the oral barrier at the gingival sulcus

6.1 Introduction

The oral barrier at the gingival sulcus is a biologically active and adaptive interface, where complex host systems interact with complex bacterial biofilms. The key characteristic, central to this chapter, is the responsiveness of the junctional epithelium to bacterial challenge that results in dynamic migration of neutrophils into the gingival sulcus, both as a steady-state surveillance mechanism and in inflammation-driven recruitment. These processes were described in detail in Section 1.1.3.1.1 and Section 1.1.3.2.1, respectively.

An *in vitro* model of the oral barrier at the gingival sulcus should therefore reflect not only the *in vivo* presence of various components but also its structure (e.g. how epithelial cells are organised into layers), spatiality (how these cells rest on the membrane, facing the biofilm), temporality (e.g. arrival of neutrophils at the site), and directionality of host processes, such as the movement of neutrophils through the epithelium towards the microbial trigger. In other words, the model of the barrier should not merely represent a static material condition or structure, but rather a directed, dynamic process that the various structures and mobile elements afford.

As already described in detail in Section 4.1.2, our group has previously developed a set of 3-, 7- and 10-species bacterial biofilms associated with health, gingivitis and periodontitis, cultured on either 13 mm Thermanox coverslips or directly on the 24-well plate surface (Brown, 2020, Millhouse, 2015). An earlier 4-species periodontitis biofilm model, comprising *S. mitis*, *F. nucleatum*, *P. gingivalis* and *A. actinomycetemcomitans*, had also been cultured on coverslips or hydroxyapatite discs (Anto, 2013). These biofilms were subsequently used in various co-culture model systems. For example, the 4- and 10-species periodontitis biofilms were co-cultured with a monolayer of OKF6/TERT-2 cells, an immortalised oral keratinocyte cell line, to mimic interactions at the biofilm-epithelium interface (Anto, 2013, Millhouse, 2015).

This model was created in two alternative versions, with one component cultured at the bottom of the well and the other grown on a Thermanox coverslip that was fixed with Vaseline to a transwell insert scaffold (Figure 6.1A and B). In the 4-species biofilm co-culture model, a hydroxyapatite disc was used instead of a Thermanox coverslip (Anto, 2013). All components were fully submerged throughout the entire culture period (4 and 24 hours at 37 °C, 5% CO_2) (Millhouse, 2015). In later studies, the wells were seeded with the TR146 cells instead of the OKF6/TERT-2 cells and incubated with the biofilm for 20 hours (Brown, 2020). A further advancement of the model was the incorporation of immune cells and a double-transwell setup (Figure 6.1C). In this system, either peripheral blood mononuclear cells (PBMCs), $CD3^+$ T cells or $CD14^+$ monocytes were added to the well of a 12-well plate. Subsequently, a commercially obtained 0.5 cm^2 insert with primary human gingival epithelium was placed in the well, followed by the addition of artificial saliva and a smaller, 0.33 cm^2 insert with a biofilm coverslip facing the epithelium. The whole construct was incubated for 20 hours at 37 °C, 5% CO_2. This setup modelled early innate and adaptive immune responses in the outer gingiva rather than at the gingival sulcus. While these models proved effective in studying the biofilm-epithelium interactions, their orientation would not allow for modelling neutrophil transepithelial migration. Specifically, the arrangements shown in Figure 6.1A and B lacked a porous membrane supporting the epithelial layer, whereas immune cells in the configuration shown in Figure 6.1C were not expected to detach and migrate upwards through the porous membrane and the overlying epithelium.

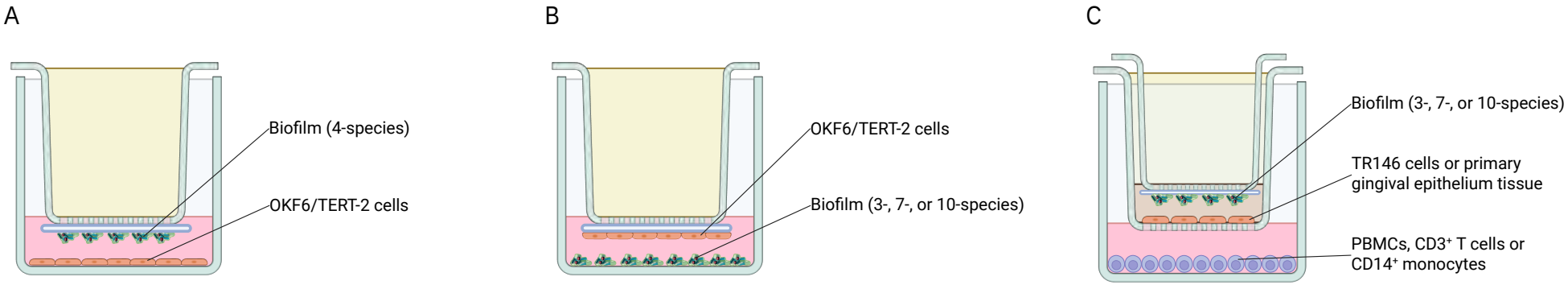

(Anto, 2013) (Millhouse, 2015) (Brown, 2020)

Figure 6.1 *In vitro* co-culture models previously developed by the group. Three model configurations are shown, each incorporating different components and spatial arrangements: (A) OKF6/TERT-2 cells grown at the bottom of the well and challenged with a 4-species biofilm* grown on a hydroxyapatite disc mounted to the transwell insert. Figure adapted from Anto (2013); (B) OKF6/TERT-2 cells grown on a Thermanox coverslip mounted to the transwell insert and challenged with a 3-species biofilm**, 7-species biofilm***, or 10-species biofilm**** grown at the bottom of the well. Figure adapted from Millhouse (2015); (C) PBMCs, $CD3^+$ T cells or $CD14^+$ monocytes added to the bottom of the well, accompanied by either TR146 cells or primary gingival epithelium grown on the membrane of the lower transwell insert. The model was challenged with a 3-species biofilm**, 7-species biofilm***, or 10-species biofilm**** grown on a Thermanox coverslip mounted to the upper transwell insert. Figure adapted from Brown (2020).
*4-species biofilm included *S. mitis*, *F. nucleatum*, *P. gingivalis* and *A. actinomycetemcomitans.*
**3-species biofilm included *S. intermedius, S. mitis* and *S. oralis.*
***7-species biofilm included *S. intermedius, S. mitis*, *S. oralis, A. naeslundii*, *F. nucleatum* subsp. *polymorphum*, *F. nucleatum* subsp. *vincentii* and *V. dispar.*
****10-species biofilm included *S. intermedius, S. mitis, S. oralis, A. naeslundii, F. nucleatum* subsp. *polymorphum, F. nucleatum* subsp. *vincentii, V. dispar, A. actinomycetemcomitans, P. intermedia* and *P. gingivalis*.
OKF6/TERT-2, an immortalised oral keratinocyte cell line; PBMCs, peripheral blood mononuclear cells. Figure created with BioRender.com.

6.2 Proposed model design

Drawing on the earlier approaches described above, a conventional transwell-based system and Thermanox coverslips were retained as supports in the proposed model (Figure 6.2). However, there were a few key differences. Bacterial biofilms were positioned at the bottom of the well, but in order to increase the versatility of the plate setup, they were grown on coverslips. The fully submerged biofilm-epithelium interface was still used, but the TR146 cells were seeded directly onto the basolateral side of the transwell membrane to mimic the *in vivo* orientation of the junctional epithelium, where the basement membrane is adjacent to the connective tissue while the outermost epithelial layers face the sulcus. The 3 µm membrane pore size was chosen to allow for active migration of neutrophils, which have a diameter of 8.3 µm, while preventing their passive passage (Downey et al., 1990). Finally, to simulate a timely, directed influx of neutrophils as early immune responders, epithelial cells were first stimulated with biofilms for 1 hour before neutrophils were added, allowing time for the release and accumulation of epithelial-derived mediators.

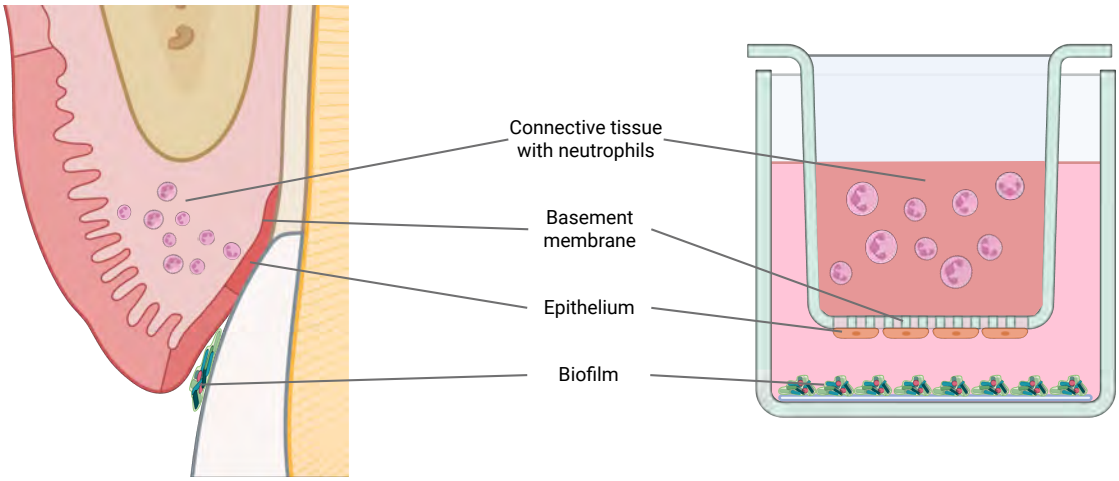

Figure 6.2 Proposed design of an *in vitro* 3D co-culture model of the oral barrier at the gingival sulcus. The proposed model utilised a conventional transwell-based system and Thermanox coverslips as supports for modelling neutrophil transepithelial migration into the gingival sulcus. The biofilm–epithelium interface was created by placing bacterial biofilms grown on coverslips at the bottom of the well, with the TR146 cell-seeded transwell insert membrane, which had 3 µm pores, positioned directly above. The epithelial layer was maintained fully submerged throughout both its formation and the co-culture period. Neutrophils were added to the transwell insert with a 1-hour delay relative to the rest of the setup to simulate a directed influx of neutrophils from the connective tissue, through the epithelium, and into the gingival sulcus. Figure created with BioRender.com.

6.3 Hypothesis and research questions

Hypothesis: There are certain components and properties of the oral barrier at the gingival sulcus that can be combined to model it *in vitro*.

The research questions raised to examine this hypothesis included:

1. In the proposed *in vitro* model system, can biofilms induce a response in the epithelial cell layer that will result in:

    a. IL-8 response from neutrophils and epithelial cells?

    b. neutrophil migration through the epithelial layer towards the bacterial biofilm?

6.4 Results

The experiments in this chapter sought to develop a proof-of-concept 3D *in vitro* model of neutrophil transepithelial migration at the junctional epithelium. To achieve this, the neutrophil transwell migration assay setup was iteratively refined through the progressive incorporation of components previously validated in Chapters 4 and 5:

- primary neutrophils;
- a TR146 epithelial cell multilayer grown on a transwell insert membrane; and
- 5- and 10-species biofilms associated with periodontal health and disease.

The assay was developed through four exploratory configurations of increasing complexity. As these experiments were conducted as preliminary proof-of-concept assays and were limited to a single independent experiment per configuration, the findings are presented descriptively and used to inform subsequent model development. The initial assay configuration was used to estimate baseline neutrophil movement through the unseeded porous transwell membrane following stimulation with soluble LPS in the well. Migration was assessed by recovering neutrophils from the wells and counting them using a haemocytometer. The next step involved introducing a TR146 cell-seeded membrane to mimic the presence of the junctional epithelium. At this stage, IL-8 measurement by ELISA was added as a readout and retained in later iterations to assess inflammatory mediator release in response to stimulation. Because direct haemocytometer counting was limited by poor recovery of migrated neutrophils from the wells, a CCK-8 assay was subsequently adopted as an indirect readout of viable cells within the migration system. The protocol was then modified to introduce an LPS gradient, with the aim of modelling directional stimulation more effectively. Finally, 5- and 10-species bacterial biofilms were incorporated as more biologically relevant stimuli to better reflect *in vivo* conditions. The final experiment was designed to compare neutrophil migration in response to the 5- and 10-species biofilm models. As the presence

of biofilms interfered with CCK-8 measurements in the wells, only transwell CCK-8 readouts were performed. A crystal violet assay was also performed to assess adherent biomass in the wells after completion of the migration assay.

6.4.1 Neutrophil transwell migration assay following stimulation with soluble LPS

Transwell inserts with porous membranes are commonly used *in vitro* tools to study neutrophil migration. In order to allow only active neutrophil movement, membranes with pores 3 µm in diameter were chosen for all experiments. The initial experiment was used to estimate baseline neutrophil movement through these unseeded membranes – in the absence of any epithelial cell layer. During the initial transwell migration assay, 1×10^6 neutrophils were added to each PC Corning transwell insert, which was placed in a well containing either HBSS(+) with LPS at 20 µg/mL or HBSS(+) alone. LPS was derived from *E. coli* O111:B4, which is reported to bind TLR4 on neutrophils, resulting in their activation (Evani et al., 2020) and enhanced motility (Boribong et al., 2019). Following a 2-hour incubation, inserts were removed and neutrophils that migrated into the wells were quantified with a haemocytometer. The total number of neutrophils detected in the wells containing LPS ($9.75 \times 10^5 \pm 1.58 \times 10^4$) did not appear markedly different from that observed in the control wells, where $8.95 \times 10^5 \pm 3.97 \times 10^4$ cells were recorded (Figure 6.3).

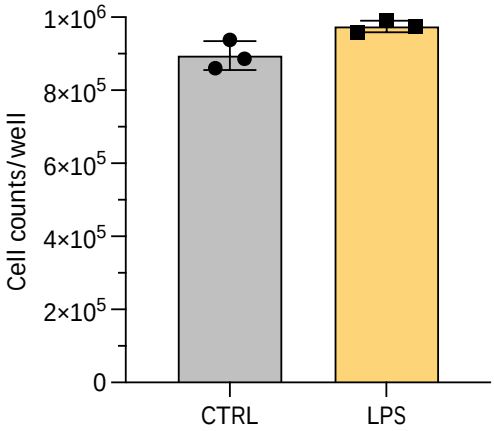

Figure 6.3 Quantification of neutrophils in the transwell migration assay following stimulation with soluble LPS. Transwell inserts with porous PC membranes were placed in wells containing HBSS(+) alone (CTRL) or HBSS(+) with LPS (20 µg/mL; LPS). Next, 1 × 10^6 neutrophils suspended in 100 µL HBSS(+) were added to each insert and incubated for 2 hours at 37 °C, 5% CO_2. Following incubation, neutrophils that migrated into the wells were quantified using an improved Neubauer haemocytometer. Data represent mean ± SD of technical triplicates from a single experiment (n = 1). Individual technical replicate values are shown as symbols. HBSS(+), Hanks' balanced salt solution with calcium and magnesium; LPS, lipopolysaccharide; PC, polycarbonate.

6.4.2 Neutrophil transepithelial migration assay following stimulation with soluble LPS

The next phase of the *in vitro* model development involved the introduction of the TR146 cell-seeded membrane to mimic the presence of the junctional epithelium. This dual-cell setup will also be referred to hereafter as PMN/Epi. For the purpose of this experiment, Millicell PET transwell inserts were seeded with 5 × 10^4 TR146 cells per transwell and incubated for 2 days at 37 °C, 5% CO_2. During the migration assay, transwells were placed in wells containing RPMI medium with or without LPS (20 µg/mL). Immediately afterwards, 1 × 10^6 neutrophils were added to each transwell insert and the full setup was incubated for either 2 or 24 hours. Following the incubation at 37 °C in 5% CO_2, recovery of neutrophils was attempted from both the wells and the apical compartments of the transwell inserts, but it did not exceed 7% of the initial input (data not shown). IL-8 ELISA analysis of supernatants retrieved from the wells suggested that stimulation of the PMN/Epi setup with LPS may have been associated with higher measured concentrations of IL-8, reaching 42.06 ± 43.83 pg/mL after 2 hours and 3058.87 ± 1928.23 pg/mL after 24 hours (Figure 6.4A and B). However, the calculated concentration for one technical replicate contributing to the 24-hour mean was extrapolated beyond the ELISA standard curve range

and should therefore be treated as an estimate. This estimated value was 4422.34 pg/mL, compared with 1695.41 pg/mL for the other replicate. IL-8 was also detected in the unstimulated dual-cell setup after 24 hours, although at a substantially lower measured concentration (157.65 ± 51.57 pg/mL).

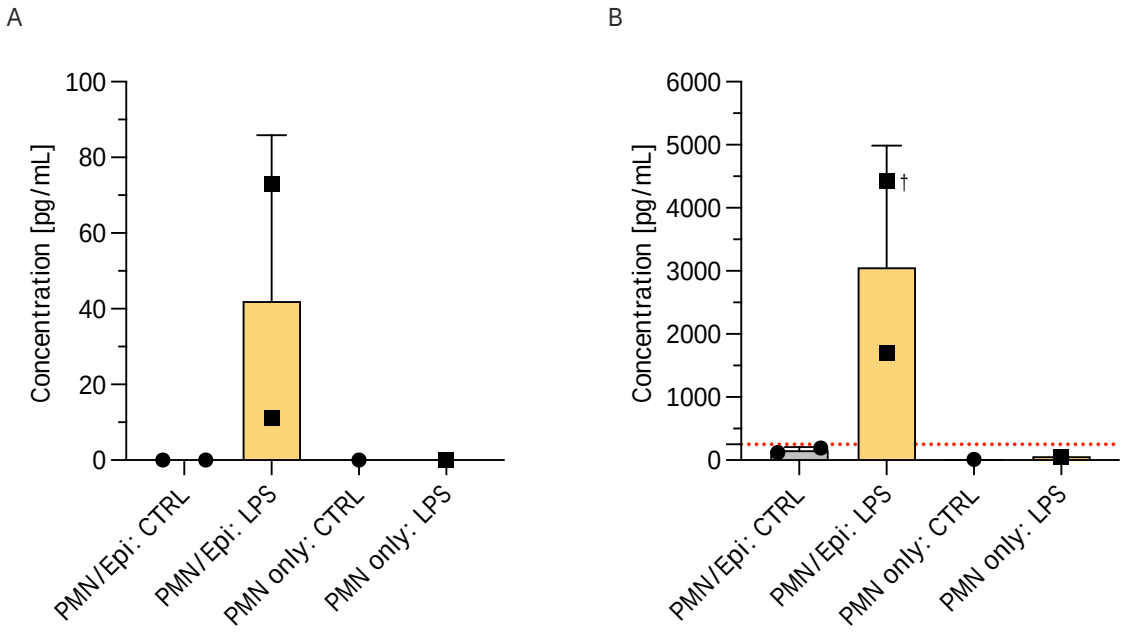

Figure 6.4 IL-8 release during the neutrophil transepithelial migration assay following stimulation with soluble LPS. Transwell inserts with porous Millicell PET membranes were seeded with 5 × 10^4 TR146 cells per transwell (PMN/Epi) or left unseeded (PMN only) and incubated for 2 days at 37 °C, 5% CO_2. Following incubation, transwells were placed in wells containing RPMI alone (CTRL) or RPMI with LPS (20 µg/mL; LPS). Next, 1 × 10^6 neutrophils suspended in 100 µL RPMI were added to each insert and incubated for (A) 2 hours or (B) 24 hours at 37 °C, 5% CO_2. Following incubation, supernatants from the wells were retrieved and evaluated for IL-8 concentrations by ELISA. Data represent mean + SD of technical duplicates (seeded transwells) or an individual measurement (unseeded control) from a single experiment (n = 1). Individual technical replicate values are shown as symbols. The red dotted line denotes the upper limit of the standard curve. The samples exceeding this limit were diluted 1:8 and re-tested, with the final concentrations adjusted for the dilution factor. One sample still exceeded the limit, but further testing at different dilutions was precluded by insufficient sample volume. Therefore, this value was extrapolated beyond the ELISA standard curve range and treated as an exploratory estimate only, and is denoted by a dagger (†) on the graph. IL-8, interleukin-8; LPS, lipopolysaccharide; PET, polyethylene terephthalate; PMN, polymorphonuclear neutrophil; PMN/Epi, dual-cell setup comprising PMNs and TR146 epithelial cells; RPMI, RPMI 1640 medium modified with L-glutamine and phenol red.

Histological analysis of the cells present on the transwell insert membranes was consistent with epithelial layer formation in all of the samples to which TR146 cells were added. Neutrophils, however, were detected only in the specimens obtained following the 2-hour incubation (Figure 6.5) and in PMN-only setups from the 24-hour incubation (data not shown).

Furthermore, at the 2-hour time point, neutrophils appeared to exhibit different distributions depending on whether membranes were TR146-seeded or unseeded. When exposed to the epithelial layer, neutrophils appeared to form clusters on the apical side of the membrane (more evident following LPS stimulation), while in the absence of TR146 cells, they were observed on both sides of the membrane as more evenly dispersed single cells.

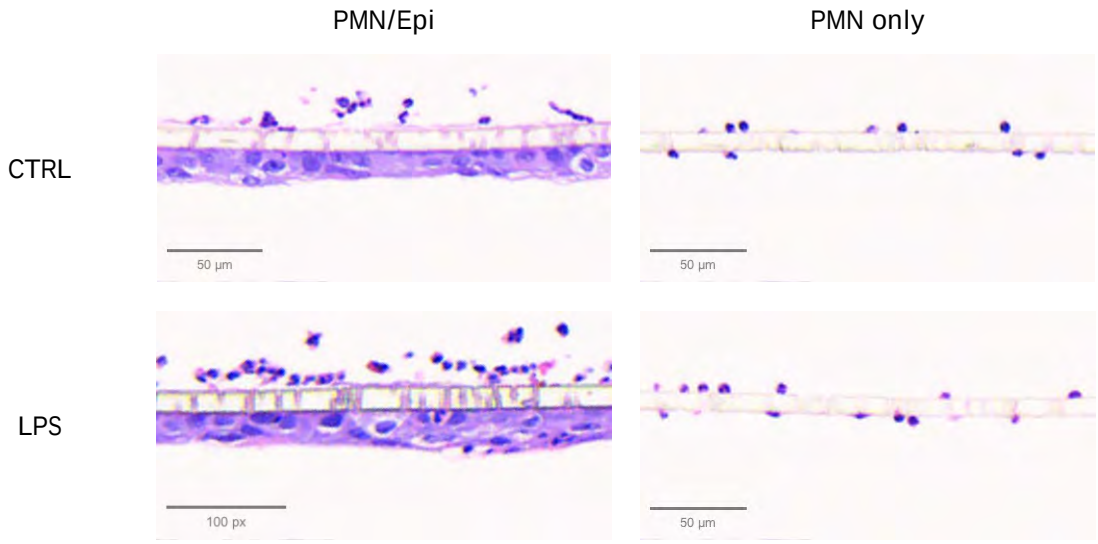

Figure 6.5 H&E-stained Millicell PET membranes from the neutrophil transepithelial migration assay following stimulation with soluble LPS. Transwell inserts with porous Millicell PET membranes were seeded with 5×10^4 TR146 cells per transwell (PMN/Epi) or left unseeded (PMN only) and incubated for 2 days at 37 °C, 5% CO_2. Following incubation, transwells were placed in wells containing RPMI alone (CTRL) or RPMI with LPS (20 µg/mL; LPS). Next, 1×10^6 neutrophils suspended in 100 µL RPMI were added to each insert and incubated for 2 hours. Following incubation, transwell membranes were fixed in 10% neutral buffered formalin overnight at 4 °C, paraffin-embedded, sectioned, and stained with H&E. Slides were scanned at 20× magnification. The experiment was performed on a single occasion (n = 1). For each condition, there were two technical replicates for PMN/Epi setups and one sample for PMN-only setups. One representative image is shown for each experimental condition.
LPS, lipopolysaccharide; PET, polyethylene terephthalate; PMN, polymorphonuclear neutrophil; PMN/Epi, dual-cell setup comprising PMNs and TR146 epithelial cells; RPMI, RPMI 1640 medium modified with L-glutamine and phenol red.

6.4.3 Neutrophil transepithelial migration assay following stimulation with surface-bound LPS

The transwell migration experiment protocol was further modified to better model directional guidance provided by the LPS gradient. LPS (100 ng/mL) was adsorbed onto the well surface pre-coated with a 1% fibrinogen solution to allow for desorption during the assay. An additional control was incorporated using a transwell insert seeded with TR146 cells, without added neutrophils, to assess the contribution of TR146 cells to IL-8 secretion. This condition also served as an

experimental negative control for the CCK-8 assay, allowing assessment of whether viable TR146 cells alone produced a detectable CCK-8 signal and whether this signal appeared to vary between stimulated and unstimulated conditions. Next, transwells were pre-incubated in the test plate for 1 hour to allow for release and accumulation of epithelial-derived IL-8 before introduction of neutrophils, consistent with reports that TR146 cells constitutively secrete IL-8 (Molero-Abraham et al., 2019) and that IL-8 release can increase following LPS exposure (Tetyczka et al., 2021). This maintained the overall stimulation period for the epithelial cells, while shortening the main incubation time for neutrophils to 1 hour due to concerns about reduced survival over longer periods. The CCK-8 assay was then carried out immediately following the incubation period to provide an estimate of viable neutrophils that remained in the apical compartment of the transwell insert and those that migrated into the well. The results of this preliminary experiment suggested that fewer neutrophils were detected in the transwell insert when its membrane was seeded with TR146 cells (Figure 6.6A). In the PMN/Epi setup, $4.00 \times 10^4 \pm 5.04 \times 10^3$ neutrophils were detected in the transwell under LPS conditions compared to the media-only control with $5.02 \times 10^4 \pm 2.86 \times 10^4$ neutrophils. When the epithelial layer was not present, higher neutrophil counts were observed in the transwells – $6.27 \times 10^4 \pm 2.26 \times 10^3$ and $8.64 \times 10^4 \pm 3.74 \times 10^4$ in the presence and absence of LPS, respectively. While an opposing pattern was observed in the wells (Figure 6.6B), the combined counts from both sides did not fully account for the initial input cell number (1×10^6 neutrophils per insert). Neutrophil counts in the PMN/Epi setup wells reached $5.91 \times 10^5 \pm 1.09 \times 10^5$ and $4.23 \times 10^5 \pm 3.74 \times 10^4$ under LPS and control conditions, respectively. Setups without the epithelial cell layer yielded lower neutrophil counts in wells, with $1.48 \times 10^5 \pm 3.94 \times 10^4$ when stimulated with LPS and $7.86 \times 10^4 \pm 2.34 \times 10^4$ under media control conditions. Within the TR146-only setup, the CCK-8 signal appeared comparable in the presence and absence of LPS, both in the transwells and the corresponding wells.

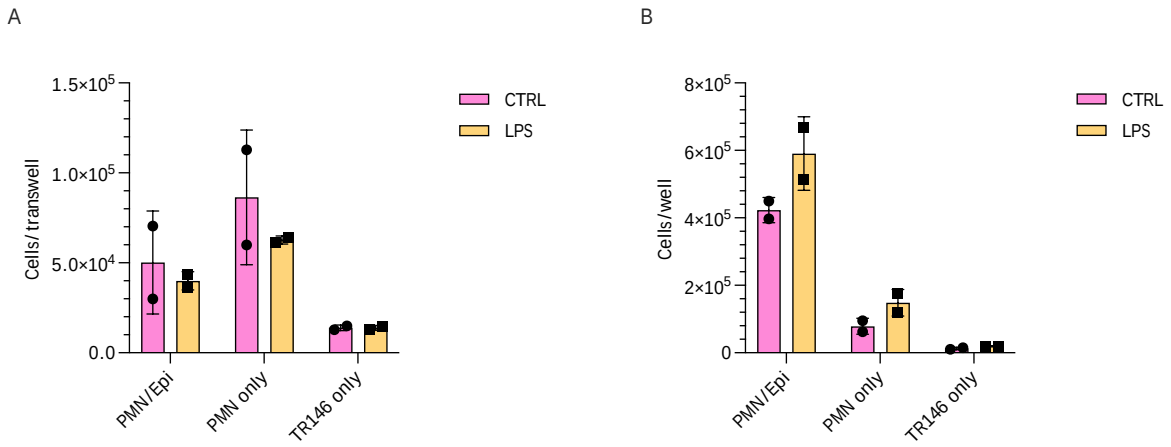

Figure 6.6 Quantification of neutrophils in the transepithelial migration assay following stimulation with surface-bound LPS. Transwell inserts with porous Millicell PET membranes were seeded with 5 × 10^4 TR146 cells per transwell (PMN/Epi and TR146 only) or left unseeded (PMN only) and incubated for 2 days at 37 °C, 5% CO_2. Following incubation, transwells were placed in RPMI-containing wells pre-treated with dPBS(−) alone (CTRL) or with LPS (100 ng/mL; LPS) and incubated for 1 hour at 37 °C, 5% CO_2. Next, 1 × 10^6 neutrophils suspended in 100 µL RPMI were added to each insert in the PMN/Epi and PMN-only conditions, while 100 µL RPMI alone was added to inserts in the TR146-only condition. All setups were then incubated for 1 hour at 37 °C, 5% CO_2. Following incubation, cell suspensions in (A) the transwell inserts and (B) the wells were analysed using the CCK-8 assay. Data represent mean ± SD of technical duplicates from a single experiment (n = 1). Individual technical replicate values are shown as symbols. dPBS(−), calcium- and magnesium-free Dulbecco's phosphate-buffered saline; LPS, lipopolysaccharide; PET, polyethylene terephthalate; PMN, polymorphonuclear neutrophil; PMN/Epi, dual-cell setup comprising PMNs and TR146 epithelial cells; RPMI, RPMI 1640 medium modified with L-glutamine and phenol red.

Supernatants recovered from the wells were assessed for the presence of IL-8 by ELISA (Figure 6.7). For this assay, only one replicate from the 1:10 dilution was available for analysis; therefore, the data are presented descriptively as single concentration values. PMN/Epi setups were associated with the highest measured IL-8 concentrations, reaching 1834.39 and 1426.15 pg/mL for LPS-stimulated and unstimulated setups, respectively. This was followed by the TR146-only setups with 1134.31 pg/mL (under LPS conditions) and 317.29 pg/mL (media control). The lowest IL-8 concentrations were detected in PMN-only setups, with values of 210.54 pg/mL under LPS conditions and 78.93 pg/mL in the absence of LPS.

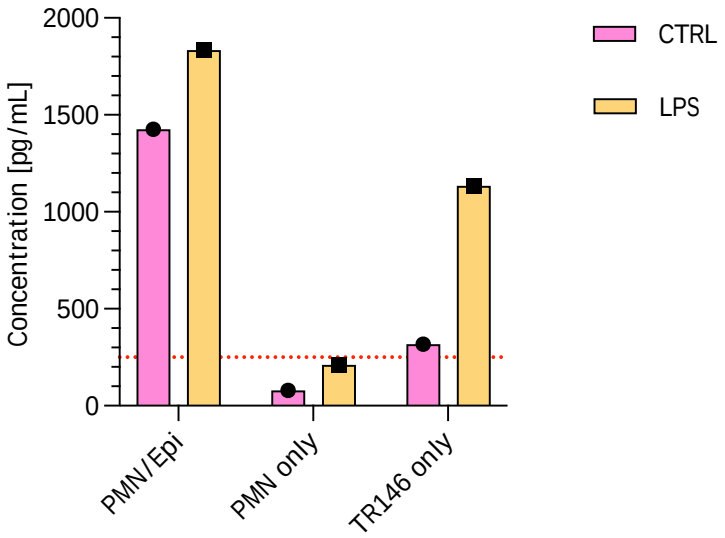

Figure 6.7 IL-8 release during the neutrophil transepithelial migration assay following stimulation with surface-bound LPS. Transwell inserts with porous Millicell PET membranes were seeded with 5 × 10^4 TR146 cells per transwell (PMN/Epi and TR146 only) or left unseeded (PMN only) and incubated for 2 days at 37 °C, 5% CO_2. Following incubation, transwells were placed in RPMI-containing wells pre-treated with dPBS(−) alone (CTRL) or with LPS (100 ng/mL; LPS) and incubated for 1 hour at 37 °C, 5% CO_2. Next, 1 × 10^6 neutrophils suspended in 100 µL RPMI were added to each insert in the PMN/Epi and PMN-only conditions, while 100 µL RPMI alone was added to inserts in the TR146-only condition. All setups were then incubated for 1 hour at 37 °C, 5% CO_2. Following incubation, supernatants from the wells were retrieved and evaluated for IL-8 levels by ELISA. Data represent individual measurements from a single experiment (n = 1), with one technical replicate from the 1:10 dilution available for analysis. Individual values are shown as symbols. The red dotted line denotes the upper limit of the standard curve. Both neat and diluted samples were analysed. The 1:10 dilution was required to fit the samples within the standard curve range, with the final concentrations adjusted for the dilution factor. Further testing of the second replicate at different dilutions was precluded by insufficient sample volume. IL-8, interleukin-8; LPS, lipopolysaccharide; PET, polyethylene terephthalate; PMN, polymorphonuclear neutrophil; PMN/Epi, dual-cell setup comprising PMNs and TR146 epithelial cells; RPMI, RPMI 1640 medium modified with L-glutamine and phenol red.

Histological analysis of the specimens obtained during the experiment was not possible due to cell detachment from the membrane in several specimens, resulting in sparse cell retention or empty slides (data not shown).

6.4.4 Neutrophil transepithelial migration assay following stimulation with 5- and 10-species biofilms

The transepithelial migration assay was advanced by incorporation of 5- and 10-species bacterial biofilms, described in detail in Chapter 4, to better reflect *in vivo* conditions. The final experiment was designed to compare neutrophil migration in response to these two biofilm models. Multispecies biofilms stored at −80 °C were revived overnight under appropriate conditions (see Section 2.1.1.9). Clean coverslips were processed in parallel with each biofilm condition using the same overnight protocol and were used as an exploratory feasibility

platform to assess whether neutrophils could be recovered from both transwell compartments. Aside from replacing surface-bound LPS with 5- or 10-species biofilms grown on Thermanox coverslips and increasing TR146-seeding density from 5×10^4 to 1×10^6 cells per transwell, the migration assay was conducted as described in the previous section.

The CCK-8 assay carried out on cell suspensions retrieved from the transwells (Figure 6.8) suggested that transwell retention of neutrophils was lower following 5-species biofilm stimulation than 10-species biofilm stimulation in both the PMN/Epi setup ($3.18 \times 10^4 \pm 2.39 \times 10^3$ vs. $1.12 \times 10^5 \pm 2.68 \times 10^4$ cells, respectively) and the PMN-only setup ($2.94 \times 10^4 \pm 1.52 \times 10^3$ vs. $8.16 \times 10^4 \pm 1.86 \times 10^4$ cells, respectively). Among coverslip-only conditions, neutrophil retention in the PMN-only setup ($1.42 \times 10^5 \pm 6.83 \times 10^4$ cells) appeared higher than in the PMN/Epi setup ($5.34 \times 10^4 \pm 2.07 \times 10^4$ cells). The PMN-only setup under this condition also showed both the highest apparent cell retention and the greatest variability among the transwell CCK-8 readouts in this experiment. Within the TR146-only setup, the CCK-8 signal in the transwells appeared comparable across all experimental conditions. The assay readout was limited to cell suspensions retrieved from transwells due to interfering signals produced by coverslips and biofilms in the wells.

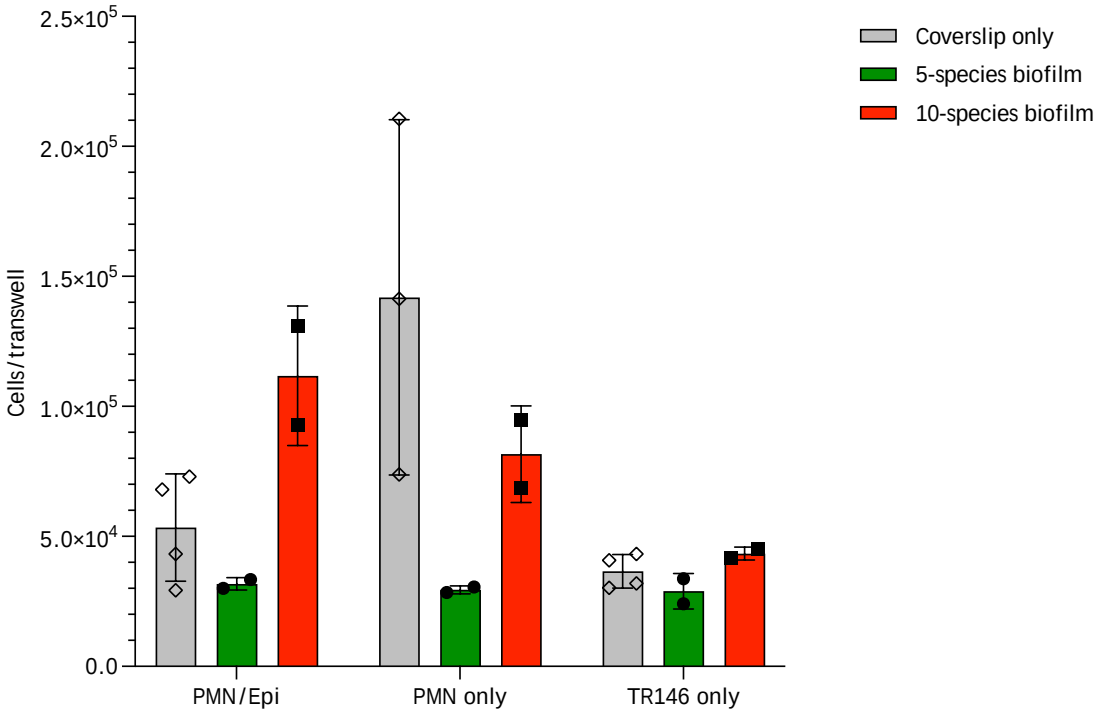

Figure 6.8 Quantification of neutrophils in the transepithelial migration assay following stimulation with 5-species* and 10-species** bacterial biofilms. Transwell inserts with porous Millicell PET membranes were seeded with 1 × 10^6 TR146 cells per transwell (PMN/Epi and TR146 only) or left unseeded (PMN only) and incubated for 2 days at 37 °C, 5% CO_2. Following incubation, transwells were placed in RPMI-containing wells with revived 5-species or 10-species biofilms, or with clean coverslips processed in parallel for each biofilm type using the same overnight protocol. Transwells were then incubated for 1 hour at 37 °C, 5% CO_2. Next, 1 × 10^6 neutrophils suspended in 100 µL RPMI were added to each insert in the PMN/Epi and PMN-only setups, while 100 µL RPMI alone was added to inserts in the TR146-only setup. All setups were then incubated for 1 hour at 37 °C, 5% CO_2. Following incubation, cell suspensions in the transwell inserts were analysed using the CCK-8 assay. Data represent mean ± SD from a single experiment (n = 1). Biofilm conditions were assessed using technical duplicates, while coverslip-only data were pooled within each experimental setup. The pooled coverslip-only conditions included four technical replicates for PMN/Epi and TR146-only setups, and three technical replicates for the PMN-only setup. One PMN-only sample was excluded prior to analysis due to suspected technical error during the assay. Individual technical replicate values are shown as symbols.
*5-species biofilms included *S. intermedius, S. mitis, S. oralis, N. mucosa* and *R. dentocariosa.*
**10-species biofilms included *S. intermedius, S. mitis, S. oralis, A. naeslundii, F. nucleatum subsp. polymorphum, F. nucleatum subsp. vincentii, V. dispar, A. actinomycetemcomitans, P. intermedia* and *P. gingivalis*.
PET, polyethylene terephthalate; PMN, polymorphonuclear neutrophil; PMN/Epi, dual-cell setup comprising PMNs and TR146 epithelial cells; RPMI, RPMI 1640 medium modified with L-glutamine and phenol red.

Additionally, macroscopic visual inspection after the experiment showed visible material in the coverslip-only wells in the PMN/Epi setup and, to a lesser extent, in the PMN-only setup. Subsequent examination under a light microscope showed small, rounded cells attached to the coverslip surface in these wells (data not shown).

Histological analysis of the transwell insert membranes was attempted; however, the cells detached from the membrane during processing, resulting in sparse cell retention or empty slides (data not shown).

Next, IL-8 concentrations in well supernatants were measured by ELISA (Figure 6.9). Stimulation with a 5-species biofilm in the PMN/Epi setup appeared to be associated with a higher mean IL-8 concentration (58.99 ± 49.05 pg/mL) compared to the 10-species biofilm and coverslip-only conditions (42.23 ± 21.84 pg/mL and 45.08 ± 17.86 pg/mL, respectively), although variability was also greater. By contrast, in the TR146-only setup, 5-species biofilm stimulation appeared to be associated with a lower mean IL-8 concentration (20.58 ± 0.34 pg/mL) and lower variability than 10-species biofilm stimulation (38.44 ± 54.36 pg/mL) or the coverslip-only condition (30.48 ± 30.64 pg/mL). Overall, IL-8 concentrations in the PMN/Epi and TR146-only setups appeared broadly comparable across conditions. Notably, IL-8 was undetectable in supernatants retrieved from PMN-only setups, regardless of stimulation conditions.

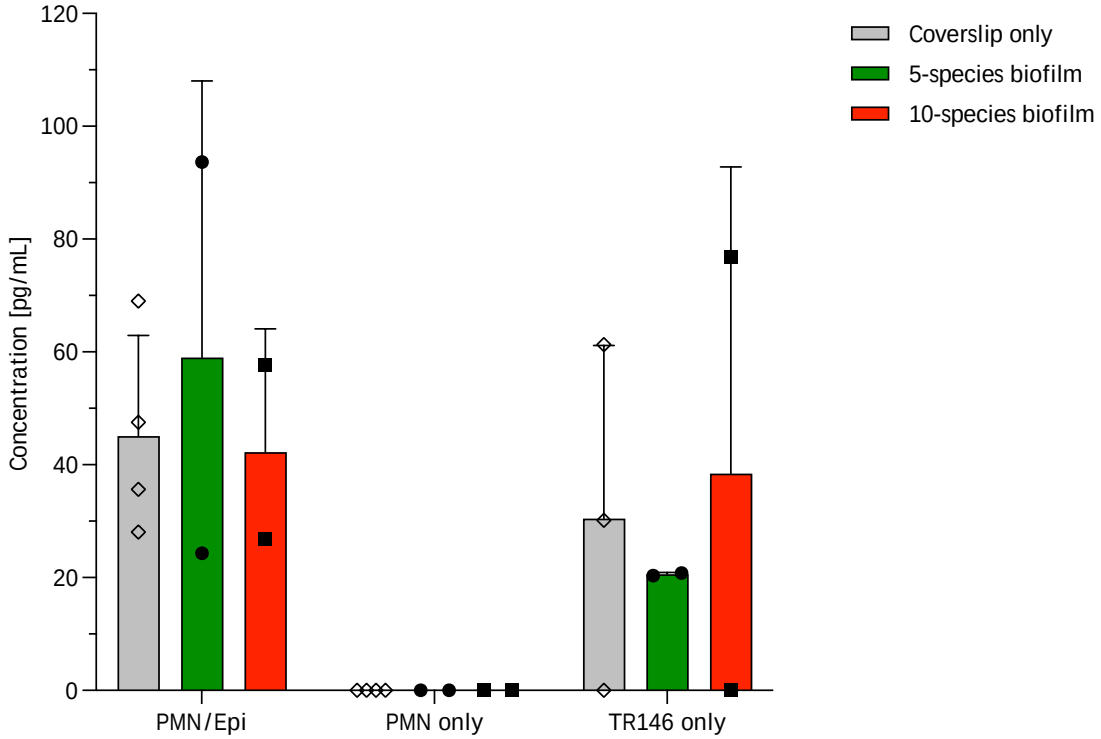

Figure 6.9 IL-8 release during the neutrophil transepithelial migration assay following stimulation with 5-species* and 10-species** bacterial biofilms. Transwell inserts with porous Millicell PET membranes were seeded with 1 × 10^6 TR146 cells per transwell (PMN/Epi and TR146 only) or left unseeded (PMN only) and incubated for 2 days at 37 °C, 5% CO_2. Following incubation, transwells were placed in RPMI-containing wells with revived 5-species or 10-species biofilms, or with clean coverslips processed in parallel for each biofilm type using the same overnight protocol. Transwells were then incubated for 1 hour at 37 °C, 5% CO_2. Next, 1 × 10^6 neutrophils suspended in 100 µL RPMI were added to each insert in the PMN/Epi and PMN-only conditions, while 100 µL RPMI alone was added to inserts in the TR146-only condition. All setups were then incubated for 1 hour at 37 °C, 5% CO_2. Following incubation, supernatants from the wells were retrieved and evaluated for IL-8 levels by ELISA. Data represent mean + SD from a single experiment (n = 1). Biofilm conditions were assessed using technical duplicates, while coverslip-only data were pooled within each experimental setup. The pooled coverslip-only conditions included four technical replicates for PMN/Epi and PMN-only setups, and three technical replicates for the TR146-only setup. One TR146-only sample was excluded prior to analysis due to suspected technical error during ELISA duplicate measurement. Individual technical replicate values are shown as symbols.
*5-species biofilms included *S. intermedius, S. mitis, S. oralis, N. mucosa* and *R. dentocariosa.*
**10-species biofilms included *S. intermedius, S. mitis, S. oralis, A. naeslundii, F. nucleatum* subsp. *polymorphum, F. nucleatum* subsp. *vincentii, V. dispar, A. actinomycetemcomitans, P. intermedia* and *P. gingivalis*.
IL-8, interleukin-8; PET, polyethylene terephthalate; PMN, polymorphonuclear neutrophil; PMN/Epi, dual-cell setup comprising PMNs and TR146 epithelial cells; RPMI, RPMI 1640 medium modified with L-glutamine and phenol red.

Following completion of the transwell migration assay, the 24-well plate with coverslips was dried and utilised for crystal violet staining (Figure 6.10) to enable macroscopic visualisation of cells that had migrated and attached under the coverslip-only conditions and to assess adherent biomass in the wells. Macroscopic inspection of the coverslip-only wells in the PMN/Epi setup after crystal violet staining showed circular stained areas corresponding to the footprint of the transwell insert membrane, with additional stained material extending beyond this area (Figure 6.10A). In the PMN-only setup, the footprint was less distinct, with weaker overall staining and a few more intensely stained punctate areas within the footprint. In the TR146-only setup, the footprint area was largely unstained, with only minimal staining outside this region. Strong crystal violet staining was observed on biofilm-containing coverslips. The 5-species biofilms appeared to be more uniformly stained, whereas the 10-species biofilms showed a more heterogeneous staining pattern. On these coverslips, the transwell footprint remained visible mainly as a lighter peripheral rim. After macroscopic imaging, retained crystal violet was solubilised and absorbance was measured as the biomass readout. The biomass appeared broadly comparable between wells with 5- and 10-species biofilms when considered across all setups, as the mean OD values were 2.019 ± 0.368 and 2.081 ± 0.3784, respectively, with corresponding CV values of 18.23% and 18.18% (Figure 6.10B). Biomass in the coverslip-only conditions appeared substantially lower than that of the biofilm-containing wells (Figure 6.10C). Nevertheless, biomass in the coverslip-only wells incubated with the PMN/Epi setup seemed slightly higher (0.1778 ± 0.025, CV = 14.34%) than in those incubated with the PMN-only setup (0.053 ± 0.02, CV = 30.16%). While it should be noted that these values are very small and should therefore be interpreted cautiously, they appeared consistent with the macroscopic appearance of the wells (Figure 6.10A).

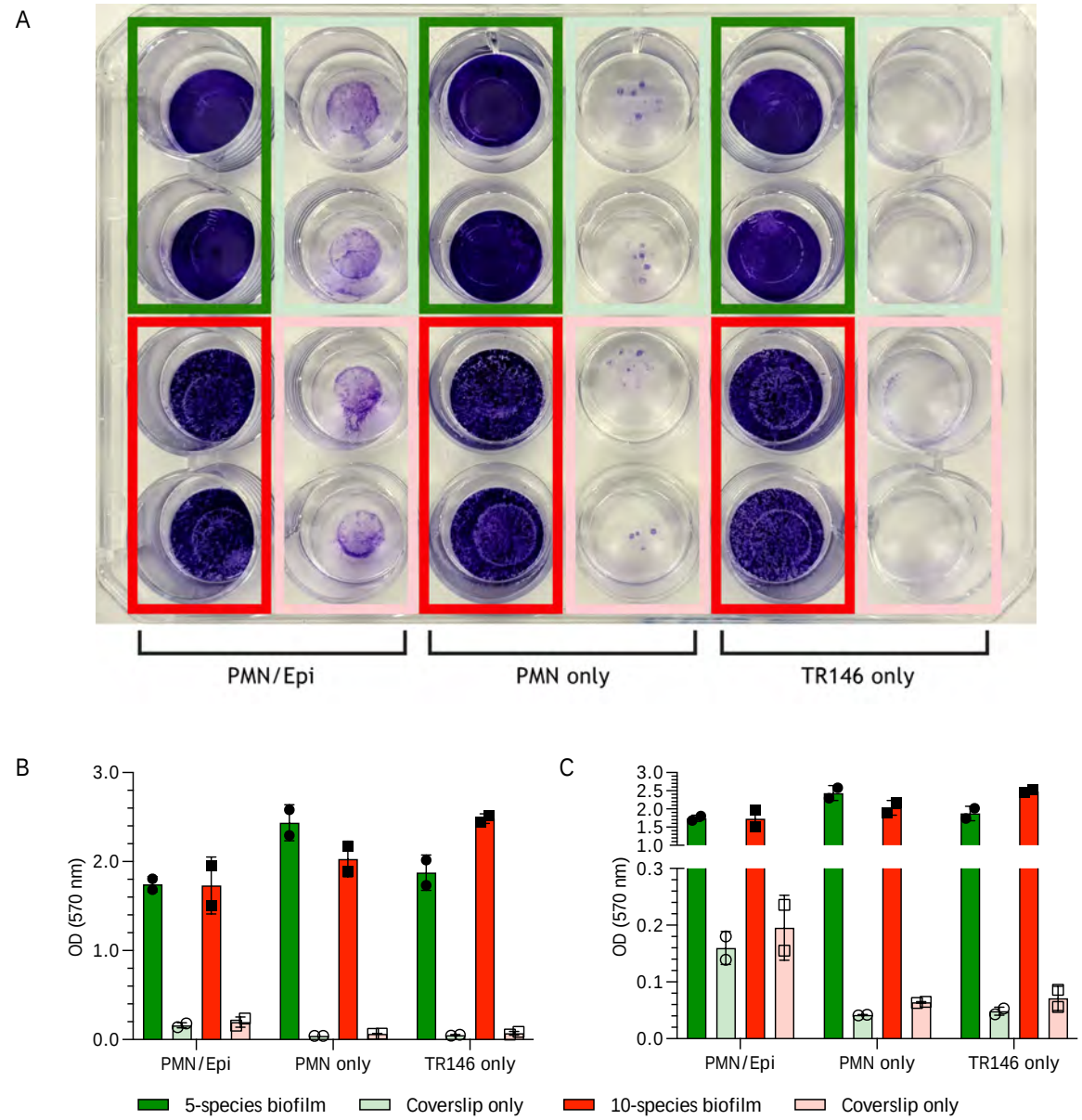

Figure 6.10 Crystal violet biomass assessment of a post-migration plate after neutrophil transepithelial migration following stimulation with 5-species* and 10-species** bacterial biofilms. Transwell inserts with porous Millicell PET membranes were seeded with 1×10^6 TR146 cells per transwell (PMN/Epi and TR146 only) or left unseeded (PMN only) and incubated for 2 days at 37 °C, 5% CO_2. Following incubation, transwells were placed in RPMI-containing wells with revived 5-species or 10-species biofilms, or with clean coverslips processed in parallel for each biofilm type using the same overnight protocol. Transwells were then incubated for 1 hour at 37 °C, 5% CO_2. Next, 1×10^6 neutrophils suspended in 100 µL RPMI were added to each insert in the PMN/Epi and PMN-only conditions, while 100 µL RPMI alone was added to inserts in the TR146-only condition. All setups were then incubated for 1 hour at 37 °C, 5% CO_2. Following incubation, the plate containing coverslips was retrieved, dried and used for the crystal violet biomass assay. (A) Post-migration plate stained with crystal violet, (B) crystal violet biomass assessment showing the full OD range, (C) crystal violet biomass assessment showing an expanded low-OD range. Image and data are from a single experiment (n = 1) performed in technical duplicate. Data represent mean ± SD, with individual technical replicate values shown as symbols.
*5-species biofilms included *S. intermedius, S. mitis, S. oralis, N. mucosa* and *R. dentocariosa.*
**10-species biofilms included *S. intermedius, S. mitis, S. oralis, A. naeslundii, F. nucleatum* subsp. *polymorphum, F. nucleatum* subsp. *vincentii, V. dispar, A. actinomycetemcomitans, P. intermedia* and *P. gingivalis*.
PET, polyethylene terephthalate; PMN, polymorphonuclear neutrophil; PMN/Epi, dual-cell setup comprising PMNs and TR146 epithelial cells; RPMI, RPMI 1640 medium modified with L-glutamine and phenol red.

6.5 Discussion

This chapter describes the stepwise development of a 3D *in vitro* model of the oral barrier at the gingival sulcus. The components used in the model were previously validated in Chapters 4 and 5 and included 5- and 10-species biofilms associated with periodontal health and disease, a TR146 epithelial cell multilayer grown on a transwell insert membrane, and primary neutrophils. These components were progressively incorporated into the setup, in configurations of increasing complexity, resulting in the development of the proof-of-concept model of neutrophil migration across the junctional epithelium. The assays were exploratory, with one independent experiment performed per configuration to assess feasibility and guide further model development.

6.5.1 LPS-stimulated transwell migration assays

The initial transwell migration assay provided an estimate of baseline neutrophil migration through the unseeded porous transwell membrane following stimulation with soluble LPS in the well (Figure 6.3). Soluble LPS did not appear to enhance neutrophil migration under the conditions tested. The comparable recovery of neutrophils from LPS-containing and control wells may reflect substantial unstimulated baseline migration through the porous membrane. This is consistent with transwell-based neutrophil chemotaxis assays in which spontaneous migration is measured as a background component of the assay (Thunström Salzer et al., 2018). The similar recovery between conditions may also have been influenced by the relatively long incubation time, which could have allowed neutrophils in the control condition to migrate to a similar extent. In addition, the finding may reflect the context-dependent nature of LPS effects on neutrophil migration. Although LPS has been reported to act as a direct chemoattractant for human neutrophils at high concentrations (Creamer et al., 1991), other studies have reported that LPS alone does not induce neutrophil chemotaxis, with migration instead occurring in response to mediators released by LPS-stimulated cells (Jung et al., 2013).

In the subsequent experiment, TR146 cells were used to seed the transwell insert membrane to generate an epithelial multilayer intended to mimic the junctional epithelium. Neutrophil recovery was low across all conditions (data

not shown). Histological assessment of H&E-stained membrane sections showed neutrophils at the 2-hour time point (Figure 6.5). In the PMN-only setup, these cells were more evenly dispersed on both sides of the membrane under both control and LPS-stimulated conditions. In contrast, neutrophils present in the PMN/Epi setup appeared to form aggregates, which may be consistent with increased activation, as activated neutrophils are known to increase adhesion molecule expression, promoting cell–cell aggregation (Kienle and Lämmermann, 2016). This may have been influenced by epithelial cell-derived signals. The absence of neutrophils in the PMN/Epi setup at 24 hours could be consistent with loss of detectable cells following prolonged or strong activation, potentially involving apoptosis or NETosis (Hsu et al., 2025, Perez-Figueroa et al., 2021). However, as apoptosis and NETosis were not directly assessed, this interpretation remains speculative. IL-8 was detected in well supernatants, with higher measured concentrations in PMN/Epi setups stimulated with LPS at both time points (Figure 6.4). TR146 cells have been reported to release IL-8, with a modest increase following LPS stimulation (Hosokawa et al., 2017, Tetyczka et al., 2021). This may suggest that the presence of TR146 cells contributed to the IL-8 response under these conditions, although a synergistic interaction between neutrophils and TR146 cells could not be excluded at this stage.

The next iteration of the model used surface-bound LPS in the wells with the aim of generating a more spatially restricted source of stimulation than soluble LPS in the well medium. Additionally, temporal control was introduced by delaying the addition of the neutrophil suspension. At this stage, the CCK-8 assay was employed because direct haemocytometer counting had been limited by poor recovery of migrated neutrophils from the wells in the previous experiment. This enabled estimation of viable neutrophil numbers in both the transwell insert apical compartments and the wells (Figure 6.6). As CCK-8 provides an indirect readout based on cell metabolic activity rather than a direct cell count, these estimates should be interpreted as approximate viable cell numbers. The data suggested that the presence of an epithelial layer, even when unstimulated, was associated with increased apparent neutrophil migration. Additionally, CCK-8-derived estimates in the wells appeared higher under LPS-stimulated conditions than under the corresponding control conditions in both neutrophil-containing setups. However, because this was based on a

single independent experiment with technical duplicates, this pattern should be interpreted descriptively rather than as evidence of a robust difference. The corresponding transwell readouts showed lower overall cell numbers than the well readouts and did not appear to show a clear condition-dependent pattern. Nevertheless, the estimated viable cell counts did not account for the full neutrophil input added to the transwell inserts, suggesting incomplete recovery and/or loss of detectable viable cells during the assay. This may reflect cells adhering to or remaining within the membrane or epithelial layer, cell death, or the indirect, viability-dependent nature of the CCK-8 assay in this setup. The CCK-8 readout from TR146 cells alone did not appear to differ markedly between LPS-stimulated and unstimulated conditions, suggesting that LPS did not substantially alter the viable cell signal from the epithelial component under the conditions tested. IL-8 concentrations were also measured in well supernatants from the same experimental setup (Figure 6.7). Across conditions, the IL-8 pattern appeared to align with the CCK-8-derived neutrophil counts in the corresponding wells, with higher apparent neutrophil migration accompanied by higher measured IL-8 concentrations. However, this possible relationship should be interpreted very cautiously, as one IL-8 technical replicate could not be quantified reliably. Both neat samples exceeded the upper detection limit, but following 1:10 dilution, only one replicate fell within the quantifiable range, while the other was below the lower limit of quantification.

This apparent alignment between migration and IL-8 readouts may reflect epithelial–neutrophil crosstalk within the PMN/Epi setup, although the direction of this relationship cannot be resolved from this experiment alone. One possible explanation is that TR146 cells constitutively release soluble mediators and express adhesion-associated molecules that may support neutrophil migration, with these responses potentially being further altered following LPS stimulation. IL-8 is a plausible contributor, although other inflammatory mediators or adhesion-associated molecules, such as IL-1β, IL-6, or ICAM-1, may also have contributed (Hagio-Izaki et al., 2018, Tetyczka et al., 2021). Further experiments would be required to measure additional epithelial-derived mediators and test whether blocking candidate signals alters neutrophil migration.

Another consideration relates to the interpretation of neutrophil counts obtained from setups with and without the epithelial cell layer, as these conditions may reflect distinct biological and assay-related processes. In the absence of the epithelial cell layer, increased migration through the membrane cannot be assumed to reflect classical chemotaxis, as the effects of LPS on neutrophil migration appear to depend on dose, timing and assay format. For example, LPS has been reported to act as a stop signal at higher concentrations in an under-agarose chemotaxis assay (Wang et al., 2017), whereas LPS pre-priming increased spontaneous migration of differentiated HL-60 cells in a microfluidic chemotaxis assay (Boribong et al., 2019). Therefore, the apparent LPS-associated migration observed in the PMN-only setup may reflect altered basal motility, neutrophil-derived mediator production, or assay-specific effects rather than a simple chemoattractant response. One possible indirect mechanism is LPS-induced IL-8 production by neutrophils, which could be amplified through autocrine or paracrine signalling (Evani et al., 2020, Kaiser et al., 2021). However, LPS desorption from the coated surface was not assessed, and the formation of an LPS or IL-8 gradient in this system remains speculative.

6.5.2 Biofilm-stimulated transwell migration assay

The concluding modification to the *in vitro* system involved substitution of the surface-bound LPS with coverslip-grown multispecies biofilms, allowing assessment of biofilm-associated IL-8 responses and neutrophil migration in the developing model. The final experiment was designed to compare responses to the 5- and 10-species biofilm models.

The CCK-8 analysis was limited to cell suspensions retrieved from the transwells only, due to interfering signals produced by coverslips and biofilms in the wells. Within the constraints of this readout, fewer neutrophils were retained in the transwells following exposure to 5-species biofilms than to 10-species biofilms, both in the presence and absence of epithelial cells (Figure 6.8). This pattern may indicate reduced neutrophil migration towards 10-species biofilms compared with 5-species biofilms. As the readout was indirect and the data were based on a single independent experiment, this finding should be interpreted cautiously and would require confirmation in additional experiments. If this pattern is confirmed, one possible explanation to explore is that differences in

bacterial composition between the biofilm models may have altered neutrophil chemotaxis through proteolytic activity or other virulence mechanisms. For example, *P. gingivalis* is known to disrupt IL-1ß, IL-6 and IL-8 signalling through the proteolytic activity of its gingipain proteases (Sochalska and Potempa, 2017, Stathopoulou et al., 2009). *A. actinomycetemcomitans* employs its outer membrane components to sequester inflammatory mediators; LPS captures IL-8 (Ahlstrand et al., 2019), while bacterial interleukin receptor I binds IL-6 and IL-8 and internalises IL-1ß (Ahlstrand et al., 2017).

IL-8 was measured as a readout of neutrophil and epithelial cell responses in the *in vitro* model (Figure 6.9). It was detected in the PMN/Epi and TR146-only setups, but was undetectable in PMN-only setups, suggesting that neutrophils were unlikely to be the main source of IL-8 under these experimental conditions. Instead, IL-8 detected in conditions containing TR146 cells may have partly reflected epithelial-derived IL-8, as TR146 cells have been reported to constitutively secrete IL-8, with secretion increasing only modestly under bacterial stimulation (Molero-Abraham et al., 2019). When considered in relation to the proposed bacterial disruption of cytokine signalling, however, the IL-8 concentrations in well supernatants did not show the reduction that would be expected if substantial sequestration or degradation had occurred. This does not exclude the possibility that other cytokines may still be relevant to this response, as these were not measured in this experiment. Overall, the IL-8 ELISA results were not sufficient to determine whether IL-8 influenced neutrophil migration. In addition, biofilm stimulation did not appear to clearly modulate the IL-8 response under these conditions. Further optimisation of the model conditions is required to assess potential changes in cytokine production by the model components under different experimental conditions.

The data also suggested that neutrophils could migrate through the transwell insert in the absence of biofilm; however, this response appeared highly variable and difficult to interpret (Figure 6.8). This coverslip-only condition provided an exploratory feasibility platform to assess whether neutrophils could be recovered from both transwell compartments. Microscopic inspection of the PMN/Epi and PMN-only wells revealed small, rounded cells attached to the

coverslip surface, with a morphology that appeared more consistent with neutrophils than epithelial cells.

This observation was consistent with neutrophil adhesion to the coverslip. Thermanox coverslips are hydrophilic, cell-culture-treated polyester surfaces designed to support cell attachment, and may also retain assay-derived molecules. Potential neutrophil adhesion at this surface could therefore be promoted by interactions with host-derived mediators or biofilm medium-derived components adsorbed to the coverslip. CD11b/CD18-dependent adhesion described for plastic surfaces may also have contributed (Yakubenko et al., 2002). Where present, IL-8 released during the assay could further contribute to inside-out activation of CD11b/CD18, increasing integrin affinity and avidity (Detmers et al., 1990). Subsequent integrin engagement and clustering on the neutrophil membrane could then reinforce outside-in signalling, adhesion and activation (Bouti et al., 2021).

Crystal violet biomass assessment did not appear to show clear differences between 5- and 10-species biofilms across the different experimental setups (PMN/Epi, PMN-only and TR146-only). Biomass detected in coverslip-only wells appeared to constitute only a fraction of that detected in wells containing biofilm-covered coverslips and was therefore low relative to the biofilm-associated signal (Figure 6.10B). As these coverslip-only wells did not contain biofilm, the low-level crystal violet staining in these wells may instead reflect non-specific dye binding to adherent cellular material, including neutrophils, neutrophil-derived debris and/or extracellular DNA/NET-like material retained on the coverslip surface. Although some OD values were very low (Figure 6.10C), they corresponded to the macroscopic staining pattern of the wells (Figure 6.10A). However, as crystal violet staining provides a semi-quantitative estimate of adherent biomass and may be insufficiently sensitive to resolve subtle differences, particularly in complex multispecies biofilms, these findings should be interpreted with caution (Azeredo et al., 2017, Castro et al., 2022, Kragh et al., 2019). The exact nature of the stained material could not be confirmed without more targeted staining approaches, such as immunostaining for neutrophil- or NET-associated markers (Allen, 2014, Pilchová et al., 2025). Therefore, the staining pattern and previous microscopic observations were

consistent with, but not confirmatory of, neutrophil-associated material in the coverslip-only wells.

NET-associated signal was also assessed in well supernatants; however, the signal detected in the samples was very low and therefore did not provide clear evidence of NET formation in this experiment. Although the 1-hour period following neutrophil addition exceeded the minimum onset time for NETosis reported in some *in vitro* studies (van der Linden et al., 2017), other reports indicate that full NET release may require 180–240 minutes, depending on the stimulus (Inozemtsev et al., 2023). Importantly, only well supernatants were analysed. NETs are surface-associated extracellular DNA–protein structures and may have remained attached to the coverslip or epithelial cell layer rather than being efficiently recovered in the supernatant. Therefore, supernatant analysis may have underestimated NET formation in this assay.

Overall, neutrophil quantification and evaluation of migration in this system remained challenging, and further work is required to enable reliable neutrophil tracking in this model. Nevertheless, the combined evidence from CCK-8-derived cell estimates, macroscopic and microscopic observations after the migration assay, and macroscopic assessment after crystal violet staining suggested that neutrophils could move through the transwell membrane in the presence or absence of an epithelial cell layer and be detected in the well.

6.5.3 Model limitations and future optimisation

A major limitation of this chapter is that each assay configuration was performed as a single independent experiment. Therefore, the findings are descriptive and should not be interpreted as statistically robust evidence of differences between conditions. Instead, the data support the practical feasibility of the model components and identify methodological issues requiring optimisation in future experiments.

Quantification of neutrophils that migrated into the wells would have provided additional insight but was not technically feasible due to biofilm metabolic interference with the CCK-8 assay. Alternative approaches for future experiments could include pre-labelling neutrophils with carboxyfluorescein

diacetate succinimidyl ester (CFDA-SE) or calcein-acetoxymethyl ester (Calcein-AM) before adding them to the transwell inserts, followed by fluorescence-based imaging or quantification after migration (Cotter et al., 2001, Frevert et al., 1998, Lammers et al., 2015). Another option would be quantification of human DNA present in the wells as a proxy for cell number; this could involve targeting single-copy nuclear genes such as ribonuclease P protein subunit p30 (*RPP30*) or mitochondrial DNA (mtDNA) genes such as NADH dehydrogenase subunit 1 (*MT-ND1*) or cytochrome b (*MT-CYB*) (Castellani et al., 2020, Dyavar et al., 2018). However, these DNA-based approaches would not distinguish intact cells from extracellular DNA released during cell death or NET formation. In dual-cell setups, detached epithelial cells could also contribute to the signal.

To address the non-specific adhesion observed under the coverslip-only conditions, future optimisation could explore surface passivation of coverslips through albumin-based blocking with human or bovine serum albumin, similar to strategies used in ELISA plate blocking (Neubert et al., 2019), or by applying non-protein anti-adhesive coatings used in biomedical devices, such as Pluronic F-127 (Jackson et al., 2000, Treter et al., 2014), with the aim of reducing non-specific neutrophil adhesion or activation at the coverslip surface.

A further technical challenge of this model system was the inability to perform histological analysis of membranes with epithelial cell layers due to poor cell retention in the specimens. As discussed in Chapter 5, this may be attributable to the need for a reduced PFA fixation time due to the exceptional thinness of the specimens. If this issue were resolved, a range of staining approaches could be used to visualise neutrophils interacting with the transwell insert membrane and the TR146 epithelial cell layer.

Despite these limitations, the sequential approach used in the development of the *in vitro* model provided several advantages. It allowed assessment of whether the model behaved in line with the intended design and helped attribute observed outcomes to specific components or technical limitations. This pilot proof-of-concept work supported the feasibility of the model and provided the groundwork for future studies with sufficient replication for statistical analysis.

6.6 Summary and findings

1. In the proposed *in vitro* model system, can biofilms induce a response in the epithelial cell layer that will result in:

    a. IL-8 response from neutrophils and epithelial cells?

    b. neutrophil migration through the epithelial layer towards the bacterial biofilm?

In the *in vitro* model system developed in this chapter, the data are consistent with the hypothesis that there are certain components and properties of the oral barrier at the gingival sulcus that can be combined to model it *in vitro*, although neutrophil quantification and evaluation of migration in this system were challenging. The CCK-8 assay was identified as a potential means of neutrophil quantification. Further work is needed for reliable neutrophil tracking in this model.

IL-8 was detected in the dual-cell setup containing neutrophils and TR146 epithelial cells. However, in the current model setup there was no obvious modulation of this response with biofilm stimulation. Further work is required to optimise the model conditions for detecting changes in cytokine production by components of the model under different experimental conditions.

6.7 Publications

Work from this chapter has been presented at the following conferences/symposia:

- Haleon Symposium, January 2025, Weybridge
- University of Glasgow School of Medicine, Dentistry and Nursing IEE Day Away, April 2025, Glasgow
- Oral Microbiology and Immunology Group ECR Meeting, May 2025, Glasgow.

7 General Discussion

The work described in this thesis shows the stepwise development of an *in vitro* model of the oral mucosal barrier by incorporating key characteristics that contribute to the maintenance of periodontal health. To the best of the author's knowledge, this is a novel model.

7.1 Summary of findings across chapters

7.1.1 Identification of taxa present in subgingival plaque that are associated with periodontal health

The narrative review comprising Chapter 3 provided a synthesis of microbiome data reported in 42 original studies conducted across 20 countries between 2012 and 2021. Analysis of the reported taxa showed higher variability in the health-associated microbiome compared to the periodontitis-associated microbiome across studies, possibly due to the relatively recent development of open-ended, high-throughput detection techniques and the historical focus on pathogens and their role in disease, rather than the more contemporary emphasis on health-associated taxa in the maintenance of health (Feres et al., 2021, Ma et al., 2024). The most frequently reported taxa associated with health included Actinobacteria, Proteobacteria and Firmicutes at the phylum level, *Corynebacterium*, *Actinomyces*, *Capnocytophaga*, *Streptococcus* at the genus level and *Corynebacterium matruchotii*, *Cardiobacterium hominis*, *Granulicatella adiacens*, *Haemophilus parainfluenzae*, *Rothia dentocariosa* and *Streptococcus sanguinis* at the species level. It is increasingly recognised that different communities of bacteria may share similar functions. Therefore, further valuable information could be obtained by complementing taxonomic characterisation with assessment of microbial metabolic activity (Duran-Pinedo et al., 2014, Jorth et al., 2014).

7.1.2 Development of periodontal health-associated *in vitro* biofilms

The work described in Chapter 4 focused on the development of a 5-species *in vitro* biofilm to emulate periodontal health. The model design was based on a previously developed 3-species Glasgow biofilm model (Brown et al., 2023), but

it was expanded by incorporating two additional species: *R. dentocariosa* and *N. mucosa*. Based on data from Chapter 3, *R. dentocariosa* was among the most frequently reported species associated with health. Moreover, one study concluded that the genus *Rothia* was most positively correlated with health, with *R. dentocariosa* numerically dominating the health-associated communities (Abusleme et al., 2013). *R. dentocariosa* has also been reported to reduce nitrate (Rosier et al., 2020), and nitrate reduction has been suggested to support oral homeostasis (Rosier et al., 2022). *Neisseria* species were consistently represented in studies of health-associated biofilms; however, as different members of this genus appeared in different studies, no single *Neisseria* species featured heavily. *N. mucosa* was therefore selected as a representative *Neisseria* species because it reduces nitrate (Barth et al., 2009) and inhibits *P. gingivalis* invasion of gingival epithelial cells (Fukuda et al., 2024). These species were added either before or after the incorporation of *Streptococcus* spp. during biofilm preparation, to determine whether they could be successfully incorporated into the developing model. Compositional analysis of the 5-species biofilms showed that all species were successfully incorporated into both variations of the 5-species model, with noticeable and consistent dominance of *Streptococcus* spp. SEM-based comparison of the 5-species and previously developed 10-species biofilm models (Brown et al., 2023) suggested differences in microarchitecture and structure that partly resembled those reported between health-associated and disease-associated *ex vivo* biofilms, including surface homogeneity, structural complexity and biomass.

7.1.3 Investigating host cell lines for use in an *in vitro* model

The TR146 cell line is widely used in oral barrier property studies (Bierbaumer et al., 2018) and was used to seed transwell insert membranes to form an epithelial multilayer. Different methods were explored to confirm its formation, among which the CCK-8 assay was identified as the most reliable method to assess intra-batch variability based on OD values. Absolute quantification of cells was not possible due to technical constraints in the preparation of a reliable reference curve. This is a known challenge associated with assessing 3D *in vitro* structures (Temple et al., 2022).

The immortality, relative ease of culture and theoretical reproducibility of established cell lines make them an appealing alternative to primary cells, which are harder to source, have limited proliferative capacity and lower survival rates. Nonetheless, in the author's experience, even established cell lines can be challenging and show variability between stored batches in terms of proliferative capacity and cell responsiveness.

Given the challenges associated with the use of primary neutrophils – namely, the requirement for same-day venepuncture from a volunteer and the subsequent variability among volunteers – immortalised promyelocytic cell lines are often employed in *in vitro* studies as their substitutes. Two different methods of HL-60 differentiation and maturation were tested here: DMSO and ATRA stimulation (Blanter et al., 2021). Both differentiated cell types were assessed alongside primary neutrophils using flow cytometry. ATRA-differentiated cells displayed cell surface markers ($CD11b^+$, $CD15^+$) similar to the primary neutrophils and were assessed further. However, when stimulated with known neutrophil agonists, fMLF and LTB_4, their response appeared to be attenuated. Therefore, primary neutrophils were used in the *in vitro* model following successful optimisation of their quantification using the CCK-8 assay.

7.1.4 Stepwise development of a 3D *in vitro* co-culture model

The three components evaluated in previous chapters were finally combined in Chapter 6 to develop a pilot proof-of-concept 3D *in vitro* co-culture model of neutrophil migration across the junctional epithelium. The final modification of the model involved incorporation of multispecies bacterial biofilms. Enumeration of neutrophils in this system was challenging. Following co-culture of the PMN/Epi setup with 5- and 10-species biofilms, the CCK-8 assay was used to determine the number of neutrophils remaining in the transwell insert. This approach was employed because neutrophils in the well could not be quantified, as the biofilms interfered with the CCK-8 assay. The data were inconclusive and suggested variable migration of neutrophils. Nevertheless, the model forms the basis for future studies.

7.2 Distinctive features of the developed model

The developed co-culture model differs from previously published systems through the integration of distinctive features within a single experimental platform: a health-associated biofilm, an epithelial–biofilm spatial configuration that enables gingival sulcus-like compartmentalisation, and the potential to model directed transepithelial neutrophil migration towards the biofilm.

7.2.1 Distinct health-associated taxa

Most published oral biofilm models have focused on disease-associated species, with periodontal health often treated as a baseline rather than a distinct microbial state. The present model addresses this gap by expanding the previous 3-species Glasgow biofilm model through the incorporation of *N. mucosa* and *R. dentocariosa*, selected to represent health-associated taxa. These species were not included in the periodontitis-associated 10-species model, making their incorporation a distinctive feature of the 5-species health-associated model.

7.2.2 Physiologically relevant compartmentalisation

Unlike the previously described models of the oral barrier, this model incorporated a physiologically oriented epithelial–biofilm interface with the potential for directed immune-cell migration. The epithelial multilayer was formed by seeding TR146 cells on the basolateral side of a porous transwell insert membrane with a pore size suitable for cell migration. As a result, the superficial epithelial layers faced the biofilm, while the deepest epithelial layers remained adjacent to the membrane and the upper chamber compartment. This design created a compartmentalised system in which epithelial–biofilm interactions could be maintained, while preserving the possibility of modelling a directed immune-cell response through the addition of immune cells to the transwell insert.

7.2.3 Transepithelial neutrophil migration

Although immune cells have been incorporated into some oral barrier models, relatively few systems have specifically sought to model neutrophil transepithelial migration, a key feature of gingival sulcus immune surveillance.

One notable exception is the transwell model described by Madianos et al. (1997), which was used to examine human neutrophil migration across a *P. gingivalis*-infected KB cell epithelial layer. However, the relevance of this model to the oral barrier is limited by the subsequent recognition that the KB cell line was misidentified and is now considered to be HeLa-derived, rather than a true oral epithelial cell line (Vaughan et al., 2017).

7.3 Technical optimisation, model validation and limitations

The model was developed using an iterative, proof-of-concept approach, in which individual components were used to establish feasibility and troubleshoot their integration prior to formal validation. These preliminary runs were therefore intended to identify observable trends, technical constraints and areas requiring optimisation to guide model development, rather than to support statistical inference or definitive comparisons between conditions. Accordingly, apparent differences observed between conditions should be interpreted as preliminary trends requiring confirmation in independent repeat experiments, which are necessary to establish reproducibility and enable quantitative validation of the model.

7.3.1 Future technical optimisation

Several practical considerations were identified across the biofilm component, neutrophil-handling steps and downstream readouts. At the biofilm level, the apparent dominance of *Streptococcus* spp. in the 5-species biofilm requires confirmation using a viability-based method, such as live/dead qPCR, to determine whether this signal reflects viable streptococci or residual DNA from non-viable cells. If viable *Streptococcus* spp. dominance is confirmed, future work could include adjustment of starting inoculum concentrations or further expansion of species diversity in this model, for example by incorporating species identified following the completion of the systematic review described in Chapter 3.

The experimental setup also presented challenges, as neutrophils appeared to adhere strongly to the coverslip surface. This could be addressed by exploring

surface passivation strategies, including ELISA plate-blocking approaches or anti-adhesive coatings developed for biomedical devices, provided that the surface treatment itself does not activate neutrophils.

Further technical constraints were also identified in relation to model readouts. The presence of the biofilms in the wells interfered with the CCK-8 assay. As already discussed in Chapter 6, this could be resolved by applying additional methods such as pre-labelling neutrophils with fluorescent dyes before they are added to the transwell inserts and measuring fluorescence intensity, or quantifying their DNA in the wells using qPCR. A further limitation of the model was the low volumes of supernatant that could be obtained after completion of the experiment. This could be addressed with the use of high-plex platforms such as Luminex or a proximity extension assay or, alternatively, using a 6-well plate alongside appropriately sized transwells. Another technical limitation was the difficulty of consistently capturing the epithelial layer on transwell inserts for staining, possibly due to detachment during processing, indicating that fixation protocols require further optimisation.

7.3.2 Logistical constraints

The setup of the final biofilm-containing iteration of the model was highly time-sensitive. This was particularly relevant for primary neutrophils, which have a short *ex vivo* lifespan and require careful handling before use. Potential solutions would include growing biofilms directly in compatible plate formats or adapting the model to an automated high-throughput screening system, provided that readouts were standardised and automation-compatible. For example, Corning offers robotics-friendly 24-well plates with transwell inserts, and suggested applications include high-throughput screening of drug transport, cell toxicity, and cell migration. In all cases, independent repeat experiments would be required to assess reproducibility and support statistical analysis.

7.3.3 Model limitations and validation

Any *in vitro* model is inherently a reductionist system and therefore has biological limitations. The model necessarily simplifies the complexity of the gingival sulcus and cannot fully reproduce the periodontal immune response

in vivo. The 5-species biofilm does not capture the full microbial diversity, spatial organisation, metabolic activity or interspecies interactions of the *in vivo* subgingival plaque. The epithelial content is also simplified, as TR146 cells do not represent junctional epithelium. Similarly, the immune component was limited to neutrophils, whereas the *in vivo* host response also involves immune and stromal cell populations in the surrounding gingival tissues, whose soluble mediators may contribute to the gingival sulcus environment (Hajishengallis and Korostoff, 2017). Finally, cell culture medium does not reproduce gingival crevicular fluid, including its nutrient and oxygen gradients, flow, pH and host proteins. These limitations reflect the controlled and reductionist nature of the model, rather than technical failure, and should be considered when interpreting the biological relevance of the findings. The findings could be contextualised by comparing results from the model with *in vivo* and *ex vivo* human data, allowing the model to be interpreted accordingly and potential modifications to be considered.

7.4 Further research and potential applications of the model

Overall, an *in vitro* model such as the one proposed could help characterise features of gingival health and identify targetable pathways to maintain gingival health under challenge, such as exposure to a dysbiotic biofilm, environmental irritants including those identified in electronic cigarettes, or inflammatory mediators generated in response to aberrant local or systemic immune responses. This could offer a different therapeutic strategy based on promoting resilience in healthy tissues rather than on the traditional disease-blocking approach, which targets disease-associated pathways.

The developed 3D *in vitro* co-culture model offers high versatility, as its components can be easily modified and substituted. Each component of the model – i) the coverslip, ii) the biofilm, iii) the epithelial cell-coated transwell membrane, iv) the cells in suspension within the transwell insert and v) the culture medium bathing the model – offers an opportunity to ask research questions. For example, at the level of the coverslip, a variety of host or bacterial mediators could be used to coat the surface to study neutrophil response to a specific surface-bound cue. This could provide a way to explore

candidate compounds intended for local delivery within the gingival sulcus. Gelatine chips, including PerioChip, are currently used to introduce chlorhexidine at this site as an adjunct to periodontal treatment (Ma and Diao, 2020). Hypothetically, other compounds could be delivered in a similar way to modulate inflammation. Alternatively, other coverslip-grown biofilm models could be employed, including *ex vivo* subgingival biofilms obtained from healthy and periodontitis patients. Biofilm modulation could be further studied by adding antibodies that neutralise bacterial enzymes such as gingipains, or by adding bacterial supernatants from probiotic strains, e.g. *L. reuteri* producing the antibacterial compound reuterin (Iniesta et al., 2012, Jansen et al., 2021). Similarly, biofilms could be grown with gene-deficient bacteria, such as the RgpA/RgpB knockout *P. gingivalis* (Popadiak et al., 2007).

The transwell insert membrane could be modified by using either other epithelial cell lines, or TR146 cell line knockouts generated, for example, with genome editing tools such as clustered regularly interspaced short palindromic repeats–CRISPR-associated protein 9. It would be interesting to target the serum amyloid A–TLR axis, which has been reported to be involved in the first-line defence against periodontal microbiota in junctional epithelium (Qian et al., 2021). Using healthy patient-derived primary cells is challenging as these can only routinely, reasonably and ethically be obtained from patients undergoing elective minor surgical procedures involving gingival tissue, for example: implant post exposure, surgical crown lengthening, or orthodontic extractions. Healthy gingival tissue can be obtained by gingival biopsy of healthy volunteers but this is invasive and can result in gingival recession, so is at best a limited source of tissue. Patients with periodontitis are more likely to be undergoing procedures from which epithelial tissues can, in theory, be obtained. However, growing epithelial cells from such tissues is extremely challenging as the fibroblasts are extremely difficult to eliminate and tend to outcompete the epithelial cells.

Peripheral blood neutrophils could be used with the *ex vivo* biofilms from the same individuals, which could model personalised immune responses, aligning with the concept of precision medicine. Combining a full model of neutrophils, biofilm and epithelial cells from the same donor would require the patient to return for a blood draw after the tissue collection procedure, as the neutrophils

would need to be obtained several days later once the epithelium was already established.

The *in vitro* model could be further expanded by incorporating more cell types such as human umbilical vein endothelial cells (HUVECs) grown in an additional insert or on top of fully modelled tissue together with human gingival fibroblasts and collagen to study neutrophil extravasation, in addition to transepithelial migration, or by including macrophages as a source of anti-inflammatory cytokines to investigate resolution of inflammation (Huang et al., 2016).

The model could be used to demonstrate proof-of-concept for drug and non-drug active agents suitable for incorporation into local delivery systems for the periodontal pocket. Such agents could be incorporated into a solid formulation – such as the gelatine chips mentioned above – or delivered in liquid or semi-solid form as an irrigant, gel or even an oral rinse. Although an oral rinse is unlikely to affect deep periodontal pockets, it may still have an effect at the gingival margin. For example, an early clinical study suggested that BLXA4-ME, a host-modulatory lipoxin analogue delivered as an oral rinse, could reduce gingival inflammation (Hasturk et al., 2021b). Such agents could be designed to maintain a homeostatic periodontal host response and promote its resilience under challenge, or restore it under gingivitis- or periodontitis-associated conditions. As a human-cell-based *in vitro* system, the model could also be used alongside *in vivo* approaches, providing an initial platform to prioritise candidates for subsequent animal-based testing and thereby support the 3Rs principles of reduction and refinement.

The platform could be adapted for the development of patient-specific functional assays. Patient-derived neutrophils could be combined with the *ex vivo* biofilms and, potentially, gingival tissue collected during clinically indicated procedures from the same individuals. This could allow personalised immune responses to be modelled, aligning with the concept of precision medicine. In the longer term, such assays could help assess individual responses to selected active agents, including host-modulating compounds or microbiome-modulating interventions. Such applications would depend on sample availability, ethical approval and practical constraints related to sample collection and processing.

With further adaptation, the model could potentially be used for large-scale compound screening, especially if implemented within an automated high-throughput screening system rather than the current single-insert and coverslip format, which is labour-intensive. However, this would require further standardisation of the model and development of automation-compatible readouts.

7.5 Concluding remarks

This thesis aimed to develop an *in vitro* model of the oral mucosal barrier by incorporating key characteristics that contribute to the maintenance of periodontal health, with the goal of generating an easy-to-use and versatile *in vitro* model that mimics *in vivo* conditions.

The key findings were:

- The subgingival microbiome associated with periodontal health differs when compared to periodontitis at phylum, genus and species levels.
- Some of the key differences between health- and periodontitis-associated subgingival biofilms, such as composition or microarchitecture and structure, could be emulated *in vitro*. Further studies are needed to evaluate how these different biofilms influence oral barrier integrity in an *in vitro* model.
- TR146 cells grown on a porous transwell insert membrane could be used to recreate an epithelial layer, modelling junctional epithelium *in vitro*.
- HL-60 cells could be differentiated with ATRA into neutrophil-like cells that expressed surface markers characteristic of primary neutrophils, consistent with previous reports, but these cells did not mimic primary neutrophil responsiveness to stimuli under the conditions tested.
- Neutrophil quantification and the evaluation of migration in this system were challenging. The CCK-8 assay was identified as a potential means of neutrophil quantification. Further work is needed to enable reliable neutrophil tracking in this model.

8 Appendices

Appendix I

Table S1 Equivalent bacterial strain identifiers across major microbial culture collections.

Microorganism	Type strain	Strain designation	Culture collection identifiers
S. intermedius	Yes	VPI 3372A, 1877, SK 54	ATCC 27335, BCCM/LMG 17840, CCUG 17827, CCUG 32759, CECT 803, CIP 103248, DSM 20573, HAMBI 1571, JCM 12996, LMG 14510, LMG 17840, NCDO 2227, NCFB 2227, NCTC 11324, VPI 3372-A, VPI 3372A
S. mitis	Yes	NS 51, SK 142	ATCC 49456, BCCM/LMG 14557, CCM 7411, CCUG 27308, CCUG 31611, CCUG 35790, CIP 103335, DSM 12643, JCM 12971, KCTC 13047, KCTC 3556, LMG 14557, NBRC 106071, NCIMB 13770, NCTC 12261
S. oralis	Yes	LVG/1, PB 182, SK 23	ATCC 35037, BCCM/LMG 14532, Carlsson LVG 1, CCUG 13229, CCUG 24891, CCUG 25610, CECT 907, CIP 102922, DSM 20627, JCM 12997, KCTC 13048, KCTC 3285, LMG 14532, NBRC 113011, NCDO 2680, NCTC 11427
N. mucosa	Yes	N 16 1959	ATCC 19696, CCUG 26877, CIP 59.51, DSM 17611, JCM 12992, NCTC 12978
R. dentocariosa	Yes	XDIA, X599	ATCC 17931, CCM 7007, CCUG 35437, CDC X599, CIP 81.83, DSM 43762, DSM 46363, IAM 14816, IFM 1284, IFO 12531, IMET 11515, IMSNU 21309, JCM 3067, KCC A-0067, KCTC 3204, NBRC 12531, NCTC 10917, NRRL B-8017, PCM 2349, XD1A
A. naeslundii	No	Bowden X600S-96, CS 1752, X-600	ATCC 19039, CCUG 35337, CDC X-600, CIP 100654, CIP 104837, CIP 82.9, DSM 17233, DSM 43325, JCM 8350, WVU 447
F. nucleatum (subsp. *polymorphum*)	Yes	555A	ATCC 10953, CCUG 9126, DSM 20482, JCM 12990, NCTC 10562
F. nucleatum (subsp. *vincentii*)	Yes	EM48	ATCC 49256, CCUG 37843, CIP 104988, DSM 19507, JCM 11023
V. dispar	Yes	ERN	AIP 10221, ATCC 17748, CCUG 54948, CIP 108002, DSM 20735, NCTC 11831

Microorganism	Type strain	Strain designation	Culture collection identifiers
P. gingivalis	No	W83	ATCC BAA-308, W83
A. actinomycetemcomitans	No	Y4	ATCC 43718, DSM 11123, JCM 8578
P. intermedia	Yes	B422, Finegold B422	ATCC 25611, DATCC 25611, BCRC 14416, CCUG 24041, CIP 101222, CIP 103682, DSM 20706, JCM 11150, JCM 12248, JCM 7365, KCTC 15693, KCTC 3692, NCTC 13070, VPI 4197

Culture collection identifiers were retrieved from ATCC (American Type Culture Collection), BacDive (Schober et al., 2025) and NCTC (National Collection of Type Cultures) databases. Bacterial strains used by the author are indicated in bold.

Appendix II

TEER measurements

Corning and Millicell transwells with PET membrane (see Table 2.7) were seeded with TR146 cells at a total density of 5×10^4 cells/transwell as described in Section 2.2.1.2 and incubated for 24 hours. Additionally, the following transwells were included: transwells with cells seeded onto the apical side of the membrane, and seeded or unseeded transwells pre-coated with poly-L-lysine [Sigma-Aldrich, Merck, Darmstadt, Germany]. Following incubation and two consecutive washes in dPBS(+), they were placed into a new 24-well plate. Wells were filled with 600 µL of dPBS(+) and an additional volume of 400 µL of dPBS(+) was added into each transwell chamber. Then, electrical resistance across the epithelial layer was measured promptly using an EVOM Manual Meter System consisting of an EVM-MT-03-01 TEER Measurement Meter and an STX4 electrode [World Precision Instruments, Hitchin, Hertfordshire, UK]. Measurements were performed three times for each transwell, for two consecutive days. Each reading was acquired immediately upon probe placement and signal stabilisation. Unseeded transwells served as a negative control. Additionally, on day 4, a single set of measurements was performed before and after visibly puncturing each membrane with a pipette tip.

Appendix III

Table S2 Taxa associated with health and periodontitis: example entries from data extraction step.

Reference	Taxa associated with periodontal health	Taxa associated with periodontitis
(Abusleme et al., 2013)	Phyla Relative abundance: Actinobacteria Genera Abundance: *Actinomyces, Burkholderia, Corynebacterium, Rothia* Species Relative abundance: *Actinomyces gerencseriae OT 618, Actinomyces sp. (Actinomyces sp. OT 170), Actinomyces sp. (Actinomyces naeslundii OT 176), Actinomyces sp. (Actinomyces odontolyticus OT 701), Actinomyces sp. (Actinomyces sp. OT 169), Actinomyces sp. (Actinomyces sp. OT 175), Actinomyces sp. OT 177 Porphyromonas sp. (Porphyromonas catoniae OT 283), Burkholderia cepacia OT 571, Rothia sp. (Rothia dentocariosa OT 587), Streptococcus sp. (Streptococcus sanguinis OT 758), Veillonellaceae [G-1] sp. (Veillonellaceae [G-1] sp. OT 155), unclassified Xanthomonadaceae, unclassified Xanthomonadaceae* Highly prevalent and highly abundant: *Actinomyces sp. OT 170, Rothia dentocariosa OT 587** Highly prevalent but present in low abundance: *Actinomyces gerencseriae OT 618, Actinomyces naeslundii OT 176* Moderately prevalent and present in low abundance: *Actinomyces odontolyticus OT 701, Actinomyces sp. OT 177, Burkholderia cepacia OT 571, Porphyromonas catoniae OT 283, Streptococcus sanguinis OT 758, unclassified Xanthomonadaceae*	Phyla Relative abundance: Chloroflexi, Firmicutes, Spirochetes, Synergistetes, Prevalence: Chloroflexi, Spirochetes, Synergistetes Genera Abundance: *Bacteroidetes [G-1], Bacteroidetes [G-3], Bacteroidetes [G-6], Chloroflexi [G-1], Desulfobulbus, Eubacterium [11] [G-1], Eubacterium [11] [G-6], Eubacterium [11] [G-6], Filifactor, Lachnospiraceae [G-4], Lachnospiraceae [G-8], Mogibacterium, Mycoplasma, Parvimonas, Peptostreptococcaceae [11] [G-2], Peptostreptococcaceae [11] [G-4], Peptostreptococcaceae [13] [G-1], Peptostreptococcus, Porphyromonas, Pseudoramibacter, Synergistestes [G-3], TM7 [G-5], Tannerella, Treponema, Veillonellaceae [G-1]* Species Relative abundance: *Bacteroidetes [G-1] sp. OT 272, Bacteroidetes [G-3] sp. OT 280, Bacteroidetes [G-6] sp. OT 516, Chloroflexi[G-1] sp. OT 439, Desulfobulbus sp. OT 041, Eubacterium [11][G-6] minutum OT 673, Eubacterium [11][G-6] nodatum OT 694, Eubacterium [XI][G-3] brachy OT 557, Eubacterium [XI][G-5] saphenum OT 759, Filifactor alocis OT 539, Filifactor alocis OT 539, Johnsonella sp. OT 166, Lachnospiraceae [G-4] sp. OT 373, Lachnospiraceae [G-8] sp. OT 500, Mogibacterium timidum OT 042, Mycoplasma faucium OT 606, Parvimonas sp. (Parvimonas micra OT 111), Peptostreptococcaceae [X1] [G-2] sp. OT 091, Peptostreptococcaceae [XIII][G-1] sp. OT 113, Peptostreptococcaceae [XI][G-4] sp. (Peptostreptococcaceae [XI][G-4] sp. OT 369), Peptostreptococcus stomatis OT 112, Porphyromonas endodontalis OT 273, Porphyromonas gingivalis OT 619, Pseudoramibacter alactolyticus OT 538, Selenomonas sputigena OT 151, Streptococcus constellatus OT 576, Streptococcus sp. (Streptococcus sp. OT 071), Synergistetes [G-3] sp. (Synergistetes [G-3] sp. OT 360),*

		Synergistetes [G-3] sp. (Synergistetes [G-3] sp. OT 362), Synergistetes [G-3] sp. OT 363, Synergistetes [G-3] sp. OT 361, TM7 [G-1] sp. OT 346, TM7 [G-5] sp. OT 356, TM7 [G-1] sp. OT 349, Tannerella forsythia OT 613, Treponema denticola OT 584, Treponema lecithinolyticum OT 653, Treponema maltophilum OT 664, Treponema socranskii OT 769, Treponema socranskii OT 769, Treponema sp. (Treponema medium OT 667), Treponema sp. (Treponema sp. OT 257), Treponema sp. OT 237, Veillonellaceae [G-1] sp. (Veillonellaceae [G-1] sp. OT 145), unclassified Clostridiales, unclassified Enterobacteriaceae (Enterobacter cancerogenus OT 565) Highly prevalent and highly abundant: *TM7 [G-1] sp. OT 346, Treponema denticola OT 584, Treponema medium OT 667, Treponema sp. OT 237* Highly prevalent but present in low abundance: *Bacteroidetes [G-1] sp. OT 272, Chloroflexi [G-1] sp. OT 439, Desulfobulbus sp. OT 041, Eubacterium [XI][G-3] brachy OT 557, Eubacterium [XI][G-5] saphenum OT 759, Eubacterium [XI][G-6] nodatum OT 694, Filifactor alocis OT 539,, Lachnospiraceae [G-8] sp. OT 500, Mogibacterium timidum OT 042, Parvimonas micra OT 111, Peptostreptococcaceae [XI][G-2] sp. OT 091, Peptostreptococcaceae [XI][G-4] sp. OT 369, Peptostreptococcaceae [XIII][G-1] sp. OT 113, Porphyromonas endodontalis OT 273, Porphyromonas gingivalis OT 619, Selenomonas sputigena OT 151, Streptococcus sp. OT 071, Synergistetes [G-3] sp. (OT 360), Synergistetes [G-3] sp. OT 362, Synergistetes [G-3] sp. OT 363, TM7 [G-1] sp. OT 349, TM7 [G-5] sp. OT 356, Tannerella forsythia OT 613, Treponema lecithinolyticum OT 653, Treponema maltophilum OT 664, Treponema socranskii OT 769, unclassified Clostridiales, Veillonellaceae [G-1] sp. OT 145* Moderately prevalent and present in low abundance: *Bacteroidetes [G-3] sp. OT 280, Bacteroidetes [G-6] sp. OT 516, Eubacterium [XI][G-6] minutum OT 673, Lachnospiraceae [G-4] sp. OT 373, Mycoplasma faucium OT 606, Peptostreptococcus stomatis OT 112, Pseudoramibacter alactolyticus OT 538, Streptococcus constellatus OT 576, Synergistetes [G-3] sp. OT 361, Treponema sp. OT 257*

(Dabdoub et al., 2016)	Phyla No data Genera No data Species Relative abundance: *Acinetobacter baumannii, Actinobaculum HOT.183, Actinomyces dentalis, Actinomyces georgiae, Actinomyces gerencseriae, Actinomyces graevenitzii, Actinomyces HOT.169, Actinomyces HOT.170, Actinomyces HOT.171, Actinomyces HOT.177, Actinomyces HOT.448, Actinomyces HOT.525, Actinomyces HOT.848, Actinomyces HOT.877, Actinomyces HOT.896, Actinomyces johnsonii, Actinomyces massiliensis, Actinomyces meyeri, Actinomyces naeslundii, Actinomyces oricola, Actinomyces oris, Actinomyces radicidentis, Aggregatibacter HOT.512, Aggregatibacter HOT.898, Alloprevotella HOT.473, Alloprevotella HOT.912, Alloprevotella HOT.913, Alloprevotella HOT.914, Alloprevotella rava, Alloscardovia omnicolens, Arcanobacterium haemolyticum, Atopobium HOT.416, Atopobium sp, Bacillus subtilis, Bacteroidales [G-3] HOT.911, Bacteroides tectus, Bacteroides ureolyticus, Bacteroidetes [G-3] HOT.365, Bacteroidetes [G-5] HOT.507, Bdellovibrio HOT.039, Bifidobacterium animalis, Bifidobacterium scardovii, Bordetella pertussis, Brevundimonas diminuta, Burkholderia cepacian, Capnocytophaga haemolytica, Capnocytophaga HOT.863, Capnocytophaga HOT.901, Cardiobacterium hominis, Caulobacter HOT.002, Corynebacterium diphtheriae, Corynebacterium durum, Corynebacterium HOT.184, Corynebacterium matruchotii, Corynebacterium mucifaciens, Corynebacterium urealyticum, Defluvibacter lusatiensis, Dialister micraerophilus, Dietzia HOT.368, Erysipelothrix tonsillarum, Fusobacterium gonidiaformans, Fusobacterium necrophorum, Haemophilus HOT.908, Helicobacter pylori, Jonquetella anthropic, Kingella kingae, Kingella oralis, Kluyvera ascorbate, Kocuria HOT.189, Kytococcus sedentarius, Lachnospiraceae [G-5] HOT.455, Lactobacillus [XVII] catenaformis, Lactobacillus buchneri, Lactobacillus jensenii, Lactobacillus panis,*	Phyla No data Genera No data Species Relative abundance: *Bulleidia extructa, Desulfobulbus HOT.041, Eubacterium [XI][G-3] brachy, Eubacterium [XI][G-5] saphenum, Eubacterium [XI][G-6] nodatum, Filifactor alocis, Fretibacterium HOT.358, Fretibacterium HOT.361, Fretibacterium HOT.362, Fretibacterium HOT.452, Fusobacterium HOT.205, Fusobacterium naviforme, Fusobacterium nucleatum, Johnsonella HOT.166, Lachnospiraceae [G-8] HOT.500, Leptotrichiaceae [G-1] HOT.220, Parvimonas micra, Peptostreptococcaceae [XI][G-2] HOT.091, Peptostreptococcaceae [XI][G-4] HOT.369, Peptostreptococcaceae [XIII][G-1] HOT.113, Porphyromonas gingivalis, Selenomonas HOT.134, Selenomonas sputigena, Streptococcus oralis, Tannerella forsythia, Treponema HOT.255, Treponema HOT.264, Treponema HOT.268, Veillonella parvula*

	Lactobacillus reuteri, Lactobacillus rhamnosus, Lactobacillus vaginalis, Lactococcus lactis, Lautropia mirabilis, Leptothrix HOT.024, Leptotrichia goodfellowii, Listeria monocytogenes, Lysinibacillus fusiformis, Megasphaera HOT.841, Mitsuokella HOT.131, Mitsuokella multacida, Mobiluncus mulieris, Mollicutes [G-2] HOT.906, Moryella HOT.419, Mycobacterium leprae, Mycobacterium neoaurum, Mycobacterium tuberculosis, Mycoplasma pneumoniae, Neisseria elongata, Neisseria weaver, Oribacterium HOT.372, Ottowia HOT.894, Paenibacillus HOT.048, Paenibacillus sp, Peptococcus HOT.168, Peptoniphilus HOT.836, Peptostreptococcus anaerobius, Porphyromonas catoniae, Porphyromonas HOT.284, Porphyromonas uenonis, Prevotella bivia, Prevotella buccalis, Prevotella enoeca, Prevotella HOT.292, Prevotella HOT.299, Prevotella HOT.305, Prevotella HOT.309, Prevotella HOT.396, Prevotella HOT.475, Prevotella HOT.515, Prevotella multisaccharivorax, Prevotella nigrescens, Prevotella oulorum, Prevotella pallens, Prevotella saccharolytica, Prevotella shahii, Propionibacterium avidum, Propionibacterium HOT.915, Propionibacterium propionicum, Proteus mirabilis, Pseudomonas stutzeri, Ralstonia HOT.027, Ralstonia HOT.406, Ralstonia pickettii, Rhodocyclus HOT.028, Rothia aeria, Rothia dentocariosa, Rothia mucilaginosa, Sanguibacter keddieii, Scardovia inopinata, Scardovia wiggsiae, Selenomonas HOT.478, Selenomonas HOT.501, Shuttleworthia satelles, Simonsiella muelleri, Streptococcus agalactiae, Streptococcus HOT.066, Streptococcus HOT.068, Streptococcus HOT.070, Streptococcus mutans, Streptococcus pyogenes, Streptococcus salivarius, Streptococcus sanguinis, TM7 [G-1] HOT.347, TM7 [G-2] HOT.350, TM7 [G-4] HOT.355, Turicella otitidis, Veillonella HOT.917	
(Wu et al., 2017)	Phyla No data Genera <u>Average relative abundance:</u> *Actinobaculum, Actinomyces, Arcanobacterium, Blastomonas, Capnocytophaga, Cardiobacterium, Chryseobacterium, Corynebacterium, Elizabethkingia, Gemella,*	Phyla No data Genera <u>Average relative abundance:</u> *Acetobacterium, Aminobacterium, Candidatus Tammella, Catonella, Desulfobulbus, Dialister, Dysgonomonas, Filifactor, Fusobacterium, Kingella, Longilinea,*

	Granulicatella, Haemophilus, Lautropia, Neisseria, Parascardovia, Propionibacterium, Rothia, Streptococcus, Streptomyces, Veillonella Species Average relative abundance: *Actinobaculum suis, Actinomyces georgiae, Actinomyces meyeri, Actinomyces odontolyticus, Arcanobacterium bernardiae, Bacteroides graminisolvens, Blastomonas natatorial, Campylobacter gracilis, Capnocytophaga gingivalis, Capnocytophaga granulosa, Capnocytophaga ochracea, Corynebacterium durum, Corynebacterium matruchotii, Elizabethkingia meningoseptica, Gemella haemolysans, Gemella sanguinis, Granulicatella adiacens, Haemophilus parainfluenzae, Lautropia mirabilis, Leptotrichia buccalis, Leptotrichia hofstadii, Leptotrichia shahii, Neisseria flavescens, Neisseria lactamica, Neisseria mucosa, Porphyromonas catoniae, Prevotella saccharolytica, Propionibacterium humerusii, Rothia aeria, Streptococcus australis, Streptococcus bovis, Streptococcus cristatus, Streptococcus fryi, Streptococcus infantis, Streptococcus oligofermentans, Streptococcus oralis, Streptococcus parasanguinis, Streptococcus pseudopneumoniae, Streptococcus sanguinis, Streptococcus tigurinus, Streptococcus vestibularis, Streptococcus gordonii, Veillonella atypica, Veillonella dispar, Veillonella parvula*	*Luteococcus, Mogibacterium, Odoribacter, Pectinatus, Peptoniphilus, Porphyromonas, Pseudoramibacter, Sedimentibacter, Slackia, Tannerella, Thermovirga, Treponema* Species Average relative abundance: *Aminobacterium colombiense, Atopobium rimae, Bacteroides denticanum, Bacteroides heparinolyticus, Candidatus Tammella caduceiae, Catonella morbi, Dialister invisus, Dysgonomonas wimpennyi, Filifactor alocis, Fusobacterium nucleatum, Kingella oralis, Longilinea arvoryzae, Luteococcus peritonei, Mogibacterium timidum, Odoribacter denticanis, Pectinatus cerevisiiphilus, Peptoniphilus indolicus, Porphyromonas endodontalis, Porphyromonas gingivalis, Prevotella dentalis, Prevotella intermedia, Sedimentibacter hydroxybenzoicus, Tannerella forsythia, Thermovirga lienii, Treponema amylovorum, Treponema denticola, Treponema maltophilum, Treponema medium, Treponema paraluiscuniculi, Treponema porcinum, Treponema putidum, Treponema socranskii, Treponema succinifaciens, Treponema vincentii*

Appendix IV

Table S3 Phyla associated with periodontal health.

Phylum	Count	Row locations*
No data	32	1; 2; 3; 5; 6; 8; 10; 11; 12; 13; 15; 16; 17; 18; 19; 20; 22; 23; 24; 25; 27; 29; 30; 33; 34; 35; 37; 38; 39; 40; 41; 42
Actinobacteria	3	4; 7; 36
Proteobacteria	3	21; 28; 32
None	3	9; 26; 31
Firmicutes	2	9; 14
Cyanobacteria	1	9
Verrucomicrobia	1	9
Bacteroidetes	1	28

*Row location refers to the row in the data extraction document.

Table S4 Genera associated with periodontal health.

Genus	Count	Row locations*
No data	28	1; 2; 5; 6; 10; 11; 12; 13; 15; 16; 17; 18; 19; 20; 21; 22; 24; 25; 26; 29; 30; 31; 33; 34; 35; 37; 39; 42
Corynebacterium	9	3; 4; 7; 8; 14; 23; 28; 32; 36
Actinomyces	7	4; 8; 14; 28; 32; 36; 38
Capnocytophaga	7	4; 8; 14; 23; 28; 32; 40
Streptococcus	5	7; 8; 14; 23; 38
Haemophilus	4	8; 14; 23; 38
Leptotrichia	4	4; 23; 28; 40
Prevotella	4	4; 9; 28; 40
Veillonella	4	4; 8; 9; 23
Granulicatella	3	8; 9; 38
Lautropia	3	8; 14; 40
Neisseria	3	8; 28; 32
Rothia	3	3; 8; 36
Campylobacter	2	28; 40
Cardiobacterium	2	8; 40
Gemella	2	8; 23
Oribacterium	2	9; 40
Paludibacter	2	4; 14

Only genera reported in more than one study are shown.
*Row location refers to the row in the data extraction document.

Table S5 Species associated with periodontal health.

Species	Count	Row locations*
None	20	1; 2; 5; 6; 11; 12; 13; 14; 15; 16; 17; 19; 20; 22; 28; 29; 30; 32; 38; 40
No data	7	3; 4; 9; 21; 23; 33; 39
Corynebacterium matruchotii	6	7; 8; 10; 29; 34; 35
Cardiobacterium hominis	5	10; 24; 29; 35; 41
Granulicatella adiacens	5	8; 18; 26; 29; 31
Haemophilus parainfluenzae	5	7; 8; 18; 24; 31
Rothia dentocariosa	5	10; 27; 29; 31; 37
Streptococcus sanguinis	5	8; 10; 18; 37; 40
Actinomyces georgiae	4	8; 10; 29; 43
Actinomyces gerencseriae	4	10; 24; 37; 40
Corynebacterium durum	4	7; 8; 10; 18
Gemella haemolysans	4	8; 18; 26; 31
Rothia aeria	4	8; 10; 34; 43
Streptococcus mitis	4	18; 24; 26; 27
Actinomyces johnsonii	3	10; 29; 43
Campylobacter gracilis	3	8; 24; 41
Capnocytophaga sputigena	3	24; 29; 35
Granulicatella elegans	3	18; 31; 43
Kingella oralis	3	10; 24; 29
Lautropia mirabilis	3	8; 10; 24
Leptotrichia hofstadii	3	8; 24; 34
Neisseria flavescens	3	8; 18; 35
Porphyromonas catoniae	3	8; 10; 37
Porphyromonas sp.	3	29; 35; 37
Prevotella loescheii	3	24; 29; 35
Selenomonas noxia	3	24; 29; 35
Streptococcus australis	3	8; 18; 31
Streptococcus oralis	3	8; 18; 31
Streptococcus parasanguinis	3	8; 18; 31
Streptococcus vestibularis	3	8; 31; 42

Only species reported in more than two studies are shown.
*Row location refers to the row in the data extraction document.

Table S6 Phyla associated with periodontitis.

Phylum	Count	Row locations*
No data	32	1; 2; 3; 5; 6; 8; 10; 11; 12; 13; 15; 16; 17; 18; 19; 20; 22; 23; 24; 25; 27; 29; 30; 34; 35; 36; 38; 39; 40; 41; 42; 43
Synergistetes	7	7; 21; 26; 28; 31; 32; 37
Bacteroidetes	6	4; 7; 14; 21; 26; 32
Spirochaetes	5	4; 7; 21; 32; 37
Chloroflexi	4	7; 28; 32; 37
Firmicutes	3	28; 32; 37
Fusobacteria	2	7; 9
Euryarchaeota	1	32
TM7 (Saccharibacteria)	1	31
Tenericutes	1	32
None	0	

*Row location refers to the row in the data extraction document.

Table S7 Genera associated with periodontitis.

Genus	Count	Row locations*
No data	26	1; 2; 5; 6; 10; 12; 13; 15; 16; 17; 18; 19; 20; 22; 24; 25; 26; 29; 30; 31; 33; 34; 35; 37; 39; 42
Filifactor	13	3; 4; 7; 8; 11; 14; 21; 23; 28; 32; 36; 40; 41
Tannerella	11	4; 7; 8; 11; 14; 23; 28; 32; 36; 38; 40
Porphyromonas	9	3; 4; 7; 8; 14; 21; 23; 32; 36
Treponema	9	3; 4; 7; 8; 14; 23; 32; 36; 38
Desulfobulbus	7	3; 4; 8; 9; 28; 36; 40
Eubacterium	6	3; 4; 7; 23; 32; 36
Peptostreptococcus	6	3; 14; 23; 28; 32; 36
Mogibacterium	5	4; 7; 8; 11; 36
TM7	5	7; 23; 28; 36; 41
Fusobacterium	4	7; 8; 11; 32
Mycoplasma	4	3; 4; 7; 36
Prevotella	4	3; 4; 7; 38
Pseudoramibacter	4	7; 8; 9; 36
Catonella	3	8; 32; 38
Dialister	3	7; 8; 11
Lachnospiraceae [G-8]	3	7; 36; 40
Parvimonas	3	7; 32; 36
Peptostreptococcaceae [XI][G-4]	3	7; 40; 41
Veillonellaceae	3	7; 28; 36
Bacteroidetes [G-3]	2	7; 36
Fretibacterium	2	7; 21
Hallella	2	4; 32
Johnsonella	2	4; 7
Megasphaera	2	7; 11
Peptostreptococcaceae [XI][G-1]	2	7; 41
Peptostreptococcaceae [XI][G-5]	2	40; 41
Slackia	2	7; 8
TM7 [G-5]	2	36; 41
Unclassified	2	4; 28
Veillonellaceae [G-1]	2	7; 36

Only genera reported in more than one study are shown.
*Row location refers to the row in the data extraction document.

Table S8 Species associated with periodontitis.

Species	Count	Row locations*
Tannerella forsythia	23	1; 2; 7; 8; 10; 11; 13; 14; 16; 17; 18; 19; 22; 26; 29; 31; 32; 34; 37; 38; 41; 42; 43
Porphyromonas gingivalis	22	1; 2; 7; 8; 10; 11; 16; 17; 18; 19; 22; 26; 27; 29; 31; 32; 34; 37; 38; 40; 42; 43
Treponema denticola	16	1; 2; 6; 7; 8; 11; 17; 18; 19; 26; 31; 32; 36; 37; 38; 43
Filifactor alocis	15	7; 8; 10; 11; 15; 16; 18; 26; 29; 31; 32; 37; 41; 42; 43
Fusobacterium nucleatum	10	1; 2; 8; 10; 11; 17; 19; 26; 27; 43
Porphyromonas endodontalis	10	2; 7; 8; 11; 15; 17; 18; 26; 31; 37
Selenomonas sputigena	10	7; 10; 12; 16; 22; 24; 29; 35; 37; 40
Parvimonas micra	8	1; 6; 7; 10; 22; 31; 32; 37
Prevotella intermedia	8	1; 2; 8; 11; 18; 22; 31; 38
No data	7	3; 4; 9; 21; 23; 33; 39
Treponema socranskii	7	1; 7; 8; 11; 18; 26; 37
Campylobacter rectus	5	1; 17; 18; 31; 38
Eubacterium saphenum	5	11; 17; 26; 29; 34
Treponema maltophilum	5	8; 18; 26; 31; 37
Aggregatibacter actinomycetemcomitans	4	1; 2; 6; 31
Dialister invisus	4	7; 8; 29; 31
Mogibacterium timidum	4	8; 26; 37; 41
Prevotella nigrescens	4	1; 6; 11; 22
Streptococcus constellatus	4	1; 6; 26; 37
Actinomyces israelii	3	1; 2; 6
Dialister pneumosintes	3	15; 19; 31
Eubacterium [XI][G-3] *brachy*	3	7; 10; 37
Eubacterium [XI][G-5] *saphenum*	3	7; 10; 37
Filifactor alocis HOT 539	3	7; 16; 18
Fretibacterium fastidiosum HOT 363	3	7; 16; 18
Fusobacterium periodonticum	3	1; 6; 11
None	3	5; 20; 30
Porphyromonas gingivalis HOT 619	3	7; 16; 18
Prevotella dentalis	3	8; 11; 18
Streptococcus anginosus	3	1; 24; 34
Tannerella forsythia HOT 613	3	7; 16; 18
Treponema lecithinolyticum	3	17; 31; 37
Treponema medium	3	8; 18; 37
Veillonella parvula	3	1; 6; 10

Only species reported in more than two studies are shown.
*Row location refers to the row in the data extraction document.

Appendix V

Table S9 Studies included in the author's data extraction document and their corresponding row locations.

No.	Reference	Title
1	(Cavalla et al., 2018)	Genetic association with subgingival bacterial colonization in chronic periodontitis
2	(Arenas Rodrigues et al., 2018)	Qualitative, quantitative and genotypic evaluation of *Aggregatibacter actinomycetemcomitans* and *Fusobacterium nucleatum* isolated from individuals with different periodontal clinical conditions
3*	(Shi et al., 2018)	The subgingival microbiome of periodontal pockets with different probing depths in chronic and aggressive periodontitis: a pilot study
4	(Chen et al., 2018)	Oral microbiota of periodontal health and disease and their changes after nonsurgical periodontal therapy
5	(Babaev et al., 2017)	Metagenomic analysis of gingival sulcus microbiota and pathogenesis of periodontitis associated with type 2 diabetes mellitus
6	(Hartenbach et al., 2018)	The effect of supragingival biofilm re-development on the subgingival microbiota in chronic periodontitis
7*	(Pérez-Chaparro et al., 2018)	Do different probing depths exhibit striking differences in microbial profiles?
8	(Wu et al., 2017)	16S rDNA analysis of periodontal plaque in chronic obstructive pulmonary disease and periodontitis patients
9	(Coretti et al., 2017)	Subgingival dysbiosis in smoker and non-smoker patients with chronic periodontitis
10*	(Dabdoub et al., 2016)	Comparative metagenomics reveals taxonomically idiosyncratic yet functionally congruent communities in periodontitis
11	(Hunter et al., 2016)	Microbial signatures of oral dysbiosis, periodontitis and edentulism revealed by Gene Meter methodology
12	(Nagpal et al., 2016)	Detection and comparison of *Selenomonas sputigena* in subgingival biofilms in chronic and aggressive periodontitis patients
13	(Ozturk et al., 2016)	Impact of aging on TREM-1 responses in the periodontium: a cross-sectional study in an elderly population
14*	(Tsai et al., 2018)	Subgingival microbiota in individuals with severe chronic periodontitis
15	(Gonçalves et al., 2016)	Association of three putative periodontal pathogens with chronic periodontitis in Brazilian subjects
16	(Oliveira et al., 2016)	Levels of candidate periodontal pathogens in subgingival biofilm
17	(Scapoli et al., 2015)	Quantitative analysis of periodontal pathogens in periodontitis and gingivitis
18	(Szafrański et al., 2015a)	Functional biomarkers for chronic periodontitis and insights into the roles of *Prevotella nigrescens* and *Fusobacterium nucleatum*; a metatranscriptome analysis
19	(Collins et al., 2016)	Periodontal pathogens and tetracycline resistance genes in subgingival biofilm of periodontally healthy and diseased Dominican adults
20	(Lages et al., 2015)	Alcohol consumption and periodontitis: quantification of periodontal pathogens and cytokines

21*	(Park et al., 2015)	Pyrosequencing analysis of subgingival microbiota in distinct periodontal conditions
22	(Gaetti-Jardim et al., 2015)	Occurrence of periodontal pathogens in ethnic groups from a native Brazilian reservation
23*	(Camelo-Castillo et al., 2015)	Subgingival microbiota in health compared to periodontitis and the influence of smoking
24	(Elabdeen et al., 2015)	Subgingival microbial profiles of Sudanese patients with aggressive periodontitis
25	(Szafrański et al., 2015b)	High-resolution taxonomic profiling of the subgingival microbiome for biomarker discovery and periodontitis diagnosis
26*	(Kirst et al., 2015)	Dysbiosis and alterations in predicted functions of the subgingival microbiome in chronic periodontitis
27	(Souto et al., 2014)	Prevalence of *Pseudomonas aeruginosa* and *Acinetobacter* spp. in subgingival biofilm and saliva of subjects with chronic periodontal infection
28*	(Galimanas et al., 2014)	Bacterial community composition of chronic periodontitis and novel oral sampling sites for detecting disease indicators
29	(Zbinden et al., 2014)	Frequent detection of *Streptococcus tigurinus* in the human oral microbial flora by a specific 16S rRNA gene real-time TaqMan PCR
30	(Lourenço et al., 2014)	Microbial signature profiles of periodontally healthy and diseased patients
31	(Al-Hebshi et al., 2015)	Quantitative analysis of classical and new putative periodontal pathogens in subgingival biofilm: a case-control study
32*	(Li et al., 2014)	Phylogenetic and functional gene structure shifts of the oral microbiomes in periodontitis patients
33*	(Duran-Pinedo et al., 2014)	Community-wide transcriptome of the oral microbiome in subjects with and without periodontitis
34	(Zhou et al., 2013)	Investigation of the effect of type 2 diabetes mellitus on subgingival plaque microbiota by high-throughput 16S rDNA pyrosequencing
35	(You et al., 2013)	Comparative analysis of oral treponemes associated with periodontal health and disease
36*	(Abusleme et al., 2013)	The subgingival microbiome in health and periodontitis and its relationship with community biomass and inflammation
37	(Ebadian et al., 2012)	Bacterial analysis of peri-implantitis and chronic periodontitis in Iranian subjects
38*	(Liu et al., 2012)	Deep sequencing of the oral microbiome reveals signatures of periodontal disease
39	(Gonçalves et al., 2012)	Levels of *Selenomonas* species in generalized aggressive periodontitis
40	(Nibali et al., 2022)	Patterns of subgingival microbiota in different periodontal phenotypes
41	(Lu et al., 2021a)	Subgingival microbial profiles of young Chinese adults with stage I/II periodontitis, gingivitis and periodontal health status
42	(Lee et al., 2021)	Subgingival microbiome and specialized pro-resolving lipid mediator pathway profiles are correlated in periodontal inflammation

*Denotes studies included in previous review (Feres et al., 2021).

Appendix VI

S. intermedius

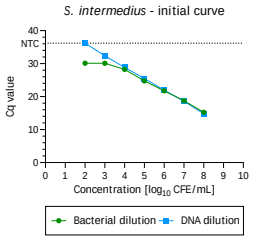

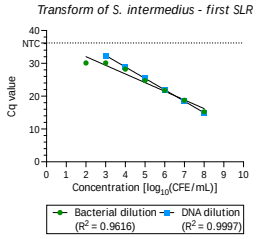

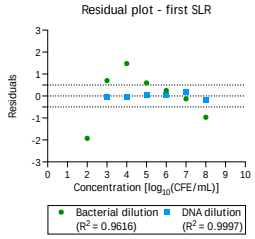

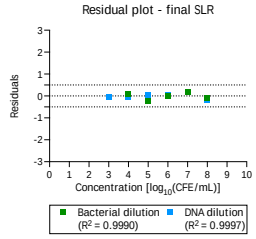

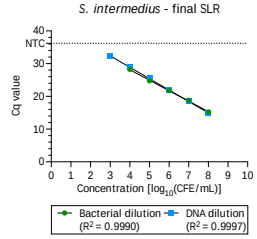

S. mitis

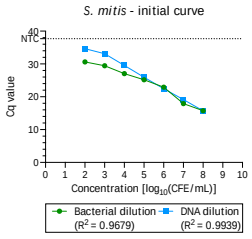

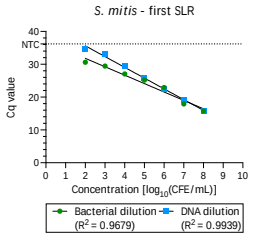

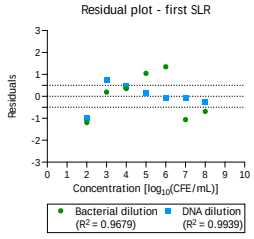

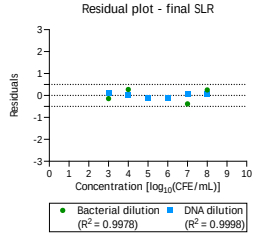

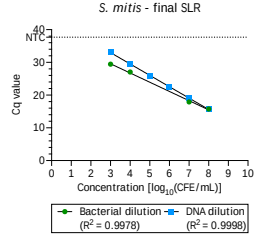

S. oralis

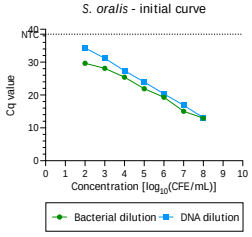

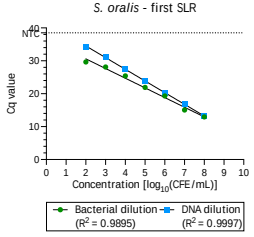

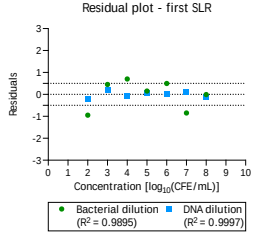

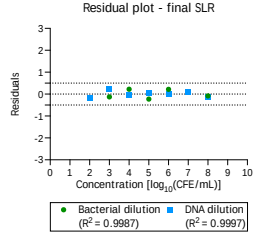

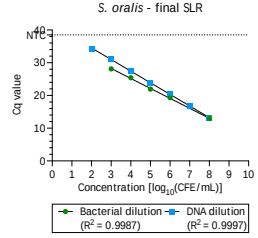

Streptococcus spp.

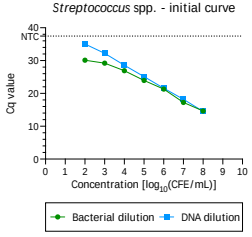

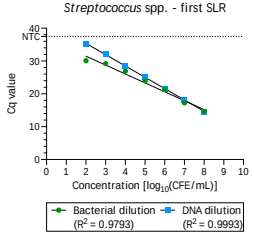

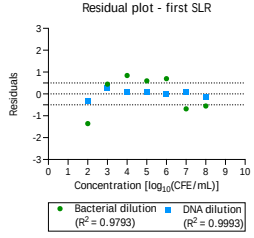

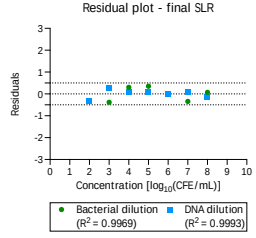

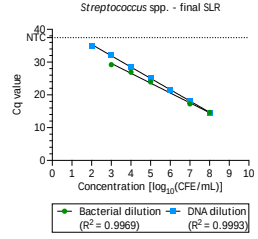

N. mucosa

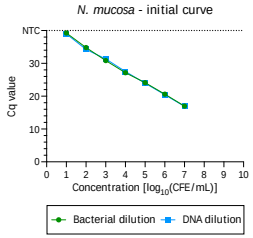

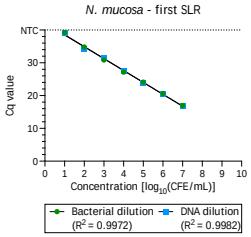

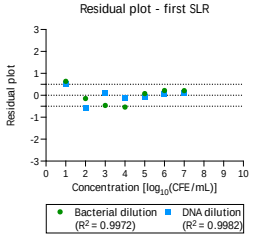

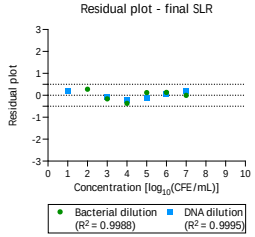

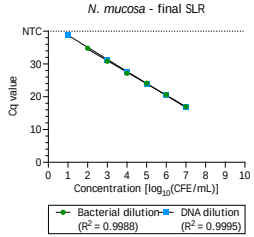

R. dentocariosa

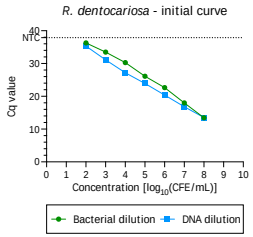

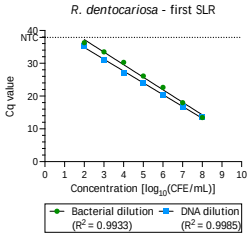

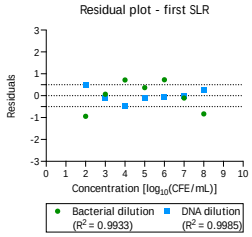

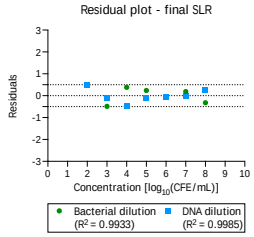

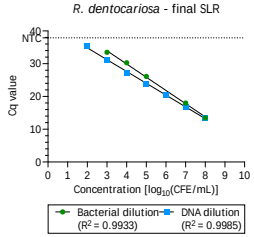

A. naeslundii

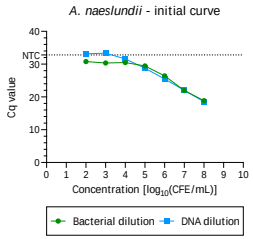

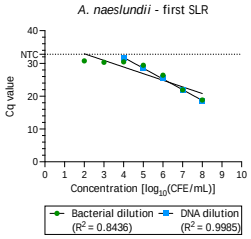

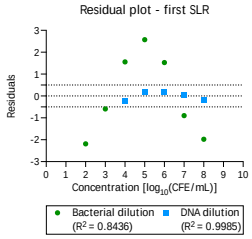

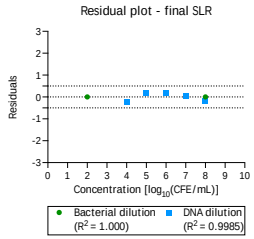

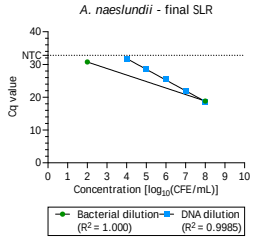

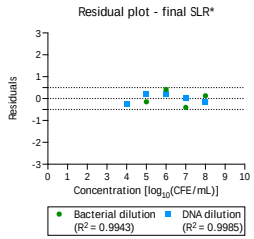

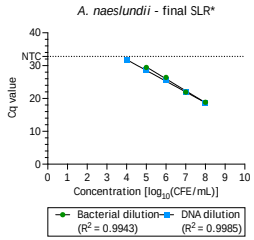

V. dispar

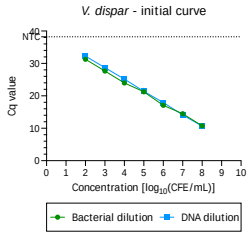

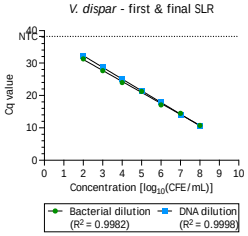

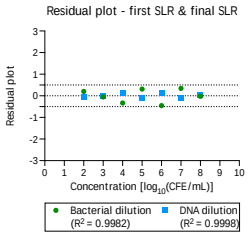

F. nucleatum subsp. *polymorphum*

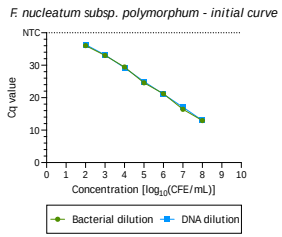

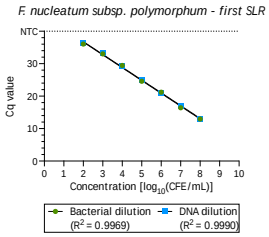

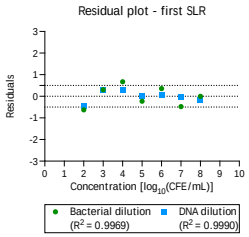

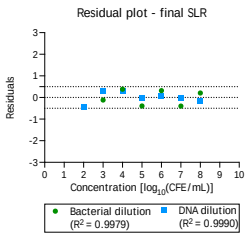

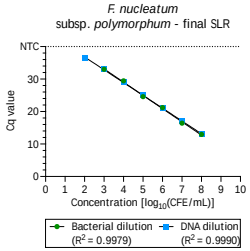

F. nucleatum subsp. *vincentii*

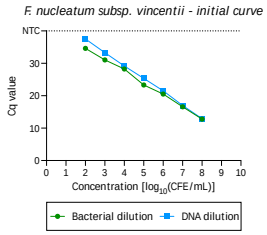

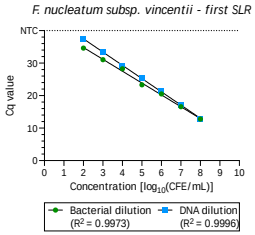

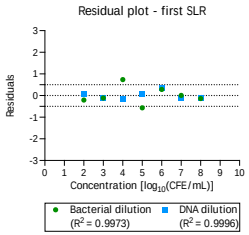

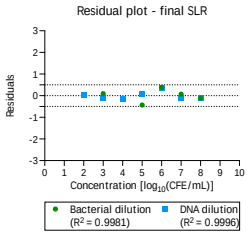

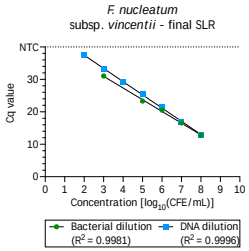

Fusobacterium spp.

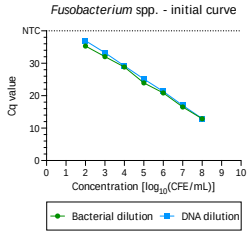

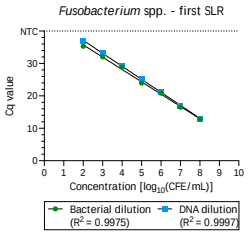

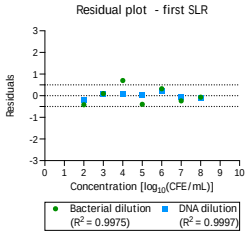

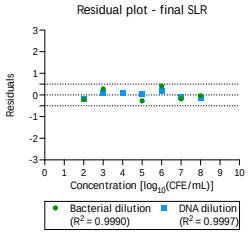

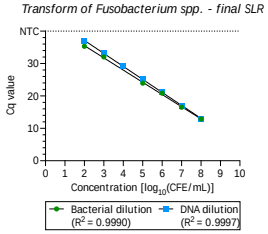

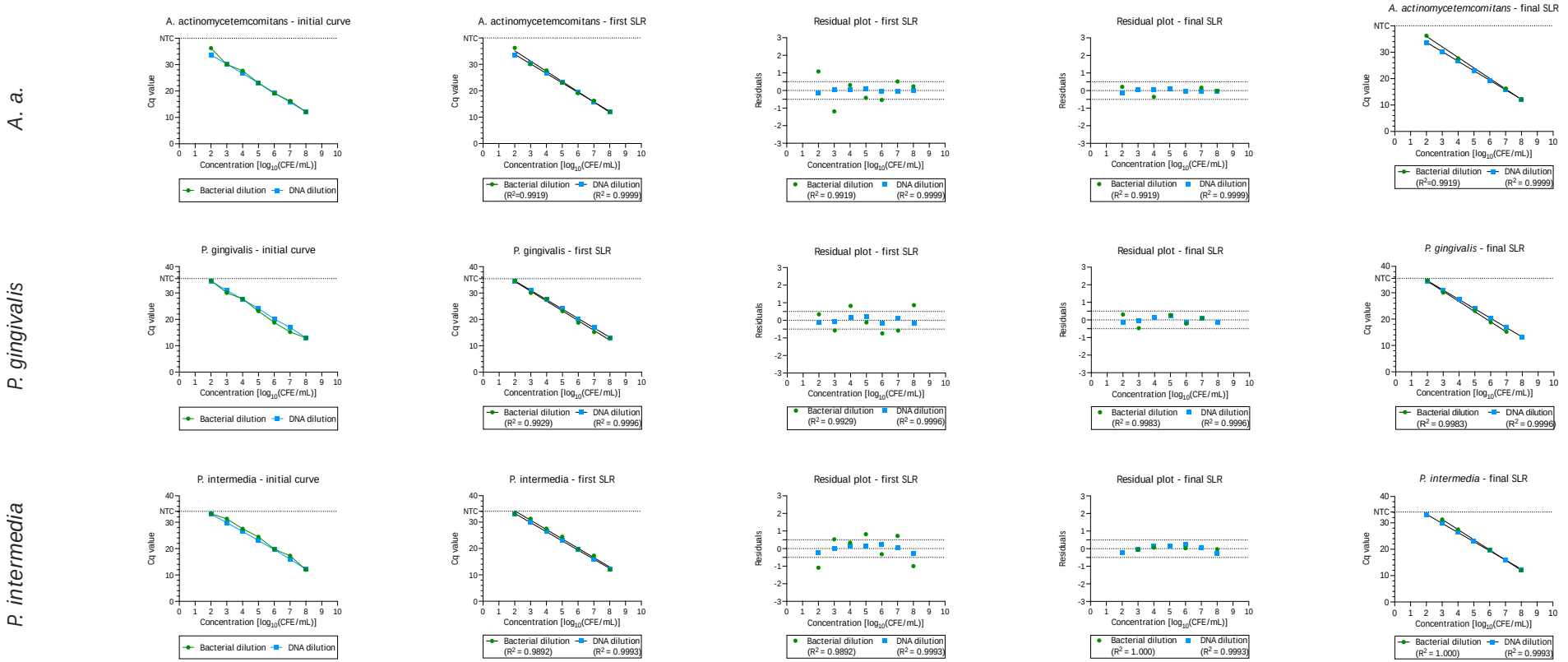

Figure S1 Full analytical workflow for generation of species-specific and genus-level qPCR standard curves. Each row represents the analytical workflow for one species-specific or genus-level standard curve. Within each row, panels are arranged from left to right as follows: initial curve, first SLR, residual plot for the first SLR, residual plot for the final SLR, and final SLR. Planktonic monocultures of *S. intermedius, S. mitis, S. oralis, N. mucosa, R. dentocariosa, A. naeslundii, V. dispar, F. nucleatum* subsp. *polymorphum, F. nucleatum* subsp. *vincentii, A. actinomycetemcomitans, P. gingivalis,* and *P. intermedia* were cultured in appropriate broths and adjusted in PBS to target concentrations of 1×10^8 CFE/mL, except for *N. mucosa*, which was adjusted to 1×10^7 CFE/mL. Bacterial suspensions were serially diluted ten-fold before DNA extraction. Additional sets of ten-fold dilutions were prepared from the DNA extracts obtained from the highest-concentration bacterial suspensions. Both dilution series were analysed using qPCR. Standard curves were generated by plotting Cq values against $\log_{10}$-transformed CFE/mL values. Curve fit was assessed iteratively using simple linear regression, R^2 values, and residual analysis, followed by sequential removal of outlying data points until residuals fell within

± 0.5 to obtain the final standard curves. For *V. dispar*, the first SLR also met the final acceptance criteria and no data points were removed from any dilution series. For *A. naeslundii*, sequential optimisation of the bacterial dilution series yielded only two remaining data points; therefore, an additional alternative analysis, denoted by an asterisk (*), was performed in which the 10^2, 10^3 and 10^4 CFE/mL data points were removed first due to the flattened shape of the curve. For each species, two dilution series were run on a single occasion (n = 1) in duplicate on the same plate under identical conditions, with a single shared set of NTCs (4 wells). Additional genus-level standard curves and corresponding NTC values were generated for *Streptococcus* spp. from the mean Cq values of *S. intermedius, S. mitis*, and *S. oralis*, and for *Fusobacterium* spp. from the mean Cq values of *F. nucleatum* subsp. *polymorphum* and *F. nucleatum* subsp. *vincentii*. In each graph showing an initial curve, first SLR or final SLR, the dotted line denotes the mean Cq value for the NTCs. *A. a.*, *Aggregatibacter actinomycetemcomitans*; NTC, no-template control. SLR, simple linear regression.

Appendix VII

Table S10 Assessment of qPCR assay performance from the bacterial standard curves.

Species/Genus	Dynamic range (CFE/mL)	Correlation coefficient (R^2)	Standard Error of Estimate ($S_{y.x}$)	Equation	Slope	Y-intercept	Mean NTC value	Efficiency (%)
S. intermedius	10^4 – 10^8	0.9990	0.1810	$y = -3.198 \times x + 40.93$	−3.198	40.930	36.193	105.44
S. mitis	10^3 – 10^8	0.9978	0.3892	$y = -2.818 \times x + 38.04$	−2.818	38.040	37.682	126.39
S. oralis	10^3 – 10^8	0.9987	0.2395	$y = -3.045 \times x + 37.38$	−3.045	37.380	38.493	113.01
Streptococcus spp.	10^3 – 10^8	0.9969	0.4022	$y = -3.007 \times x + 38.63$	−3.007	38.630	37.358	115.06
N. mucosa	10^3 – 10^8	0.9988	0.2596	$y = -3.512 \times x + 45.07$	−3.512	45.070	40.000	92.64
R. dentocariosa	10^3 – 10^8	0.9979	0.4387	$y = -4.037 \times x + 46.07$	−4.037	46.070	37.876	76.89
A. naeslundii	10^2 – 10^8	1.000	-	$y = -1.986 \times x + 34.75$	−1.986	34.750	32.791	218.80
*A. naeslundii**	10^4 – 10^8	0.9943	0.4326	$y = -3.628 \times x + 47.75$	−3.628	47.750	32.791	88.64
V. dispar	10^2 – 10^8	0.9982	0.3378	$y = -3.390 \times x + 37.88$	−3.390	37.880	38.205	97.24
F. nucleatum subsp. *polymorphum*	10^3 – 10^8	0.9979	0.3910	$y = -4.078 \times x + 45.37$	−4.078	45.370	40.000	75.88
F. nucleatum subsp. *vincentii*	10^3 – 10^8	0.9981	0.3456	$y = -3.612 \times x + 41.80$	−3.612	41.800	40.000	89.17
F. nucleatum spp.	10^2 – 10^8	0.9990	0.3152	$y = -3.769 \times x + 43.06$	−3.769	43.060	40.000	84.21
A. actinomycetemcomitans	10^2 – 10^8	0.9995	0.3149	$y = -3.990 \times x + 44.01$	−3.990	44.010	40.000	78.08
P. gingivalis	10^2 – 10^7	0.9983	0.3844	$y = -3.853 \times x + 42.09$	−3.853	42.090	35.436	81.78
P. intermedia	10^3 – 10^8	1.000	0.0657	$y = -3.858 \times x + 42.90$	−3.858	42.900	34.113	81.64

Bacterial dilution series values were derived from a single experimental run (n = 1), performed in technical duplicate. A shared set of NTCs (4 wells) was used for both the bacterial and DNA standard curves.
*Alternative analysis for *A. naeslundii*, in which the 10^2, 10^3 and 10^4 CFE/mL data points were removed first due to the flattened shape of the curve.

Table S11 Assessment of qPCR assay performance from the DNA standard curves.

Species/Genus	Dynamic range (CFE/mL)	Correlation coefficient (R^2)	Standard Error of Estimate ($S_{y.x}$)	Equation	Slope	Y-intercept	Mean NTC value	Efficiency (%)
S. intermedius	$10^3 - 10^8$	0.9997	0.1268	$y = -3.488 \times x + 42.86$	−3.488	42.860	36.193	93.51
S. mitis	$10^3 - 10^8$	0.9998	0.1105	$y = -3.475 \times x + 43.43$	−3.475	43.430	37.682	93.99
S. oralis	$10^2 - 10^8$	0.9997	0.1562	$y = -3.548 \times x + 41.62$	−3.548	41.620	38.493	91.36
Streptococcus spp.	$10^2 - 10^8$	0.9993	0.2152	$y = -3.450 \times x + 42.30$	−3.450	42.300	37.358	94.92
N. mucosa	$10^1 - 10^7$	0.9995	0.1967	$y = -3.678 \times x + 46.14$	−3.678	46.140	40.000	87.02
R. dentocariosa	$10^2 - 10^8$	0.9985	0.3305	$y = -3.601 \times x + 42.04$	−3.601	42.040	37.876	89.54
A. naeslundii	$10^4 - 10^8$	0.9985	0.2336	$y = -3.278 \times x + 44.94$	−3.278	44.940	32.791	101.87
V. dispar	$10^2 - 10^8$	0.9998	0.1061	$y = -3.612 \times x + 39.52$	−3.612	39.520	38.205	89.17
F. nucleatum subsp. *polymorphum*	$10^2 - 10^8$	0.9990	0.2896	$y = -3.943 \times x + 44.69$	−3.943	44.690	40.000	79.31
F. nucleatum subsp. *vincentii*	$10^2 - 10^8$	0.9996	0.1965	$y = -4.077 \times x + 45.63$	−4.077	45.630	40.000	75.91
F. nucleatum spp.	$10^2 - 10^8$	0.9997	0.1546	$y = -4.010 \times x + 45.16$	−4.010	45.160	40.000	77.57
A. actinomycetemcomitans	$10^2 - 10^8$	0.9999	0.0894	$y = -3.603 \times x + 41.00$	−3.603	41.000	40.000	89.47
P. gingivalis	$10^2 - 10^8$	0.9996	0.1762	$y = -3.560 \times x + 41.69$	−3.560	41.690	35.436	90.94
P. intermedia	$10^2 - 10^8$	0.9993	0.2153	$y = -3.472 \times x + 40.24$	−3.472	40.240	34.113	94.10

DNA dilution series values were derived from a single experimental run (n = 1), performed in technical duplicate. A shared set of NTCs (4 wells) was used for both the bacterial and DNA standard curves.

Appendix VIII

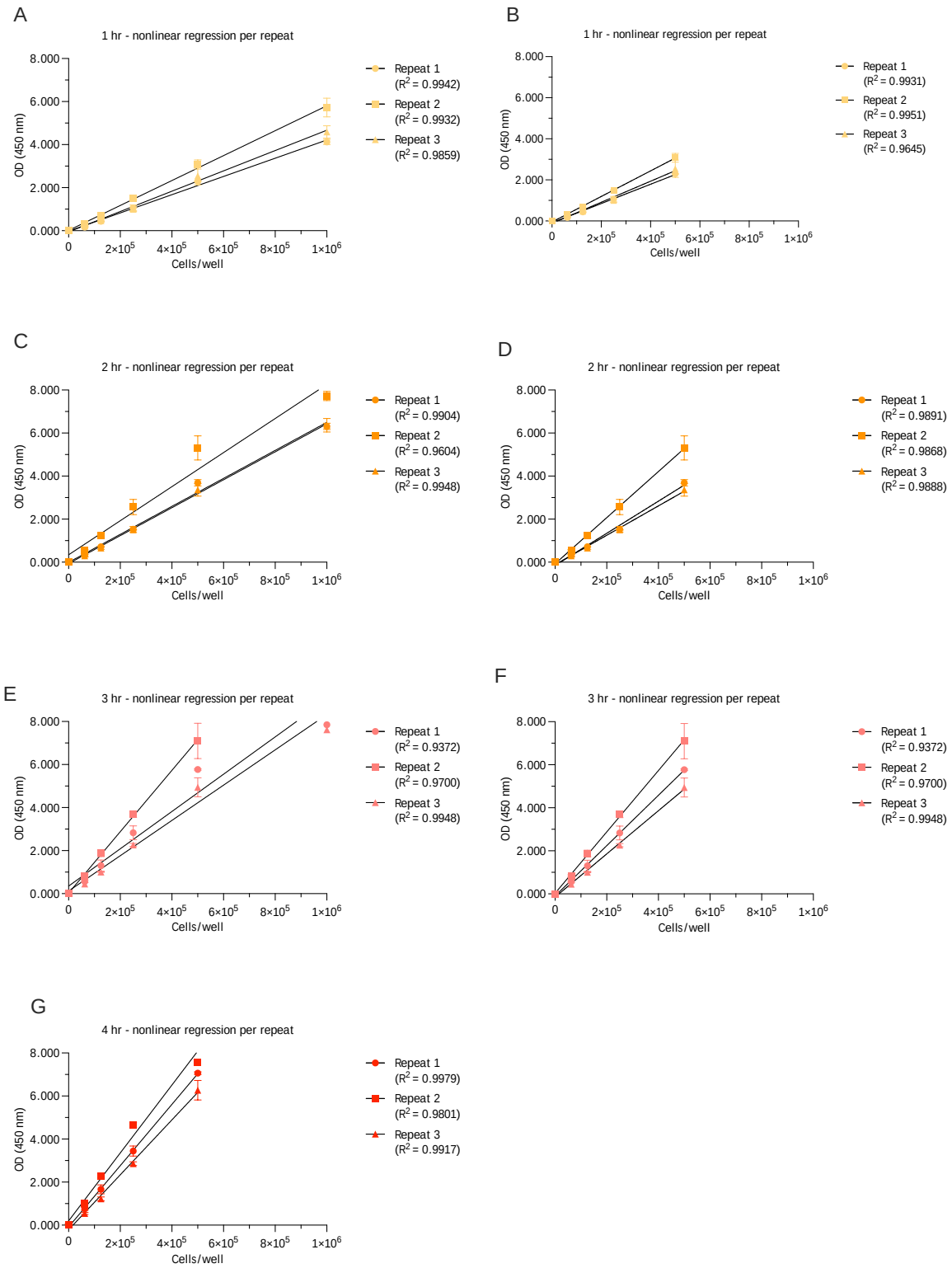

Figure S2 TR146 cell standard curves generated using the CCK-8 assay. Nonlinear regression (straight line fit) was performed on blank-corrected OD values obtained from serial dilutions of TR146 cell suspensions during the CCK-8 assay. Serial dilutions of TR146 cell suspensions were incubated with CCK-8 for 1 hour (A, B), 2 hours (C, D), 3 hours (E, F) and 4 hours (G). Nonlinear regression was performed on all available data points (A, C, E, G) or with the top concentration excluded from the analysis (B, D, F). For the 4-hour time point, OD values for the top concentration exceeded the plate reader's measurable range and were unavailable for analysis. Data are presented as mean ± SD of blank-corrected OD values from three independent experiments (n = 3) performed in technical duplicate for each time point.

Appendix IX

Brand	Treatment		Parts with strongest growth	Parts with average growth	Parts with weakest growth
Corning	Media	A	----	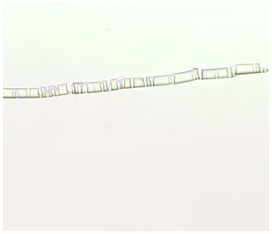	----
Corning	Media	B	----	----	----
Corning	Cells only	A	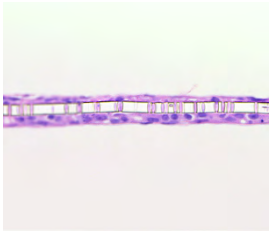	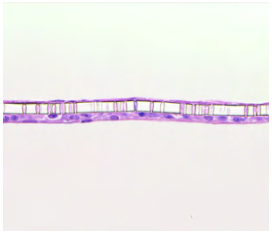	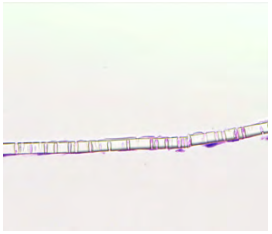
Corning	Cells only	B	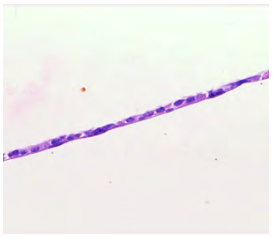	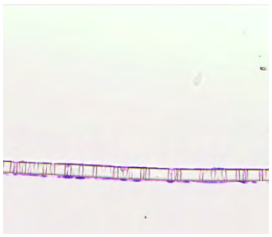	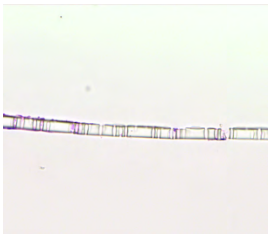
Corning	$CaCl_2$	A	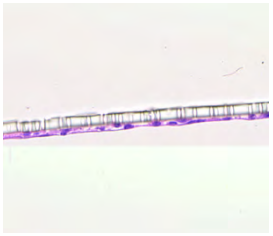	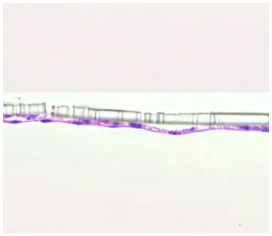	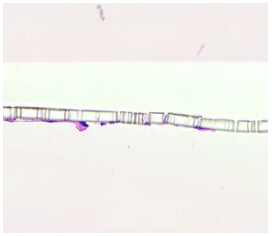
Corning	$CaCl_2$	B	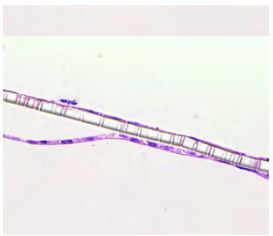	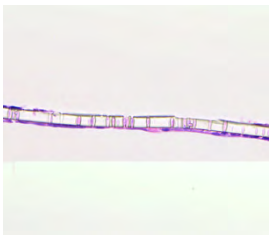	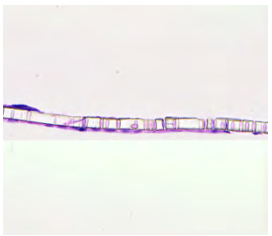
Corning	Collagen I	A	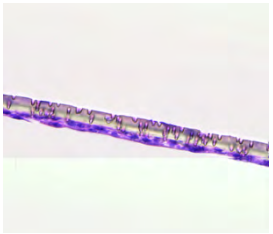	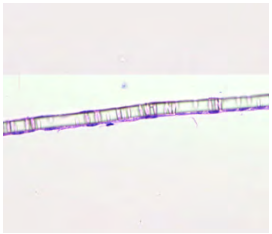	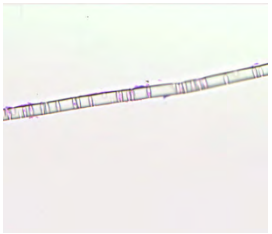
Corning	Collagen I	B	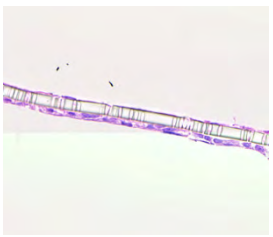	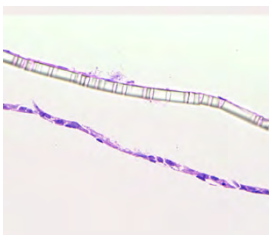	

Corning	FBS	A	----	----	----
Corning	FBS	B	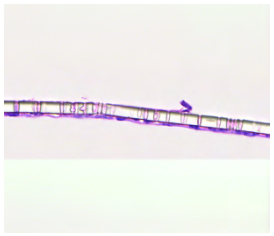	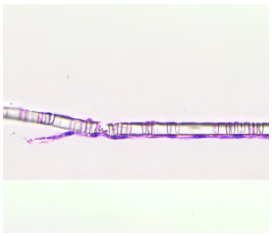	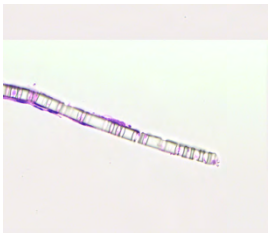
Millicell	Media	A	----	----	----
Millicell	Media	B	----	----	----
Millicell	Cells only	A	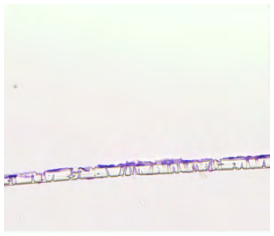	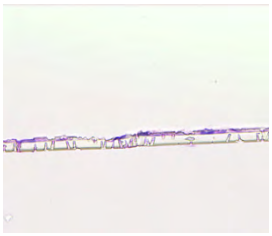	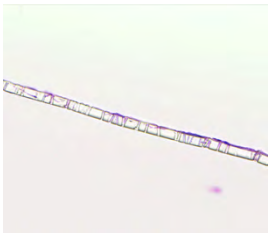
Millicell	Cells only	B	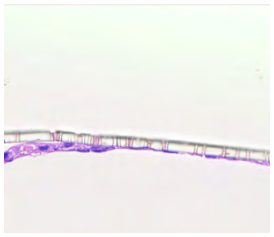	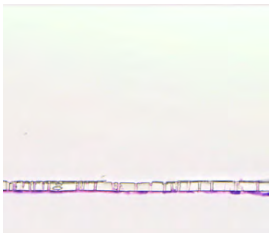	
Millicell	$CaCl_2$	A		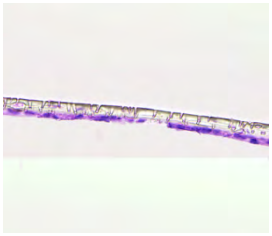	
Millicell	$CaCl_2$	B		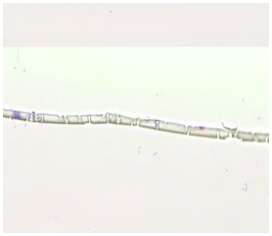	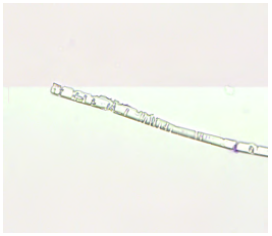
Millicell	Collagen I	A		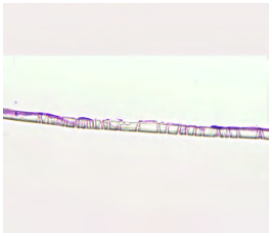	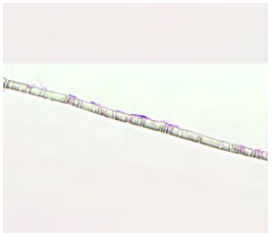

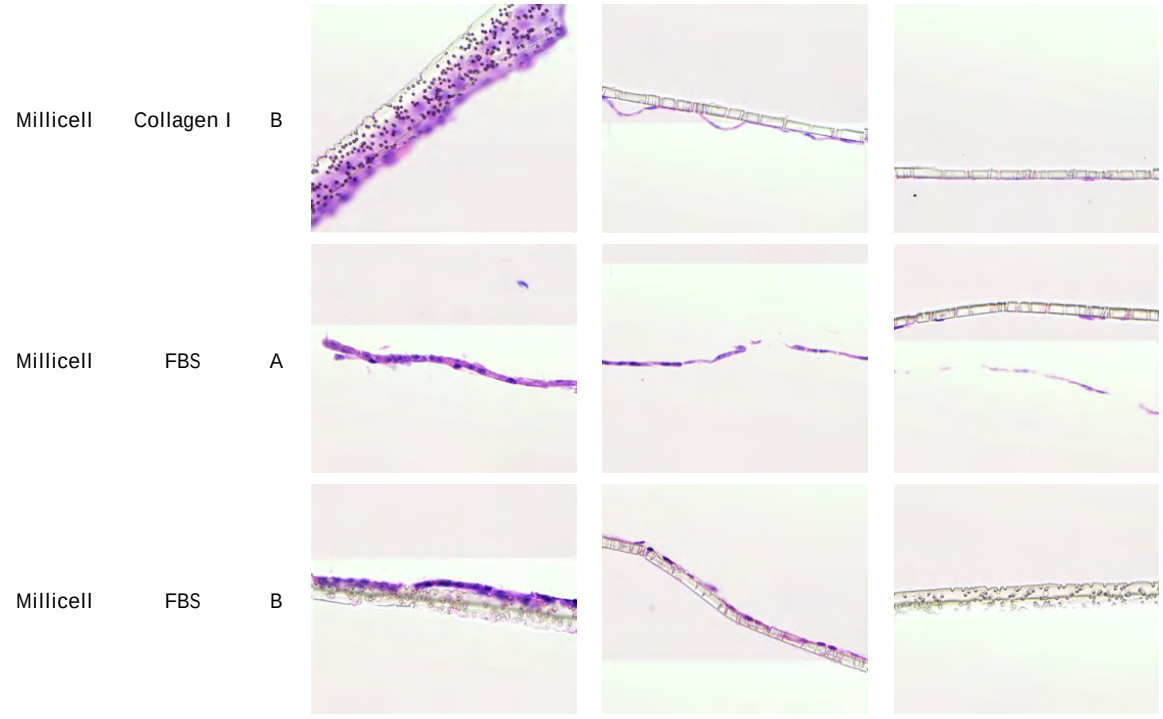

Figure S3 Histology of TR146 epithelial cell layers grown on Corning and Millicell PET transwell insert membranes. Panels A and B show duplicate membranes, each seeded with 5×10^4 cells with or without pre-coating with $CaCl_2$, type I collagen or FBS and incubated for 4 days at 37 °C, 5% CO_2. Subsequently, they were fixed, excised, embedded in paraffin blocks, sectioned and stained with H&E. Slides were scanned at 80× magnification. Each image is representative of a part of a single membrane showing the strongest, average or weakest cell growth. Membrane thickness is 10 µm (Corning) or 9–16 µm (Millicell). Membranes that could not be imaged are indicated by a dash placeholder (----). PET, polyethylene terephthalate.

Appendix X

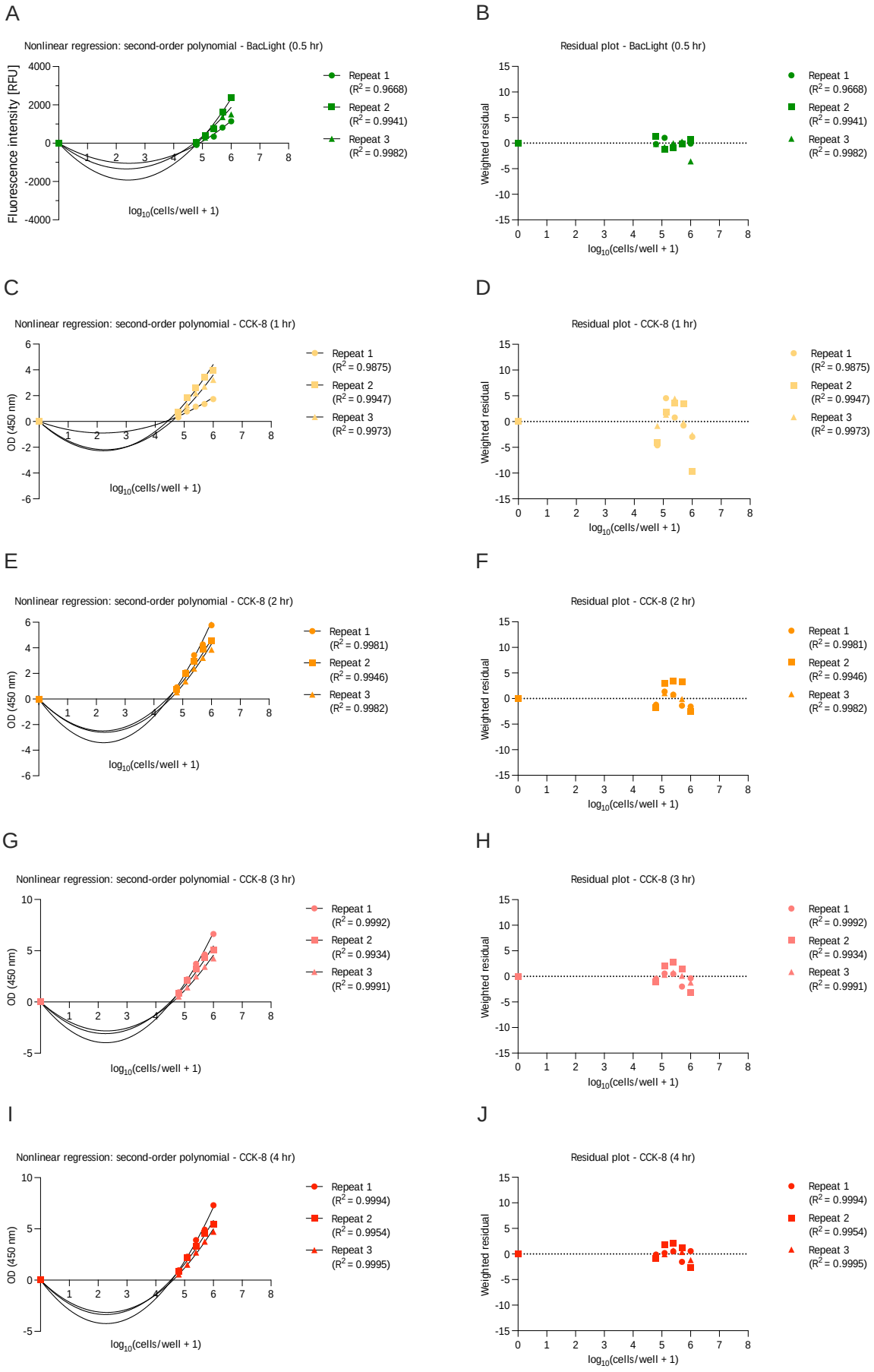

Figure S4 Neutrophil standard curves generated in 96-well plates using BacLight and CCK-8 assays. Nonlinear regression (second order polynomial (quadratic) fit) was performed on blank-corrected fluorescence values for the BacLight assay and blank-corrected OD values for the CCK-8 assay. Serial dilutions of neutrophil suspensions were incubated in 96-well plates with

BacLight for 0.5 hours (A, B) or with CCK-8 for 1 hour (C, D), 2 hours (E, F), 3 hours (G, H) and 4 hours (I, J) at 37 °C, 5% CO_2. Nonlinear regression was performed on all obtained data points (A, C, E, G, I) with corresponding residual plots (B, D, F, H, J). Data are presented as mean ± SD of blank-corrected fluorescence values for BacLight and blank-corrected OD values for CCK-8 from 3 independent experiments for each time point. RFU, relative fluorescence units.

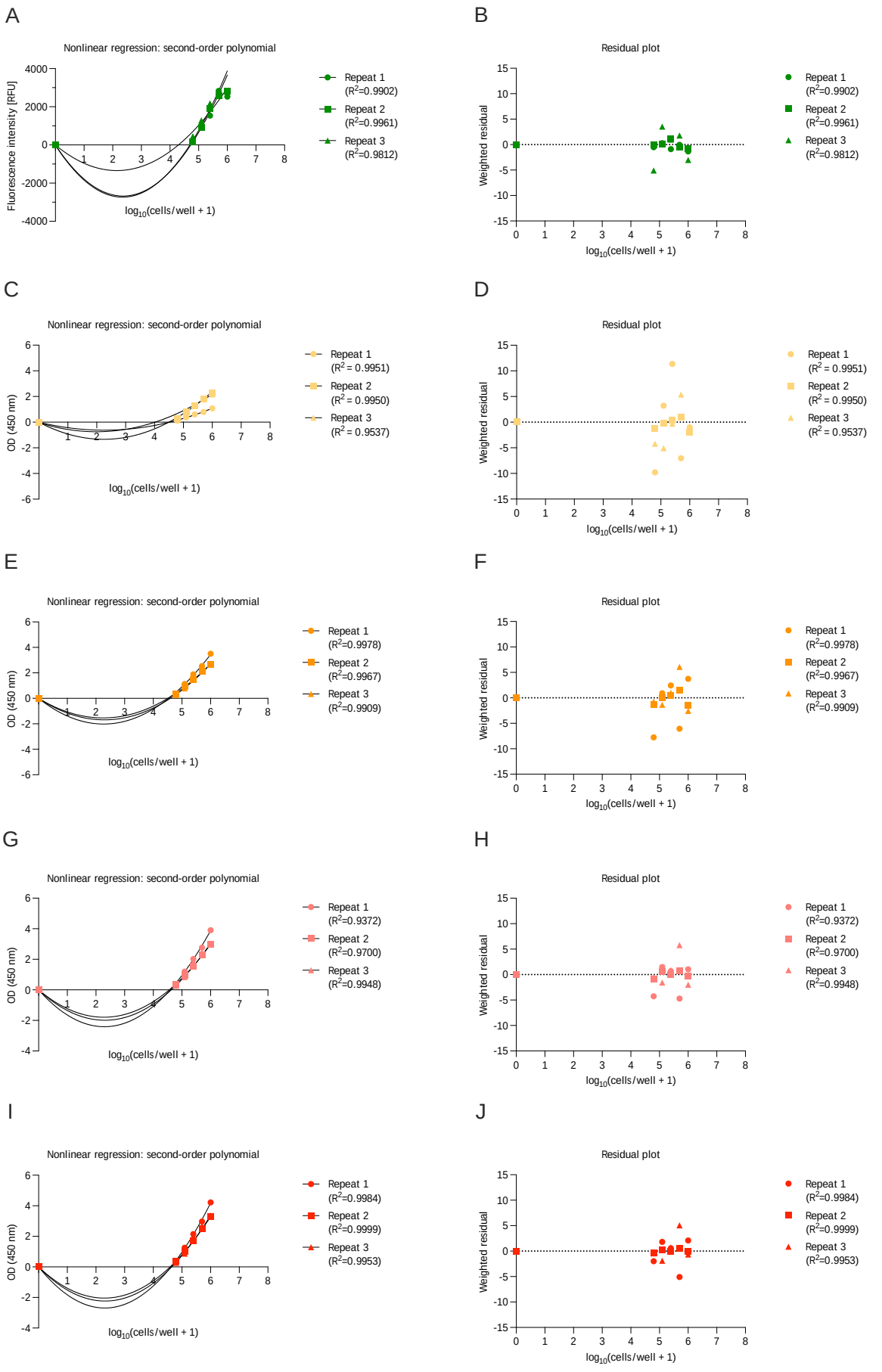

Figure S5 Neutrophil standard curves generated in 24-well plates using BacLight and CCK-8 assays. Nonlinear regression (second order polynomial (quadratic) fit) was performed on blank-corrected fluorescence values for the BacLight assay and blank-corrected OD values for the CCK-8 assay. Serial dilutions of neutrophil suspensions were incubated in 24-well plates with

BacLight for 0.5 hours (A, B) or with CCK-8 for 1 hour (C, D), 2 hours (E, F), 3 hours (G, H) and 4 hours (I, J) at 37 °C, 5% CO_2. Nonlinear regression was performed on all obtained data points (A, C, E, G, I) with corresponding residual plots (B, D, F, H, J). Data are presented as mean ± SD of blank-corrected fluorescence values for BacLight and blank-corrected OD values for CCK-8 from 3 independent experiments for each time point. RFU, relative fluorescence units.

List of References

Abe, T., AlSarhan, M., Benakanakere, M.R., Maekawa, T., Kinane, D.F., Cancro, M.P., Korostoff, J.M. and Hajishengallis, G. (2015) The B cell–stimulatory cytokines BLyS and APRIL are elevated in human periodontitis and are required for B cell–dependent bone loss in experimental murine periodontitis. *The Journal of Immunology,* 195(4), 1427–1435. https://doi.org/10.4049/jimmunol.1500496

Abusleme, L., Dupuy, A.K., Dutzan, N., Silva, N., Burleson, J.A., Strausbaugh, L.D., Gamonal, J. and Diaz, P.I. (2013) The subgingival microbiome in health and periodontitis and its relationship with community biomass and inflammation. *The ISME Journal,* 7(5), 1016–1025. https://doi.org/10.1038/ismej.2012.174

Abusleme, L., Hoare, A., Hong, B.-Y. and Diaz, P.I. (2021) Microbial signatures of health, gingivitis, and periodontitis. *Periodontology 2000,* 86(1), 57–78. https://doi.org/10.1111/prd.12362

Ahlstrand, T., Kovesjoki, L., Maula, T., Oscarsson, J. and Ihalin, R. (2019) *Aggregatibacter actinomycetemcomitans* LPS binds human interleukin-8. *Journal of Oral Microbiology,* 11(1), 1549931. https://doi.org/10.1080/20002297.2018.1549931

Ahlstrand, T., Tuominen, H., Beklen, A., Torittu, A., Oscarsson, J., Sormunen, R., Pollanen, M.T., Permi, P. and Ihalin, R. (2017) A novel intrinsically disordered outer membrane lipoprotein of *Aggregatibacter actinomycetemcomitans* binds various cytokines and plays a role in biofilm response to interleukin-1ß and interleukin-8. *Virulence,* 8(2), 115–134. https://doi.org/10.1080/21505594.2016.1216294

Akatsu, T., Souno, H., Fujii, A., Minegishi, Y., Ota, N. and Yamashita, Y. (2025) Characteristics of subgingival plaque microbiome in Japanese older adults with healthy gingiva. *Journal of Clinical Periodontology,* 52(9), 1314–1326. https://doi.org/10.1111/jcpe.14192

Al Kawas, S., Al-Marzooq, F., Rahman, B., Shearston, J.A., Saad, H., Benzina, D. and Weitzman, M. (2021) The impact of smoking different tobacco types on the subgingival microbiome and periodontal health: a pilot study. *Scientific Reports,* 11, 1113. https://doi.org/10.1038/s41598-020-80937-3

Al-Fatlawi, Z., Huang, M., Chau, D.Y.S. and D'Aiuto, F. (2023) Three dimensional (3D) gingival models in periodontal research: a systematic review. *Journal of Materials Science: Materials in Medicine,* 34(11), 58. https://doi.org/10.1007/s10856-023-06761-z

Al-Hebshi, N.N., Al-Alimi, A., Taiyeb-Ali, T. and Jaafar, N. (2015) Quantitative analysis of classical and new putative periodontal pathogens in subgingival biofilm: a case-control study. *Journal of Periodontal Research,* 50(3), 320–329. https://doi.org/10.1111/jre.12210

Alessandri, G., Rizzo, S.M., Mancabelli, L., Fontana, F., Longhi, G., Turroni, F., van Sinderen, D. and Ventura, M. (2024) Impact of cryoprotective agents on human gut microbes and *in vitro* stabilized artificial gut microbiota communities. *Microbial Biotechnology,* 17(6), e14509. https://doi.org/10.1111/1751-7915.14509

Allen, L.-A.H. (2014) Immunofluorescence and confocal microscopy of neutrophils. In: Quinn, M.T. and DeLeo, F.R. (eds.) *Neutrophil methods and protocols.* Totowa, NJ: Humana Press, pp. 251–268. https://doi.org/10.1007/978-1-62703-845-4_16

Alshatti, F., Almutairi, R., Alkandari, S., Haneef, A., Bhardwaj, R. and Karched, M. (2023) Bioinformatics analysis of the *Rothia dentocariosa* proteome and assessment of the proinflammatory potential of biofilm and planktonic cells. *The Open Dentistry Journal,* 17, e187421062211300. https://doi.org/10.2174/18742106-v16-e221130-2022-71

Alvarez, G., Gonzalez, M., Isabal, S., Blanc, V. and Leon, R. (2013) Method to quantify live and dead cells in multi-species oral biofilm by real-time PCR with propidium monoazide. *AMB Express,* 3, 1. https://doi.org/10.1186/2191-0855-3-1

American Academy of Periodontology (2011) Comprehensive periodontal therapy: a statement by the American Academy of Periodontology. *Journal of Periodontology,* 82(7), 943–949. https://doi.org/10.1902/jop.2011.117001

American Type Culture Collection *ATCC Strain Database* [Online]. Available at: https://www.atcc.org (Accessed: 1 July 2025).

Ammann, T.W., Belibasakis, G.N. and Thurnheer, T. (2013) Impact of early colonizers on *in vitro* subgingival biofilm formation. *PLOS ONE,* 8(12), e83090. https://doi.org/10.1371/journal.pone.0083090

Ammann, T.W., Gmur, R. and Thurnheer, T. (2012) Advancement of the 10-species subgingival Zurich biofilm model by examining different nutritional conditions and defining the structure of the *in vitro* biofilms. *BMC Microbiology,* 12, 227. https://doi.org/10.1186/1471-2180-12-227

Antezack, A., Etchecopar-Etchart, D., La Scola, B. and Monnet-Corti, V. (2023) New putative periodontopathogens and periodontal health-associated species: a systematic review and meta-analysis. *Journal of Periodontal Research,* 58(5), 893–906. https://doi.org/10.1111/jre.13173

Anto, J. (2013) *Investigating the effects of oral microbial biofilms on oral epithelial cells.* PhD thesis, University of Glasgow.

Aoki, A., Mizutani, K., Schwarz, F., Sculean, A., Yukna, R.A., Takasaki, A.A., Romanos, G.E., Taniguchi, Y., Sasaki, K.M., Zeredo, J.L., Koshy, G., Coluzzi, D.J., White, J.M., Abiko, Y., Ishikawa, I. and Izumi, Y. (2015) Periodontal and peri-implant wound healing following laser therapy. *Periodontology 2000,* 68(1), 217–269. https://doi.org/10.1111/prd.12080

Araújo, J.P., Lourenço, P., Azevedo, A., Friões, F., Rocha-Gonçalves, F., Ferreira, A. and Bettencourt, P. (2009) Prognostic value of high-sensitivity C-reactive protein in heart failure: a systematic review. *Journal of Cardiac Failure,* 15(3), 256–266. https://doi.org/10.1016/j.cardfail.2008.10.030

Arenas Rodrigues, V.A., de Avila, E.D., Nakano, V. and Avila-Campos, M.J. (2018) Qualitative, quantitative and genotypic evaluation of *Aggregatibacter actinomycetemcomitans* and *Fusobacterium nucleatum* isolated from individuals with different periodontal clinical conditions. *Anaerobe,* 52, 50–58. https://doi.org/10.1016/j.anaerobe.2018.05.015

Armitage, G.C. (1999) Development of a classification system for periodontal diseases and conditions. *Annals of Periodontology,* 4(1), 1–6. https://doi.org/10.1902/annals.1999.4.1.1

Armitage, G.C. (2002) Classifying periodontal diseases—a long-standing dilemma. *Periodontology 2000,* 30(1), 9–23. https://doi.org/10.1034/j.1600-0757.2002.03002.x

Arredondo, A., Àlvarez, G., Isabal, S., Teughels, W., Laleman, I., Contreras, M.J., Isbej, L., Huapaya, E., Gerardo, M.-A., Mor, C., Nart, J., Blanc, V. and León, R. (2025) Geographic influence on subgingival microbiota in health and periodontitis: a multinational shotgun metagenomic study. *Journal of Periodontal Research,* 60(9), 910–922. https://doi.org/10.1111/jre.13406

Ashraf, A. and Bruce, E.D. (2025) Differentiation and histological analysis of primary human bronchial epithelial cells cultured on transwell membranes using air-liquid interface culture. *MethodsX,* 15, 103492. https://doi.org/10.1016/j.mex.2025.103492

Assinder, S.J. (1995) Effects of pH and acid end-products on acid production in oral streptococci. *Microbial Ecology in Health and Disease,* 8(3), 113–119. https://doi.org/10.3109/08910609509140088

Azeredo, J., Azevedo, N.F., Briandet, R., Cerca, N., Coenye, T., Costa, A.R., Desvaux, M., Di Bonaventura, G., Hébraud, M., Jaglic, Z., Kačániová, M., Knøchel, S., Lourenço, A., Mergulhão, F., Meyer, R.L., Nychas, G., Simões, M., Tresse, O. and Sternberg, C. (2017) Critical review on biofilm methods. *Critical Reviews in Microbiology,* 43(3), 313–351. https://doi.org/10.1080/1040841X.2016.1208146

Babaev, E.A., Balmasova, I.P., Mkrtumyan, A.M., Kostryukova, S.N., Vakhitova, E.S., Il'ina, E.N., Tsarev, V.N., Gabibov, A.G. and Arutyunov, S.D. (2017) Metagenomic analysis of gingival sulcus microbiota and pathogenesis of periodontitis associated with type 2 diabetes mellitus. *Bulletin of Experimental Biology and Medicine,* 163(6), 718–721. https://doi.org/10.1007/s10517-017-3888-6

Babatunde, K.A., Wang, X., Hopke, A., Lannes, N., Mantel, P.-Y. and Irimia, D. (2021) Chemotaxis and swarming in differentiated HL-60 neutrophil-like cells. *Scientific Reports,* 11, 778. https://doi.org/10.1038/s41598-020-78854-6

Babcock, J.F. (1870) Periodontitis. *The American Journal of Dental Science,* 3(10), 473–476.

Baddouri, L. and Hannig, M. (2024) Probiotics as an adjunctive therapy in periodontitis treatment-reality or illusion-a clinical perspective. *npj Biofilms and Microbiomes,* 10, 148. https://doi.org/10.1038/s41522-024-00614-5

Baik, S.Y., Lim, Y.A., Kang, S.J., Ahn, S.H., Lee, W.G. and Kim, C.H. (2014) Effects of platelet lysate preparations on the proliferation of HaCaT cells. *Annals of Laboratory Medicine,* 34(1), 43–50. https://doi.org/10.3343/alm.2014.34.1.43

Balta, M.G., Papathanasiou, E., Blix, I.J. and Van Dyke, T.E. (2021) Host modulation and treatment of periodontal disease. *Journal of Dental Research,* 100(8), 798–809. https://doi.org/10.1177/0022034521995157

Bankhead, P., Loughrey, M.B., Fernandez, J.A., Dombrowski, Y., McArt, D.G., Dunne, P.D., McQuaid, S., Gray, R.T., Murray, L.J., Coleman, H.G., James, J.A., Salto-Tellez, M. and Hamilton, P.W. (2017) QuPath: open source software for digital pathology image analysis. *Scientific Reports,* 7, 16878. https://doi.org/10.1038/s41598-017-17204-5

Barth, K.R., Isabella, V.M. and Clark, V.L. (2009) Biochemical and genomic analysis of the denitrification pathway within the genus *Neisseria*. *Microbiology,* 155(12), 4093–4103. https://doi.org/10.1099/mic.0.032961-0

Bashyal, S., Seo, J.E., Keum, T., Noh, G., Choi, Y.W. and Lee, S. (2018) Facilitated permeation of insulin across TR146 cells by cholic acid derivatives-modified elastic bilosomes. *International Journal of Nanomedicine,* 13, 5173–5186. https://doi.org/10.2147/IJN.S168310

Basso, F.G., Soares, D.G., de Souza Costa, C.A. and Hebling, J. (2016) Low-level laser therapy in 3D cell culture model using gingival fibroblasts. *Lasers in Medical Science,* 31, 973–978. https://doi.org/10.1007/S10103-016-1945-4

Bedran, T.B.L., Mayer, M.P.A., Spolidorio, D.P. and Grenier, D. (2014) Synergistic anti-inflammatory activity of the antimicrobial peptides human beta-defensin-3 (hBD-3) and cathelicidin (LL-37) in a three-dimensional co-culture model of gingival epithelial cells and fibroblasts. *PLOS ONE,* 9(9), e106766. https://doi.org/10.1371/journal.pone.0106766

Belibasakis, G.N., Kast, J.I., Thurnheer, T., Akdis, C.A. and Bostanci, N. (2015) The expression of gingival epithelial junctions in response to subgingival biofilms. *Virulence,* 6(7), 704–709. https://doi.org/10.1080/21505594.2015.1081731

Belibasakis, G.N., Schmidlin, P.R. and Sahrmann, P. (2014) Molecular microbiological evaluation of subgingival biofilm sampling by paper point and curette. *APMIS,* 122(4), 347–352. https://doi.org/10.1111/apm.12151

Belibasakis, G.N., Thurnheer, T. and Bostanci, N. (2013) Interleukin-8 responses of multi-layer gingival epithelia to subgingival biofilms: role of the "red complex" species. *PLOS ONE,* 8(12), e81581. https://doi.org/10.1371/journal.pone.0081581

Bernabe, E., Marcenes, W., Abdulkader, R.S., Abreu, L.G., Afzal, S., Alhalaiqa, F.N., Al-Maweri, S., Alsharif, U., Anyasodor, A.E., Arora, A., Asgary, S., Ashraf, T., Balasubramanian, M., Banakar, M., Barrow, A., Bashiri, A., Belay, S.A., Belgaumi, U.I., Berhie, A.Y., Bhardwaj, P., Bhaskar, S., Bijani, A., Bouaoud, S., Cao, Y., Chaurasia, A., Chen, M.X., Chu, D.-T., Cruz-Martins, N., Dadras, O., Dai, X., Diaz, D., Du, M., Ekholuenetale, M., Ekundayo, T.C., El Tantawi, M., Elhadi, M., Fagbamigbe, A.F., Farshidfar, N., Fatehizadeh, A., Fischer, F., Folayan, M.O., Gaewkhiew, P., Gajdács, M., Golechha, M., Gupta, B., Gupta, S., Hagins, H., Halboub, E.S., Hamidi, S., Hariyani, N., Hay, S.I., Heidari, M., Herrera-Serna, B.Y., Heyi, D.Z., Hostiuc, S., Humphrey, K.M., Ibitoye, S.E., Ilic, M.D., Isola, G., Kandaswamy, E., Kantar, R.S., Kaur, N., Kemmer, L., Khader, Y.S., Khateri, S., Kisa, A., Krishan, K., Kruger, E., Lalloo, R., Li, A., Lim, S.S., Mestrovic, T., Mokdad, A.H., Moreira, R.S., Morrison, S.D., Murray, C.J.L., Natto, Z.S., Nayak, B.P., Nguyen, T., Nguyen, V.T., Omotayo, A.O., Padron-Monedero, A., Patel, J., Patil, S., Pawar, S., Petcu, I.-R., Qattea, I., Rahman, M., Ratan, Z.A., Riad, A., S, M., S N, C., Sabour, S., Saheb Sharif-Askari, F., Sahebkar, A., Sakshaug, J.W., Samy, A.M., Sarode, S.C., Sawhney, M., Schwendicke, F., et al. (2025) Trends in the global, regional, and national burden of oral conditions from 1990 to 2021: a systematic analysis for the Global Burden of Disease Study 2021. *The Lancet,* 405(10482), 897–910. https://doi.org/10.1016/S0140-6736(24)02811-3

Bertolini, M., Costa, R.C., Barão, V.A., Villar, C.C., Retamal-Valdes, B., Feres, M. and Silva Souza, J.G. (2022) Oral microorganisms and biofilms: new insights to defeat the main etiologic factor of oral diseases. *Microorganisms,* 10(12), 2413. https://doi.org/10.3390/microorganisms10122413

Beyer, K., Brandt, B.W., Buijs, M.J., Brun, J.G., Crielaard, W., Bolstad, A.I. and Zaura, E. (2017) Comparison of paperpoint and curette sampling of subgingival microbiome composition as analyzed by 16S rRNA gene amplicon sequencing. *Journal of Oral Microbiology,* 9(Suppl. 1), 1325260. https://doi.org/10.1080/20002297.2017.1325260

Bierbaumer, L., Schwarze, U.Y., Gruber, R. and Neuhaus, W. (2018) Cell culture models of oral mucosal barriers: a review with a focus on applications, culture conditions and barrier properties. *Tissue Barriers,* 6(3), e1479568. https://doi.org/10.1080/21688370.2018.1479568

Bizhang, M., Ellerbrock, B., Preza, D., Raab, W., Singh, P., Beikler, T., Henrich, B. and Zimmer, S. (2011) Detection of nine microorganisms from the initial carious root lesions using a TaqMan-based real-time PCR. *Oral Diseases,* 17(7), 642–652. https://doi.org/10.1111/j.1601-0825.2011.01815.x

Blanter, M., Gouwy, M. and Struyf, S. (2021) Studying neutrophil function *in vitro*: cell models and environmental factors. *Journal of Inflammation Research,* 14, 141–162. https://doi.org/10.2147/JIR.S284941

Bloch, S., Hager-Mair, F.F., Andrukhov, O. and Schaffer, C. (2024) Oral streptococci: modulators of health and disease. *Frontiers in Cellular and Infection Microbiology,* 14, 1357631. https://doi.org/10.3389/fcimb.2024.1357631

Bluhmki, T., Bitzer, S., Gindele, J.A., Schruf, E., Kiechle, T., Webster, M., Schymeinsky, J., Ries, R., Gantner, F., Bischoff, D., Garnett, J. and Heilker, R. (2020) Development of a miniaturized 96-Transwell air-liquid interface human small airway epithelial model. *Scientific Reports,* 10, 13022. https://doi.org/10.1038/s41598-020-69948-2

Boisen, G., Davies, J.R. and Neilands, J. (2021) Acid tolerance in early colonizers of oral biofilms. *BMC Microbiology,* 21, 45. https://doi.org/10.1186/s12866-021-02089-2

Boribong, B.P., Lenzi, M.J., Li, L. and Jones, C.N. (2019) Super-low dose lipopolysaccharide dysregulates neutrophil migratory decision-making. *Frontiers in Immunology,* 10, 359. https://doi.org/10.3389/fimmu.2019.00359

Bosshardt, D.D. and Lang, N.P. (2005) The junctional epithelium: from health to disease. *Journal of Dental Research,* 84(1), 9–20. https://doi.org/10.1177/154405910508400102

Botelho, J., Machado, V., Leira, Y., Proenca, L., Chambrone, L. and Mendes, J.J. (2022) Economic burden of periodontitis in the United States and Europe: an updated estimation. *Journal of Periodontology,* 93(3), 373–379. https://doi.org/10.1002/JPER.21-0111

Bouchery, T. and Harris, N. (2019) Neutrophil-macrophage cooperation and its impact on tissue repair. *Immunology and Cell Biology,* 97(3), 289–298. https://doi.org/10.1111/imcb.12241

Bouti, P., Webbers, S.D.S., Fagerholm, S.C., Alon, R., Moser, M., Matlung, H.L. and Kuijpers, T.W. (2021) ß2 integrin signaling cascade in neutrophils: more than a single function. *Frontiers in Immunology,* 11, 619925. https://doi.org/10.3389/fimmu.2020.619925

Brown, J.L. (2020) *Enrichment of innate lymphoid cell populations in gingival tissue: cellular responses in oral health and disease.* PhD thesis, University of the West of Scotland.

Brown, J.L., Butcher, M.C., Veena, C.L.R., Chogule, S., Johnston, W. and Ramage, G. (2023) Generation of multispecies oral bacteria biofilm models. In: Seymour, G.J., Cullinan, M.P., Heng, N.C. and Cooper, P.R. (eds.) *Oral Biology.* New York, NY: Humana Press, pp. 187–199. https://doi.org/10.1007/978-1-0716-2780-8_12

Brown, J.L., Johnston, W., Delaney, C., Rajendran, R., Butcher, J., Khan, S., Bradshaw, D., Ramage, G. and Culshaw, S. (2019) Biofilm-stimulated epithelium modulates the inflammatory responses in co-cultured immune cells. *Scientific Reports,* 9, 15779. https://doi.org/10.1038/s41598-019-52115-7

Bryan, N.S. and Grisham, M.B. (2007) Methods to detect nitric oxide and its metabolites in biological samples. *Free Radical Biology and Medicine,* 43(5), 645–657. https://doi.org/10.1016/j.freeradbiomed.2007.04.026

Bunaes, D.F., Mustafa, M., Mohamed, H.G., Lie, S.A. and Leknes, K.N. (2017) The effect of smoking on inflammatory and bone remodeling markers in gingival crevicular fluid and subgingival microbiota following periodontal therapy. *Journal of Periodontal Research,* 52(4), 713–724. https://doi.org/10.1111/jre.12438

Buskermolen, J.K., Reijnders, C.M., Spiekstra, S.W., Steinberg, T., Kleverlaan, C.J., Feilzer, A.J., Bakker, A.D. and Gibbs, S. (2016) Development of a full-thickness human gingiva equivalent constructed from immortalized keratinocytes and fibroblasts. *Tissue Engineering Part C: Methods,* 22(8), 781–791. https://doi.org/10.1089/ten.TEC.2016.0066

Bustin, S.A., Benes, V., Garson, J.A., Hellemans, J., Huggett, J., Kubista, M., Mueller, R., Nolan, T., Pfaffl, M.W., Shipley, G.L., Vandesompele, J. and Wittwer, C.T. (2009) The MIQE guidelines: minimum information for publication of quantitative real-time PCR experiments. *Clinical Chemistry,* 55(4), 611–622. https://doi.org/10.1373/clinchem.2008.112797

Byrne, S.J., Chang, D., Adams, G.G., Butler, C.A., Reynolds, E.C., Darby, I.B. and Dashper, S.G. (2022) Microbiome profiles of non-responding and responding paired periodontitis sites within the same participants following non-surgical treatment. *Journal of Oral Microbiology,* 14(1), 2043595. https://doi.org/10.1080/20002297.2022.2043595

Camacho-Fernandez, C., Hervas, D., Rivas-Sendra, A., Marin, M.P. and Segui-Simarro, J.M. (2018) Comparison of six different methods to calculate cell densities. *Plant Methods,* 14, 30. https://doi.org/10.1186/s13007-018-0297-4

Camelo-Castillo, A.J., Mira, A., Pico, A., Nibali, L., Henderson, B., Donos, N. and Tomas, I. (2015) Subgingival microbiota in health compared to periodontitis and the influence of smoking. *Frontiers in Microbiology,* 6, 119. https://doi.org/10.3389/fmicb.2015.00119

Canut-Delgado, N., Giovannoni, M.L. and Chimenos-Küstner, E. (2021) Are probiotics a possible treatment of periodontitis? Probiotics against periodontal disease: a systematic review. *British Dental Journal,* 231(10). https://doi.org/10.1038/s41415-021-3624-5

Cardoso, L.M., Pansani, T.N., Hebling, J., de Souza Costa, C.A. and Basso, F.G. (2020) Photobiomodulation of inflammatory-cytokine-related effects in a 3-D culture model with gingival fibroblasts. *Lasers in Medical Science,* 35, 1205–1212. https://doi.org/10.1007/S10103-020-02974-8

Carrion, J., Scisci, E., Miles, B., Sabino, G.J., Zeituni, A.E., Gu, Y., Bear, A., Genco, C.A., Brown, D.L. and Cutler, C.W. (2012) Microbial carriage state of peripheral blood dendritic cells (DCs) in chronic periodontitis influences DC differentiation, atherogenic potential. *The Journal of Immunology,* 189(6), 3178–3187. https://doi.org/10.4049/jimmunol.1201053

Casale, T.B. and Abbas, M.K. (1990) Comparison of leukotriene B4-induced neutrophil migration through different cellular barriers. *American Journal of Physiology-Cell Physiology,* 258(4), C639–C647. https://doi.org/10.1152/ajpcell.1990.258.4.C639

Casanova, L., Hughes, F.J. and Preshaw, P.M. (2014) Diabetes and periodontal disease: a two-way relationship. *British Dental Journal,* 217(8), 433–437. https://doi.org/10.1038/sj.bdj.2014.907

Caselli, E., Fabbri, C., D'Accolti, M., Soffritti, I., Bassi, C., Mazzacane, S. and Franchi, M. (2020) Defining the oral microbiome by whole-genome sequencing and resistome analysis: the complexity of the healthy picture. *BMC Microbiology,* 20, 120. https://doi.org/10.1186/s12866-020-01801-y

Castellani, C.A., Longchamps, R.J., Sun, J., Guallar, E. and Arking, D.E. (2020) Thinking outside the nucleus: mitochondrial DNA copy number in health and disease. *Mitochondrion,* 53, 214–223. https://doi.org/10.1016/j.mito.2020.06.004

Castellani, S., D'Oria, S., Diana, A., Polizzi, A.M., Di Gioia, S., Mariggiò, M.A., Guerra, L., Favia, M., Vinella, A., Leonetti, G., De Venuto, D., Gallo, C., Montemurro, P. and Conese, M. (2019) G-CSF and GM-CSF modify neutrophil functions at concentrations found in cystic fibrosis. *Scientific Reports,* 9, 12937. https://doi.org/10.1038/s41598-019-49419-z

Castro, J., Lima, Â., Sousa, L.G.V., Rosca, A.S., Muzny, C.A. and Cerca, N. (2022) Crystal violet staining alone is not adequate to assess synergism or antagonism in multi-species biofilms of bacteria associated with bacterial vaginosis. *Frontiers in Cellular and Infection Microbiology,* 11, 795797. https://doi.org/10.3389/fcimb.2021.795797

Caton, J.G., Armitage, G., Berglundh, T., Chapple, I.L.C., Jepsen, S., Kornman, K.S., Mealey, B.L., Papapanou, P.N., Sanz, M. and Tonetti, M.S. (2018) A new classification scheme for periodontal and peri-implant diseases and conditions - Introduction and key changes from the 1999 classification. *Journal of Clinical Periodontology,* 45(Suppl. 20), S1–S8. https://doi.org/10.1111/jcpe.12935

Catz, S.D. and McLeish, K.R. (2020) Therapeutic targeting of neutrophil exocytosis. *Journal of Leukocyte Biology,* 107(3), 393–408. https://doi.org/10.1002/JLB.3RI0120-645R

Cavalla, F., Biguetti, C.C., Melchiades, J.L., Tabanez, A.P., Azevedo, M.C.S., Trombone, A.P.F., Faveri, M., Feres, M. and Garlet, G.P. (2018) Genetic association with subgingival bacterial colonization in chronic periodontitis. *Genes,* 9(6), 271. https://doi.org/10.3390/genes9060271

Cázares-Preciado, J.A., Cruz-Cárdenas, J.A., López-Arredondo, A., Gallardo-Camarena, M.V. and Brunck, M.E.G. (2025) IMDM-20 enhances neutrophilic features during 1.3% DMSO-mediated differentiation of HL-60 cells. *Biochemistry and Biophysics Reports,* 43, 102215. https://doi.org/10.1016/j.bbrep.2025.102215

Cázares-Preciado, J.A., López-Arredondo, A., Cruz-Cárdenas, J.A., Luévano-Martínez, L.A., García-Rivas, G., Prado-García, H. and Brunck, M.E.G. (2024) Metabolic features of neutrophilic differentiation of HL-60 cells in hyperglycemic environments. *BMJ Open Diabetes Research & Care,* 12(4), e004181. https://doi.org/10.1136/bmjdrc-2024-004181

Chang, A.M., Kantrong, N. and Darveau, R.P. (2021) Maintaining homeostatic control of periodontal epithelial tissue. *Periodontology 2000,* 86(1), 188–200. https://doi.org/10.1111/prd.12369

Chapple, I.L., Bouchard, P., Cagetti, M.G., Campus, G., Carra, M.C., Cocco, F., Nibali, L., Hujoel, P., Laine, M.L., Lingstrom, P., Manton, D.J., Montero, E., Pitts, N., Range, H., Schlueter, N., Teughels, W., Twetman, S., Van Loveren, C., Van der Weijden, F., Vieira, A.R. and Schulte, A.G. (2017) Interaction of lifestyle, behaviour or systemic diseases with dental caries and periodontal diseases: consensus report of group 2 of the joint EFP/ORCA workshop on the boundaries between caries and periodontal diseases. *Journal of Clinical Periodontology,* 44(Suppl. 18), S39–S51. https://doi.org/10.1111/jcpe.12685

Chapple, I.L.C., Hirschfeld, J., Kantarci, A., Wilensky, A. and Shapira, L. (2023) The role of the host–neutrophil biology. *Periodontology 2000,* 00, 1–47. https://doi.org/10.1111/prd.12490

Chapple, I.L.C., Mealey, B.L., Van Dyke, T.E., Bartold, P.M., Dommisch, H., Eickholz, P., Geisinger, M.L., Genco, R.J., Glogauer, M., Goldstein, M., Griffin, T.J., Holmstrup, P., Johnson, G.K., Kapila, Y., Lang, N.P., Meyle, J., Murakami, S., Plemons, J., Romito, G.A., Shapira, L., Tatakis, D.N., Teughels, W., Trombelli, L., Walter, C., Wimmer, G., Xenoudi, P. and Yoshie, H. (2018) Periodontal health and gingival diseases and conditions on an intact and a reduced periodontium: consensus report of workgroup 1 of the 2017 World Workshop on the Classification of Periodontal and Peri-Implant Diseases and Conditions. *Journal of Clinical Periodontology,* 45(Suppl. 20), S68–S77. https://doi.org/10.1111/jcpe.12940

Chen, C., Hemme, C., Beleno, J., Shi, Z.J., Ning, D., Qin, Y., Tu, Q., Jorgensen, M., He, Z., Wu, L. and Zhou, J. (2018) Oral microbiota of periodontal health and disease and their changes after nonsurgical periodontal therapy. *The ISME Journal,* 12(5), 1210–1224. https://doi.org/10.1038/s41396-017-0037-1

Chen, C.-L., Wang, Y., Sesaki, H. and Iijima, M. (2012) Myosin I links PIP_3 signaling to remodeling of the actin cytoskeleton in chemotaxis. *Science Signaling,* 5(209), ra10. https://doi.org/10.1126/scisignal.2002446

Chen, T., Marsh, P.D. and Al-Hebshi, N.N. (2022) SMDI: an index for measuring subgingival microbial dysbiosis. *Journal of Dental Research,* 101(3), 331–338. https://doi.org/10.1177/00220345211035775

Chew, R.J.J., Goh, C.E., Sriram, G., Preshaw, P.M. and Tan, K.S. (2023) Microbial biomarkers as a predictor of periodontal treatment response: A systematic review. *Journal of Periodontal Research,* 58(6), 1113–1127. https://doi.org/10.1111/jre.13188

Chu, K.K., Kusek, M.E., Liu, L., Som, A., Yonker, L.M., Leung, H., Cui, D., Ryu, J., Eaton, A.D., Tearney, G.J. and Hurley, B.P. (2017) Illuminating dynamic neutrophil trans-epithelial migration with micro-optical coherence tomography. *Scientific Reports,* 8, 45789. https://doi.org/10.1038/srep45789

Cieplik, F., Deng, D., Crielaard, W., Buchalla, W., Hellwig, E., Al-Ahmad, A. and Maisch, T. (2018) Antimicrobial photodynamic therapy - what we know and what we don't. *Critical Reviews in Microbiology,* 44(5), 571–589. https://doi.org/10.1080/1040841X.2018.1467876

Collins, J.R., Arredondo, A., Roa, A., Valdez, Y., Leon, R. and Blanc, V. (2016) Periodontal pathogens and tetracycline resistance genes in subgingival biofilm of periodontally healthy and diseased Dominican adults. *Clinical Oral Investigations,* 20(2), 349–356. https://doi.org/10.1007/s00784-015-1516-2

Collins, S.J., Gallo, R.C. and Gallagher, R.E. (1977) Continuous growth and differentiation of human myeloid leukaemic cells in suspension culture. *Nature,* 270(5635), 347–349. https://doi.org/10.1038/270347a0

Connolly, E., Millhouse, E., Doyle, R., Culshaw, S., Ramage, G. and Moran, G.P. (2017) The *Porphyromonas gingivalis* hemagglutinins HagB and HagC are major mediators of adhesion and biofilm formation. *Molecular Oral Microbiology,* 32(1), 35–47. https://doi.org/10.1111/omi.12151

Cooper, K.N., Terekhova, M., Potempa, B., D'Aubeterre, A., Timbol, J., Chen, S.A., Dufour, A., Jin, S., Artyomov, M.N., Potempa, J. and Bagaitkar, J. (2025) The trapping of live neutrophils by macrophages during infection. *Cell Death & Disease,* 16, 488. https://doi.org/10.1038/s41419-025-07808-5

Coretti, L., Cuomo, M., Florio, E., Palumbo, D., Keller, S., Pero, R., Chiariotti, L., Lembo, F. and Cafiero, C. (2017) Subgingival dysbiosis in smoker and

non-smoker patients with chronic periodontitis. *Molecular Medicine Reports,* 15(4), 2007–2014. https://doi.org/10.3892/mmr.2017.6269

Costa, F.O., Guimaraes, A.N., Cota, L.O., Pataro, A.L., Segundo, T.K., Cortelli, S.C. and Costa, J.E. (2009) Impact of different periodontitis case definitions on periodontal research. *Journal of Oral Science,* 51(2), 199–206. https://doi.org/10.2334/josnusd.51.199

Costerton, J.W., Irvin, R.T. and Cheng, K.J. (1981) The role of bacterial surface structures in pathogenesis. *Critical Reviews in Microbiology,* 8(4), 303–338. https://doi.org/10.3109/10408418109085082

Cotter, M.J., Norman, K.E., Hellewell, P.G. and Ridger, V.C. (2001) A novel method for isolation of neutrophils from murine blood using negative immunomagnetic separation. *American Journal of Pathology,* 159(2), 473–481. https://doi.org/10.1016/s0002-9440(10)61719-1

Cozlin, A., Barthelemy, S., Garnotel, R., Antonicelli, F., Kaplan, H., Hornebeck, W. and Lorimier, S. (2006) Elastolysis induces collagenolysis in a gingival lamina propria model. *Journal of Dental Research,* 85(8), 745–750. https://doi.org/10.1177/154405910608500811

Creamer, H.R., Hunter, N., Bullock, W.W. and Gabler, W.L. (1991) Concurrent lipopolysaccharide enhances chemotactic response of human polymorphonuclear leukocytes to bacterial chemotaxin. *Inflammation,* 15(3), 201–211. https://doi.org/10.1007/BF00918646

Culture Collections (n.d.-a) *Cell line passage numbers explained* [Online]. Available at: https://www.culturecollections.org.uk/training-and-support/cell-line-passage-numbers-explained/ (Accessed: 1 June 2026).

Culture Collections (n.d.-b) *Cell lines FAQs* [Online]. Available at: https://www.culturecollections.org.uk/training-and-support/frequently-asked-questions/cell-lines-faqs/ (Accessed: 22 May 2026).

D'Aiuto, F., Ready, D., Parkar, M. and Tonetti, M.S. (2005) Relative contribution of patient-, tooth-, and site-associated variability on the clinical outcomes of subgingival debridement. I. Probing depths. *Journal of Periodontology,* 76(3), 398–405. https://doi.org/10.1902/jop.2005.76.3.398

da Silva, M.K., de Carvalho, A.C.G., Alves, E.H.P., da Silva, F.R.P., Pessoa, L.D.S. and Vasconcelos, D.F.P. (2017) Genetic factors and the risk of periodontitis development: findings from a systematic review composed of 13 studies of meta-analysis with 71,531 participants. *International Journal of Dentistry,* 2017, 1914073. https://doi.org/10.1155/2017/1914073

Dabdoub, S.M., Ganesan, S.M. and Kumar, P.S. (2016) Comparative metagenomics reveals taxonomically idiosyncratic yet functionally congruent communities in periodontitis. *Scientific Reports,* 6, 38993. https://doi.org/10.1038/srep38993

Dabija-Wolter, G., Bakken, V., Cimpan, M.R., Johannessen, A.C. and Costea, D.E. (2013) *In vitro* reconstruction of human junctional and sulcular epithelium. *Journal of Oral Pathology & Medicine,* 42(5), 396–404. https://doi.org/10.1111/JOP.12005

Dahlén, G., Gmür, R. and Yoshino, T. (2007) Phenotypes, serotypes and antibiotic susceptibility of Swedish *Porphyromonas gingivalis* isolates from periodontitis and periodontal abscesses. *Oral Microbiology and Immunology,* 22(2), 80–86. https://doi.org/10.1111/j.1399-302X.2007.00324.x

Darveau, R.P. (2010) Periodontitis: a polymicrobial disruption of host homeostasis. *Nature Reviews Microbiology,* 8(7), 481–490. https://doi.org/10.1038/nrmicro2337

Davey, H.M. (2011) Life, death, and in-between: meanings and methods in microbiology. *Applied and Environmental Microbiology,* 77(16), 5571–5576. https://doi.org/10.1128/AEM.00744-11

de Sousa, E.T., de Araújo, J.S.M., Pires, A.C. and Lira Dos Santos, E.J. (2021) Local delivery natural products to treat periodontitis: a systematic review and meta-analysis. *Clinical Oral Investigations,* 25(7), 4599–4619. https://doi.org/10.1007/s00784-021-03774-2

Dean, R. (2017) The periodontal ligament: development, anatomy and function. *Oral Health and Dental Management*, 16(6), 1–7. Available at: https://www.walshmedicalmedia.com/open-access/the-periodontal-ligament-development-anatomy-and-function.pdf (Accessed: 20 February 2026).

DeForge, L.E., Kenney, J.S., Jones, M.L., Warren, J.S. and Remick, D.G. (1992) Biphasic production of IL-8 in lipopolysaccharide (LPS)-stimulated human whole blood. Separation of LPS- and cytokine-stimulated components using anti-tumor necrosis factor and anti-IL-1 antibodies. *The Journal of Immunology,* 148(7), 2133–2141. https://doi.org/10.4049/jimmunol.148.7.2133

Delgado-Rizo, V., Martinez-Guzman, M.A., Iniguez-Gutierrez, L., Garcia-Orozco, A., Alvarado-Navarro, A. and Fafutis-Morris, M. (2017) Neutrophil extracellular traps and its implications in inflammation: an overview. *Frontiers in Immunology,* 8, 81. https://doi.org/10.3389/fimmu.2017.00081

Delima, A.J. and Van Dyke, T.E. (2003) Origin and function of the cellular components in gingival crevice fluid. *Periodontology 2000,* 31, 55–76. https://doi.org/10.1034/J.1600-0757.2003.03105.X

Detmers, P.A., Lo, S.K., Olsen-Egbert, E., Walz, A., Baggiolini, M. and Cohn, Z.A. (1990) Neutrophil-activating protein 1/interleukin 8 stimulates the binding activity of the leukocyte adhesion receptor CD11b/CD18 on human neutrophils. *Journal of Experimental Medicine,* 171(4), 1155–1162. https://doi.org/10.1084/jem.171.4.1155

Diaz, P.I., Chalmers, N.I., Rickard, A.H., Kong, C., Milburn, C.L., Palmer, R.J., Jr. and Kolenbrander, P.E. (2006) Molecular characterization of subject-specific oral microflora during initial colonization of enamel. *Applied and Environmental Microbiology,* 72(4), 2837–2848. https://doi.org/10.1128/AEM.72.4.2837-2848.2006

Doel, J.J., Benjamin, N., Hector, M.P., Rogers, M. and Allaker, R.P. (2005) Evaluation of bacterial nitrate reduction in the human oral cavity. *European Journal of Oral Sciences,* 113(1), 14–19. https://doi.org/10.1111/j.1600-0722.2004.00184.x.

Dominy, S.S., Lynch, C., Ermini, F., Benedyk, M., Marczyk, A., Konradi, A., Nguyen, M., Haditsch, U., Raha, D., Griffin, C., Holsinger, L.J., Arastu-Kapur, S., Kaba, S., Lee, A., Ryder, M.I., Potempa, B., Mydel, P., Hellvard, A., Adamowicz, K., Hasturk, H., Walker, G.D., Reynolds, E.C., Faull, R.L.M., Curtis, M.A., Dragunow, M. and Potempa, J. (2019) *Porphyromonas gingivalis* in Alzheimer's disease brains: evidence for disease causation and treatment with small-molecule inhibitors. *Science Advances,* 5(1), eaau3333. https://doi.org/10.1126/sciadv.aau3333

Donati, C., Zolfo, M., Albanese, D., Tin Truong, D., Asnicar, F., Iebba, V., Cavalieri, D., Jousson, O., De Filippo, C., Huttenhower, C. and Segata, N. (2016) Uncovering oral *Neisseria* tropism and persistence using metagenomic sequencing. *Nature Microbiology,* 1(7), 16070. https://doi.org/10.1038/nmicrobiol.2016.70

Dongari-Bagtzoglou, A. and Kashleva, H. (2006) Development of a highly reproducible three-dimensional organotypic model of the oral mucosa. *Nature Protocols,* 1(4), 2012–2018. https://doi.org/10.1038/nprot.2006.323

Donos, N., Calciolari, E., Brusselaers, N., Goldoni, M., Bostanci, N. and Belibasakis, G.N. (2020) The adjunctive use of host modulators in non-surgical periodontal therapy. A systematic review of randomized, placebo-controlled clinical studies. *Journal of Clinical Periodontology,* 47(Suppl. 22), 199–238. https://doi.org/10.1111/jcpe.13232

Downey, G.P., Doherty, D.E., Schwab, B., 3rd, Elson, E.L., Henson, P.M. and Worthen, G.S. (1990) Retention of leukocytes in capillaries: role of cell size and deformability. *Journal of Applied Physiology,* 69(5), 1767–1778. https://doi.org/10.1152/jappl.1990.69.5.1767

Duran-Pinedo, A.E., Chen, T., Teles, R., Starr, J.R., Wang, X., Krishnan, K. and Frias-Lopez, J. (2014) Community-wide transcriptome of the oral microbiome in subjects with and without periodontitis. *The ISME Journal,* 8(8), 1659–1672. https://doi.org/10.1038/ismej.2014.23

Dyavar, S.R., Ye, Z., Byrareddy, S.N., Scarsi, K.K., Winchester, L.C., Weinhold, J.A., Fletcher, C.V. and Podany, A.T. (2018) Normalization of cell associated antiretroviral drug concentrations with a novel RPP30 droplet digital PCR assay. *Scientific Reports,* 8, 3626. https://doi.org/10.1038/s41598-018-21882-0

Easter, Q.T., Fernandes Matuck, B., Beldorati Stark, G., Worth, C.L., Predeus, A.V., Fremin, B., Huynh, K., Ranganathan, V., Ren, Z., Pereira, D., Rupp, B.T., Weaver, T., Miller, K., Perez, P., Hasuike, A., Chen, Z., Bush, M., Qu, X., Lee, J., Randell, S.H., Wallet, S.M., Sequeira, I., Koo, H., Tyc, K.M., Liu, J., Ko, K.I., Teichmann, S.A. and Byrd, K.M. (2024) Single-cell and spatially resolved interactomics of tooth-associated keratinocytes in periodontitis. *Nature Communications,* 15, 5016. https://doi.org/10.1038/s41467-024-49037-y

Ebadian, A.R., Kadkhodazadeh, M., Zarnegarnia, P. and Dahlen, G. (2012) Bacterial analysis of peri-implantitis and chronic periodontitis in Iranian subjects. *Acta Medica Iranica,* 50(7), 486–492.

Ebersole, J.L., Graves, C.L., Gonzalez, O.A., Dawson, D., 3rd, Morford, L.A., Huja, P.E., Hartsfield, J.K., Jr., Huja, S.S., Pandruvada, S. and Wallet, S.M. (2016) Aging, inflammation, immunity and periodontal disease. *Periodontology 2000,* 72(1), 54–75. https://doi.org/10.1111/prd.12135

Edmisson, J.S., Tian, S., Armstrong, C.L., Vashishta, A., Klaes, C.K., Miralda, I., Jimenez-Flores, E., Le, J., Wang, Q., Lamont, R.J. and Uriarte, S.M. (2018) *Filifactor alocis* modulates human neutrophil antimicrobial functional responses. *Cellular Microbiology,* 20(6), e12829. https://doi.org/10.1111/cmi.12829

Eickholz, P., Kaltschmitt, J., Berbig, J., Reitmeir, P. and Pretzl, B. (2008) Tooth loss after active periodontal therapy. 1: patient-related factors for risk, prognosis, and quality of outcome. *Journal of Clinical Periodontology,* 35(2), 165–174. https://doi.org/10.1111/j.1600-051X.2007.01184.x

Elabdeen, H.R., Mustafa, M., Hasturk, H., Klepac-Ceraj, V., Ali, R.W., Paster, B.J., Van Dyke, T. and Bolstad, A.I. (2015) Subgingival microbial profiles of Sudanese patients with aggressive periodontitis. *Journal of Periodontal Research,* 50(5), 674–682. https://doi.org/10.1111/jre.12250

Ellen, R.P. (1976) Establishment and distribution of *Actinomyces viscosus* and *Actinomyces naeslundii* in the human oral cavity. *Infection and Immunity,* 14(5), 1119–1124. https://doi.org/10.1128/iai.14.5.1119-1124.1976

Erbeck, K., Klein, J.B. and McLeish, K.R. (1993) Differential uncoupling of chemoattractant receptors from G proteins in retinoic acid-differentiated HL-60 granulocytes. *The Journal of Immunology,* 150(5), 1913–1921.

Ergin, C., Can, R. and Kaya, C. (2002) Catalase-negative *Rothia dentocariosa*: evaluation of additional descriptive tests. *Mikrobiyoloji Bülteni,* 36(1), 49–55.

Erlandsen, S.L., Kristich, C.J., Dunny, G.M. and Wells, C.L. (2004) High-resolution visualization of the microbial glycocalyx with low-voltage scanning electron microscopy: dependence on cationic dyes. *The Journal of Histochemistry and Cytochemistry,* 52(11), 1427–1435. https://doi.org/10.1369/jhc.4A6428.2004

Escapa, I.F., Chen, T., Huang, Y., Gajare, P., Dewhirst, F.E. and Lemon, K.P. (2018) New insights into human nostril microbiome from the expanded human oral microbiome database (eHOMD): a resource for the microbiome of the human aerodigestive tract. *mSystems,* 3(6), e00187-00118. https://doi.org/10.1128/mSystems.00187-18

Esposito, M.V., Nardelli, C., Granata, I., Pagliuca, C., D'Argenio, V., Russo, I., Guarracino, M.R., Salvatore, P., Del Vecchio Blanco, G., Ciacci, C. and Sacchetti, L. (2019) Setup of quantitative PCR for oral *Neisseria* spp. evaluation in celiac disease diagnosis. *Diagnostics,* 10(1), 12. https://doi.org/10.3390/diagnostics10010012

Evani, S.J., Karna, S.L.R., Seshu, J. and Leung, K.P. (2020) Pirfenidone regulates LPS mediated activation of neutrophils. *Scientific Reports,* 10, 19936. https://doi.org/10.1038/s41598-020-76271-3

Exterkate, R.A.M., Crielaard, W. and Ten Cate, J.M. (2010) Different response to amine fluoride by *Streptococcus mutans* and polymicrobial biofilms in a novel high-throughput active attachment model. *Caries Research,* 44(4), 372–379. https://doi.org/10.1159/000316541

Fan, J., Schiemer, T., Vaska, A., Jahed, V. and Klavins, K. (2024) Cell via cell viability assay changes cellular metabolic characteristics by intervening with glycolysis and pentose phosphate pathway. *Chemical Research in Toxicology,* 37(2), 208–211. https://doi.org/10.1021/acs.chemrestox.3c00339

Faurschou, M. and Borregaard, N. (2003) Neutrophil granules and secretory vesicles in inflammation. *Microbes and Infection,* 5(14), 1317–1327. https://doi.org/10.1016/j.micinf.2003.09.008

Feres, M., Retamal-Valdes, B., Gonçalves, C., Figueiredo, L.C. and Teles, F. (2021) Did Omics change periodontal therapy? *Periodontology 2000,* 85(1), 182–209. https://doi.org/10.1111/prd.12358

Ferrà-Cañellas, M.d.M., Munar-Bestard, M., Garcia-Sureda, L., Lejeune, B., Ramis, J.M. and Monjo, M. (2021) BMP4 micro-immunotherapy increases collagen deposition and reduces PGE2 release in human gingival fibroblasts and increases tissue viability of engineered 3D gingiva under inflammatory conditions. *Journal of Periodontology,* 92, 1448–1459. https://doi.org/10.1002/JPER.20-0552

Fouchard, J., Wyatt, T.P.J., Proag, A., Lisica, A., Khalilgharibi, N., Recho, P., Suzanne, M., Kabla, A. and Charras, G. (2020) Curling of epithelial monolayers reveals coupling between active bending and tissue tension. *Proceedings of the National Academy of Sciences of the United States of America,* 117(17), 9377–9383. https://doi.org/10.1073/pnas.1917838117

Franceschi, C., Bonafe, M., Valensin, S., Olivieri, F., De Luca, M., Ottaviani, E. and De Benedictis, G. (2000) Inflamm-aging. An evolutionary perspective

on immunosenescence. *Annals of the New York Academy of Sciences,* 908, 244–254. https://doi.org/10.1111/j.1749-6632.2000.tb06651.x

Frevert, C.W., Wong, V.A., Goodman, R.B., Goodwin, R. and Martin, T.R. (1998) Rapid fluorescence-based measurement of neutrophil migration *in vitro*. *Journal of Immunological Methods,* 213(1), 41–52. https://doi.org/10.1016/S0022-1759(98)00016-7

Friedman, M.T., Barber, P.M., Mordan, N.J. and Newman, H.N. (1992) The "plaque-free zone" in health and disease: a scanning electron microscope study. *Journal of Periodontology,* 63(11), 890–896. https://doi.org/10.1902/jop.1992.63.11.890

Fu, Y.W., Li, X.X., Xu, H.Z., Gong, Y.Q. and Yang, Y. (2016) Effects of periodontal therapy on serum lipid profile and proinflammatory cytokines in patients with hyperlipidemia: a randomized controlled trial. *Clinical Oral Investigations,* 20(6), 1263–1269. https://doi.org/10.1007/s00784-015-1621-2

Fukuda, S., Akatsu, T., Fujii, A., Kawano, S., Minegishi, Y. and Ota, N. (2024) Commensal *Neisseria* inhibit *Porphyromonas gingivalis* invasion of gingival epithelial cells. *Oral Health & Preventive Dentistry,* 22, 609–616. https://doi.org/10.3290/j.ohpd.b5866430

Gaetti-Jardim, E., Jr., Pereira, M.F., Vieira, E.M., Schweitzer, C.M., Okamoto, A.C. and Avila-Campos, M.J. (2015) Occurrence of periodontal pathogens in ethnic groups from a native Brazilian reservation. *Archives of Oral Biology,* 60(6), 959–965. https://doi.org/10.1016/j.archoralbio.2015.01.002

Gaffen, S.L. and Moutsopoulos, N.M. (2020) Regulation of host-microbe interactions at oral mucosal barriers by type 17 immunity. *Science Immunology,* 5(43), eaau4594. https://doi.org/10.1126/sciimmunol.aau4594

Galimanas, V., Hall, M.W., Singh, N., Lynch, M.D., Goldberg, M., Tenenbaum, H., Cvitkovitch, D.G., Neufeld, J.D. and Senadheera, D.B. (2014) Bacterial community composition of chronic periodontitis and novel oral sampling sites for detecting disease indicators. *Microbiome,* 2, 32. https://doi.org/10.1186/2049-2618-2-32

Gallagher, R., Collins, S., Trujillo, J., McCredie, K., Ahearn, M., Tsai, S., Metzgar, R., Aulakh, G., Ting, R., Ruscetti, F. and Gallo, R. (1979) Characterization of the continuous, differentiating myeloid cell line (HL-60) from a patient with acute promyelocytic leukemia. *Blood,* 54(3), 713–733.

Gavriiloglou, M., Hammad, M., Iliopoulos, J.M., Layrolle, P. and Apazidou, D.A. (2024) Bioengineering the junctional epithelium in 3D oral mucosa models. *Journal of Functional Biomaterials,* 15(11), 330. https://doi.org/10.3390/jfb15110330

Gawron, K., Lazarz-Bartyzel, K., Lazarz, M., Steplewska, K., Pyrc, K., Potempa, J. and Chomyszyn-Gajewska, M. (2014) *In vitro* testing the potential of a novel chimeric IgG variant for inhibiting collagen fibrils formation in recurrent hereditary gingival fibromatosis: chimeric antibody in a gingival model. *Journal of Physiology and Pharmacology,* 65(4), 585–591.

Genco, R.J. and Van Dyke, T.E. (2010) Prevention: reducing the risk of CVD in patients with periodontitis. *Nature Reviews Cardiology,* 7(9), 479–480. https://doi.org/10.1038/nrcardio.2010.120

Gibbs, S., Roffel, S., Meyer, M. and Gasser, A. (2019) Biology of soft tissue repair: gingival epithelium in wound healing and attachment to the tooth and abutment surface. *European Cells and Materials,* 38, 63–78. https://doi.org/10.22203/eCM.v038a06

Golub, L.M., Elburki, M.S., Walker, C., Ryan, M., Sorsa, T., Tenenbaum, H., Goldberg, M., Wolff, M. and Gu, Y. (2016) Non-antibacterial tetracycline formulations: host-modulators in the treatment of periodontitis and relevant systemic diseases. *International Dental Journal,* 66(3), 127–135. https://doi.org/10.1111/idj.12221

Gonçalves, C., Soares, G.M., Faveri, M., Pérez-Chaparro, P.J., Lobão, E., Figueiredo, L.C., Baccelli, G.T. and Feres, M. (2016) Association of three putative periodontal pathogens with chronic periodontitis in Brazilian subjects. *Journal of Applied Oral Science,* 24(2), 181–185. https://doi.org/10.1590/1678-775720150445

Gonçalves, L.F., Fermiano, D., Feres, M., Figueiredo, L.C., Teles, F.R., Mayer, M.P. and Faveri, M. (2012) Levels of *Selenomonas* species in generalized aggressive periodontitis. *Journal of Periodontal Research,* 47(6), 711–718. https://doi.org/10.1111/j.1600-0765.2012.01485.x

Gonzalez-Mariscal, L., Contreras, R.G., Bolivar, J.J., Ponce, A., Chavez De Ramirez, B. and Cereijido, M. (1990) Role of calcium in tight junction formation between epithelial cells. *American Journal of Physiology-Cell Physiology,* 259(6 Pt 1), C978–C986. https://doi.org/10.1152/ajpcell.1990.259.6.C978

Griffiths, G.S. (2003) Formation, collection and significance of gingival crevice fluid. *Periodontology 2000,* 31(1), 32–42. https://doi.org/10.1034/j.1600-0757.2003.03103.x.

Guerra, F., Mazur, M., Ndokaj, A., Corridore, D., La Torre, G., Polimeni, A. and Ottolenghi, L. (2018) Periodontitis and the microbiome: a systematic review and meta-analysis. *Minerva Stomatologica,* 67(6), 250–258. https://doi.org/10.23736/S0026-4970.18.04198-5

Guggenheim, B., Gmur, R., Galicia, J.C., Stathopoulou, P.G., Benakanakere, M.R., Meier, A., Thurnheer, T. and Kinane, D.F. (2009) *In vitro* modeling of host-parasite interactions: the 'subgingival' biofilm challenge of primary human epithelial cells. *BMC Microbiology,* 9, 280. https://doi.org/10.1186/1471-2180-9-280

Guo, N., Wei, Q. and Xu, Y. (2020) Optimization of cryopreservation of pathogenic microbial strains. *Journal of Biosafety and Biosecurity,* 2(2), 66–70. https://doi.org/10.1016/j.jobb.2020.11.003

Guo, Y., Yang, Y., Xu, Y., Meng, Y., Ye, J., Xia, X. and Liu, Y. (2022) Deformable nanovesicle-loaded gel for buccal insulin delivery. *Pharmaceutics,* 14(11), 2262. https://doi.org/10.3390/pharmaceutics14112262

Gurav, A.N. (2012) Periodontitis and insulin resistance: casual or causal relationship? *Diabetes & Metabolism Journal,* 36(6), 404–411. https://doi.org/10.4093/dmj.2012.36.6.404

Hagio-Izaki, K., Yasunaga, M., Yamaguchi, M., Kajiya, H., Morita, H., Yoneda, M., Hirofuji, T. and Ohno, J. (2018) Lipopolysaccharide induces bacterial autophagy in epithelial keratinocytes of the gingival sulcus. *BMC Cell Biology,* 19(1), 18. https://doi.org/10.1186/s12860-018-0168-x

Hajishengallis, G. and Chavakis, T. (2021) Local and systemic mechanisms linking periodontal disease and inflammatory comorbidities. *Nature Reviews Immunology,* 21(7), 426–440. https://doi.org/10.1038/s41577-020-00488-6

Hajishengallis, G., Chavakis, T. and Lambris, J.D. (2020) Current understanding of periodontal disease pathogenesis and targets for host-modulation therapy. *Periodontology 2000,* 84(1), 14–34. https://doi.org/10.1111/prd.12331

Hajishengallis, G. and Korostoff, J.M. (2017) Revisiting the Page & Schroeder model: the good, the bad and the unknowns in the periodontal host

response 40 years later. *Periodontology 2000,* 75(1), 116–151. https://doi.org/10.1111/prd.12181

Hajishengallis, G. and Lamont, R.J. (2012) Beyond the red complex and into more complexity: the polymicrobial synergy and dysbiosis (PSD) model of periodontal disease etiology. *Molecular Oral Microbiology,* 27(6), 409–419. https://doi.org/10.1111/j.2041-1014.2012.00663.x

Hajishengallis, G., Lamont, R.J. and Koo, H. (2023) Oral polymicrobial communities: assembly, function, and impact on diseases. *Cell Host & Microbe,* 31(4), 528–538. https://doi.org/10.1016/j.chom.2023.02.009

Hajishengallis, G., Liang, S., Payne, M.A., Hashim, A., Jotwani, R., Eskan, M.A., McIntosh, M.L., Alsam, A., Kirkwood, K.L., Lambris, J.D., Darveau, R.P. and Curtis, M.A. (2011) Low-abundance biofilm species orchestrates inflammatory periodontal disease through the commensal microbiota and complement. *Cell Host & Microbe,* 10(5), 497–506. https://doi.org/10.1016/j.chom.2011.10.006

Hammond, B.F. (1970) Isolation and serological characterization of a cell wall antigen of *Rothia dentocariosa*. *Journal of Bacteriology,* 103(3), 634–640. https://doi.org/10.1128/jb.103.3.634-640.1970

Hanazawa, S., Kawata, Y., Takeshita, A., Kumada, H., Okithu, M., Tanaka, S., Yamamoto, Y., Masuda, T., Umemoto, T. and Kitano, S. (1993) Expression of monocyte chemoattractant protein 1 (MCP-1) in adult periodontal disease: increased monocyte chemotactic activity in crevicular fluids and induction of MCP-1 expression in gingival tissues. *Infection and Immunity,* 61(12), 5219–5224. https://doi.org/10.1128/iai.61.12.5219-5224.1993

Hao, C.P., Cao, N.J., Zhu, Y.H. and Wang, W. (2023) The impact of smoking on periodontitis patients' GCF/serum cytokine profile both before and after periodontal therapy: a meta-analysis. *BMC Oral Health,* 23(1), 60. https://doi.org/10.1186/s12903-023-02768-8

Hart, S.P., Ross, J.A., Ross, K., Haslett, C. and Dransfield, I. (2000) Molecular characterization of the surface of apoptotic neutrophils: implications for functional downregulation and recognition by phagocytes. *Cell Death & Differentiation,* 7(5), 493–503. https://doi.org/10.1038/sj.cdd.4400680

Hartenbach, F., Silva-Boghossian, C.M. and Colombo, A.P.V. (2018) The effect of supragingival biofilm re-development on the subgingival microbiota in chronic periodontitis. *Archives of Oral Biology,* 85, 51–57. https://doi.org/10.1016/j.archoralbio.2017.10.007

Hasturk, H., Hajishengallis, G., Lambris, J.D., Mastellos, D.C. and Yancopoulou, D. (2021a) Phase IIa clinical trial of complement C3 inhibitor AMY-101 in adults with periodontal inflammation. *Journal of Clinical Investigation,* 131(23), e152973. https://doi.org/10.1172/JCI152973

Hasturk, H., Schulte, F., Martins, M., Sherzai, H., Floros, C., Cugini, M., Chiu, C.J., Hardt, M. and Van Dyke, T. (2021b) Safety and preliminary efficacy of a novel host-modulatory therapy for reducing gingival inflammation. *Frontiers in Immunology,* 12, 704163. https://doi.org/10.3389/fimmu.2021.704163

Heller, D., Helmerhorst, E.J., Gower, A.C., Siqueira, W.L., Paster, B.J. and Oppenheim, F.G. (2016) Microbial diversity in the early in vivo-formed dental biofilm. *Applied and Environmental Microbiology,* 82(6), 1881–1888. https://doi.org/10.1128/AEM.03984-15

Herrera, D., Sanz, M., Kebschull, M., Jepsen, S., Sculean, A., Berglundh, T., Papapanou, P.N., Chapple, I., Tonetti, M.S. and EFP Workshop Participants and Methodological Consultant (2022) Treatment of stage IV periodontitis:

The EFP S3 level clinical practice guideline. *Journal of Clinical Periodontology,* 49(Suppl. 24), 4–71. https://doi.org/10.1111/jcpe.13639

Herrero, E.R., Slomka, V., Bernaerts, K., Boon, N., Hernandez-Sanabria, E., Passoni, B.B., Quirynen, M. and Teughels, W. (2016) Antimicrobial effects of commensal oral species are regulated by environmental factors. *Journal of Dentistry,* 47, 23–33. https://doi.org/10.1016/j.jdent.2016.02.007

Hidalgo, M.A., Carretta, M.D., Teuber, S.E., Zarate, C., Carcamo, L., Concha, I.I. and Burgos, R.A. (2015) fMLP-induced IL-8 release is dependent on NADPH oxidase in human neutrophils. *Journal of Immunology Research,* 2015, 120348. https://doi.org/10.1155/2015/120348

Highfield, J. (2009) Diagnosis and classification of periodontal disease. *Australian Dental Journal,* 54(Suppl. 1), S11–S26. https://doi.org/10.1111/j.1834-7819.2009.01140.x

Hirschfeld, J. (2020) Neutrophil subsets in periodontal health and disease: a mini review. *Frontiers in Immunology,* 10, 3001. https://doi.org/10.3389/fimmu.2019.03001

Hirschfeld, L. and Wasserman, B. (1978) A long-term survey of tooth loss in 600 treated periodontal patients. *Journal of Periodontology,* 49(5), 225–237. https://doi.org/10.1902/jop.1978.49.5.225

Holliday, R., Preshaw, P.M., Bowen, L. and Jakubovics, N.S. (2015) The ultrastructure of subgingival dental plaque, revealed by high-resolution field emission scanning electron microscopy. *BDJ Open,* 1, 15003. https://doi.org/10.1038/bdjopen.2015.3

Horbach, S. and Halffman, W. (2017) The ghosts of HeLa: How cell line misidentification contaminates the scientific literature. *PLOS ONE,* 12(10), e0186281. https://doi.org/10.1371/journal.pone.0186281

Hornstein, T. and Unfried, K. (2025) Differentiation of HL-60 cells into primed neutrophils for the evaluation of antiapoptotic effects of poorly soluble nanoparticles. *PLOS ONE,* 20(7), e0328717. https://doi.org/10.1371/journal.pone.0328717

Hosokawa, Y., Hosokawa, I., Ozaki, K. and Matsuo, T. (2017) IL-27 modulates chemokine production in TNF-alpha-stimulated human oral epithelial cells. *Cellular Physiology and Biochemistry,* 43(3), 1198–1206. https://doi.org/10.1159/000481760

Hsu, A.Y., Huang, Q., Liu, F., Balasubramanian, A. and Luo, H.R. (2025) Neutrophil death–more than meets the eye. *Experimental Hematology,* 150, 104857. https://doi.org/10.1016/j.exphem.2025.104857

Huang, C.B., Alimova, Y., Myers, T.M. and Ebersole, J.L. (2016) Macrophage polarization in response to oral commensals and pathogens. *FEMS Pathogens and Disease,* 74(3), ftw011. https://doi.org/10.1093/femspd/ftw011

Huang, L.C., Lin, W., Yagami, M., Tseng, D., Miyashita-Lin, E., Singh, N., Lin, A. and Shih, S.J. (2010) Validation of cell density and viability assays using Cedex automated cell counter. *Biologicals,* 38(3), 393–400. https://doi.org/10.1016/j.biologicals.2010.01.009

Huang, S., He, T., Yue, F., Xu, X., Wang, L., Zhu, P., Teng, F., Sun, Z., Liu, X., Jing, G., Su, X., Jin, L., Liu, J. and Xu, J. (2021a) Longitudinal multi-omics and microbiome meta-analysis identify an asymptomatic gingival state that links gingivitis, periodontitis, and aging. *mBio,* 12(2), e03281-03220. https://doi.org/10.1128/mBio.03281-20

Huang, Y., Bell, J., Kuksin, D., Sarkar, S., Pierce, L.T., Newton, D., Qiu, J. and Chan, L.L.-Y. (2021b) Practical application of cell counting method

performance evaluation and comparison derived from the ISO Cell Counting Standards Part 1 and 2. *Cell & Gene Therapy Insights,* 7(9), 937–960. https://doi.org/10.18609/cgti.2021.126

Hubálek, Z. (2003) Protectants used in the cryopreservation of microorganisms. *Cryobiology,* 46(3), 205–229. https://doi.org/10.1016/S0011-2240(03)00046-4

Huggett, J.F., Novak, T., Garson, J.A., Green, C., Morris-Jones, S.D., Miller, R.F. and Zumla, A. (2008) Differential susceptibility of PCR reactions to inhibitors: an important and unrecognised phenomenon. *BMC Research Notes,* 1, 70. https://doi.org/10.1186/1756-0500-1-70

Hunter, M.C., Pozhitkov, A.E. and Noble, P.A. (2016) Microbial signatures of oral dysbiosis, periodontitis and edentulism revealed by Gene Meter methodology. *Journal of Microbiological Methods,* 131, 85–101. https://doi.org/10.1016/j.mimet.2016.09.019

Ihara, Y., Takeshita, T., Kageyama, S., Matsumi, R., Asakawa, M., Shibata, Y., Sugiura, Y., Ishikawa, K., Takahashi, I. and Yamashita, Y. (2019) Identification of initial colonizing bacteria in dental plaques from young adults using full-length 16S rRNA gene sequencing. *mSystems,* 4(5), e00360-00319. https://doi.org/10.1128/mSystems.00360-19

Ince, G., Gursoy, H., Ipci, S.D., Cakar, G., Emekli-Alturfan, E. and Yilmaz, S. (2015) Clinical and biochemical evaluation of lozenges containing *Lactobacillus reuteri* as an adjunct to non-surgical periodontal therapy in chronic periodontitis. *Journal of Periodontology,* 86(6), 746–754. https://doi.org/10.1902/jop.2015.140612

Iniesta, M., Herrera, D., Montero, E., Zurbriggen, M., Matos, A.R., Marin, M.J., Sanchez-Beltran, M.C., Llama-Palacio, A. and Sanz, M. (2012) Probiotic effects of orally administered *Lactobacillus reuteri*-containing tablets on the subgingival and salivary microbiota in patients with gingivitis. A randomized clinical trial. *Journal of Clinical Periodontology,* 39(8), 736–744. https://doi.org/10.1111/j.1600-051X.2012.01914.x

Inozemtsev, V., Sergunova, V., Vorobjeva, N., Kozlova, E., Sherstyukova, E., Lyapunova, S. and Chernysh, A. (2023) Stages of NETosis development upon stimulation of neutrophils with activators of different types. *International Journal of Molecular Sciences,* 24(15), 12355. https://doi.org/10.3390/ijms241512355

International Cell Line Authentication Committee (2024) *ICLAC register of misidentified cell lines* [Online]. International Cell Line Authentication Committee. Available at: https://iclac.org/databases/cross-contaminations/ (Accessed: 5 October 2025).

Itzek, A., Zheng, L., Chen, Z., Merritt, J. and Kreth, J. (2011) Hydrogen peroxide-dependent DNA release and transfer of antibiotic resistance genes in *Streptococcus gordonii*. *Journal of Bacteriology,* 193(24), 6912–6922. https://doi.org/10.1128/jb.05791-11

Jackson, J.K., Springate, C.M.K., Hunter, W.L. and Burt, H.M. (2000) Neutrophil activation by plasma opsonized polymeric microspheres: inhibitory effect of Pluronic F127. *Biomaterials,* 21(14), 1483–1491. https://doi.org/10.1016/S0142-9612(00)00034-X

Jacobsen, J., Nielsen, E.B., Brondum-Nielsen, K., Christensen, M.E., Olin, H.B., Tommerup, N. and Rassing, M.R. (1999) Filter-grown TR146 cells as an *in vitro* model of human buccal epithelial permeability. *European Journal of Oral Sciences,* 107(2), 138–146. https://doi.org/10.1046/j.0909-8836.1999.eos107210.x

Jacobsen, J., van Deurs, B., Pedersen, M. and Rassing, M.R. (1995) TR146 cells grown on filters as a model for human buccal epithelium: I. Morphology, growth, barrier properties, and permeability. *International Journal of Pharmaceutics,* 125(2), 165–184. https://doi.org/10.1016/0378-5173(95)00109-V

Jacobsen, L.C., Theilgaard-Mönch, K., Christensen, E.I. and Borregaard, N. (2007) Arginase 1 is expressed in myelocytes/metamyelocytes and localized in gelatinase granules of human neutrophils. *Blood,* 109(7), 3084–3087. https://doi.org/10.1182/blood-2006-06-032599

Jakubovics, N.S., Gill, S.R., Vickerman, M.M. and Kolenbrander, P.E. (2008) Role of hydrogen peroxide in competition and cooperation between *Streptococcus gordonii* and *Actinomyces naeslundii*. *FEMS Microbiology Ecology,* 66(3), 637–644. https://doi.org/10.1111/j.1574-6941.2008.00585.x

Jakubovics, N.S., Goodman, S.D., Mashburn-Warren, L., Stafford, G.P. and Cieplik, F. (2021) The dental plaque biofilm matrix. *Periodontology 2000,* 86(1), 32–56. https://doi.org/10.1111/prd.12361

Jansen, P.M., Abdelbary, M.M.H. and Conrads, G. (2021) A concerted probiotic activity to inhibit periodontitis-associated bacteria. *PLOS ONE,* 16(3), e0248308. https://doi.org/10.1371/journal.pone.0248308

Janus, M.M., Keijser, B.J., Bikker, F.J., Exterkate, R.A., Crielaard, W. and Krom, B.P. (2015) *In vitro* phenotypic differentiation towards commensal and pathogenic oral biofilms. *Biofouling,* 31(6), 503–510. https://doi.org/10.1080/08927014.2015.1067887

Jayawardena, D.S., Yates, R., West, N.X. and Pollard, A.J. (2021) Implementing the 2017 Classification of Periodontal and Peri-Implant Diseases - how are we doing in the South West region of the UK? *British Dental Journal,* 231(11), 1–5. https://doi.org/10.1038/s41415-021-3716-2

Johanson, M., Zhao, X.R., Huynh-Ba, G. and Villar, C.C. (2013) Matrix metalloproteinases, tissue inhibitors of matrix metalloproteinases, and inflammation in cyclosporine A–induced gingival enlargement: a pilot *in vitro* study using a three-dimensional model of the human oral mucosa. *Journal of Periodontology,* 84(5), 634–640. https://doi.org/10.1902/JOP.2012.120224

Johnson, D.E. and Redner, R.L. (2015) An ATRActive future for differentiation therapy in AML. *Blood Reviews,* 29(4), 263–268. https://doi.org/10.1016/j.blre.2015.01.002

Jorth, P., Turner Keith, H., Gumus, P., Nizam, N., Buduneli, N. and Whiteley, M. (2014) Metatranscriptomics of the human oral microbiome during health and disease. *mBio,* 5(2), e01012-01014. https://doi.org/10.1128/mbio.01012-14

Jung, Y.S., Lee, H.Y., Kim, S.D., Park, J.S., Kim, J.K., Suh, P.-G. and Bae, Y.-S. (2013) Wnt5a stimulates chemotactic migration and chemokine production in human neutrophils. *Experimental & Molecular Medicine,* 45(6), e27–e27. https://doi.org/10.1038/emm.2013.48

Kaiser, R., Leunig, A., Pekayvaz, K., Popp, O., Joppich, M., Polewka, V., Escaig, R., Anjum, A., Hoffknecht, M.L., Gold, C., Brambs, S., Engel, A., Stockhausen, S., Knottenberg, V., Titova, A., Haji, M., Scherer, C., Muenchhoff, M., Hellmuth, J.C., Saar, K., Schubert, B., Hilgendorff, A., Schulz, C., Kaab, S., Zimmer, R., Hubner, N., Massberg, S., Mertins, P., Nicolai, L. and Stark, K. (2021) Self-sustaining IL-8 loops drive a prothrombotic neutrophil phenotype in severe COVID-19. *JCI Insight,* 6(18), e150862. https://doi.org/10.1172/jci.insight.150862

Kanmaz, M., Kanmaz, B. and Buduneli, N. (2021) Periodontal treatment outcomes in smokers: a narrative review. *Tobacco Induced Diseases,* 19, 77. https://doi.org/10.18332/tid/142106

Karlsson Linnér, R., Biroli, P., Kong, E., Meddens, S.F.W., Wedow, R., Fontana, M.A., Lebreton, M., Tino, S.P., Abdellaoui, A., Hammerschlag, A.R., Nivard, M.G., Okbay, A., Rietveld, C.A., Timshel, P.N., Trzaskowski, M., de Vlaming, R., Zünd, C.L., Bao, Y., Buzdugan, L., Caplin, A.H., Chen, C.-Y., Eibich, P., Fontanillas, P., Gonzalez, J.R., Joshi, P.K., Karhunen, V., Kleinman, A., Levin, R.Z., Lill, C.M., Meddens, G.A., Muntané, G., Sanchez-Roige, S., van Rooij, F.J., Taskesen, E., Wu, Y., Zhang, F., 23and Me Research Team, eQTLgen Consortium, International Cannabis Consortium, Social Science Genetic Association Consortium, Auton, A., Boardman, J.D., Clark, D.W., Conlin, A., Dolan, C.C., Fischbacher, U., Groenen, P.J.F., Harris, K.M., Hasler, G., Hofman, A., Ikram, M.A., Jain, S., Karlsson, R., Kessler, R.C., Kooyman, M., MacKillop, J., Männikkö, M., Morcillo-Suarez, C., McQueen, M.B., Schmidt, K.M., Smart, M.C., Sutter, M., Thurik, A.R., Uitterlinden, A.G., White, J., de Wit, H., Yang, J., Bertram, L., Boomsma, D.I., Esko, T., Fehr, E., Hinds, D.A., Johannesson, M., Kumari, M., Laibson, D., Magnusson, P.K.E., Meyer, M.N., Navarro, A., Palmer, A.A., Pers, T.H., Posthuma, D., Schunk, D., Stein, M.B., Svento, R., Tiemeier, H., Timmers, P.R.H.J., Turley, P., Ursano, R.J., Wagner, G.G., Wilson, J.F., Gratten, J., Lee, J.J., Cesarini, D., Benjamin, D.J., Koellinger, P.D. and Beauchamp, J.P. (2019) Genome-wide association analyses of risk tolerance and risky behaviors in over 1 million individuals identify hundreds of loci and shared genetic influences. *Nature Genetics,* 51(2), 245–257. https://doi.org/10.1038/s41588-018-0309-3

Kavlick, M.F. (2018) Development of a universal internal positive control. *BioTechniques,* 65(5), 275–280. https://doi.org/10.2144/btn-2018-0034

Kawai, T., Matsuyama, T., Hosokawa, Y., Makihira, S., Seki, M., Karimbux, N.Y., Goncalves, R.B., Valverde, P., Dibart, S., Li, Y.-P., Miranda, L.A., Ernst, C.W.O., Izumi, Y. and Taubman, M.A. (2006) B and T lymphocytes are the primary sources of RANKL in the bone resorptive lesion of periodontal disease. *The American Journal of Pathology,* 169(3), 987–998. https://doi.org/10.2353/ajpath.2006.060180

Kerdreux, M., Edin, S., Lowenmark, T., Bronnec, V., Lofgren-Burstrom, A., Zingmark, C., Ljuslinder, I., Palmqvist, R. and Ling, A. (2023) *Porphyromonas gingivalis* in colorectal cancer and its association to patient prognosis. *Journal of Cancer,* 14(9), 1479–1485. https://doi.org/10.7150/jca.83395

Keum, T., Noh, G., Seo, J.E., Bashyal, S., Sohn, D.H. and Lee, S. (2022) Examination of effective buccal absorption of salmon calcitonin using cell-penetrating peptide-conjugated liposomal drug delivery system. *International Journal of Nanomedicine,* 17, 697–710. https://doi.org/10.2147/IJN.S335774

Khan, M.A., Farahvash, A., Douda, D.N., Licht, J.-C., Grasemann, H., Sweezey, N. and Palaniyar, N. (2017) JNK activation turns on LPS- and gram-negative bacteria-induced NADPH oxidase-dependent suicidal NETosis. *Scientific Reports,* 7, 3409. https://doi.org/10.1038/s41598-017-03257-z

Kienle, K. and Lämmermann, T. (2016) Neutrophil swarming: an essential process of the neutrophil tissue response. *Immunological Reviews,* 273(1), 76–93. https://doi.org/10.1111/imr.12458

Kim, T.S. and Moutsopoulos, N.M. (2024) Neutrophils and neutrophil extracellular traps in oral health and disease. *Experimental & Molecular Medicine,* 56(5), 1055–1065. https://doi.org/10.1038/s12276-024-01219-w

Kinane, D.F., Stathopoulou, P.G. and Papapanou, P.N. (2017) Periodontal diseases. *Nature Reviews Disease Primers,* 3, 17038. https://doi.org/10.1038/nrdp.2017.38

Kirst, M.E., Li, E.C., Alfant, B., Chi, Y.Y., Walker, C., Magnusson, I. and Wang, G.P. (2015) Dysbiosis and alterations in predicted functions of the subgingival microbiome in chronic periodontitis. *Applied and Environmental Microbiology,* 81(2), 783–793. https://doi.org/10.1128/AEM.02712-14

Kiser, P.K., Lohr, C.V., Meritet, D., Spagnoli, S.T., Milovancev, M. and Russell, D.S. (2018) Histologic processing artifacts and inter-pathologist variation in measurement of inked margins of canine mast cell tumors. *Journal of Veterinary Diagnostic Investigation,* 30(3), 377–385. https://doi.org/10.1177/1040638718757582

Kistler, J.O., Booth, V., Bradshaw, D.J. and Wade, W.G. (2013) Bacterial community development in experimental gingivitis. *PLOS ONE,* 8(8), e71227. https://doi.org/10.1371/journal.pone.0071227

Klausner, M., Handa, Y. and Aizawa, S. (2021) *In vitro* three-dimensional organotypic culture models of the oral mucosa. *In Vitro Cellular and Developmental Biology – Animal,* 57(2), 148–159. https://doi.org/10.1007/s11626-020-00539-1

Kolenbrander, P.E., Andersen, R.N., Blehert, D.S., Egland, P.G., Foster, J.S. and Palmer, R.J. (2002) Communication among oral bacteria. *Microbiology and Molecular Biology Reviews,* 66(3), 486–505. https://doi.org/10.1128/mmbr.66.3.486-505.2002

Kolenbrander, P.E., Palmer Jr, R.J., Rickard, A.H., Jakubovics, N.S., Chalmers, N.I. and Diaz, P.I. (2006) Bacterial interactions and successions during plaque development. *Periodontology 2000,* 42(1), 47–79. https://doi.org/10.1111/j.1600-0757.2006.00187.x

Kolenbrander, P.E., Palmer, R.J., Jr., Periasamy, S. and Jakubovics, N.S. (2010) Oral multispecies biofilm development and the key role of cell-cell distance. *Nature Reviews Microbiology,* 8(7), 471–480. https://doi.org/10.1038/nrmicro2381

Kononen, E., Gursoy, M. and Gursoy, U.K. (2019) Periodontitis: a multifaceted disease of tooth-supporting tissues. *Journal of Clinical Medicine,* 8(8), 1135. https://doi.org/10.3390/jcm8081135

Kornman, K.S. (2018) Contemporary approaches for identifying individual risk for periodontitis. *Periodontology 2000,* 78(1), 12–29. https://doi.org/10.1111/prd.12234

Kotsakis, G.A., Javed, F., Hinrichs, J.E., Karoussis, I.K. and Romanos, G.E. (2015) Impact of cigarette smoking on clinical outcomes of periodontal flap surgical procedures: a systematic review and meta-analysis. *Journal of Periodontology,* 86(2), 254–263. https://doi.org/10.1902/jop.2014.140452

Kragh, K.N., Alhede, M., Kvich, L. and Bjarnsholt, T. (2019) Into the well—a close look at the complex structures of a microtiter biofilm and the crystal violet assay. *Biofilm,* 1, 100006. https://doi.org/10.1016/j.bioflm.2019.100006

Kralik, P. and Ricchi, M. (2017) A basic guide to real time PCR in microbial diagnostics: Definitions, parameters, and everything. *Frontiers in Microbiology,* 8, 108. https://doi.org/10.3389/fmicb.2017.00108

Kusek, M.E., Pazos, M.A., Pirzai, W. and Hurley, B.P. (2014) *In vitro* coculture assay to assess pathogen induced neutrophil trans-epithelial migration. *Journal of Visualized Experiments,* 83, e50823. https://doi.org/10.3791/50823

Kusumoto, Y., Hirano, H., Saitoh, K., Yamada, S., Takedachi, M., Nozaki, T., Ozawa, Y., Nakahira, Y., Saho, T., Ogo, H., Shimabukuro, Y., Okada, H. and Murakami, S. (2004) Human gingival epithelial cells produce chemotactic factors interleukin-8 and monocyte chemoattractant protein-1 after stimulation with *Porphyromonas gingivalis* via Toll-like receptor 2. *Journal of Periodontology,* 75(3), 370–379. https://doi.org/10.1902/jop.2004.75.3.370

Lages, E.J., Costa, F.O., Cortelli, S.C., Cortelli, J.R., Cota, L.O., Cyrino, R.M., Lages, E.M., Nobre-Franco, G.C., Brito, J.A. and Gomez, R.S. (2015) Alcohol consumption and periodontitis: quantification of periodontal pathogens and cytokines. *Journal of Periodontology,* 86(9), 1058–1068. https://doi.org/10.1902/jop.2015.150087

Lammers, K.M., Chieppa, M., Liu, L., Liu, S., Omatsu, T., Janka-Junttila, M., Casolaro, V., Reinecker, H.-C., Parent, C.A. and Fasano, A. (2015) Gliadin induces neutrophil migration via engagement of the formyl peptide receptor, FPR1. *PLOS ONE,* 10(9), e0138338. https://doi.org/10.1371/journal.pone.0138338

Lamont, R., J., Hajishengallis, G. and Koo, H. (2023) Social networking at the microbiome-host interface. *Infection and Immunity,* 91(9), e00124-00123. https://doi.org/10.1128/iai.00124-23

Lamont, R.J., Koo, H. and Hajishengallis, G. (2018) The oral microbiota: dynamic communities and host interactions. *Nature Reviews Microbiology,* 16(12), 745–759. https://doi.org/10.1038/s41579-018-0089-x

Lang, N.P. and Bartold, P.M. (2018) Periodontal health. *Journal of Periodontology,* 89(Suppl. 1), S9–S16. https://doi.org/10.1002/JPER.16-0517

Lang, N.P. and Tonetti, M.S. (2003) Periodontal risk assessment (PRA) for patients in supportive periodontal therapy (SPT). *Oral Health & Preventive Dentistry,* 1(1), 7–16.

Ledderose, C., Hashiguchi, N., Valsami, E.-A., Rusu, C. and Junger, W.G. (2023) Optimized flow cytometry assays to monitor neutrophil activation in human and mouse whole blood samples. *Journal of Immunological Methods,* 512, 113403. https://doi.org/10.1016/j.jim.2022.113403

Lee, C.T., Li, R., Zhu, L., Tribble, G.D., Zheng, W.J., Ferguson, B., Maddipati, K.R., Angelov, N. and Van Dyke, T.E. (2021) Subgingival microbiome and specialized pro-resolving lipid mediator pathway profiles are correlated in periodontal inflammation. *Frontiers in Immunology,* 12, 691216. https://doi.org/10.3389/fimmu.2021.691216

Lee, C.T., Teles, R., Kantarci, A., Chen, T., McCafferty, J., Starr, J.R., Brito, L.C., Paster, B.J. and Van Dyke, T.E. (2016) Resolvin E1 reverses experimental periodontitis and dysbiosis. *The Journal of Immunology,* 197(7), 2796–2806. https://doi.org/10.4049/jimmunol.1600859

Leite, F.R.M., Nascimento, G.G., Scheutz, F. and Lopez, R. (2018) Effect of smoking on periodontitis: a systematic review and meta-regression. *American Journal of Preventive Medicine,* 54(6), 831–841. https://doi.org/10.1016/j.amepre.2018.02.014

Leitinger, B. (2011) Transmembrane collagen receptors. *Annual Review of Cell and Developmental Biology,* 27, 265–290. https://doi.org/10.1146/annurev-cellbio-092910-154013

Leoni, G., Gripentrog, J., Lord, C., Riesselman, M., Sumagin, R., Parkos, C.A., Nusrat, A. and Jesaitis, A.J. (2015) Human neutrophil formyl peptide receptor phosphorylation and the mucosal inflammatory response. *Journal of Leukocyte Biology,* 97(1), 87–101. https://doi.org/10.1189/jlb.4A0314-153R

Li, Y., He, J., He, Z., Zhou, Y., Yuan, M., Xu, X., Sun, F., Liu, C., Li, J., Xie, W., Deng, Y., Qin, Y., VanNostrand, J.D., Xiao, L., Wu, L., Zhou, J., Shi, W. and Zhou, X. (2014) Phylogenetic and functional gene structure shifts of the oral microbiomes in periodontitis patients. *The ISME Journal,* 8(9), 1879–1891. https://doi.org/10.1038/ismej.2014.28

Lin, G.C., Leitgeb, T., Vladetic, A., Friedl, H.P., Rhodes, N., Rossi, A., Roblegg, E. and Neuhaus, W. (2020) Optimization of an oral mucosa *in vitro* model based on cell line TR146. *Tissue Barriers,* 8(2), 1748459. https://doi.org/10.1080/21688370.2020.1748459

Lind, S., Dahlgren, C., Holmdahl, R., Olofsson, P. and Forsman, H. (2021) Functional selective FPR1 signaling in favor of an activation of the neutrophil superoxide generating NOX2 complex. *Journal of Leukocyte Biology,* 109(6), 1105–1120. https://doi.org/10.1002/JLB.2HI0520-317R

Lindhe, J. and Nyman, S. (1984) Long-term maintenance of patients treated for advanced periodontal disease. *Journal of Clinical Periodontology,* 11(8), 504–514. https://doi.org/10.1111/j.1600-051x.1984.tb00902.x

Liu, B., Faller, L.L., Klitgord, N., Mazumdar, V., Ghodsi, M., Sommer, D.D., Gibbons, T.R., Treangen, T.J., Chang, Y.C., Li, S., Stine, O.C., Hasturk, H., Kasif, S., Segre, D., Pop, M. and Amar, S. (2012) Deep sequencing of the oral microbiome reveals signatures of periodontal disease. *PLOS ONE,* 7(6), e37919. https://doi.org/10.1371/journal.pone.0037919

Loe, H., Anerud, A., Boysen, H. and Morrison, E. (1986) Natural history of periodontal disease in man. Rapid, moderate and no loss of attachment in Sri Lankan laborers 14 to 46 years of age. *Journal of Clinical Periodontology,* 13(5), 431–445. https://doi.org/10.1111/j.1600-051x.1986.tb01487.x

Loesche, W.J. (1976) Chemotherapy of dental plaque infections. *Oral Science Reviews,* 9, 65–107.

Lombard, V., Golaconda Ramulu, H., Drula, E., Coutinho, P.M. and Henrissat, B. (2014) The carbohydrate-active enzymes database (CAZy) in 2013. *Nucleic Acids Research,* 42(D1), D490–D495. https://doi.org/10.1093/nar/gkt1178

Lombardo Bedran, T.B., Palomari Spolidorio, D. and Grenier, D. (2015) Green tea polyphenol epigallocatechin-3-gallate and cranberry proanthocyanidins act in synergy with cathelicidin (LL-37) to reduce the LPS-induced inflammatory response in a three-dimensional co-culture model of gingival epithelial cells and fibroblasts. *Archives of Oral Biology,* 60(6), 845–853. https://doi.org/10.1016/j.archoralbio.2015.02.021

Loozen, G., Boon, N., Pauwels, M., Quirynen, M. and Teughels, W. (2011) Live/dead real-time polymerase chain reaction to assess new therapies against dental plaque-related pathologies. *Molecular Oral Microbiology,* 26(4), 253–261. https://doi.org/10.1111/j.2041-1014.2011.00615.x

Lourenço, T.G.B., Heller, D., Silva-Boghossian, C.M., Cotton, S.L., Paster, B.J. and Colombo, A.P. (2014) Microbial signature profiles of periodontally healthy and diseased patients. *Journal of Clinical Periodontology,* 41(11), 1027–1036. https://doi.org/10.1111/jcpe.12302

Lowenmark, T., Lofgren-Burstrom, A., Zingmark, C., Eklof, V., Dahlberg, M., Wai, S.N., Larsson, P., Ljuslinder, I., Edin, S. and Palmqvist, R. (2020) Parvimonas micra as a putative non-invasive faecal biomarker for

colorectal cancer. *Scientific Reports,* 10, 15250. https://doi.org/10.1038/s41598-020-72132-1

Lu, C., Chu, Y., Liu, J.R., Liu, W.Y. and Ouyang, X.Y. (2021a) Subgingival microbial profiles of young Chinese adults with stage I/II periodontitis, gingivitis and periodontal health status. *Journal of Dental Research,* 24(3), 167–175. https://doi.org/10.3290/j.cjdr.b1965003

Lu, E.M.-C., Hobbs, C., Ghuman, M. and Hughes, F.J. (2021b) Development of an *in vitro* model of the dentogingival junction using 3D organotypic constructs. *Journal of Periodontal Research,* 56(1), 147–153. https://doi.org/10.1111/jre.12804

Luchian, I., Goriuc, A., Sandu, D. and Covasa, M. (2022) The role of matrix metalloproteinases (MMP-8, MMP-9, MMP-13) in periodontal and peri-implant pathological processes. *International Journal of Molecular Sciences,* 23(3), 1806. https://doi.org/10.3390/ijms23031806

Ma, L. and Diao, X. (2020) Effect of chlorhexidine chip as an adjunct in non-surgical management of periodontal pockets: a meta-analysis. *BMC Oral Health,* 20, 262. https://doi.org/10.1186/s12903-020-01247-8

Ma, Z., Zuo, T., Frey, N. and Rangrez, A.Y. (2024) A systematic framework for understanding the microbiome in human health and disease: from basic principles to clinical translation. *Signal Transduction and Targeted Therapy,* 9(1), 237. https://doi.org/10.1038/s41392-024-01946-6

Madianos, P.N., Papapanou, P.N. and Sandros, J. (1997) *Porphyromonas gingivalis* infection of oral epithelium inhibits neutrophil transepithelial migration. *Infection and Immunity,* 65(10), 3983–3990. https://doi.org/10.1128/iai.65.10.3983-3990.1997

Maekawa, T., Krauss, J.L., Abe, T., Jotwani, R., Triantafilou, M., Triantafilou, K., Hashim, A., Hoch, S., Curtis, M.A., Nussbaum, G., Lambris, J.D. and Hajishengallis, G. (2014) *Porphyromonas gingivalis* manipulates complement and TLR signaling to uncouple bacterial clearance from inflammation and promote dysbiosis. *Cell Host & Microbe,* 15(6), 768–778. https://doi.org/10.1016/j.chom.2014.05.012

Mahanonda, R., Champaiboon, C., Subbalekha, K., Sa-Ard-Iam, N., Rattanathammatada, W., Thawanaphong, S., Rerkyen, P., Yoshimura, F., Nagano, K., Lang, N.P. and Pichyangkul, S. (2016) Human memory B cells in healthy gingiva, gingivitis, and periodontitis. *The Journal of Immunology,* 197(3), 715–725. https://doi.org/10.4049/jimmunol.1600540

Mahomed, A.G. and Anderson, R. (2000) Activation of human neutrophils with chemotactic peptide, opsonized zymosan and the calcium ionophore A23187, but not with a phorbol ester, is accompanied by efflux and store-operated influx of calcium. *Inflammation,* 24(6), 559–569. https://doi.org/10.1023/A:1007029524141

Malmqvist, S., Strandberg, P., Victorin, I., Boberg, E. and Johannsen, A. (2025) The new system for classification of periodontal and peri-implant disease: a questionnaire study of implementation by Swedish dental hygienists. *International Journal of Dental Hygiene,* 23(3), 625–631. https://doi.org/10.1111/idh.12816

Maloney, W. (2010) A tooth is worth a treasure. *WebmedCentral DENTISTRY*, 1(9), WMC00576. Available at: http://www.webmedcentral.com/article_view/576 (Accessed: 21 February 2026).

Mammen, M.J., Scannapieco, F.A. and Sethi, S. (2020) Oral-lung microbiome interactions in lung diseases. *Periodontology 2000,* 83(1), 234–241. https://doi.org/10.1111/prd.12301

Manda-Handzlik, A., Bystrzycka, W., Wachowska, M., Sieczkowska, S., Stelmaszczyk-Emmel, A., Demkow, U. and Ciepiela, O. (2018) The influence of agents differentiating HL-60 cells toward granulocyte-like cells on their ability to release neutrophil extracellular traps. *Immunology and Cell Biology,* 96(4), 413–425. https://doi.org/10.1111/imcb.12015

Mandeville, J.T.H., Lawson, M.A. and Maxfield, F.R. (1997) Dynamic imaging of neutrophil migration in three dimensions: mechanical interactions between cells and matrix. *Journal of Leukocyte Biology,* 61(2), 188–200. https://doi.org/10.1002/jlb.61.2.188

Manoil, D. and Belibasakis, G.N. (2025) Subgingival ecology of the periodontal pocket. In: Koo, H.M., Jakubovics, N.S. and Krom, B.P. (eds.) *Oral Biofilms in Health and Disease.* Cham: Springer Nature Switzerland AG, pp. 311–323. https://doi.org/10.1007/978-3-031-82202-5_12

Mariotti, A. (1999) Dental plaque-induced gingival diseases. *Annals of Periodontology,* 4(1), 7–19. https://doi.org/10.1902/annals.1999.4.1.7

Mark Welch, J.L., Dewhirst, F.E. and Borisy, G.G. (2019) Biogeography of the oral microbiome: the site-specialist hypothesis. *Annual Review of Microbiology,* 73, 335–358. https://doi.org/10.1146/annurev-micro-090817-062503

Mark Welch, J.L., Rossetti, B.J., Rieken, C.W., Dewhirst, F.E. and Borisy, G.G. (2016) Biogeography of a human oral microbiome at the micron scale. *Proceedings of the National Academy of Sciences,* 113(6), E791–E800. https://doi.org/10.1073/pnas.1522149113

Marsh, P.D. (1994) Microbial ecology of dental plaque and its significance in health and disease. *Advances in Dental Research,* 8(2), 263–271. https://doi.org/10.1177/08959374940080022001

Marsh, P.D. (2003) Are dental diseases examples of ecological catastrophes? *Microbiology,* 149(2), 279–294. https://doi.org/10.1099/mic.0.26082-0

Marsh, P.D. (2006) Dental plaque as a biofilm and a microbial community – implications for health and disease. *BMC Oral Health,* 6(Suppl. 1), S14. https://doi.org/10.1186/1472-6831-6-S1-S14

Martin, S.J., Bradley, J.G. and Cotter, T.G. (1990) HL-60 cells induced to differentiate towards neutrophils subsequently die via apoptosis. *Clinical and Experimental Immunology,* 79(3), 448–453. https://doi.org/10.1111/j.1365-2249.1990.tb08110.x

Mashimo, P.A., Yamamoto, Y., Nakamura, M., Reynolds, H.S. and Genco, R.J. (1985) Lactic acid production by oral *Streptococcus mitis* inhibits the growth of oral *Capnocytophaga*. *Journal of Periodontology,* 56(9), 548–552. https://doi.org/10.1902/jop.1985.56.9.548

Masters, J.R. (2002) HeLa cells 50 years on: the good, the bad and the ugly. *Nature Reviews Cancer,* 2(4), 315–319. https://doi.org/10.1038/nrc775

Matsuo, M. and Takahashi, K. (2002) Scanning electron microscopic observation of microvasculature in periodontium. *Microscopy Research and Technique,* 56(1), 3–14. https://doi.org/10.1002/jemt.10008

Matsushima, K., Yang, D. and Oppenheim, J.J. (2022) Interleukin-8: an evolving chemokine. *Cytokine,* 153, 155828. https://doi.org/10.1016/j.cyto.2022.155828

Matsuyama, T., Izumi, Y. and Sueda, T. (1997) Culture and characterization of human junctional epithelial cells. *Journal of Periodontology,* 68(3), 229–239. https://doi.org/10.1902/jop.1997.68.3.229

Matuliene, G., Studer, R., Lang, N.P., Schmidlin, K., Pjetursson, B.E., Salvi, G.E., Bragger, U. and Zwahlen, M. (2010) Significance of Periodontal Risk Assessment in the recurrence of periodontitis and tooth loss. *Journal of*

Clinical Periodontology, 37(2), 191–199. https://doi.org/10.1111/j.1600-051X.2009.01508.x

Mazurel, D., Carda-Diéguez, M., Langenburg, T., Ziemyte, M., Johnston, W., Martinez, C.P., Albalat, F., Llena, C., Al-Hebshi, N., Culshaw, S., Mira, A. and Rosier, B.T. (2023) Nitrate and a nitrate-reducing *Rothia aeria* strain as potential prebiotic or synbiotic treatments for periodontitis. *npj Biofilms and Microbiomes,* 9, 40. https://doi.org/10.1038/s41522-023-00406-3

Mazzinelli, E., Favuzzi, I., Arcovito, A., Castagnola, R., Fratocchi, G., Mordente, A. and Nocca, G. (2023) Oral mucosa models to evaluate drug permeability. *Pharmaceutics,* 15(5), 1559. https://doi.org/10.3390/pharmaceutics15051559

McCain, R.W., Holden, E.P., Blackwell, T.R. and Christman, J.W. (1994) Leukotriene B4 stimulates human polymorphonuclear leukocytes to synthesize and release interleukin-8 *in vitro*. *American Journal of Respiratory Cell and Molecular Biology,* 10(6), 651–657. https://doi.org/10.1165/ajrcmb.10.6.8003341

McClintock, S.D., Attili, D., Dame, M.K., Richter, A., Silvestri, S.S., Berner, M.M., Bohm, M.S., Karpoff, K., McCarthy, C.L., Spence, J.R., Varani, J. and Aslam, M.N. (2020) Differentiation of human colon tissue in culture: effects of calcium on trans-epithelial electrical resistance and tissue cohesive properties. *PLOS ONE,* 15(3), e0222058. https://doi.org/10.1371/journal.pone.0222058

McFall, W.T., Jr. (1982) Tooth loss in 100 treated patients with periodontal disease. A long-term study. *Journal of Periodontology,* 53(9), 539–549. https://doi.org/10.1902/jop.1982.53.9.539

Mehta, A., Blumenthal, R.S., Gluckman, T.J., Feldman, D.I. and Kohli, P. (2025) High-sensitivity C-reactive protein in atherosclerotic cardiovascular disease: to measure or not to measure? *US Cardiology,* 19, e06. https://doi.org/10.15420/usc.2024.25

Menditto, A., Patriarca, M. and Magnusson, B. (2007) Understanding the meaning of accuracy, trueness and precision. *Accreditation and Quality Assurance,* 12(1), 45–47. https://doi.org/10.1007/s00769-006-0191-z

Merriam-Webster (2025) *Periodontitis* [Online]. Merriam-Webster. Available at: https://www.merriam-webster.com/dictionary/periodontitis (Accessed: 4 October 2025).

Metzemaekers, M., Gouwy, M. and Proost, P. (2020) Neutrophil chemoattractant receptors in health and disease: double-edged swords. *Cellular & Molecular Immunology,* 17(5), 433–450. https://doi.org/10.1038/s41423-020-0412-0

Meuric, V., Le Gall-David, S., Boyer, E., Acuna-Amador, L., Martin, B., Fong, S.B., Barloy-Hubler, F. and Bonnaure-Mallet, M. (2017) Signature of microbial dysbiosis in periodontitis. *Applied and Environmental Microbiology,* 83(14), e00462-00417. https://doi.org/10.1128/AEM.00462-17

Meyer, K.F. (1917) The present status of dental bacteriology. *The Journal of the National Dental Association,* 4(9), 966–996.

Michaud, M., Balardy, L., Moulis, G., Gaudin, C., Peyrot, C., Vellas, B., Cesari, M. and Nourhashemi, F. (2013) Proinflammatory cytokines, aging, and age-related diseases. *Journal of the American Medical Directors Association,* 14(12), 877–882. https://doi.org/10.1016/j.jamda.2013.05.009

Miles, A.A., Misra, S.S. and Irwin, J.O. (1938) The estimation of the bactericidal power of the blood. *The Journal of Hygiene,* 38(6), 732–749. https://doi.org/10.1017/s002217240001158x

Miller, W.D. (1890) *The micro-organisms of the human mouth.* Philadelphia: The S.S. White Dental Manufacturing Co.

Millhouse, E. (2015) *Microbial biofilm composition influences the host immune response.* PhD thesis, University of Glasgow.

Mills, G.A. (1885) Rigg's disease. *The American Journal of Dental Science,* 19(5), 218–223.

Mira, P., Yeh, P. and Hall, B.G. (2022) Estimating microbial population data from optical density. *PLOS ONE,* 17(10), e0276040. https://doi.org/10.1371/journal.pone.0276040

Miralda, I., Vashishta, A., Rogers, M.N., Lamont, R.J. and Uriarte, S.M. (2022) The emerging oral pathogen, *Filifactor alocis*, extends the functional lifespan of human neutrophils. *Molecular Microbiology,* 117(6), 1340–1351. https://doi.org/10.1111/mmi.14911

Moghaddam, B., Yang, J. and Roohpour, N. (2016) Biologic evaluation of devices with chronic exposure using 3D human gingival model. Paper presented at: 10th World Biomaterials Congress, Montréal, Canada, 17–22 May 2016. https://doi.org/10.3389/conf.FBIOE.2016.01.01697

Moharamzadeh, K., Brook, I.M., Van Noort, R., Scutt, A.M. and Thornhill, M.H. (2007) Tissue-engineered oral mucosa: a review of the scientific literature. *Journal of Dental Research,* 86(2), 115–124. https://doi.org/10.1177/154405910708600203

Moher, D., Liberati, A., Tetzlaff, J. and Altman, D.G. (2009) Preferred reporting items for systematic reviews and meta-analyses: the PRISMA statement. *BMJ,* 339, b2535. https://doi.org/10.1136/bmj.b2535

Molero-Abraham, M., Sanchez-Trincado, J.L., Gomez-Perosanz, M., Torres-Gomez, A., Subiza, J.L., Lafuente, E.M. and Reche, P.A. (2019) Human oral epithelial cells impair bacteria-mediated maturation of dendritic cells and render T cells unresponsive to stimulation. *Frontiers in Immunology,* 10, 1434. https://doi.org/10.3389/fimmu.2019.01434

Morin, M.-P. and Grenier, D. (2017) Regulation of matrix metalloproteinase secretion by green tea catechins in a three-dimensional co-culture model of macrophages and gingival fibroblasts. *Archives of Oral Biology,* 75, 89–99. https://doi.org/10.1016/j.archoralbio.2016.10.035

Mountcastle, S.E., Cox, S.C., Sammons, R.L., Jabbari, S., Shelton, R.M. and Kuehne, S.A. (2020) A review of co-culture models to study the oral microenvironment and disease. *Journal of Oral Microbiology,* 12(1), 1773122. https://doi.org/10.1080/20002297.2020.1773122

Moutsopoulos, N.M. and Konkel, J.E. (2018) Tissue-specific immunity at the oral mucosal barrier. *Trends in Immunology,* 39(4), 276–287. https://doi.org/10.1016/j.it.2017.08.005

Moutsopoulos, N.M., Zerbe, C.S., Wild, T., Dutzan, N., Brenchley, L., DiPasquale, G., Uzel, G., Axelrod, K.C., Lisco, A., Notarangelo, L.D., Hajishengallis, G., Notarangelo, L.D. and Holland, S.M. (2017) Interleukin-12 and interleukin-23 blockade in leukocyte adhesion deficiency type 1. *The New England Journal of Medicine,* 376(12), 1141–1146. https://doi.org/10.1056/NEJMoa1612197

Munar-Bestard, M., Llopis-Grimalt, M.A., Ramis, J.M. and Monjo, M. (2021) Comparative *in vitro* evaluation of commercial periodontal gels on antibacterial, biocompatibility and wound healing ability. *Pharmaceutics,* 13(9), 1502. https://doi.org/10.3390/pharmaceutics13091502

Nagpal, D., Prakash, S., Bhat, K.G. and Singh, G. (2016) Detection and comparison of *Selenomonas sputigena* in subgingival biofilms in chronic and aggressive periodontitis patients. *Journal of Indian Society of*

Periodontology, 20(3), 286–291. https://doi.org/10.4103/0972-124X.181247

Nakamura, M. (2018) Histological and immunological characteristics of the junctional epithelium. *Japanese Dental Science Review,* 54(2), 59–65. https://doi.org/10.1016/j.jdsr.2017.11.004

Nakatomi, K., Aida, Y., Kusumoto, K., Pabst, M.J. and Maeda, K. (1998) Neutrophils responded to immobilized lipopolysaccharide in the absence of lipopolysaccharide-binding protein. *Journal of Leukocyte Biology,* 64(2), 177–184. https://doi.org/10.1002/jlb.64.2.177

Nascimento, G.G., Alves-Costa, S. and Romandini, M. (2024) Burden of severe periodontitis and edentulism in 2021, with projections up to 2050: The Global Burden of Disease 2021 study. *Journal of Periodontal Research,* 59(5), 823–867. https://doi.org/10.1111/jre.13337

National Academies of Sciences Engineering and Medicine (2020) Necessity, Use, and Care of Laboratory Dogs at the U.S. Department of Veterans Affairs. Washington, DC: National Academies Press. https://doi.org/10.17226/25772

National Collection of Type Cultures *NCTC Online Catalogue* [Online]. Available at: https://www.culturecollections.org.uk/nop/product/neisseria-mucosa-3 (Accessed: 1 July 2025).

Nepomuceno, R., Pigossi, S.C., Finoti, L.S., Orrico, S.R.P., Cirelli, J.A., Barros, S.P., Offenbacher, S. and Scarel-Caminaga, R.M. (2017) Serum lipid levels in patients with periodontal disease: a meta-analysis and meta-regression. *Journal of Clinical Periodontology,* 44(12), 1192–1207. https://doi.org/10.1111/jcpe.12792

Nesse, W., Abbas, F., van der Ploeg, I., Spijkervet, F.K., Dijkstra, P.U. and Vissink, A. (2008) Periodontal inflamed surface area: quantifying inflammatory burden. *Journal of Clinical Periodontology,* 35(8), 668–673. https://doi.org/10.1111/j.1600-051X.2008.01249.x

Neubert, E., Senger-Sander, S.N., Manzke, V.S., Busse, J., Polo, E., Scheidmann, S.E.F., Schön, M.P., Kruss, S. and Erpenbeck, L. (2019) Serum and serum albumin inhibit *in vitro* formation of neutrophil extracellular traps (NETs). *Frontiers in Immunology,* 10, 12. https://doi.org/10.3389/fimmu.2019.00012

Nguyen, C.H., Grandits, A.M., Purton, L.E., Sill, H. and Wieser, R. (2020) All-trans retinoic acid in non-promyelocytic acute myeloid leukemia: driver lesion dependent effects on leukemic stem cells. *Cell Cycle,* 19(20), 2573–2588. https://doi.org/10.1080/15384101.2020.1810402

Nibali, L., Bayliss-Chapman, J., Almofareh, S.A., Zhou, Y., Divaris, K. and Vieira, A.R. (2019) What is the heritability of periodontitis? A systematic review. *Journal of Dental Research,* 98(6), 632–641. https://doi.org/10.1177/0022034519842510

Nibali, L., Sousa, V., Davrandi, M., Liu, L.S., Spratt, D. and Donos, N. (2022) Patterns of subgingival microbiota in different periodontal phenotypes. *Journal of Dentistry,* 117, 103912. https://doi.org/10.1016/j.jdent.2021.103912

Nobbs, A.H., Jenkinson, H.F. and Everett, D.B. (2015) Generic determinants of *Streptococcus* colonization and infection. *Infection, Genetics and Evolution,* 33, 361–370. https://doi.org/10.1016/j.meegid.2014.09.018

Nocker, A., Cheung, C.Y. and Camper, A.K. (2006) Comparison of propidium monoazide with ethidium monoazide for differentiation of live vs. dead bacteria by selective removal of DNA from dead cells. *Journal of*

Microbiological Methods, 67(2), 310–320. https://doi.org/10.1016/j.mimet.2006.04.015

Nolan, T., Hands, R.E., Ogunkolade, W. and Bustin, S.A. (2006) SPUD: a quantitative PCR assay for the detection of inhibitors in nucleic acid preparations. *Analytical Biochemistry,* 351(2), 308–310. https://doi.org/10.1016/j.ab.2006.01.051

Ochôa, C., Castro, F., Bulhosa, J.F., Manso, C., Fernandes, J.C.H. and Fernandes, G.V.O. (2023) Influence of the probiotic *L. reuteri* on periodontal clinical parameters after nonsurgical treatment: a systematic review. *Microorganisms,* 11(6), 1449. https://doi.org/10.3390/microorganisms11061449

Oh, C., Kim, H.J. and Kim, H.M. (2022) Transepithelial channels for leukocytes in the junctional epithelium. *Journal of Periodontal Research,* 57(5), 1093–1100. https://doi.org/10.1111/jre.13043

Ohshima, M., Otsuka, K. and Suzuki, K. (1994) Interleukin-1β stimulates collagenase production by cultured human periodontal ligament fibroblasts. *Journal of Periodontal Research,* 29(6), 421–429. https://doi.org/10.1111/J.1600-0765.1994.tb01244.x

Ohshima, M., Yamaguchi, Y., Ambe, K., Horie, M., Saito, A., Nagase, T., Nakashima, K., Ohki, H., Kawai, T., Abiko, Y., Micke, P. and Kappert, K. (2016) Fibroblast VEGF-receptor 1 expression as molecular target in periodontitis. *Journal of Clinical Periodontology,* 43(2), 128–137. https://doi.org/10.1111/jcpe.12495

Ohshima, M., Yamaguchi, Y., Matsumoto, N., Micke, P., Takenouchi, Y., Nishida, T., Kato, M., Komiyama, K., Abiko, Y., Ito, K., Otsuka, K. and Kappert, K. (2010) TGF-β signaling in gingival fibroblast-epithelial interaction. *Journal of Dental Research,* 89(11), 1315–1321. https://doi.org/10.1177/0022034510378423

Okahashi, N., Sumitomo, T., Nakata, M., Sakurai, A., Kuwata, H. and Kawabata, S. (2014) Hydrogen peroxide contributes to the epithelial cell death induced by the oral mitis group of streptococci. *PLOS ONE,* 9(1), e88136. https://doi.org/10.1371/journal.pone.0088136

Oliveira, R.R., Fermiano, D., Feres, M., Figueiredo, L.C., Teles, F.R., Soares, G.M. and Faveri, M. (2016) Levels of candidate periodontal pathogens in subgingival biofilm. *Journal of Dental Research,* 95(6), 711–718. https://doi.org/10.1177/0022034516634619

Ozturk, V.O., Belibasakis, G.N., Emingil, G. and Bostanci, N. (2016) Impact of aging on TREM-1 responses in the periodontium: a cross-sectional study in an elderly population. *BMC Infectious Diseases,* 16(1), 429. https://doi.org/10.1186/s12879-016-1778-6

Ozuna, H., Uriarte, S.M. and Demuth, D.R. (2021) The Hunger Games: *Aggregatibacter actinomycetemcomitans* exploits human neutrophils as an epinephrine source for survival. *Frontiers in Immunology,* 12, 707096. https://doi.org/10.3389/fimmu.2021.707096

Padrell, M., Llorente, M. and Amici, F. (2021) Invasive research on non-human primates—time to turn the page. *Animals,* 11(10), 2999. https://doi.org/10.3390/ani11102999

Page, R.C. and Schroeder, H.E. (1976) Pathogenesis of inflammatory periodontal disease. A summary of current work. *Laboratory Investigation,* 34(3), 235–249.

Palmer, R. and Floyd, P. (2023) Periodontal examination and screening. *British Dental Journal,* 235(9), 707–713. https://doi.org/10.1038/s41415-023-6410-8

Palmer, R.J., Jr., Shah, N., Valm, A., Paster, B., Dewhirst, F., Inui, T. and Cisar, J.O. (2017) Interbacterial adhesion networks within early oral biofilms of single human hosts. *Applied and Environmental Microbiology,* 83(11), e00407-00417. https://doi.org/10.1128/AEM.00407-17

Pan, W., Wang, Q. and Chen, Q. (2019) The cytokine network involved in the host immune response to periodontitis. *International Journal of Oral Science,* 11(3), 30. https://doi.org/10.1038/s41368-019-0064-z

Papapanou, P.N., Madianos, P.N., Dahlen, G. and Sandros, J. (1997) "Checkerboard" versus culture: a comparison between two methods for identification of subgingival microbiota. *European Journal of Oral Sciences,* 105(5 Pt 1), 389–396. https://doi.org/10.1111/j.1600-0722.1997.tb02135.x

Papapanou, P.N., Sanz, M., Buduneli, N., Dietrich, T., Feres, M., Fine, D.H., Flemmig, T.F., Garcia, R., Giannobile, W.V., Graziani, F., Greenwell, H., Herrera, D., Kao, R.T., Kebschull, M., Kinane, D.F., Kirkwood, K.L., Kocher, T., Kornman, K.S., Kumar, P.S., Loos, B.G., Machtei, E., Meng, H., Mombelli, A., Needleman, I., Offenbacher, S., Seymour, G.J., Teles, R. and Tonetti, M.S. (2018) Periodontitis: consensus report of workgroup 2 of the 2017 World Workshop on the Classification of Periodontal and Peri-Implant Diseases and Conditions. *Journal of Clinical Periodontology,* 45(Suppl. 20), S162–S170. https://doi.org/10.1111/jcpe.12946

Park, O.J., Yi, H., Jeon, J.H., Kang, S.S., Koo, K.T., Kum, K.Y., Chun, J., Yun, C.H. and Han, S.H. (2015) Pyrosequencing analysis of subgingival microbiota in distinct periodontal conditions. *Journal of Dental Research,* 94(7), 921–927. https://doi.org/10.1177/0022034515583531

Park, S.N., Park, J.Y. and Kook, J.K. (2011) Development of *Porphyromonas gingivalis*-specific quantitative real-time PCR primers based on the nucleotide sequence of rpoB. *Journal of Microbiology,* 49(2), 315–319. https://doi.org/10.1007/s12275-011-1028-y

Pérez-Chaparro, P.J., Duarte, P.M., Pannuti, C.M., Figueiredo, L.C., Mestnik, M.J., Gonçalves, C.P., Faveri, M. and Feres, M. (2015) Evaluation of human and microbial DNA content in subgingival plaque samples collected by paper points or curette. *Journal of Microbiological Methods,* 111, 19–20. https://doi.org/10.1016/j.mimet.2015.01.023

Pérez-Chaparro, P.J., Gonçalves, C., Figueiredo, L.C., Faveri, M., Lobão, E., Tamashiro, N., Duarte, P. and Feres, M. (2014) Newly identified pathogens associated with periodontitis: a systematic review. *Journal of Dental Research,* 93, 846–858. https://doi.org/10.1177/0022034514542468

Pérez-Chaparro, P.J., McCulloch, J.A., Mamizuka, E.M., Moraes, A., Faveri, M., Figueiredo, L.C., Duarte, P.M. and Feres, M. (2018) Do different probing depths exhibit striking differences in microbial profiles? *Journal of Clinical Periodontology,* 45(1), 26–37. https://doi.org/10.1111/jcpe.12811

Perez-Figueroa, E., Alvarez-Carrasco, P., Ortega, E. and Maldonado-Bernal, C. (2021) Neutrophils: many ways to die. *Frontiers in Immunology,* 12, 631821. https://doi.org/10.3389/fimmu.2021.631821

Periasamy, S., Chalmers, N.I., Du-Thumm, L. and Kolenbrander, P.E. (2009) *Fusobacterium nucleatum* ATCC 10953 requires *Actinomyces naeslundii* ATCC 43146 for growth on saliva in a three-species community that includes *Streptococcus oralis* 34. *Applied and Environmental Microbiology,* 75(10), 3250–3257. https://doi.org/10.1128/AEM.02901-08

Periasamy, S. and Kolenbrander, P.E. (2009) *Aggregatibacter actinomycetemcomitans* builds mutualistic biofilm communities with

Fusobacterium nucleatum and *Veillonella* species in saliva. *Infection and Immunity,* 77(9), 3542–3551. https://doi.org/10.1128/IAI.00345-09

Perio Tools (2025) *Perio Tools* [Online]. Available at: https://www.perio-tools.com/ (Accessed: 23 February 2026).

Persson, K., Esberg, A., Claesson, R. and Strömberg, N. (2012) The pilin protein FimP from *Actinomyces oris*: crystal structure and sequence analyses. *PLOS ONE,* 7(10), e48364. https://doi.org/10.1371/journal.pone.0048364

Peyyala, R., Kirakodu, S., Novak, K.F. and Ebersole, J.L. (2011a) Epithelial interleukin-8 responses to oral bacterial biofilms. *Clinical and Vaccine Immunology,* 18(10), 1770–1772. https://doi.org/10.1128/CVI.05162-11

Peyyala, R., Kirakodu, S.S., Ebersole, J.L. and Novak, K.F. (2011b) Novel model for multispecies biofilms that uses rigid gas-permeable lenses. *Applied and Environmental Microbiology,* 77(10), 3413–3421. https://doi.org/10.1128/AEM.00039-11

Peyyala, R., Kirakodu, S.S., Novak, K.F. and Ebersole, J.L. (2012) Oral microbial biofilm stimulation of epithelial cell responses. *Cytokine,* 58(1), 65–72. https://doi.org/10.1016/j.cyto.2011.12.016

Piazza, F., Ravaglia, B., Caporale, A., Svetic, A., Parisse, P., Asaro, F., Grassi, G., Secco, L., Sgarra, R., Marsich, E., Donati, I. and Sacco, P. (2024) Elucidating the unexpected cell adhesive properties of agarose substrates. The effect of mechanics, fetal bovine serum and specific peptide sequences. *Acta Biomaterialia,* 189, 286–297. https://doi.org/10.1016/j.actbio.2024.09.042

Pilchová, V., Richter, A., Meurer, M., Schulz, C. and von Köckritz-Blickwede, M. (2025) The effect of chemical fixation with paraformaldehyde, glutardialdehyde or methanol on immunofluorescence staining of neutrophils and neutrophil extracellular traps. *Innate Immunity,* 31, 17534259241307563. https://doi.org/10.1177/17534259241307563

Popadiak, K., Potempa, J., Riesbeck, K. and Blom, A.M. (2007) Biphasic effect of gingipains from *Porphyromonas gingivalis* on the human complement system. *The Journal of Immunology,* 178(11), 7242–7250. https://doi.org/10.4049/jimmunol.178.11.7242

Popescu, D.M., Cândea, A., Beuran, I.A., Rauten, A.-M. and Pitru, A.R. (2025) The role of smoking in periodontal diseases: action mechanisms and clinical implications. A review article. *International Journal of Applied Dental Sciences,* 11(2), 278–281. https://doi.org/10.22271/oral.2025.v11.i2d.2165

Postgate, J.R. and Hunter, J.R. (1963) Metabolic injury in frozen bacteria. *Journal of Applied Bacteriology,* 26(3), 405–414. https://doi.org/10.1111/j.1365-2672.1963.tb04791.x

Preshaw, P.M. (2018) Host modulation therapy with anti-inflammatory agents. *Periodontology 2000,* 76(1), 131–149. https://doi.org/10.1111/prd.12148

Pretzl, B., Kaltschmitt, J., Kim, T.S., Reitmeir, P. and Eickholz, P. (2008) Tooth loss after active periodontal therapy. 2: tooth-related factors. *Journal of Clinical Periodontology,* 35(2), 175–182. https://doi.org/10.1111/j.1600-051X.2007.01182.x

Pretzl, B., Wiedemann, D., Cosgarea, R., Kaltschmitt, J., Kim, T.S., Staehle, H.J. and Eickholz, P. (2009) Effort and costs of tooth preservation in supportive periodontal treatment in a German population. *Journal of Clinical Periodontology,* 36(8), 669–676. https://doi.org/10.1111/j.1600-051X.2009.01409.x

Priyanka, T.G., Athul, A., Harini, D., Thasneem, S., Nasser, I., Benedict, C., Vijayarangan, A., Balachandran, A. and Muthukali, S. (2024) Clinical

incorporation of the 2017 classification of periodontal diseased conditions: part I (diagnosis of periodontitis involving data from 4,993 patients). *Cureus,* 16(6), e63423. https://doi.org/10.7759/cureus.63423

Qian, S.J., Huang, Q.R., Chen, R.Y., Mo, J.J., Zhou, L.Y., Zhao, Y., Li, B. and Lai, H.C. (2021) Single-cell RNA sequencing identifies new inflammation-promoting cell subsets in Asian patients with chronic periodontitis. *Frontiers in Immunology,* 12, 711337. https://doi.org/10.3389/fimmu.2021.711337

Radu, C.M., Radu, C.C., Arbanasi, E.M., Hogea, T., Murvai, V.R., Chis, I.A. and Zaha, D.C. (2024) Exploring the efficacy of novel therapeutic strategies for periodontitis: a literature review. *Life,* 14(4), 468. https://doi.org/10.3390/life14040468

Raittio, E., Leite, F.R.M., Machado, V., Botelho, J. and Nascimento, G.G. (2025) Do all individuals benefit equally from non-surgical periodontal therapy? Secondary analyses of systematic review data. *Journal of Periodontal Research,* 60(4), 315–325. https://doi.org/10.1111/jre.13347

Ramseier, C.A., Woelber, J.P., Kitzmann, J., Detzen, L., Carra, M.C. and Bouchard, P. (2020) Impact of risk factor control interventions for smoking cessation and promotion of healthy lifestyles in patients with periodontitis: a systematic review. *Journal of Clinical Periodontology,* 47(Suppl. 22), 90–106. https://doi.org/10.1111/jcpe.13240

Ray, B. and Speck, M.L. (1972) Metabolic process during the repair of freeze-injury in *Escherichia coli*. *Applied Microbiology,* 24(4), 585–590. https://doi.org/10.1128/am.24.4.585-590.1972

Ray, B. and Speck, M.L. (1973) Freeze-injury in bacteria. *CRC Critical Reviews in Clinical Laboratory Sciences,* 4(2), 161–213. https://doi.org/10.3109/10408367309151556

Raza, M., Abud, D.G., Wang, J. and Shariff, J.A. (2024) Ease and practicability of the 2017 classification of periodontal diseases and conditions: a study of dental electronic health records. *BMC Oral Health,* 24(1), 621. https://doi.org/10.1186/s12903-024-04385-5

Redanz, S., Cheng, X., Giacaman, R.A., Pfeifer, C.S., Merritt, J. and Kreth, J. (2018) Live and let die: hydrogen peroxide production by the commensal flora and its role in maintaining a symbiotic microbiome. *Molecular Oral Microbiology,* 33(5), 337–352. https://doi.org/10.1111/omi.12231

Rickard, A.H., Gilbert, P., High, N.J., Kolenbrander, P.E. and Handley, P.S. (2003) Bacterial coaggregation: an integral process in the development of multi-species biofilms. *Trends in Microbiology,* 11(2), 94–100. https://doi.org/10.1016/S0966-842X(02)00034-3

Rodrigues, L., Banat, I.M., Teixeira, J. and Oliveira, R. (2007) Strategies for the prevention of microbial biofilm formation on silicone rubber voice prostheses. *Journal of Biomedical Materials Research Part B: Applied Biomaterials,* 81B(2), 358–370. https://doi.org/10.1002/jbm.b.30673

Rosales, C. (2018) Neutrophil: a cell with many roles in inflammation or several cell types? *Frontiers in Physiology,* 9, 113. https://doi.org/10.3389/fphys.2018.00113

Rosan, B. and Lamont, R.J. (2000) Dental plaque formation. *Microbes and Infection,* 2(13), 1599–1607. https://doi.org/10.1016/S1286-4579(00)01316-2

Rosier, B.T., De Jager, M., Zaura, E. and Krom, B.P. (2014) Historical and contemporary hypotheses on the development of oral diseases: are we there yet? *Frontiers in Cellular and Infection Microbiology,* 4, 92. https://doi.org/10.3389/fcimb.2014.00092

Rosier, B.T., Johnston, W., Carda-Diéguez, M., Simpson, A., Cabello-Yeves, E., Piela, K., Reilly, R., Artacho, A., Easton, C., Burleigh, M., Culshaw, S. and Mira, A. (2024) Nitrate reduction capacity of the oral microbiota is impaired in periodontitis: potential implications for systemic nitric oxide availability. *International Journal of Oral Science,* 16(1), 1. https://doi.org/10.1038/s41368-023-00266-9

Rosier, B.T., Moya-Gonzalvez, E.M., Corell-Escuin, P. and Mira, A. (2020) Isolation and characterization of nitrate-reducing bacteria as potential probiotics for oral and systemic health. *Frontiers in Microbiology,* 11, 555465. https://doi.org/10.3389/fmicb.2020.555465

Rosier, B.T., Takahashi, N., Zaura, E., Krom, B.P., Martínez-Espinosa, R.M., van Breda, S.G.J., Marsh, P.D. and Mira, A. (2022) The importance of nitrate reduction for oral health. *Journal of Dental Research,* 101(8), 887–897. https://doi.org/10.1177/00220345221080982

Rozen, R., Bachrach, G., Bronshteyn, M., Gedalia, I. and Steinberg, D. (2001) The role of fructans on dental biofilm formation by *Streptococcus sobrinus*, *Streptococcus mutans*, *Streptococcus gordonii* and *Actinomyces viscosus*. *FEMS Microbiology Letters,* 195(2), 205–210. https://doi.org/10.1111/j.1574-6968.2001.tb10522.x

Ruhl, S., Eidt, A., Melzl, H., Reischl, U. and Cisar, J.O. (2014) Probing of microbial biofilm communities for coadhesion partners. *Applied and Environmental Microbiology,* 80(21), 6583–6590. https://doi.org/10.1128/AEM.01826-14

Rupniak, H.T., Rowlatt, C., Lane, E.B., Steele, J.G., Trejdosiewicz, L.K., Laskiewicz, B., Povey, S. and Hill, B. (1985) Characteristics of four new human cell lines derived from squamous cell carcinomas of the head and neck. *Journal of the National Cancer Institute,* 75(4), 621–635. https://doi.org/10.1093/jnci/75.4.621

Ryder, M.I. (2010) Comparison of neutrophil functions in aggressive and chronic periodontitis. *Periodontology 2000,* 53, 124–137. https://doi.org/10.1111/j.1600-0757.2009.00327.x

Saleh, M.H.A., Dukka, H., Troiano, G., Ravida, A., Galli, M., Qazi, M., Greenwell, H. and Wang, H.L. (2021) External validation and comparison of the predictive performance of 10 different tooth-level prognostic systems. *Journal of Clinical Periodontology,* 48(11), 1421–1429. https://doi.org/10.1111/jcpe.13542

Saleh, M.H.A., Dukka, H., Troiano, G., Ravida, A., Qazi, M., Wang, H.L. and Greenwell, H. (2022) Long term comparison of the prognostic performance of PerioRisk, periodontal risk assessment, periodontal risk calculator, and staging and grading systems. *Journal of Periodontology,* 93(1), 57–68. https://doi.org/10.1002/JPER.20-0662

Salvi, G.E., Stahli, A., Schmidt, J.C., Ramseier, C.A., Sculean, A. and Walter, C. (2020) Adjunctive laser or antimicrobial photodynamic therapy to non-surgical mechanical instrumentation in patients with untreated periodontitis: a systematic review and meta-analysis. *Journal of Clinical Periodontology,* 47(Suppl. 22), 176–198. https://doi.org/10.1111/jcpe.13236

Sanchez, M.C., Marin, M.J., Figuero, E., Llama-Palacios, A., Leon, R., Blanc, V., Herrera, D. and Sanz, M. (2014) Quantitative real-time PCR combined with propidium monoazide for the selective quantification of viable periodontal pathogens in an *in vitro* subgingival biofilm model. *Journal of Periodontal Research,* 49(1), 20–28. https://doi.org/10.1111/jre.12073

Sansores-España, L.D., Melgar-Rodríguez, S., Vernal, R., Carrillo-Ávila, B.A., Martínez-Aguilar, V.M. and Díaz-Zúñiga, J. (2022) Neutrophil N1 and N2 subsets and their possible association with periodontitis: a scoping review. *International Journal of Molecular Sciences,* 23(20), 12068. https://doi.org/10.3390/ijms232012068

Sanz, M., Herrera, D., Kebschull, M., Chapple, I., Jepsen, S., Berglundh, T., Sculean, A., Tonetti, M.S. and EFP Workshop Participants and Methodological Consultants (2020) Treatment of stage I–III periodontitis—the EFP S3 level clinical practice guideline. *Journal of Clinical Periodontology,* 47(Suppl. 22), 4–60. https://doi.org/10.1111/jcpe.13290

Sarkar, S., Lund, S.P., Vyzasatya, R., Vanguri, P., Elliott, J.T., Plant, A.L. and Lin-Gibson, S. (2017) Evaluating the quality of a cell counting measurement process via a dilution series experimental design. *Cytotherapy,* 19(12), 1509–1521. https://doi.org/10.1016/j.jcyt.2017.08.014

Sasaki, N., Takeuchi, H., Kitano, S., Irie, S., Amano, A. and Matsusaki, M. (2021) Dynamic analysis of *Porphyromonas gingivalis* invasion into blood capillaries during the infection process in host tissues using a vascularized three-dimensional human gingival model. *Biomaterials Science,* 9(19), 6574–6583. https://doi.org/10.1039/D1BM00831E

Scapoli, L., Girardi, A., Palmieri, A., Martinelli, M., Cura, F., Lauritano, D. and Carinci, F. (2015) Quantitative analysis of periodontal pathogens in periodontitis and gingivitis. *Journal of Biological Regulators and Homeostatic Agents,* 29(3 Suppl. 1), 101–110.

Schaefer, A.S., Nibali, L., Zoheir, N., Moutsopoulos, N.M. and Loos, B.G. (2025) Genetic risk variants implicate impaired maintenance and repair of periodontal tissues as causal for periodontitis—a synthesis of recent findings. *Periodontology 2000,* 00, 1–18. https://doi.org/10.1111/prd.12622

Schober, I., Koblitz, J., Sardà Carbasse, J., Ebeling, C., Schmidt, M.L., Podstawka, A., Gupta, R., Ilangovan, V., Chamanara, J., Overmann, J. and Reimer, L.C. (2025) BacDive in 2025: the core database for prokaryotic strain data. *Nucleic Acids Research,* 53(D1), D748–D756. https://doi.org/10.1093/nar/gkae959

Schoenborn, J.R. and Wilson, C.B. (2007) Regulation of interferon-γ during innate and adaptive immune responses. In: Alt, F.W. (ed.) *Advances in Immunology.* Academic Press, pp. 41–101. https://doi.org/10.1016/S0065-2776(07)96002-2

Schrader, C., Schielke, A., Ellerbroek, L. and Johne, R. (2012) PCR inhibitors - occurrence, properties and removal. *Journal of Applied Microbiology,* 113(5), 1014–1026. https://doi.org/10.1111/j.1365-2672.2012.05384.x

Schroeder, H.E. and Listgarten, M.A. (1997) The gingival tissues: the architecture of periodontal protection. *Periodontology 2000,* 13(1), 91–120. https://doi.org/10.1111/j.1600-0757.1997.tb00097.x

Scully, C. and Challacombe, S.J. (1979) The migration of ^{111}Indium-labelled polymorphonuclear leucocytes into the oral cavity in the rhesus monkey. *Journal of Periodontal Research,* 14(6), 475–481. https://doi.org/10.1111/j.1600-0765.1979.tb00247.x

Sham, R.L., Phatak, P.D., Belanger, K.A. and Packman, C.H. (1995) Functional properties of HL60 cells matured with all-trans-retinoic acid and DMSO: differences in response to interleukin-8 and fMLP. *Leukemia Research,* 19(1), 1–6. https://doi.org/10.1016/0145-2126(94)00063-g

Shang, F.M. and Liu, H.L. (2018) *Fusobacterium nucleatum* and colorectal cancer: a review. *World Journal of Gastrointestinal Oncology,* 10(3), 71–81. https://doi.org/10.4251/wjgo.v10.i3.71

Shang, L., Deng, D., Buskermolen, J.K., Janus, M.M., Krom, B.P., Roffel, S., Waaijman, T., van Loveren, C., Crielaard, W. and Gibbs, S. (2018) Multi-species oral biofilm promotes reconstructed human gingiva epithelial barrier function. *Scientific Reports,* 8, 16061. https://doi.org/10.1038/s41598-018-34390-y

Shang, L., Deng, D., Buskermolen, J.K., Roffel, S., Janus, M.M., Krom, B.P., Crielaard, W. and Gibbs, S. (2019) Commensal and pathogenic biofilms alter Toll-like receptor signaling in reconstructed human gingiva. *Frontiers in Cellular and Infection Microbiology,* 9, 282. https://doi.org/10.3389/fcimb.2019.00282

Shapiro, S., Giertsen, E. and Guggenheim, B. (2002) An *in vitro* oral biofilm model for comparing the efficacy of antimicrobial mouthrinses. *Caries Research,* 36(2), 93–100. https://doi.org/10.1159/000057866

Sherry, L., Lappin, G., O'Donnell, L.E., Millhouse, E., Millington, O.R., Bradshaw, D.J., Axe, A.S., Williams, C., Nile, C.J. and Ramage, G. (2016) Viable compositional analysis of an eleven species oral polymicrobial biofilm. *Frontiers in Microbiology,* 7, 912. https://doi.org/10.3389/fmicb.2016.00912

Shi, M., Wei, Y., Hu, W., Nie, Y., Wu, X. and Lu, R. (2018) The subgingival microbiome of periodontal pockets with different probing depths in chronic and aggressive periodontitis: a pilot study. *Frontiers in Cellular and Infection Microbiology,* 8, 124. https://doi.org/10.3389/fcimb.2018.00124

Shimabukuro, Y., Murakami, S. and Okada, H. (1996) Antigen-presenting-cell function of interferon gamma-treated human gingival fibroblasts. *Journal of Periodontal Research,* 31(3), 217–228. https://doi.org/10.1111/j.1600-0765.1996.tb00486.x

Shin, S.B., Kim, Y.M. and Park, H.Y. (2025) Pinoresinol enhances oral barrier integrity and function in human buccal cell monolayers. *PLOS ONE,* 20(9), e0331242. https://doi.org/10.1371/journal.pone.0331242

Sochalska, M. and Potempa, J. (2017) Manipulation of neutrophils by *Porphyromonas gingivalis* in the development of periodontitis. *Frontiers in Cellular and Infection Microbiology,* 7, 197. https://doi.org/10.3389/fcimb.2017.00197

Socransky, S.S., Haffajee, A.D., Cugini, M.A., Smith, C. and Kent, R.L. (1998) Microbial complexes in subgingival plaque. *Journal of Clinical Periodontology,* 25(2), 134–144. https://doi.org/10.1111/j.1600-051X.1998.tb02419.x

Souto, R., Silva-Boghossian, C.M. and Colombo, A.P. (2014) Prevalence of *Pseudomonas aeruginosa* and *Acinetobacter* spp. in subgingival biofilm and saliva of subjects with chronic periodontal infection. *Brazilian Journal of Microbiology,* 45(2), 495–501. https://doi.org/10.1590/s1517-83822014000200017

Stadler, A.F., Angst, P.D.M., Arce, R.M., Gomes, S.C., Oppermann, R.V. and Susin, C. (2016) Gingival crevicular fluid levels of cytokines/chemokines in chronic periodontitis: a meta-analysis. *Journal of Clinical Periodontology,* 43(9), 727–745. https://doi.org/10.1111/jcpe.12557

Stark, M.A., Huo, Y., Burcin, T.L., Morris, M.A., Olson, T.S. and Ley, K. (2005) Phagocytosis of apoptotic neutrophils regulates granulopoiesis via IL-23

and IL-17. *Immunity,* 22(3), 285–294. https://doi.org/10.1016/j.immuni.2005.01.011

Stathopoulou, P.G., Benakanakere, M.R., Galicia, J.C. and Kinane, D.F. (2009) The host cytokine response to *Porphyromonas gingivalis* is modified by gingipains. *Oral Microbiology and Immunology,* 24(1), 11–17. https://doi.org/10.1111/j.1399-302X.2008.00467.x

Strieter, R.M., Kasahara, K., Allen, R.M., Standiford, T.J., Rolfe, M.W., Becker, F.S., Chensue, S.W. and Kunkel, S.L. (1992) Cytokine-induced neutrophil-derived interleukin-8. *American Journal of Pathology,* 141(2), 397–407.

Sutton, J.D., Salas Martinez, M.L. and Gerkovich, M.M. (2017) Environmental tobacco smoke and periodontitis in United States non-smokers, 2009 to 2012. *Journal of Periodontology,* 88(6), 565–574. https://doi.org/10.1902/jop.2017.160725

Sutton, S. (2012) The limitations of CFU: compliance to CGMP requires good science. *Journal of GXP Compliance,* 16(1), 74–80.

Szafrański, S.P., Deng, Z.L., Tomasch, J., Jarek, M., Bhuju, S., Meisinger, C., Kühnisch, J., Sztajer, H. and Wagner-Döbler, I. (2015a) Functional biomarkers for chronic periodontitis and insights into the roles of *Prevotella nigrescens* and *Fusobacterium nucleatum*; a metatranscriptome analysis. *npj Biofilms and Microbiomes,* 1, 15017. https://doi.org/10.1038/npjbiofilms.2015.17

Szafrański, S.P., Wos-Oxley, M.L., Vilchez-Vargas, R., Jáuregui, R., Plumeier, I., Klawonn, F., Tomasch, J., Meisinger, C., Kühnisch, J., Sztajer, H., Pieper, D.H. and Wagner-Döbler, I. (2015b) High-resolution taxonomic profiling of the subgingival microbiome for biomarker discovery and periodontitis diagnosis. *Applied and Environmental Microbiology,* 81(3), 1047–1058. https://doi.org/10.1128/AEM.03534-14

Szkaradkiewicz, A.K., Stopa, J. and Karpiński, T.M. (2014) Effect of oral administration involving a probiotic strain of *Lactobacillus reuteri* on pro-inflammatory cytokine response in patients with chronic periodontitis. *Archivum Immunologiae et Therapiae Experimentalis,* 62(6), 495–500. https://doi.org/10.1007/s00005-014-0277-y

Takahashi, N., Mizuno, F. and Takamori, K. (1983) Isolation and properties of levanase from *Streptococcus salivarius* KTA-19. *Infection and Immunity,* 42(1), 231–236. https://doi.org/10.1128/iai.42.1.231-236.1983

Takamori, K., Mizuno, F., Yamamoto, A., Etoh, Y., Takahashi, M. and Takahashi, N. (1985) Preliminary studies of fructan-hydrolyzing bacteria from human dental plaque. *Microbiology and Immunology,* 29(4), 359–363. https://doi.org/10.1111/j.1348-0421.1985.tb00834.x

Tamashiro, R., Strange, L., Schnackenberg, K., Santos, J., Gadalla, H., Zhao, L., Li, E.C., Hill, E., Hill, B., Sidhu, G., Kirst, M., Walker, C. and Wang, G.P. (2021) Stability of healthy subgingival microbiome across space and time. *Scientific Reports,* 11, 23987. https://doi.org/10.1038/s41598-021-03479-2

Tamashiro, R., Strange, L., Schnackenberg, K., Santos, J., Gadalla, H., Zhao, L., Li, E.C., Hill, E., Hill, B., Sidhu, G.S., Kirst, M., Walker, C. and Wang, G.P. (2023) Smoking-induced subgingival dysbiosis precedes clinical signs of periodontal disease. *Scientific Reports,* 13, 3755. https://doi.org/10.1038/s41598-023-30203-z

Tannenbaum, J. and Bennett, B.T. (2015) Russell and Burch's 3Rs then and now: the need for clarity in definition and purpose. *Journal of the American Association for Laboratory Animal Science,* 54(2), 120–132.

Tattar, R., Jackson, J. and Holliday, R. (2025) The impact of e-cigarette use on periodontal health: a systematic review and meta-analysis. *Evidence-Based Dentistry,* 26(2), 117–118. https://doi.org/10.1038/s41432-025-01119-6

Taylor, J.J., Preshaw, P.M. and Lalla, E. (2013) A review of the evidence for pathogenic mechanisms that may link periodontitis and diabetes. *Journal of Clinical Periodontology,* 40(Suppl. 14), S113–S134. https://doi.org/10.1111/jcpe.12059

Tecchio, C., Micheletti, A. and Cassatella, M.A. (2014) Neutrophil-derived cytokines: facts beyond expression. *Frontiers in Immunology,* 5, 508. https://doi.org/10.3389/fimmu.2014.00508

Tekce, M., Ince, G., Gursoy, H., Dirikan Ipci, S., Cakar, G., Kadir, T. and Yılmaz, S. (2015) Clinical and microbiological effects of probiotic lozenges in the treatment of chronic periodontitis: a 1-year follow-up study. *Journal of Clinical Periodontology,* 42(4), 363–372. https://doi.org/10.1111/jcpe.12387

Teles, F.R., Teles, R.P., Uzel, N.G., Song, X.Q., Torresyap, G., Socransky, S.S. and Haffajee, A.D. (2012) Early microbial succession in redeveloping dental biofilms in periodontal health and disease. *Journal of Periodontal Research,* 47(1), 95–104. https://doi.org/10.1111/j.1600-0765.2011.01409.x

Temple, J., Velliou, E., Shehata, M. and Levy, R. (2022) Current strategies with implementation of three-dimensional cell culture: the challenge of quantification. *Interface Focus,* 12(5), 20220019. https://doi.org/10.1098/rsfs.2022.0019

Tetyczka, C., Hartl, S., Jeitler, R., Absenger-Novak, M., Meindl, C., Frohlich, E., Riedl, S., Zweytick, D. and Roblegg, E. (2021) Cytokine-mediated inflammation in the oral cavity and its effect on lipid nanocarriers. *Nanomaterials,* 11(5), 1330. https://doi.org/10.3390/nano11051330

Teubl, B.J., Absenger, M., Fröhlich, E., Leitinger, G., Zimmer, A. and Roblegg, E. (2013) The oral cavity as a biological barrier system: design of an advanced buccal *in vitro* permeability model. *European Journal of Pharmaceutics and Biopharmaceutics,* 84, 386–393. https://doi.org/10.1016/j.ejpb.2012.10.021

Theilade, E. (1986) The non-specific theory in microbial etiology of inflammatory periodontal diseases. *Journal of Clinical Periodontology,* 13(10), 905–911. https://doi.org/10.1111/j.1600-051X.1986.tb01425.x

Theofilou, V.I., Fraser, D., Kanasi, E., Brenchley, L., Greenwell-Wild, T., Adade, E.E., Valm, A.M., Douagi, I., Belkaid, Y., Tran, D.T., Williams, D.W. and Moutsopoulos, N.M. (2026) Distinct spatial organization governs oral mucosal immunity. *Nature Immunology,* 27(3), 624–635. https://doi.org/10.1038/s41590-025-02398-y

Thunström Salzer, A., Niemiec, M.J., Hosseinzadeh, A., Stylianou, M., Åström, F., Röhm, M., Ahlm, C., Wahlin, A., Ermert, D. and Urban, C.F. (2018) Assessment of neutrophil chemotaxis upon G-CSF treatment of healthy stem cell donors and in allogeneic transplant recipients. *Frontiers in Immunology,* 9, 1968. https://doi.org/10.3389/fimmu.2018.01968

Thurnheer, T., Bostanci, N. and Belibasakis, G.N. (2016) Microbial dynamics during conversion from supragingival to subgingival biofilms in an *in vitro* model. *Molecular Oral Microbiology,* 31(2), 125–135. https://doi.org/10.1111/omi.12108

Tokede, B., Brandon, R., Lee, C.T., Lin, G.H., White, J., Yansane, A., Jiang, X., Kalenderian, E. and Walji, M. (2024) Development and validation of a

rule-based algorithm to identify periodontal diagnosis using structured electronic health record data. *Journal of Clinical Periodontology,* 51(5), 547–557. https://doi.org/10.1111/jcpe.13938

Tonetti, M.S., Greenwell, H. and Kornman, K.S. (2018) Staging and grading of periodontitis: framework and proposal of a new classification and case definition. *Journal of Clinical Periodontology,* 45(Suppl. 20), S149–S161. https://doi.org/10.1111/jcpe.12945

Tonetti, M.S., Imboden, M.A., Gerber, L., Lang, N.P., Laissue, J. and Mueller, C. (1994) Localized expression of mRNA for phagocyte-specific chemotactic cytokines in human periodontal infections. *Infection and Immunity,* 62(9), 4005–4014. https://doi.org/10.1128/iai.62.9.4005-4014.1994

Tonetti, M.S., Imboden, M.A. and Lang, N.P. (1998) Neutrophil migration into the gingival sulcus is associated with transepithelial gradients of interleukin-8 and ICAM-1. *Journal of Periodontology,* 69(10), 1139–1147. https://doi.org/10.1902/jop.1998.69.10.1139

Tønjum, T. and van Putten, J. (2017) *Neisseria*. In: Cohen, J., Powderly, W.G. and Opal, S.M. (eds.) *Infectious Diseases.* 4th ed. London: Elsevier, pp. 1553–1564. https://doi.org/10.1016/B978-0-7020-6285-8.00179-9

Trayner, I.D., Bustorff, T., Etches, A.E., Mufti, G.J., Foss, Y. and Farzaneh, F. (1998) Changes in antigen expression on differentiating HL60 cells treated with dimethylsulphoxide, all-trans retinoic acid, α1,25-dihydroxyvitamin D3 or 12-O-tetradecanoyl phorbol-13-acetate. *Leukemia Research,* 22(6), 537–547. https://doi.org/10.1016/S0145-2126(98)00041-1

Treter, J., Bonatto, F., Krug, C., Soares, G.V., Baumvol, I.J.R. and Macedo, A.J. (2014) Washing-resistant surfactant coated surface is able to inhibit pathogenic bacteria adhesion. *Applied Surface Science,* 303, 147–154. https://doi.org/10.1016/j.apsusc.2014.02.123

Trombelli, L., Farina, R., Pollard, A., Claydon, N., Franceschetti, G., Khan, I. and West, N. (2020) Efficacy of alternative or additional methods to professional mechanical plaque removal during supportive periodontal therapy: a systematic review and meta-analysis. *Journal of Clinical Periodontology,* 47(Suppl. 22), 144–154. https://doi.org/10.1111/jcpe.13269

Trombelli, L., Farina, R., Silva, C.O. and Tatakis, D.N. (2018) Plaque-induced gingivitis: Case definition and diagnostic considerations. *Journal of Clinical Periodontology,* 45(Suppl. 20), S44–S67. https://doi.org/10.1002/JPER.17-0576

Tsai, C.Y., Tang, C.Y., Tan, T.S., Chen, K.H., Liao, K.H. and Liou, M.L. (2018) Subgingival microbiota in individuals with severe chronic periodontitis. *Journal of Microbiology, Immunology and Infection,* 51(2), 226–234. https://doi.org/10.1016/j.jmii.2016.04.007

Tsukasaki, M., Komatsu, N., Nagashima, K., Nitta, T., Pluemsakunthai, W., Shukunami, C., Iwakura, Y., Nakashima, T., Okamoto, K. and Takayanagi, H. (2018) Host defense against oral microbiota by bone-damaging T cells. *Nature Communications,* 9, 701. https://doi.org/10.1038/s41467-018-03147-6

Twain, M. (2010) Happy memories of the dental chair. In: *Who is Mark Twain?* 1st ed. New York, NY: HarperStudio, pp. 77–85.

Uchibori, S., Tsudukibashi, O., Goto, H., Kobayashi, T. and Aida, M. (2012) A novel selective medium for the isolation and distribution of *Rothia dentocariosa* in oral cavities. *Journal of Microbiological Methods,* 91(1), 205–207. https://doi.org/10.1016/j.mimet.2012.07.004

Uriarte, S.M. and Hajishengallis, G. (2023) Neutrophils in the periodontium: interactions with pathogens and roles in tissue homeostasis and inflammation. *Immunological Reviews,* 314(1), 93–110. https://doi.org/10.1111/imr.13152

Van den Steen, P.E., Proost, P., Wuyts, A., Van Damme, J. and Opdenakker, G. (2000) Neutrophil gelatinase B potentiates interleukin-8 tenfold by aminoterminal processing, whereas it degrades CTAP-III, PF-4, and GRO-alpha and leaves RANTES and MCP-2 intact. *Blood,* 96(8), 2673–2681. https://doi.org/10.1182/blood.V96.8.2673

van der Linden, M., Westerlaken, G.H.A., van der Vlist, M., van Montfrans, J. and Meyaard, L. (2017) Differential signalling and kinetics of neutrophil extracellular trap release revealed by quantitative live imaging. *Scientific Reports,* 7, 6529. https://doi.org/10.1038/s41598-017-06901-w

van der Reijden, W.A., Brunner, J., Bosch-Tijhof, C.J., van Trappen, S., Rijnsburger, M.C., de Graaff, M.P., van Winkelhoff, A.J., Cleenwerck, I. and de Vos, P. (2010) Phylogenetic variation of *Aggregatibacter actinomycetemcomitans* serotype e reveals an aberrant distinct evolutionary stable lineage. *Infection, Genetics and Evolution,* 10(7), 1124–1131. https://doi.org/10.1016/j.meegid.2010.07.011

Van Dyke, T.E. (2020) Shifting the paradigm from inhibitors of inflammation to resolvers of inflammation in periodontitis. *Journal of Periodontology,* 91(Suppl. 1), S19–S25. https://doi.org/10.1002/JPER.20-0088

Van Dyke, T.E., Bartold, P.M. and Reynolds, E.C. (2020) The nexus between periodontal inflammation and dysbiosis. *Frontiers in Immunology,* 11, 511. https://doi.org/10.3389/fimmu.2020.00511

van Houte, J., Lopman, J. and Kent, R. (1996) The final pH of bacteria comprising the predominant flora on sound and carious human root and enamel surfaces. *Journal of Dental Research,* 75(4), 1008–1014. https://doi.org/10.1177/00220345960750040201

Vaughan, L., Glanzel, W., Korch, C. and Capes-Davis, A. (2017) Widespread use of misidentified cell line KB (HeLa): incorrect attribution and its impact revealed through mining the scientific literature. *Cancer Research,* 77(11), 2784–2788. https://doi.org/10.1158/0008-5472.CAN-16-2258

Vesel, A., Zaplotnik, R., Primc, G. and Mozetič, M. (2020) Evolution of the surface wettability of PET polymer upon treatment with an atmospheric-pressure plasma jet. *Polymers,* 12(1), 87. https://doi.org/10.3390/polym12010087

Waite, W.H. (1870) Periodontitis. *The American Journal of Dental Science,* 4(8), 369–373.

Wake, N., Asahi, Y., Noiri, Y., Hayashi, M., Motooka, D., Nakamura, S., Gotoh, K., Miura, J., Machi, H., Iida, T. and Ebisu, S. (2016) Temporal dynamics of bacterial microbiota in the human oral cavity determined using an in situ model of dental biofilms. *npj Biofilms and Microbiomes,* 2, 16018. https://doi.org/10.1038/npjbiofilms.2016.18

Walter, E., Brock, T., Lahoud, P., Werner, N., Czaja, F., Tichy, A., Bumm, C., Bender, A., Castro, A., Teughels, W., Schwendicke, F. and Folwaczny, M. (2025) Predictive modeling for step II therapy response in periodontitis - model development and validation. *npj Digital Medicine,* 8, 445. https://doi.org/10.1038/s41746-025-01828-3

Wang, H., Divaris, K., Pan, B., Li, X., Lim, J.H., Saha, G., Barovic, M., Giannakou, D., Korostoff, J.M., Bing, Y., Sen, S., Moss, K., Wu, D., Beck, J.D., Ballantyne, C.M., Natarajan, P., North, K.E., Netea, M.G., Chavakis, T. and Hajishengallis, G. (2024) Clonal hematopoiesis driven by mutated

DNMT3A promotes inflammatory bone loss. *Cell,* 187(14), 3690–3711.e3619. https://doi.org/10.1016/j.cell.2024.05.003

Wang, X., Qin, W., Xu, X., Xiong, Y., Zhang, Y., Zhang, H. and Sun, B. (2017) Endotoxin-induced autocrine ATP signaling inhibits neutrophil chemotaxis through enhancing myosin light chain phosphorylation. *Proceedings of the National Academy of Sciences of the United States of America,* 114(17), 4483–4488. https://doi.org/10.1073/pnas.1616752114

Wen, S.-H., Hong, Z.-W., Chen, C.-C., Chang, H.-W. and Fu, H.-W. (2021) *Helicobacter pylori* neutrophil-activating protein directly interacts with and activates Toll-like receptor 2 to induce the secretion of interleukin-8 from neutrophils and ATRA-induced differentiated HL-60 cells. *International Journal of Molecular Sciences,* 22(21), 11560. https://doi.org/10.3390/ijms222111560

West, N.X., Gormley, A., Pollard, A.J., Izzetti, R., Marruganti, C. and Graziani, F. (2025) Evaluating the performance and implementation of the 2018 Classification of Periodontal Diseases: a systematic review and survey. *Journal of Clinical Periodontology,* 52(Suppl. 29), 34–57. https://doi.org/10.1111/jcpe.14170

Wewer, C., Seibt, A., Wolburg, H., Greune, L., Schmidt, M.A., Berger, J., Galla, H.J., Quitsch, U., Schwerk, C., Schroten, H. and Tenenbaum, T. (2011) Transcellular migration of neutrophil granulocytes through the blood-cerebrospinal fluid barrier after infection with *Streptococcus suis*. *Journal of Neuroinflammation,* 8(1), 51. https://doi.org/10.1186/1742-2094-8-51

Williams, D.W., Greenwell-Wild, T., Brenchley, L., Dutzan, N., Overmiller, A., Sawaya, A.P., Webb, S., Martin, D., Hajishengallis, G., Divaris, K., Morasso, M., Haniffa, M. and Moutsopoulos, N.M. (2021) Human oral mucosa cell atlas reveals a stromal-neutrophil axis regulating tissue immunity. *Cell,* 184(15), 4090–4104.e4015. https://doi.org/10.1016/j.cell.2021.05.013

Wilson, C.J., Clegg, R.E., Leavesley, D.I. and Pearcy, M.J. (2005) Mediation of biomaterial–cell interactions by adsorbed proteins: a review. *Tissue Engineering,* 11(1–2), 1–18. https://doi.org/10.1089/ten.2005.11.1

World Health Organization (2024) *Global strategy and action plan on oral health 2023–2030*. Geneva: World Health Organization. Available at: https://www.who.int/publications/i/item/9789240090538 (Accessed: 24 February 2026).

Wright, L.C., Nouri-Sorkhabi, M.H., May, G.L., Danckwerts, L.S., Kuchel, P.W. and Sorrell, T.C. (1997) Changes in cellular and plasma membrane phospholipid composition after lipopolysaccharide stimulation of human neutrophils, studied by ^{31}P NMR. *European Journal of Biochemistry,* 243(1–2), 328–335. https://doi.org/10.1111/j.1432-1033.1997.0328a.x

Wu, X., Chen, J., Xu, M., Zhu, D., Wang, X., Chen, Y., Wu, J., Cui, C., Zhang, W. and Yu, L. (2017) 16S rDNA analysis of periodontal plaque in chronic obstructive pulmonary disease and periodontitis patients. *Journal of Oral Microbiology,* 9(1), 1324725. https://doi.org/10.1080/20002297.2017.1324725

Xiao, L., Okamura, H. and Kumazawa, Y. (2018) Three-dimensional inflammatory human tissue equivalents of gingiva. *Journal of Visualized Experiments,* 2018(134), e57157. https://doi.org/10.3791/57157

Yakubenko, V.P., Lishko, V.K., Lam, S.C.T. and Ugarova, T.P. (2002) A molecular basis for integrin $\alpha_M\beta_2$ ligand binding promiscuity. *Journal of Biological Chemistry,* 277(50), 48635–48642. https://doi.org/10.1074/jbc.M208877200

Yin, J., Li, Y., Feng, M. and Li, L. (2022) Understanding the feelings and experiences of patients with periodontal disease: a qualitative meta-synthesis. *Health and Quality of Life Outcomes,* 20(1), 126. https://doi.org/10.1186/s12955-022-02042-5

You, M., Mo, S., Leung, W.K. and Watt, R.M. (2013) Comparative analysis of oral treponemes associated with periodontal health and disease. *BMC Infectious Diseases,* 13(1), 174. https://doi.org/10.1186/1471-2334-13-174

Zbinden, A., Aras, F., Zbinden, R., Mouttet, F., Schmidlin, P.R., Bloemberg, G.V. and Bostanci, N. (2014) Frequent detection of *Streptococcus tigurinus* in the human oral microbial flora by a specific 16S rRNA gene real-time TaqMan PCR. *BMC Microbiology,* 14(1), 231. https://doi.org/10.1186/s12866-014-0231-5

Zhou, B., Mobberley, J., Shi, K. and Chen, I.A. (2022) Effects of preservation and propagation methodology on microcosms derived from the oral microbiome. *Microorganisms,* 10(11), 2146. https://doi.org/10.3390/microorganisms10112146

Zhou, M., Rong, R., Munro, D., Zhu, C., Gao, X., Zhang, Q. and Dong, Q. (2013) Investigation of the effect of type 2 diabetes mellitus on subgingival plaque microbiota by high-throughput 16S rDNA pyrosequencing. *PLOS ONE,* 8(4), e61516. https://doi.org/10.1371/journal.pone.0061516

Zhu, L. and Kreth, J. (2012) The role of hydrogen peroxide in environmental adaptation of oral microbial communities. *Oxidative Medicine and Cellular Longevity,* 2012(1), 717843. https://doi.org/10.1155/2012/717843

Zijnge, V., van Leeuwen, M.B., Degener, J.E., Abbas, F., Thurnheer, T., Gmur, R. and Harmsen, H.J. (2010) Oral biofilm architecture on natural teeth. *PLOS ONE,* 5(2), e9321. https://doi.org/10.1371/journal.pone.0009321